REPORT NO. GDC-DDB-70-003
CONTRACT NAS8-21291
NASA CR 109847

EVALUATION AND APPLICATION OF DATA FROM LOW-GRAVITY ORBITAL EXPERIMENT

PHASE I - FINAL REPORT

GENERAL DYNAMICS
Convair Division

REPORT NO. GDC-DDB-70-003

EVALUATION AND APPLICATION OF DATA FROM LOW-GRAVITY ORBITAL EXPERIMENT

PHASE I - FINAL REPORT

R. D. Bradshaw

1 April 1970

Prepared Under
Contract NAS8-21291
DCN1-8-52-10101

Prepared by
CONVAIR DIVISION OF GENERAL DYNAMICS
San Diego, California

FOREWORD

This report covers work performed in the Research and Engineering Department of the Convair division of General Dynamics at San Diego, California, under contract Number NAS8-21291, "Evaluation and Application of Data From Low-Gravity Orbital Experiment" for the George C. Marshall Space Flight Center (MSFC) of the National Aeronautics and Space Administration (NASA), during the period 21 February 1968 to 30 June 1969. Contract control number was DCN1-8-52-10101. Project manager for this phase of the study was Dr. R. D. Bradshaw. Other Convair personnel contributing to this phase of the study were Messrs. M. H. Blatt, L. R. Kaszas, K. M. Kneisel, A. R. Marchese, and A. B. Walburn. The study was under the technical direction of Mr. Leon J. Hastings, NASA/MSFC, S&E-ASTN-PF.

TABLE OF CONTENTS

			Page
LIST OF FIGURES			v
NOMENCLATURE			xi
SUMMARY			xvii
1	INTRODUCTION		1-1
2	REPRESSURIZATION		2-1
	2.1	REPRESSURIZATION SEQUENCES FOR FOR AS-203	2-1
	2.2	ENERGY EVALUATION	2-4
	2.3	THE PRISM PROGRAM	2-4
	2.4	S-II PRESSURIZATION MODEL APPLICABILITY	2-8
	2.4.1	Pressure Rise Without Recirculation Simulation	2-8
3	CLOSED TANK PRESSURE RISE		3-1
	3.1	PROPELLANT TANK HEATING	3-1
	3.1.1	Orbital Heating	3-2
	3.1.2	Hydrogen Tank Energy Balance	3-5
	3.2	PRESSURE RISE RATE	3-11
4	DEPRESSURIZATION AND LIQUID LEVEL RISE		4-1
	4.1	AS-203 DATA ANALYSIS	4-1
	4.2	ANALYTICAL MODEL FOR BULK LIQUID	4-10
	4.2.1	Level Rise Due to Pressure Reduction	4-10
	4.2.2	Effects of Liquid Superheat	4-13
	4.2.3	Influence of Wall Heat Transfer	4-15
	4.2.4	Consideration of Both Superheat and Wall Heat Transfer	4-16
	4.3	BOUNDARY LAYER MODEL FOR LIQUID LEVEL RISE	4-17
	4.3.1	Description of Boundary Layer Analytical Model	4-17
	4.3.2	Parametric Analysis	4-26
	4.4	BUBBLE DYNAMICS MODEL FOR LOW-G	4-27
	4.4.1	Analytical Model	4-31

TABLE OF CONTENTS, Contd

			Page
	4.4.2	Demonstration Problem For S-IVB Liquid Level Rise	4-40
	4.5	LIQUID LEVEL RISE CONCLUSIONS AND RECOMMENDATIONS	4-48
5	PROPELLANT CONTROL AND SETTLING ANALYSIS		5-1
	5.1	PROPELLANT SLOSHING MATHEMATICAL MODEL	5-1
	5.1.1	S-IVB Propellant Sloshing Parameters	5-3
	5.1.2	Drop Tower Model Propellant Sloshing Parameters	5-3
	5.2	BAFFLE DAMPING MATHEMATICAL MODEL	5-3
	5.3	DROP TOWER PROPELLANT SLOSHING ANALYSIS	5-8
	5.3.1	Maximum Liquid Amplitude With Clean Tank Configuration (No Baffles)	5-10
	5.3.2	Maximum Liquid Amplitude With Baffled Tank Configuration	5-17
	5.3.3	Amplification Factor	5-18
	5.4	S-IVB AS-203 SLOSH SIMULATION	5-19
	5.4.1	Vehicle Dynamic Model	5-19
	5.4.2	Simulation Results	5-24
	5.4.3	Summary of Simulation Results	5-28
	5.5	SIMULATIONS WITH MARKER AND CELL MODEL	5-29
	5.5.1	Sloshing Simulation Mechanics	5-29
	5.5.2	Settling Demonstration Model	5-30
	5.5.3	Stratification/Destratification Modeling	5-32
	5.5.4	Marker and Cell Merits	5-32
6	CONCLUSIONS AND RECOMMENDATIONS		6-1
7	REFERENCES		7-1
APPENDIX A	PRISM PROGRAM		A-1
APPENDIX B	LIQLEV PROGRAM		B-1
APPENDIX C	EVOLVE PROGRAM		C-1

LIST OF FIGURES

Figure		Page
1-1	Events Sequence for S-IVB-203 Experiment	1-2
1-2	Instrumentation Schematic for S-IVB-AS-203 Vehicle	1-3
2-1	Sequence of Events Effecting Repressurization of LH_2 Tank S-IVB-203	2-1
2-2	Fuel Tank Ullage Pressure During Repressurization and Engine Chilldown	2-2
2-3	LH_2 Tank Repressurization Schematic	2-3
2-4	Ullage Heating Rate Comparison	2-5
2-5	Liquid Heating Rate Comparisons	2-5
2-6	Comparison of Prism Repressurization Runs	2-7
2-7	Pressure History During Helium Addition - Comparison of Prism Runs	2-7
2-8	Comparison of Propellant Heat Fluxes Predicted With P2162 and Those Achieved in P3542	2-9
2-9	Flight Data and Pressure Prediction With P3542 For Repressurization Phase	2-10
3-1	Orbital Radiative Heating of the Cylindrical Sidewall of the AS-203 Vehicle	3-3
3-2	Orbital Radiative Heating of the Conical Nose Fairing of the AS-203 Vehicle	3-4
3-3	Forward Dome Wall Temperature Difference at Station 652.7 for the AS-203 Pressure Rise Experiment	3-7
3-4	Wall Gradients for S-IVB Thermal Modeling	3-9
3-5	Comparison of Ullage Heating Rates For Two Absorptivities With AS-203 Data	3-10
3-6	Heat Fluxes to Sections of AS-203 During Long Term Coast	3-10
3-7	Comparison of Ullage Heating Rates With Calculated Values From AS-203 Data	3-12
3-8	Comparison of Liquid Heating Rates With Measured AS-203 Data	3-12

Figures		Page
3-9	Comparison of Predicted Pressures With AS-203 Pressure History During Long Term Coast	3-14
3-10	Comparison of Propellant Heat Fluxes Predicted With P2162 and Those Achieved in P3542	3-15
4-1	LH_2 Temperature Sensor Location in S-IVB Tank	4-3
4-2	Temperature Versus Range Time During First Depressurization For Temperature Sensors in Vicinity of Initial Liquid Level	4-4
4-3	Temperature Versus Range Time During Second Depressurization For Temperature Sensors in Vicinity of Initial Liquid Level	4-5
4-4	Response of Liquid-Vapor Sensor N052 During Second Depressurization	4-6
4-5	Response of Liquid-Vapor Sensor N052 During Initial Part of Third Depressurization	4-8
4-6	Response of Liquid-Vapor Sensor N052 During Final Part of Third Depressurization	4-9
4-7	Relative Liquid Level Rise Versus Pressure Reduction	4-12
4-8	Maximum Pressure Drop Relationship For Fractional Fill Levels	4-13
4-9	Bubble Boundary Layer Model	4-18
4-10	Bubble Geometric Spacing Factors	4-19
4-11	Mass Balance for Differential Film Layer Section For Unsteady State Boundary Layer	4-20
4-12	Mass Conservation in the Boundary Layer	4-24
4-13	Dimensionless Liquid Level Increase With Time For a Range of ϵ Values	4-28
4-14	Dimensionless Liquid Level Increase With Time for Various Vent Rates	4-28
4-15	Film Thickness Variation With Time for Various Vent Rates	4-29

LIST OF FIGURES, Contd

Figures		Page
4-16	Dimensionless Liquid Level With Time for Various Bubble Spacings	4-29
4-17	Dimensionless Liquid Level Increase Dependence on Pressure Decay Rate	4-30
4-18	Dimensionless Liquid Level Increase Dependence on g-Level	4-30
4-19	Bubble Population Produced Compared to Number Existing After Agglomeration For Wake and No Wake Cases as a Time-Dependent Function	4-41
4-20	Bubble Distribution After 30 Seconds in a Typical Radial Plane of S-IVB For Wake Interaction Case	4-42
4-21	Bubble Distribution After 30 Seconds in a Typical Radial Plane of S-IVB For No Wake Interaction Case	4-43
4-22	Bubble Population and Areas for S-IVB Simulation	4-44
4-23	Liquid Level Rise and Entrained Volume for S-IVB Simulation	4-45
4-24	Lead Bubble Characteristics for S-IVB Simulation	4-46
4-25	Important Effects of Bubble Agglomeration and Void Fraction in Finite Media Define Bubble Trajectories	4-47
5-1	Propellant Sloshing Parameters for Pendulum Slosh Analogy	5-2
5-2a	S-IVB Fuel Tank Slosh Parameters as a Function of Propellant Interface Level	5-3
5-2b	S-IVB Fuel Tank Slosh Parameters as a Function of Propellant Interface Level	5-3
5-2c	S-IVB Fuel Tank Slosh Parameters as a Function of Propellant Interface Level	5-4
5-3a	S-IVB Oxidizer Tank Slosh Parameters as a Function of Propellant Interface Level	5-4
5-3b	S-IVB Oxidizer Tank Slosh Parameters as a Function of Propellant Interface Level	5-5

Figures		Page
5-3c	S-IVB Oxidizer Tank Slosh Parameters as a Function of Propellant Interface Level	5-5
5-4	S-IVB Scale Model LH_2 Tank Slosh Parameters as a Function of Propellant Interface Level	5-7
5-5	Baffle Damping Energy Dissipation Constant as a Function of Quiescent Liquid Level for S-IVB - AS-203 Vehicle	5-9
5-6	Baffle Damping Energy Dissipation Constant as a Function of Quiescent Liquid Level for S-IVB Drop Tower Model	5-9
5-7	Drop Tower Propellant Slosh Analogy Parameters	5-10
5-8	Maximum Liquid Slosh Amplitude Determined From Analytical Model for Several Bond Numbers	5-12
5-9	Liquid Amplitude History of a Typical Simulation Run	5-13
5-10	Propellant Slosh Liquid-Vapor Interface Profiles	5-14
5-11	Drop Tower Test Data for Maximum Liquid Slosh Amplitude	5-15
5-12	Drop Tower Slosh Test 2F-41 Slosh Amplitude History	5-16
5-13	Liquid Vapor Profile Test 2F-41 at 2.5 Seconds	5-17
5-14	Comparison of Theoretical Slosh Amplification Factor With Simulation Result for No Baffle and Baffled Tank Configurations	5-20
5-15	Comparison of Theoretical Amplitude Factor With Modified Drop Tower Test Results	5-21
5-16	S-IVB Propellant Slosh Dynamic Model	5-23
5-17	Saturn S-IVB Attitude Control System Engine Locations	5-24
5-18	S-IVB Attitude Control System Autopilot Block Diagram	5-25
5-19	AS-203 Propellant Slosh Wave	5-26
5-20	Sloshing Simulation With MAC for Scale Model S-IVB in a Drop Tower Test	5-31

LIST OF FIGURES, Contd

Figure		Page
5-21	Fluid Simulation Study on S-IVB Liquid Hydrogen Tank During Engine Restart in Orbit	5-33
5-22	Stratification From Combined Sidewall and Bottom Heating	5-34

NOMENCLATURE

A_c	cross sectional area of tank, sq ft
A_x, A_y, A_z	inertial acceleration of cg along body X, Y, Z axis, ft/sec
a	acceleration, ft/sec^2
Bo	Bond number, $R^2 \, a \rho/\sigma \, g_c$
C	liquid specific heat, Btu/lb_m °R
C_ξ	baffle energy dissipation constant, ft-lb_f-sec^2/$rad^{5/2}$
C_{NL}	non linear oxidizer energy dissipation constant, deg^{-1}
D_T	tank diameter, ft
d	bubble diameter, ft
e	unit vector
E	energy
Eö	Etovos number, $R_B{}^2 \, g \, (\rho_\ell - \rho_g)/\sigma \, g_c$
E_c	control threshold, deg/sec
E_o	engine command single, N.D.
F	force, lb_f
F_x, F_y, F_z	forces on vehicle, lb_f
Fr	Froude number, v^2/aR
g	gravitational acceleration, ft/sec^2
g_c	gravitational constant, 32.17 lb_m-ft/lb_f-sec^2
H	meniscus height, ft
H	height of tank, ft
h	liquid level height, ft
h	switching hysteresis signal, deg/sec
I_R	moment of inertia of total propellant mass (Fig. 5-1), slug-ft^2
I_{OR}	moment of inertia of reduced propellant mass (Fig. 5-1), slug-ft^2

$\bar{h}_g$	average bubble enthalpy, Btu/lb_m
$\bar{h}_{fg}$	average heat of vaporization, Btu/lb_m
I_{xx_o}, I_{yy_o}, I_{zz_o}	reduced moments of inertia about vehicle centerline, slug-ft^2
I_{xy_o}, I_{xz_o}	reduced products of inertia about vehicle centerline, slug-ft^2
J	conversion constant, 778 ft-lb_f/Btu
K_f	lag feedback gain, deg/sec
K_o	switching hysteresis gain, deg/sec
$K_{R'}$	ratio of attitude to rate, sec
L_{PF}, L_{PO}	fuel and oxidizer pendulum lengths, ft
L, M, N	externally applied torques about roll, pitch, and yaw axis, ft-lb_f
ℓ_F, ℓ_o	length from reduced cg to fuel and oxidizer pendulum hinge points, ft
M_o	vehicle mass excluding mass of slosh pendulums, slugs
M_T	vehicle total mass, slugs
M_{PF}, M_{PO}	fuel and oxidizer pendulum masses, slugs
m	mass, lb_m
$\dot{m}_v$	vent flow rate, lb_m/sec
P, Q, R	angular rates in roll, pitch, and yaw, deg/sec
p	tank pressure, lb_f/in^2
Q_w	wall heat transfer, Btu/hr
R	tank radius, ft
R	gas constant of vapor, ft-lb_f/lb_m-°R
r	cavity radius, in
S_ℓ	lateral bubble spacing, dimensionless
S_v	vertical bubble spacing, dimensionless

S_W	side wall tank wetted area, ft^2
T	temperature, °R
t	time, sec
u	bubble or vapor film velocity, ft/sec
V_{max}	fluid velocity, ft/sec
V	lag feedback signal, deg/sec
V	ullage volume, ft^3
V_{BL}	volume of vapor film boundary layer, ft^3
v	slosh interface velocity, ft/sec
v	bubble velocity, ft/sec
x	station number on vehicle
Δy_o, Δz_o	pitch and yaw reduced cg offsets, ft
Z	compressibility factor
Z	coordinate along tank side wall, ft
α	local void fraction
α_F	pitch pendulum displacement angle for fuel, deg
α_O	pitch pendulum displacement angle for oxidizer, deg
α_S	solar absorptivity
α_T	thermal absorptivity
β	fractional amount of entrained vapor
β_F	yaw pendulum displacement angle for fuel, deg
β_O	yaw pendulum displacement angle for oxidizer, deg
δ	vapor film thickness, ft
ϵ	error signal, deg/sec
ϵ_c	contractor actuation signal, deg/sec
ζ	maximum liquid amplitude, ft
ζ_F	fuel linear damping ratios

ζ_L	slosh waveheight right side, ft
ζ_ℓ	maximum slosh waveheight in low-g, ft
ζ_O	oxidizer linear damping ratios
ζ_R	slosh waveheight right side, ft
Θ	time, sec; polar angle
λ	heat of evaporation, Btu/lb_m
ρ_ℓ	liquid density, lb_m/ft^3
ρ_v	vapor density, lb_m/ft^3
σ	liquid surface tension, lb_f/ft
τ_f	log feedback time constant, sec
ϕ	slosh phase angle, deg
ψ	ratio of superheated liquid mass to total liquid mass
ω_F	fuel slosh natural frequency, rad/sec
ω_O	oxidizer slosh natural frequency, rad/sec
Subscripts	
B	bubble
BL	vapor film boundary layer
e	evaporated
f	final
g	gravity, gas
h	high gravity conditions
i	incipient boiling value
L	liquid
ℓ	low gravity conditions, liquid
o	initial
s	saturated
T	tank
v	velocity, vapor

W	wall
x, y, z	axis directions
Z	local value along tank wall

SUMMARY

A fourteen month study was performed under NASA/MSFC contract NAS8-21291 to analyze the S-IVB - AS-203 data and other available data to determine the applicability and adequacy of analytical models in several areas of thermodynamics and fluid mechanics. In particular, areas considered were repressurization, vehicle heating, pressure rise, liquid level phenomena during venting, boiling and propellant sloshing. Analytical models were developed and models were verified in each of these areas. Areas requiring further study are identified.

The repressurization of the AS-203 vehicle for restart in orbit was analyzed with two existing pressurization programs. Heating programs were used to determine the contribution of ullage heating during this 360 second sequence. With heating rates determined, the reliability of the analytical pressurization models to analyze pressure changes during periods of helium addition and recirculation flow were ascertained. The program PRISM was used for a parametric study of the contributions of these variables. This program indicated options for ullage heating with interfacial heat transfer provide a good simulation of the pressure history. This model further represented the large potential effect of recirculation flow. The S-II pressurization model lacks recirculation flow capability but was used to analyze helium addition and ullage heating effects. This latter model over predicted the helium addition period pressure rise just as PRISM had done, but failed to match the ensuing pressure rise actually experienced. This suggests some effects of recirculation exist but are obviously not modeled in the S-II model. PRISM serves as an excellent pre-design tool for a parametric look at gross effects.

The closed tank pressure rise for AS-203 was analyzed with existing analytical models, the S-II Pressurization Program and REPORTER. Prior to the pressure rise analysis, considerable effort was expended in obtaining and verifying the heating analyses for input to the thermodynamic models. Heating inputs were predicted theoretically from radiant absorbed heat fluxes and from conduction-radiation models of the fuel tank and its surrounding environment. The measurements of AS-203 skin temperatures provided a confirmation of the predicted heating rates. Although energy conducted through the forward dome is small, this heat transfer analysis within the forward skirt area proved difficult because of an indefinite absorptivity for the mylar insulation. The magnitude of heating rates for the various areas are presented and compared with previous investigations. The sensitivity of the pressure rise thermodynamic models to ullage heating inputs is discussed. Good agreement with test data was obtained for both heating and pressure rise models.

The depressurization phase of the AS-203 experiment in a low-g environment was successful, however, it did not provide enlightenment on these areas of liquid behavior: liquid level rise, bubble evolution, boiling, or interfacial break-up. These phenomena increase the possibility of venting liquid if the venting rate is too rapid for a given initial liquid level. A gross bulk boiling analysis was performed to provide parametric data for liquid level rise. For this worst case analysis, a potential excessive liquid level rise was indicated. In a second analytical model, LIQLEV, boiling was assumed to occur only at the interface and in the boundary layer. A residence time was determined for bubbles based on their size. Thus, boundary layer growth occurred during a vent down; this resulted in an approximately ten percent liquid level rise for the AS-203 geometry. Parametric plots are given to show the effect of g-level and vent rate on the change in liquid level.

The phenomena of boiling, liquid level rise, and bubble motion are rigorously treated in a Convair computer code, EVOLVE, developed under company funding. This model along with LIQLEV are both listed in the appendices of this report. The analytical model computes the forces exerted on a bubble in a low-g field due to buoyancy, drag, and surface tension. The effects of adjacent bubbles and void fraction in a confined media are calculated. Studies conducted indicated that wake effects are an important consideration in the agglomeration process. The AS-203 geometry was used to evaluate bubble characteristics and liquid level rise during a depressurization. This model confirms the findings of model LIQLEV. Liquid level rise is probably not a problem except for full tanks at high vent rates. Bubble populations determined with this model are described.

Propellant sloshing analysis is based on an analytical solution of the hydrodynamic equations of motion. The solution assumes perturbational displacements of the free surface of an ideal liquid in an environment dominated by g dependent forces. Effects such as stratification or thermally driven motions are not included here. In addition splashing, geysering, or breakaway liquid is not accounted for. For simplicity the hydrodynamic solution is represented by the pendulum analogy. The forces and moments produced by the oscillating propellants are represented by a set of pendulums.

The effect of baffle damping on liquid propellant motion is treated purely as an energy dissipation device. The propellant motion is not physically constrained, instead kinetic energy is removed in accordance with the theoretical energy dissipation provided by the baffle. This baffle damping model provides an instantaneous rate of energy dissipation rather than the average value over a full cycle. Unfortunately the solution assumes the baffle to remain below the free surface level. When the baffle is allowed to become uncovered the solution is in error.

The propellant slosh parameters based on this analytical model were obtained for both the S-IVB fuel and oxidizer tanks along with the 6-inch scale model S-IVB fuel tank as a function of the undisturbed propellant interface level. These data show the second and higher propellant modes to be insignificant, hence they are omitted in the analysis.

The drop tower slosh test results provide a direct evaluation of the propellant slosh analytical solution as applied to the low-g condition. A digital computer program was established to simulate the drop tower slosh dynamics. A comparison of maximum liquid amplitude as a function of Froude number obtained from simulation results was made with published test results. Data on liquid level amplification factor was also obtained. Unfortunately not enough raw test data were available to expand on the correlation analysis. From the test data available it appeared that in addition to slosh motion, low-g meniscus effects were present. Under this condition the propellant slosh model was inadequate to completely describe the propellant slosh motion observed in test data.

The same analytical model was used to simulate AS-203 orbital coast conditions. The results show decaying liquid oscillations at their natural frequencies with small perturbations produced by the reaction control motor firings. No coupled frequencies were observed. These results are in general agreement with published flight results.

The Marker and Cell computer code affords a simulation model for fluid dynamics problems under low-g conditions. The computer code was used during this study phase for an evaluation of sloshing. Simulation of model S-IVB drop tower test results was programmed. The absence of surface tension in the model resulted in perturbations at the interface which masked the major sloshing motion. These simulation difficulties should be removed when surface tension is included in the model. This report also indicates applications of MAC to settling and stratification.

Several areas have been defined which merit further study. The quality of recirculation flow for recirculation application is not adequately defined with existing models. Pressure rise rate with unsettled propellant requires analytical modeling and verification. The break-up of the interface into globules during depressurization can result in severe liquid carryover problems. Program EVOLVE provides an excellent tool to examine bubble phenomena in low gravity storage including hot spot heat leak evaluation and ullage definition. Further analytical development and verification with test data is required for slosh damping analyses for uncovered baffles. The Marker and Cell program provides an excellent tool to examine fluid phenomena such as sloshing, settling, outflow, and stratification and destratification.

The computer codes used in this study are those already in the NASA/MSFC library with the exception of MAC, PRISM, LIQLEV, and EVOLVE. These latter three programs are supplied with input/output procedures in the appendices to this report. An improved version of MAC will be delivered at the completion of Phase II of this contract.

1

INTRODUCTION

The S-IVB Stage was launched into a nominal 100 mile circular earth orbit on 5 July 1966. This flight (AS-203) provided the most complete data on thermodynamic and fluid dynamic performance of any orbital experiment performed to date. With data from that experiment reduced and analyzed, a logical step was to verify available analytical models to determine applicability and degree of correlation. Additional data from drop tower tests were also evaluated and compared with predictions of analytical models.

Previous presentations of the AS-203 experimental data have been made (Ref. 1-1, 1-2 and 1-3). Of the many areas of low-gravity propellant behavior for which data was obtained, the particular areas of interest for this study were determined to be repressurization, pressure rise during coast, liquid level rise bubble dynamics and liquid carryover, and sloshing and settling. The sequence of events shown in Figure 1-1 gives a good overview of the experiments conducted, their duration, and the periods of time for which data was available. Data acquisition was excellent except for a period of no data during the long term coast pressure rise. The vehicle configuration and the instrumentation locations are shown in Figure 1-2. Hydrogen liquid level was at approximately station 438 at insertion.

During this fourteen month study, data which were presented in the above reports were evaluated in conjunction with the analytical models available. In the area of liquid level rise, new analytical models were developed. Where possible, test data were compared with analytical predictions. Where models show good correlation with test data, parametric studies were performed to define the range of operating conditions.

The design of future upper stage vehicles and the extension of operating conditions, i.e. coast times, of present vehicles requires verification of available analytical models. It was the further aim of this study to define areas in which further effort is required, either through analytical development or additional experiments.

The applicability of two computer codes to predict pressure history during repressurization is discussed in Section 2. The heating analysis for the S-IVB vehicles and the models for prediction of pressure history for the settled coast condition are considered in Section 3. The phenomena of liquid level rise in an S-IVB vehicle is presented in Section 4 with a model for analysis of bubble dynamics in low-g. Section 5 examines the applicability of an analytical model to sloshing, considering drop tower data and AS-203 data. The applicability of the MAC technique to sloshing and other fluid dynamics problems is examined. The conclusions and recommendations for additional work are presented in Section 6.

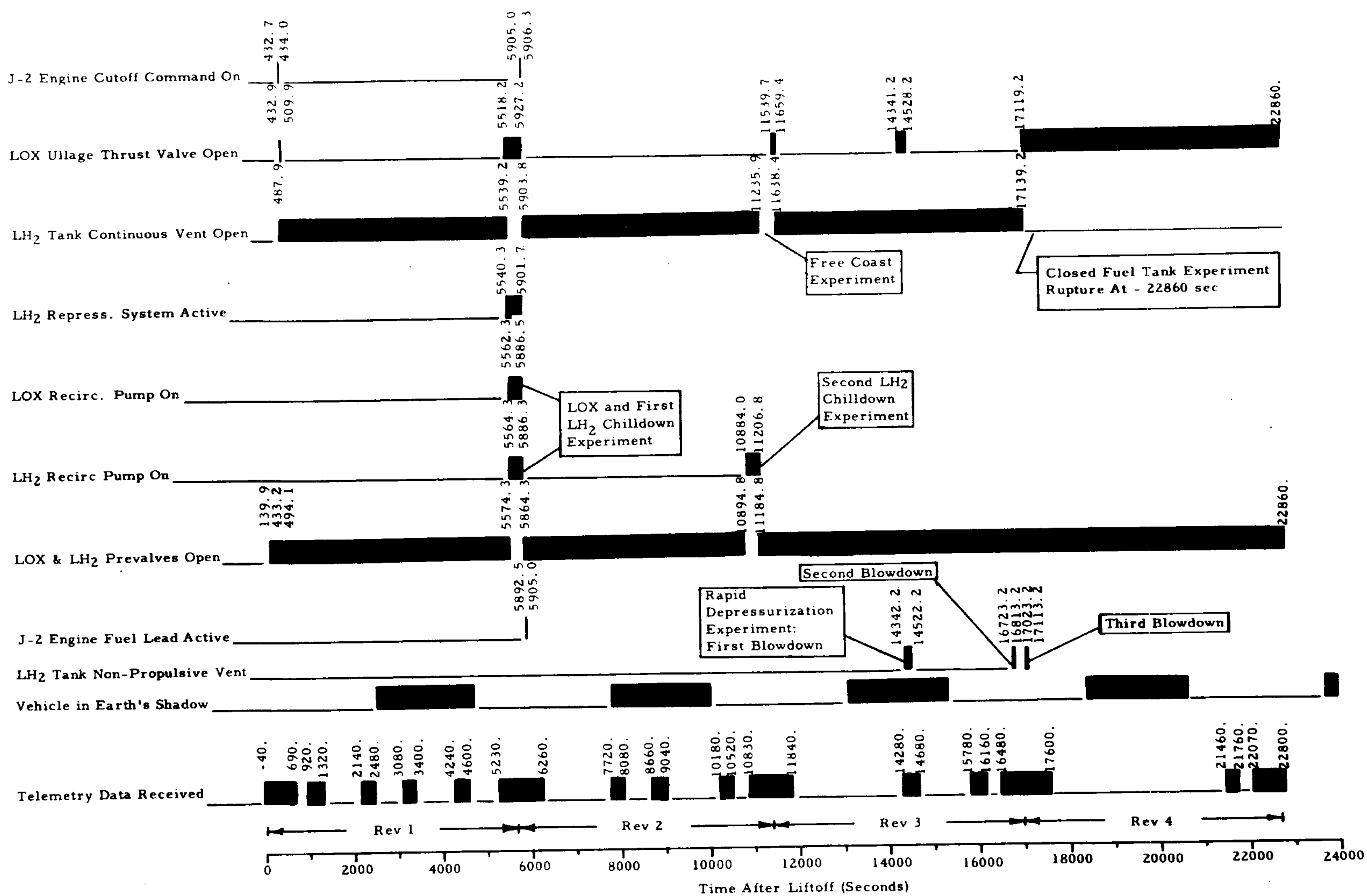

Figure 1-1. Events Sequence for S-IVB-203 Experiment (Reference 1-1)

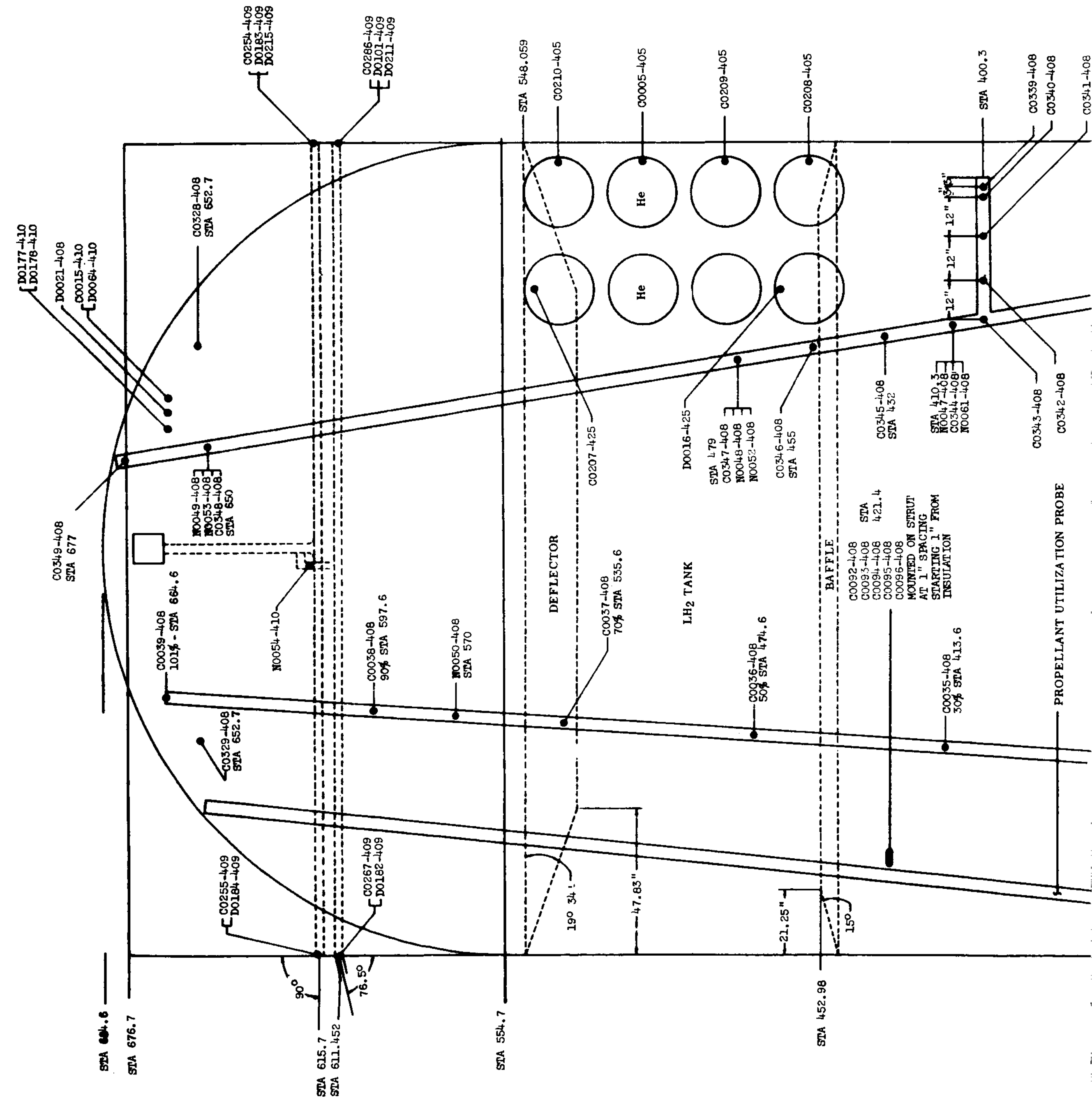

Figure 1-2. Instrumentation Schem

FOLD-OUT #1

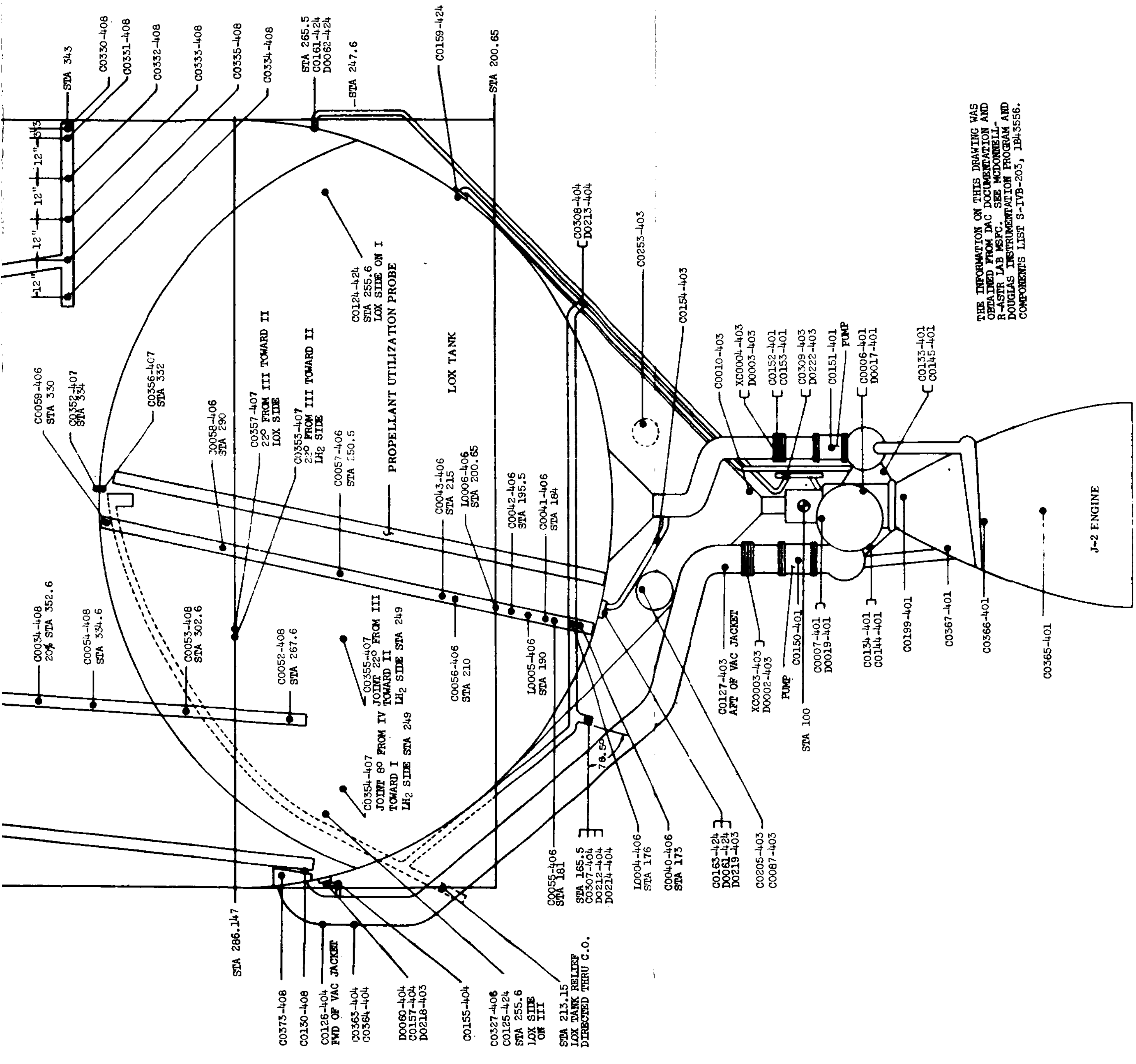

atic for S-IVB - AS-203 Vehicle (Reference 1-1)

FOLD-OUT #2

2

REPRESSURIZATION

Reliable computer codes are required for the design of pressurization systems for analysis of conditions during engine restart in orbit. The interactions between pressurant gas and existing ullage gas and also the interaction with the liquid interface are not generally defined, thus empirical correlation and model verification are required. Similarly, the effects of recirculation chilldown flow on pressure rise during this repressurization period are not specifically defined in existing computer codes. It is the aim of this section to examine these interactions within the scope of two existing computer codes utilizing the experimental data available from the AS-203 flight for variable definition and as a comparison standard.

2.1 REPRESSURIZATION SEQUENCES FOR AS-203

The objective is to correlate the LH_2 tank repressurization data during the first and second orbits of the AS-203 experiment. The sequence of events during the period of interest are described in Figure 2-1.

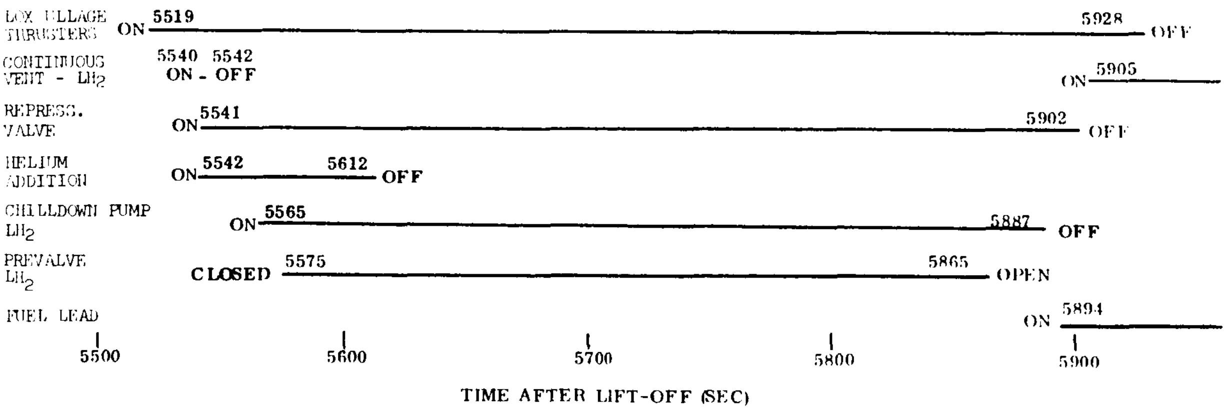

Figure 2-1. Sequence of Events Effecting Repressurization of LH_2 Tank S-IVB-203

With the LOX ullage thrusters on to provide settling acceleration, the continuous vent valve is closed and helium is added to the LH_2 tank. Following the initiation of helium addition the chilldown system was turned on to prepare the engines for firing.

The tank pressure history for this period is shown in Figure 2-2. A schematic illustrating the mass and heat transfer to the S-IVB-203 LH_2 tank is shown in Figure 2-3. The schematic indicated that heat is being added to the tank at the sidewall and

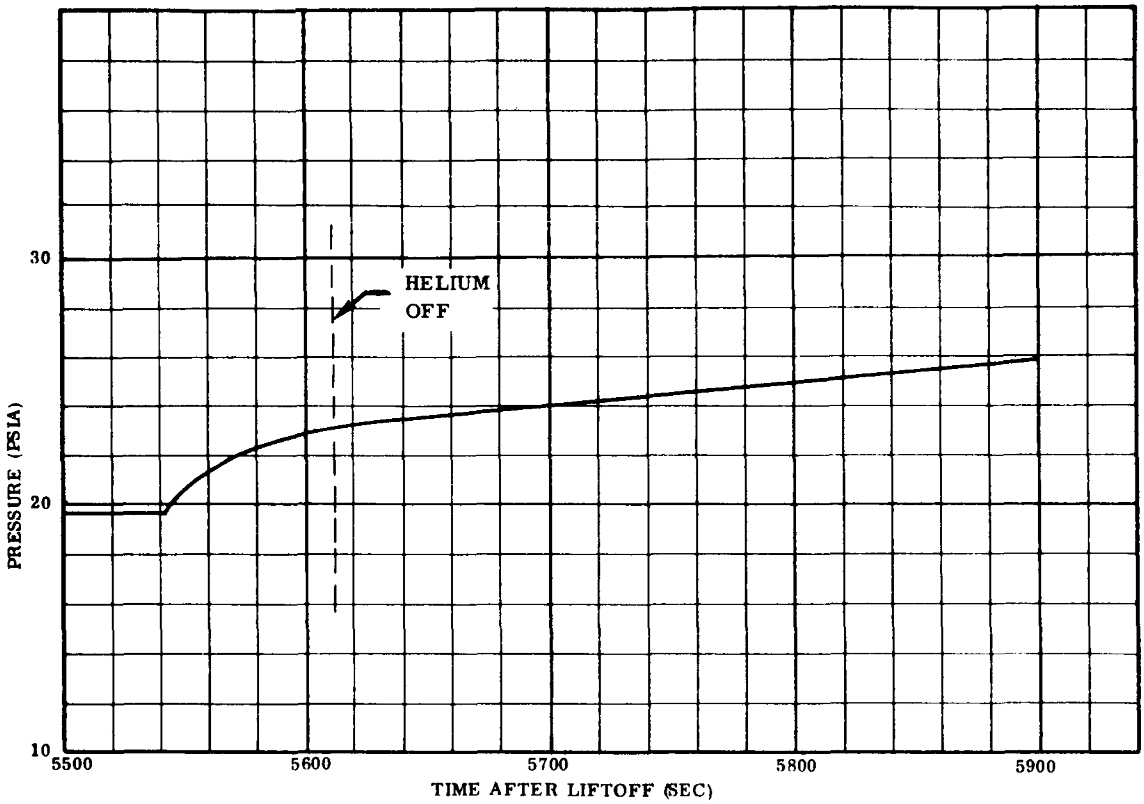

Figure 2-2. Fuel Tank Ullage Pressure During Repressurization and Engine Chilldown

forward bulkhead due to heating from the environment while heat is also added along the intermediate bulkhead from the LOX tank. Recirculation flow is also a heat input to the LH_2 since the fluid leaving the tank returns to the tank at a higher enthalpy. The only mass being added is the helium added to the ullage.

Initially a review was made of the Chrysler, Douglas and Marshall Space Flight Center reports concerning the AS-203 experiment (Ref. 1-1, 1-2, and 1-3). These reports were examined in order to become familiar with the general S-IVB configuration with specific emphasis on restart systems.

A survey of the literature was then made to find analytical or experimental models which could accurately predict the ullage pressure history, Figure 2-2, of a control volume as shown in Figure 2-3. These models were then compared with the tools existing at Convair.

Some of the more pertinent studies which were reviewed were NAS7-169, "Design Guide for Pressurization System Evaluation," Aerojet General, (Ref. 2-1); NAS7-388,

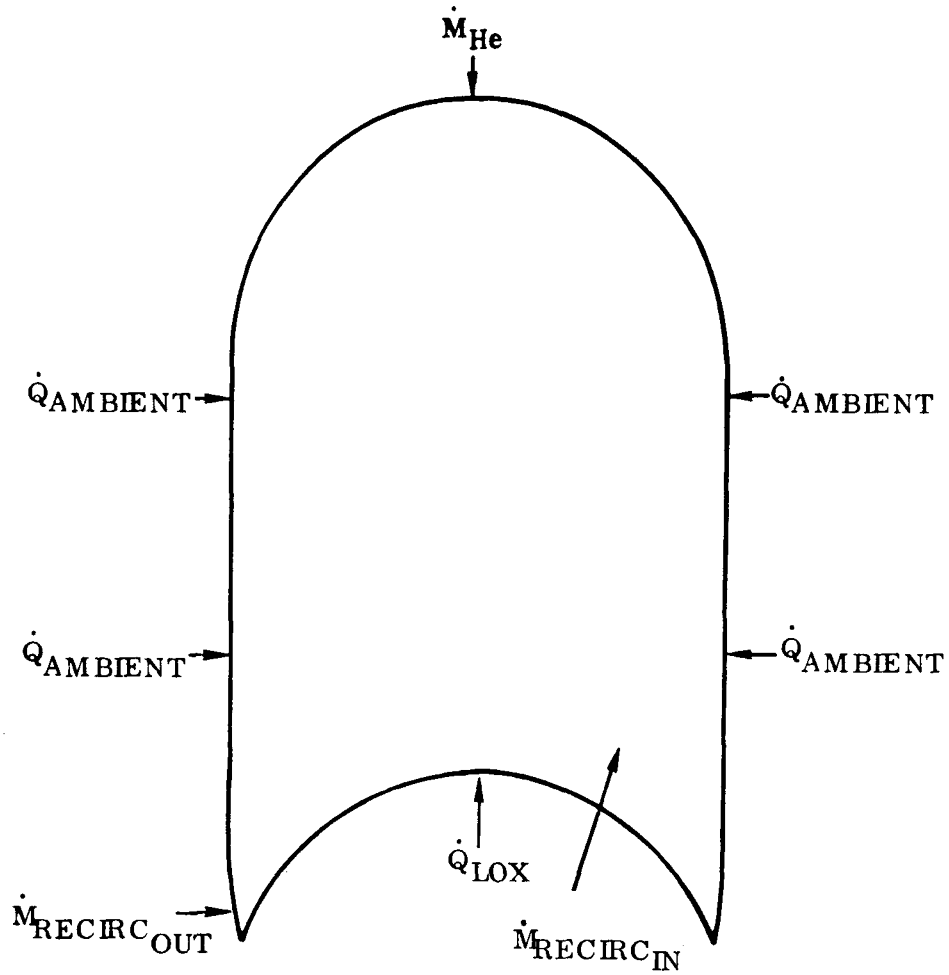

Figure 2-3. LH_2 Tank Repressurization Schematic

"Design Guide for Pressurized Gas Systems," IIT Research Institute (Ref. 2-2); NAS3-2574, "Advanced Pressurization Systems for Cryogenic Propellants," Martin Marietta (Ref. 2-3) and NASA TN D-3451, "Prediction of Propellant Tank Pressurization Requirements by Dimensional Analysis," George C. Marshall Space Flight Center (Ref. 2-4).

The Aerojet, IIT and Martin programs are set up as predesign tools for selecting optimum pressurization systems. They do not have the application to the recirculation analysis provided in the method discussed below. These three programs were not studied further or applied in this analysis. Additionally, the treatment of the tank thermodynamics in the above programs is not as refined as the NAA S-II Pressurization Program (Ref. 2-5), and the restriction of constant conditions for many of the factors which vary considerably in the AS-203 experiment limit the value of these tools. The dimensional analysis technique of Thompson and Nein (Ref. 2-4) is a simple approach to obtaining pressurant requirements, however, it assumes a constant ullage pressure and simultaneous outflow.

The two tools which were used to simulate the AS-203 LH_2 tank pressure history during repressurization are the S-II Pressurization Program and the PRISM program (Ref. 2-6). The latest version of the S-II Pressurization Program (October 23, 1964) was developed for NASA by North American Aviation. The PRISM program, developed at Convair for the Centaur vehicle, has been successfully used to predict pressurant requirements on several recent Centaur flights. Input for these programs was obtained from drawings, microfiche, reports and telecons. Configuration geometry was obtained from MSFC supplied drawings and reports and from telephone conversations with MDAC. Thermodynamic properties and data were obtained from reports and microfiche.

2.2 ENERGY EVALUATION

Ambient incident energy on the LH_2 tank was determined using the Convair Space Vehicle Radiant Energy Program (SAINT NERO) (Ref. 2-7), Convair Radiation Configuration Factors Program (Ref. 2-8) and the Convair Variable Boundary II Heat Conduction Program (P2162), (Ref. 2-9). These programs are explained in detail in Section 3. The SAINT NERO program was input with the orbital parameters, surface optical properties and vehicle geometry in order to calculate the thermal energy absorbed and reflected by the exposed surfaces. The configuration factors program was used to determine the view factors between the forward skirt, instrumentation unit and nose fairing and the hydrogen tank forward bulkhead. Heat flux calculations are completed using the Variable Boundary II Heat Conduction Program. This program was input using free convection from the tank wall to the fluid, with cases run for several different values of insulation conductivity, specific heat and emissivity in order to accurately reconstruct the heat flux history to the LH_2 tank. Several heat flux comparisons are made with "measured" values in Figures 2-4 and 2-5.

2.3 THE PRISM PROGRAM

The PRISM program was initially developed for predicting pressurant requirements and pressure histories for the Centaur fuel and oxidizer tanks. Basically the program is a first law analysis of the propellant tank allowing pressurant inflow, propellant outflow, tank wall heating and recirculation flow. Some modifications were required in order to use the program for the S-IVB repressurization simulation. These modifications included addition of a subroutine to handle transient heat transfer through thick walls of two different types of materials, alteration of block data and call statements to account for geometry differences between the Centaur and S-IVB vehicles, and modifications to the recirculation and pressurant inflow routines to allow input as a function of time. A listing of the program as it was used is given in Appendix A.

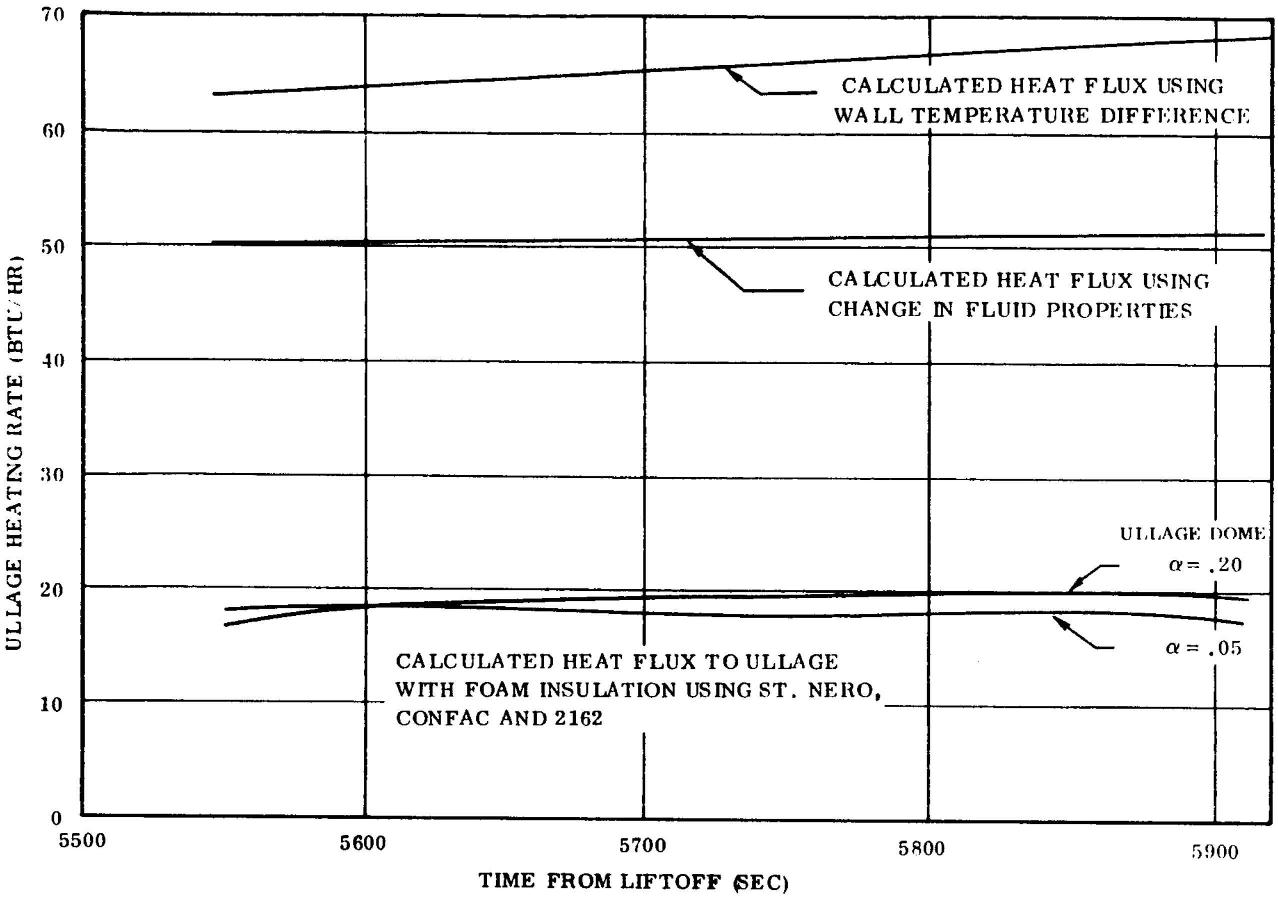

Figure 2-4. Ullage Heating Rate Comparison

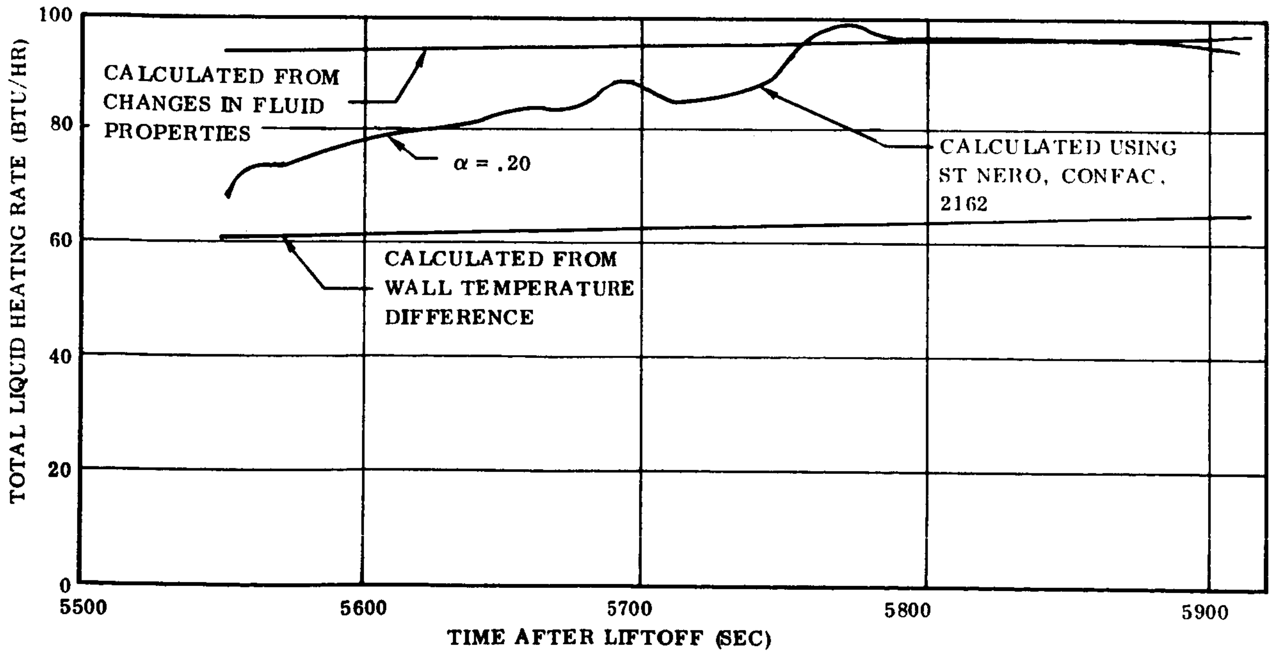

Figure 2-5. Liquid Heating Rate Comparisons

Several options are available in using the PRISM program which can be easily used to examine the influence of significant variables on the tank pressure history. Using the heat flux conditions shown for $\alpha = .20$ in Figures 2-4 and 2-5 the PRISM program was run for the following cases:

1. Full heat transfer between the liquid and ullage: Wall heating of liquid does not directly produce vapor, all recirculation heat addition contributes to the liquid sensible heat.

2. No heat transfer between the liquid and ullage: Wall heating of liquid does not directly produce vapor, all recirculation heat addition contributes to the liquid sensible heat.

3. Full heat transfer between the liquid and ullage: Wall heating of liquid does produce vapor directly at the wall, all recirculation heat addition contributes to the liquid sensible heat.

4. Full heat transfer between the liquid and ullage: Wall heating of liquid does not directly produce vapor, all recirculation heat addition contributes to boiloff.

Comparison of cases 1 and 2 shows the influence of interfacial heat transfer. Comparison of 1 and 3 illustrates the significance of the side wall heat flux. Comparison of 1 and 4 shows the effect of recirculation flow. All comparisons are between the maximum and minimum expected values of each of the three parameters being examined. The maximum pressure occurs for case 4 when ullage heat transfer variables are set to their maximum value.

Figures 2-6 and 2-7 give the pressure history for each of the above four cases along with the pressure history recorded in the AS-203 flight (previously shown in Figure 2-2).

Analysis of the comparisons of Figures 2-6 and 2-7 illustrates that of the cases run, case 1 most accurately represents the pressure history inside the S-IVB tank during repressurization. Case 1, which is the minimum heat transfer condition, gives a slightly higher pressure rise than actually occurred in the AS-203 experiment repressurization. All cases show a higher initial pressure rise when helium is being added, indicating that the mixing of the helium entering the tank is not as efficient as assumed in the model. The pressure rise subsequent to helium addition is higher in the actual flight case, probably due to the higher ullage heating rates indicated in Figure 2-4. The recirculation however appears to possess as important a part as the difference in ullage heat flux. For a more accurate modeling of the AS-203 case it is necessary to alter the mixing process, increase the heating rate to the ullage and reduce the importance of recirculation flow.

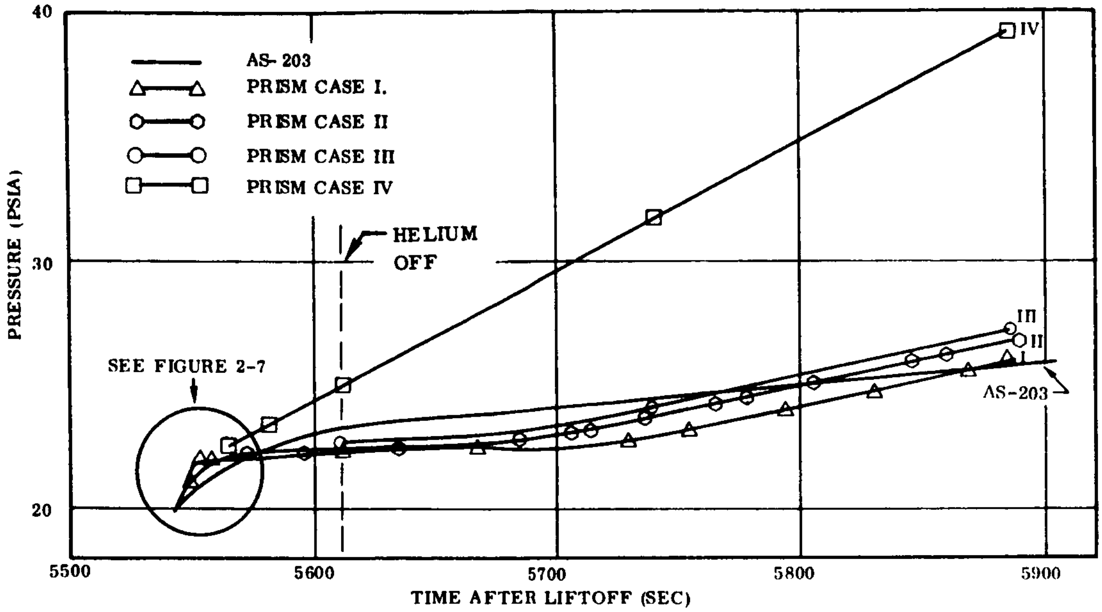

Figure 2-6. Comparison of Prism Repressurization Runs

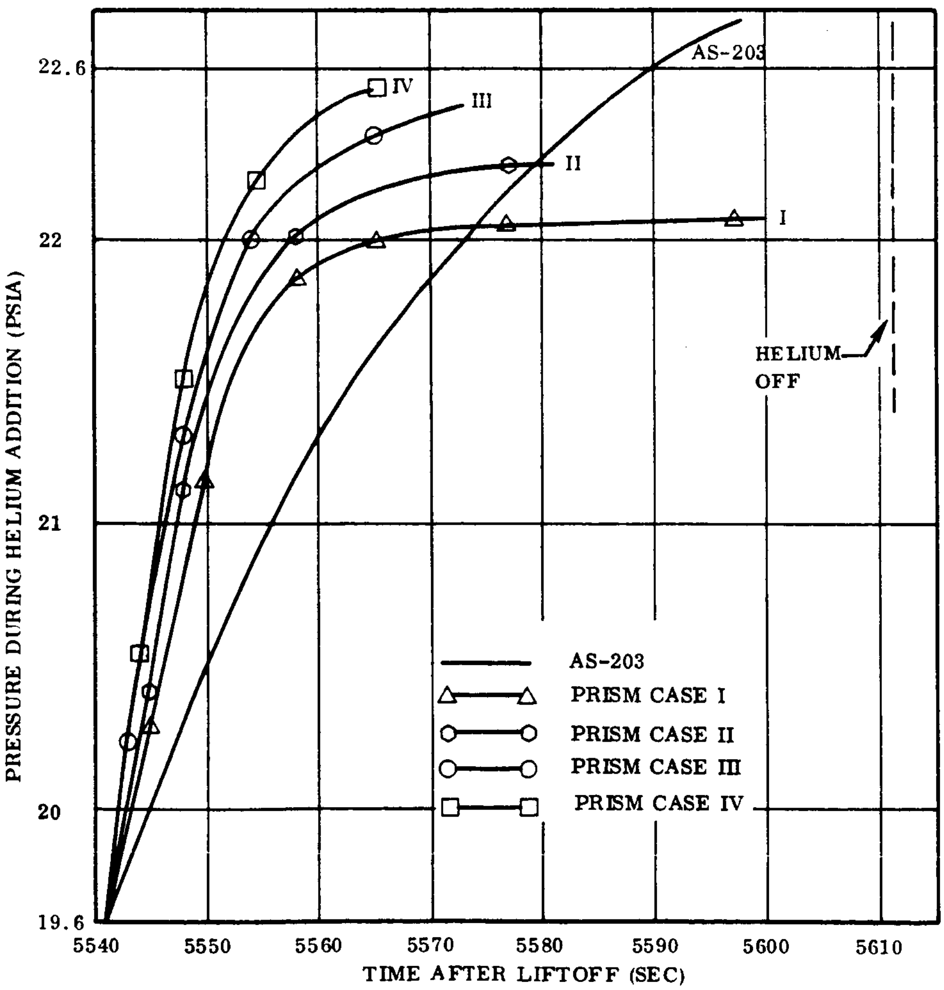

Figure 2-7. Pressure History During Helium Addition - Comparison of Prism Runs

Examining the comparative results of Figures 2-6 and 2-7 by comparing case 1 to case 2 indicates the ullage is actually cooled by the liquid in case 1 making the pressure rise rate for no interfacial heat transfer in case 2 higher than that of case 1. Case 3 illustrates the effect of treating the wall heating as producing vapor at the wall. The final variable studied was the most significant in controlling pressure rise. The difference between cases 1 and 4 is due to the recirculation flow being treated as contributing directly to either the liquid or ullage. When recirculation energy is added directly to the ullage, the pressure rise is significantly greater than experienced for only sensible heating from recirculation flow.

Conclusions of the study are that the PRISM program has given reasonable results in cases 1, 2 and 3. Modifications could improve the mixing capability and handling of the recirculation flow. The difference in heat flux between the experiment and analysis could be adjusted by modifying coefficients in the Variable Boundary II Heat Conduction Program although it is not obvious how this would be done at this time. If additional correlations are attempted, these modifications would be applicable in developing an appropriate model for pressurization analysis.

2.4 S-II PRESSURIZATION MODEL APPLICABILITY

A second computer model applicable to repressurization analyses is the NAA S-II pressurization model (Ref. 2-5). This computer program has a comprehensive treatment of ullage free and forced convection mechanisms which make the program particularly applicable to pressurization analyses. The multi-node, multi-component ullage model provides descriptive information on gradients resulting from pressurization with warm helium. A significant portion of the AS-203 restart sequence involved recirculation of engine coolant flow which entered near the bottom of the bulk liquid. The consequence of this flow in modeling the resultant pressure rise led to difficulties which could not be handled within the scope of this study.

2.4.1 PRESSURE RISE WITHOUT RECIRCULATION SIMULATION. A computer simulation of the AS-203 flight for range time of 5541-5911 seconds was performed with the S-II pressurization program, P3542, with recirculation flow absent. The utility of this approach lies in establishing the importance of the input of quality recirculation flow into the liquid. The ullage heat fluxes are also of significant importance in this model. The methods for obtaining heat flux data were described in Section 2.1. Other facets of the determination of heat flux data are discussed in Section 3. The desired heat flux values for ullage and liquid as obtained from P2162 are presented in Figure 2-8.

A shortcoming of this pressurization program is the difficulty in achieving the desired heat input to the program. The heat input is achieved by a time-dependent ambient coefficient U_A multiplied by a temperature difference resulting from an input time-dependent ambient temperature and a program calculated outer wall temperature. A

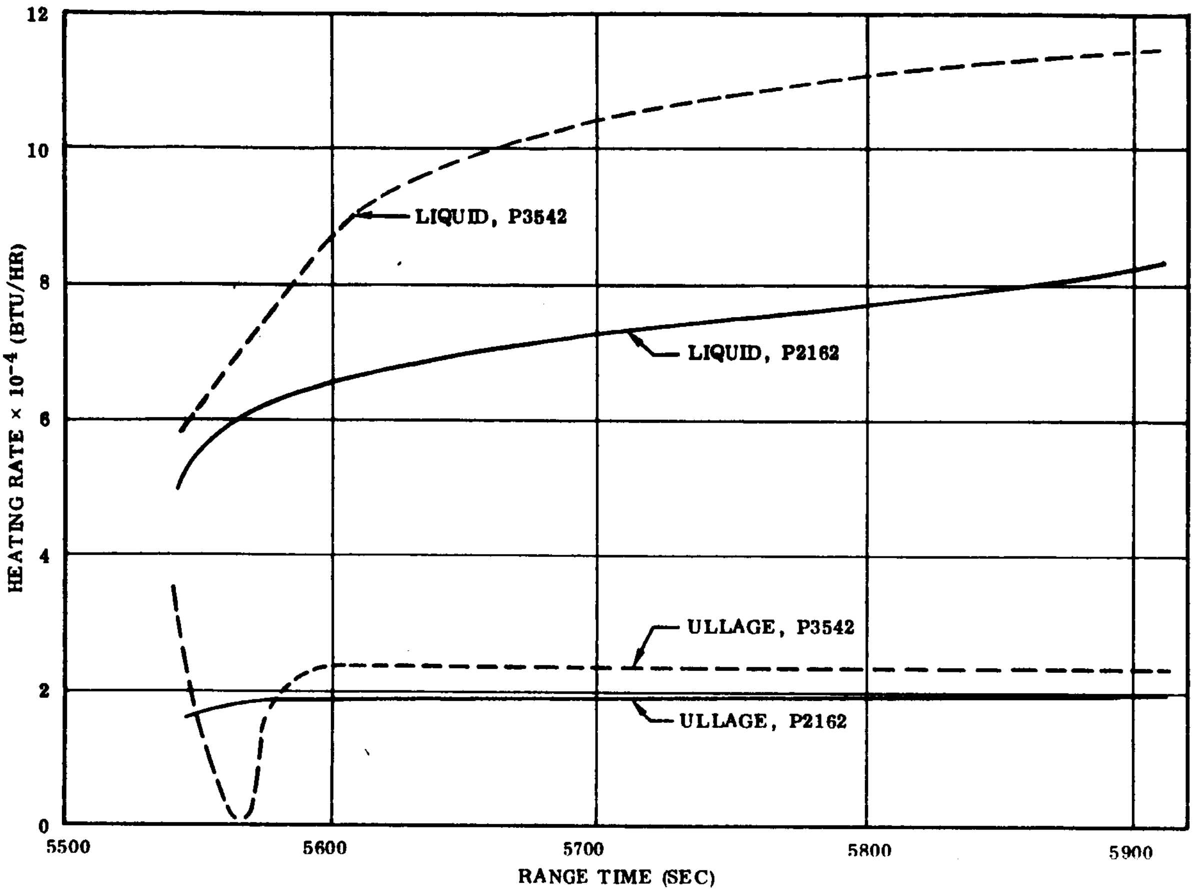

Figure 2-8. Comparison of Propellant Heat Fluxes Predicted With P2162 and Those Achieved in P3542

convenient solution here is to diminish the coefficient such that the overall temperature difference is only slightly dependent on the wall temperature. With this achieved, additional knowledge of the inner gas to wall heat transfer coefficient is required to select initial temperature gradients and temperatures for the insulation. This is frequently only available through a trial and error approach. This approach may be unique here at Convair in that heat transfer calculations are performed with other programs as described in Section 2.1 prior to using the pressurization program. These heat transfer programs permit a variation in heating to the various quadrants which is significant but is not an available option in pressurization programs. These programs as indicated earlier, also afford more accurate modeling of shroud effects on forward bulkhead heating. Thus, the procedure becomes one of accurately defining the heat transfer, then lumping heating rates for all quadrants to express them only as a function of axial location and time, and finally transmitting this information to the selected pressurization program.

In the S-II pressurization program, minor modifications have been made to afford a check between the achieved heat flux and the desired heat flux obtained from the heat transfer programs. These include the heat flux at each node, the energy addition to ullage and liquid during a time step, and the summation of this energy over the run.

It then becomes a simple matter to compare the heating information from P2162 with that obtained in a given pressurization run. These modifications are recommended to this program to provide a check on performance; energy input is frequently a quantity of interest.

In the simulation run for the period 5541 to 5911 seconds, the desired heat flux is compared with that achieved in P3542 in Figure 2-8. The agreement between the ullage heat flux is of considerable more importance in this investigation since ullage pressure is little affected by heating the subcooled liquid. The liquid was initially saturated before the pressure increase resulting from the helium pressurization resulted in the subcooled liquid state. This period started at 5541 seconds with the helium addition rate trailing off to zero at 5573 seconds after the addition of 8.7 lbs of helium.

The pressure rise history from the simulation run with computer program P3542 is shown in Figure 2-9. The steeper initial slope and the rapid change in pressure rise rate at 5560 seconds are attributed to unrealistic matching of ullage heating for this time period as indicated in Figure 2-8. More careful matching during this time period could have resulted in a better matching of AS-203 data; however the P3542 prediction would still exhibit a lower pressure rise rate after 5600 seconds. As expected, without the contribution from recirculation flow, the pressure rise does not come up to the level experienced with AS-203. Since heat flux to the ullage in this simulation slightly exceeded the predicted requirement from heat transfer programs, it appears the additional difference in pressure may be attributable to recirculation flow. Hand calculations indicate the additional energy requirements to match the observed pressure rise rate is approximately 2800 BTU.

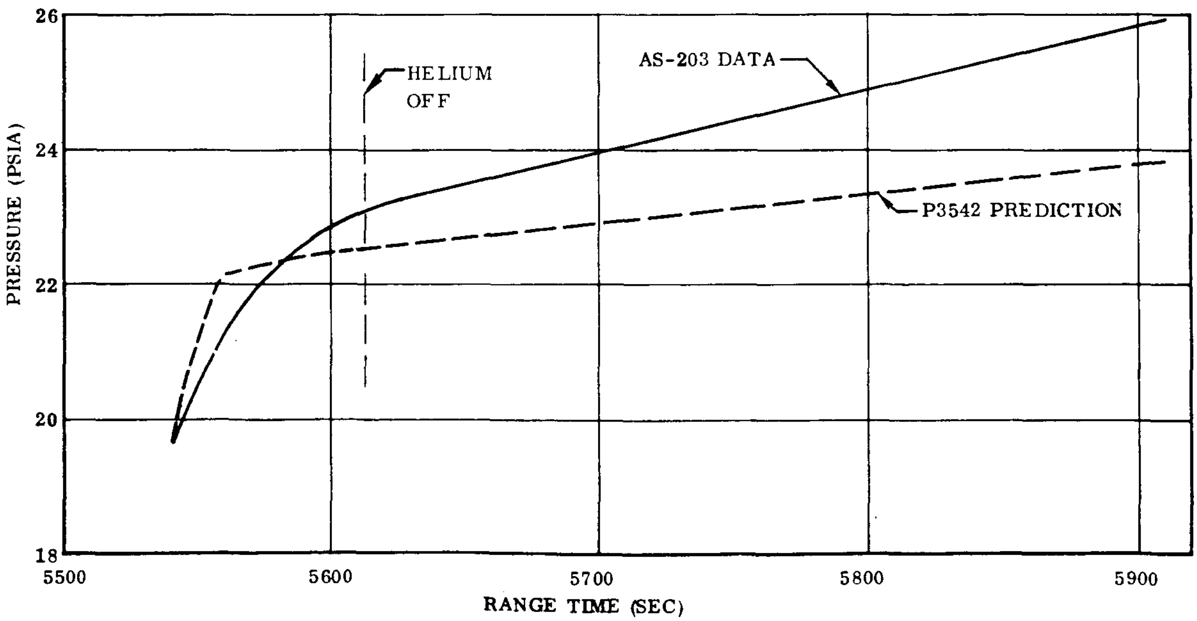

Figure 2-9. Flight Data and Pressure Prediction With P3542 For Repressurization Phase

This is equivalent to an energy flux of 27,000 BTU/hr which could result from a time average quality of only ten percent for the recirculation flow for 100 seconds. Such a situation is highly probable.

Although injecting a point heat flux at the tank location of recirculation return was considered, the degree to which the liquid is subcooled for AS-203 simulation negates any ullage contribution from such an energy input. The test data confirmed that the liquid did remain subcooled during this period. Evaporation due to liquid heating only occurs when the energy reaches the vicinity of the interface and the interface nodes become saturated.

Major modifications to the P3542 program would be required to distribute the recirculation energy in a representative manner to the appropriate nodes. Such distribution would be dependent on the flowrate and quality of the recirculation flow, the decrement in temperature below saturation, liquid depth, and gravity level. Essentially, it becomes a problem of bubble collapse or bubble migration which requires an elaborate model on its own.

In conclusion, while the program P3542 is quite satisfactory for pressurization and ullage heating simulations, it is deficient in being capable of predicting pressure histories when recirculation flow is involved. Modifications to the program could be made to incorporate data from another program which defines recirculation flow energy distribution, as a compromise solution. The second program referred to above could well be a form of the program EVOLVE discussed in Section 4.4.

3

CLOSED TANK PRESSURE RISE

Analytical models to predict pressure rise during orbital coast required verification. The AS-203 vehicle is unique in providing extensive temperature and pressure data for a tank with considerable liquid hydrogen remaining aboard. Future space missions require the storage of propellants during short coast periods as well as up to many weeks in orbit. These analyses conducted here were aimed toward reviewing the status of available tools for predicting the heat input to the tank, determining the important contributions to pressure rise rate in a closed tank, and verifying the available analytical tools with the AS-203 data.

A knowledge of pressure rise rate is an important parameter in defining propellant requirements and also tank venting requirements for orbiting vehicles. The methods examined here are quite appropriate for determining the thermal environment of the vehicle. One may still anticipate some variation between the settled propellant results attained here for pressure rise rate and those predicted for an unsettled propellant. Accurate estimates of the wetted wall area will enable the methods verified here to be used for both cases.

3.1 PROPELLANT TANK HEATING

The propellant pressure rise correlation task was performed for the locked-up hydrogen tank portion (4th orbit) of the AS-203 flight. The method of approach was to model the known vehicle geometry, surface optical properties and orbital parameters using the Convair Space Vehicle Radiant Energy Program (SAINT NERO) (Ref. 2-7), to calculate the thermal energy incident on the exposed surfaces of the vehicle and that portion of the incident energy which is absorbed by the vehicle surface. The next step was to determine the radiant geometric view factors between heated vehicle surfaces in the forward skirt, instrumentation unit and nose fairing and the hydrogen tank forward bulkhead which is seen by these surfaces. This calculation is done using the Convair Radiation Configuration Factors Program (CONFAC) (Ref. 2-8). The third step in the analysis was to perform a complete energy balance on the hydrogen tank using the Convair Variable-Boundary II Heat Conduction Program (Ref. 2-9). Subroutines of this program accommodate boundary conditions of free or forced convection, radiation to an external environment, radiative heat exchange between elements, or any other time-dependent heat flux. Calculations were made for wall conductivity values represented by the foam insulation, gaseous hydrogen, and gaseous helium. The propellant heating data from above was utilized in the various propellant thermodynamics computer programs to determine the propellant tank pressure rise prediction. A similar analysis was reported under Contract NAS8-20165 in References 3-1 and 3-2 involving orbital data from Saturn S-IV stage flights.

3.1.1 <u>ORBITAL HEATING</u>. The geometrical configuration of the orbital vehicle being analyzed for the closed tank pressure rise test correlation is somewhat complicated by the fact that the forward skirt, instrumentation unit and nose fairing remain attached to the S-IVB vehicle during flight. The thermal energy balance on the "locked-up" fuel tank involves the determination of the heat leak into the tank through the side wall, the forward bulkhead, and the aft bulkhead and aft skirt joint. The first two heat leaks are caused by radiant energy exchange with the orbital space environment. Side wall heating is due to direct environmental irradiation. Forward bulkhead heating is due to environmental irradiation only indirectly, since the bulkhead is completely enclosed by the forward skirt, instrumentation unit (IU) and nose fairing.

Prior to conducting an energy balance on the orbital fuel tank, a geometrical model of the problem configuration is established. The environmental irradiation is calculated for the cylindrical tank side wall, forward skirt and IU as well as the conical nose fairing. To do this, the cylinder and cone are divided into quadrants corresponding to the boost vehicle fin lines. This vehicle surface geometry and the fourth revolution orbital parameters (Ref. 3-3) are input to the Convair SAINT NERO program (Ref. 2-7) to determine the incident and surface absorbed heat flux due to radiation and free molecular aerodynamic heating. In the SAINT NERO program, the curved surface geometry is approximated by small flat plate elements and the surface heat flux calculated on each element due to direct solar radiation, earth reflected solar radiation (albedo), earth thermal radiation, and free molecular aerodynamic heating. The incident heating calculations are made at twenty-four locations around the orbit with special calculations made just prior to and following both ingress and egress of the vehicle from the earth's umbra. Since the tank energy balance is concerned with the surface absorbed energy, the vehicle paint radiation surface absorption coefficients for both solar and earth thermal radiation wave lengths are input to the program. The program output then provides net surface absorbed heat flux. The values of surface absorptance used for the calculations are $\alpha_S = .24$ and $\alpha_T = .23$ for the conical section (Ref. 1-3) and $\alpha_S = .33$ and $\alpha_T = .89$ for the cylindrical section (Ref. 1-2). The value of the abledo used in the SAINT NERO calculations was obtained from Reference 3-4 where radiation measurement values are obtained from satellite launches on similar trajectories to that flown by the AS-203 vehicle. The value used is 0.29 times the solar constant.

In the program, the vehicle is flown nose first and flight path oriented with fin position I oriented toward the earth. The surface absorbed heat flux for the cylindrical and conical sections is shown respectively on Figures 3-1 and 3-2. The heating data are shown for the four quadrants of each section. Quadrants I-IV and I-II are on the side of the vehicle pointed toward the earth; it is readily seen that there is little variation in surface heat flux during the orbit period. For the quadrants positioned opposite the

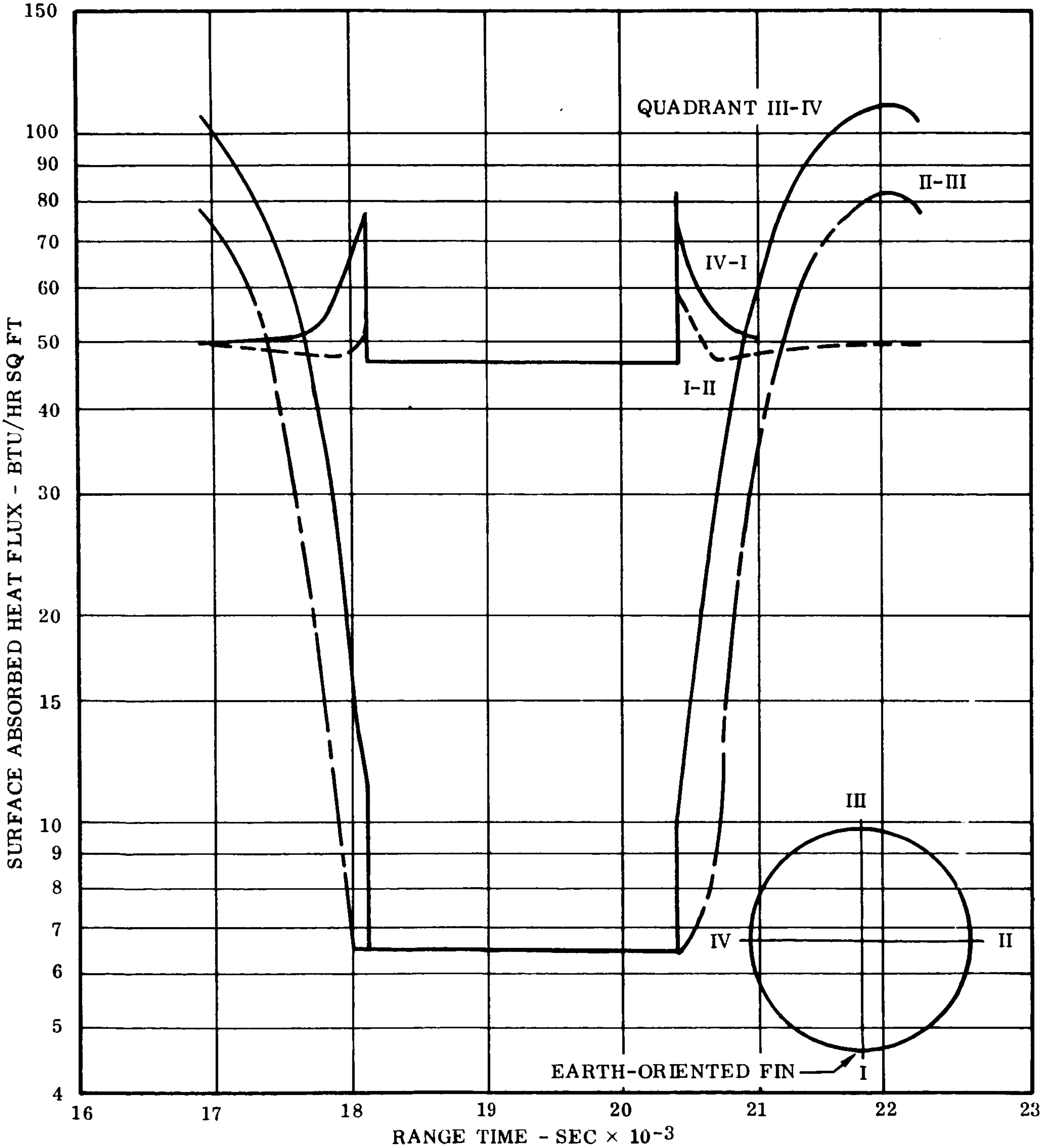

Figure 3-1. Orbital Radiative Heating of the Cylindrical Sidewall of the AS-203 Vehicle

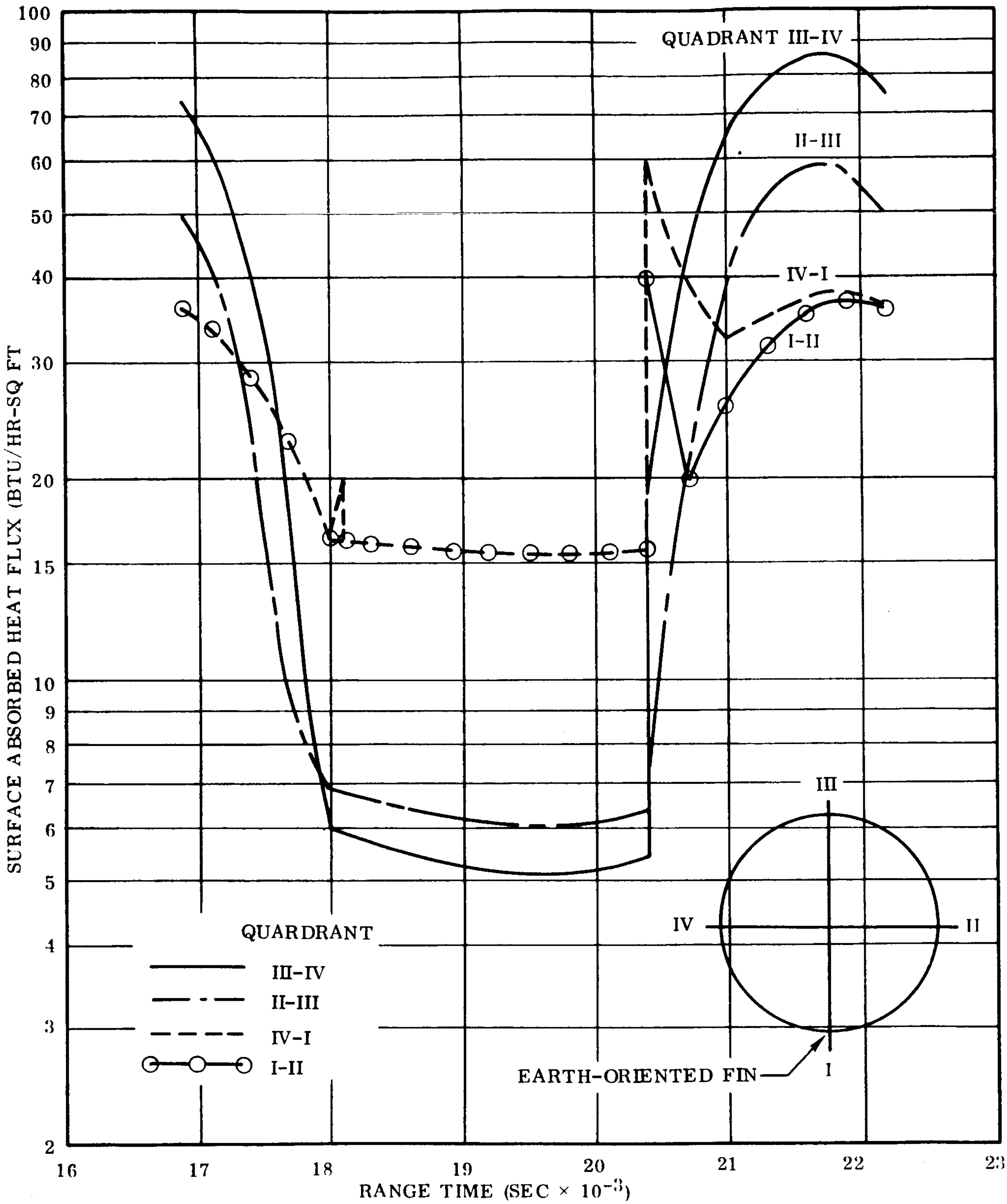

Figure 3-2. Orbital Radiative Heating of the Conical Nose Fairing of the AS-203 Vehicle

earth-vehicle line of sight, there are large variations in heat flux with time. This is especially true as the vehicle enters and leaves the earth's shadow. It is because of these large angular variations in surface absorbed energy that the vehicle is broken into quadrants for the heating analysis. The heat flux values shown are average values over the surfaces indicated. The data shown on Figures 3-1 and 3-2 are utilized as boundary conditions for the fuel tank energy balance calculation.

3.1.2 HYDROGEN TANK ENERGY BALANCE. The energy balance on the fuel tank is performed in a transient calculation as a function of flight time. Before the calculation can be performed, however, it is necessary to further specify the geometrical model of the vehicle. Since the thermal energy interchange between the tank forward bulkhead and the skirt, IU and nose fairing is principally by radiation, the geometrical shape (view) factors must be determined between the heated outside surface nodes (sources) and the bulkhead surface nodes (sinks). This is done by again dividing the forward structure and bulkhead into quadrant nodes. Calculations are performed using the Convair Radiation Configuration Factors program (Ref. 2-8), to define the view factors between nodes. For purposes of the incident heat transfer analysis, the S-IVB fuel tank was divided into quadrants and into three axial sections, at STA 555 where the forward bulkhead ends and at STA 445 near the nominal wetted liquid level during fourth orbit, a total of twelve sections. Little difficulty occurred in the analysis of the lower two sections; however the forward dome area presented some unusual analytical problems.

The energy input to this forward bulkhead area is by radiation from the forward shroud cylindrical and conical sections. McDonnell-Douglas indicated the forward bulkhead was covered with three layers of aluminized mylar with an aluminized side out having an absorptivity of 0.05. If the mylar side had been out, the appropriate absorptivity may have been as high as 0.55. Environmental conditions during the period prior to lift-off may also have resulted in deterioration of the first value to a significantly higher value. Through temperature differences in the forward wall and the magnitude of predicted fluxes, it is shown to be highly probable that the absorptivity was considerably above 0.05 although possibly not as high as 0.55. Although two or three layers of aluminized mylar may have been used, the outer surface absorptivity is controlling and the inner layers only tend to modify the effective k of the insulation; additionally, the mylar insulation k is not considered to be a significant variable in this configuration.

For the absorbed energy analysis to the propellant, the forward bulkhead was thermally modeled in P2162 by dividing the dome into quadrants along the fin lines and into four thickness nodes in each quadrant. To determine the thermal energy transferred to the dome from its external environment, radiation view factors were calculated between the dome quadrants and the quadrant sections of both the cylindrical instrumentation unit and forward interstage adapter and the conical nose fairing. A time dependent energy balance was taken on the cylindrical and conical sections and the energy input to the bulkhead calculated by performing a simultaneous energy balance on the dome itself. The bounding heat flux on the outside of the bulkhead was radiative while free convection was assumed to govern the transfer of energy away from the inner dome surface to the gaseous propellant sink for the closed tank calculation. For the free convection calculations, the vehicle acceleration level was varied from 3.27×10^{-4} g's at tank lock-up to 7.3×10^{-5} g's at the time of final loss of communication. These inputs were obtained from AS-203 flight acceleration data.

An appropriate method to check the adequacy of propellant tank thermodynamic modeling techniques is to compare the temperature difference measured across the tank wall with that predicted from the computer simulation. Data obtained for the fuel tank forward bulkhead are used for this temperature modeling comparison. The difference in temperature between the inside and outside surfaces of the bulkhead wall along fin lines I and III at Station 652.7 are shown on Figure 3-3. The temperature differences were obtained from temperature sensors C85 and C328 (fin line I) and C86 and C329 (fin line III) on the AS-203 orbital vehicle.

For this investigation, the tank energy balance was made using both the extremum values for dome absorptivity. The acceptability of either value in the thermal modeling was based upon both the comparison of analytical test dome wall temperature differences and tank pressure rise rates. From the values of both predicted and experimental temperature differences shown on Figure 3-3, it is readily apparent that the values obtained with the value of 0.05 are entirely too low and that this value of surface absorptivity is incorrect. On the other hand, the predicted temperature difference values obtained with an absorptivity value of 0.55 are somewhat too high. It appears that the value is somewhere between the two extremes. This anomaly was resolved in the selection of a dome absorptivity of 0.20 which is a compromise between the extremes studied earlier; the value has some basis according to mylar deterioration studies made by Lemke (Ref. 3-5). The use of this value on forward dome wall temperature differences is also shown in Figure 3-3. This prediction does represent the data satisfactorily except for discrepancies during the initial transient which are discussed in the following paragraph.

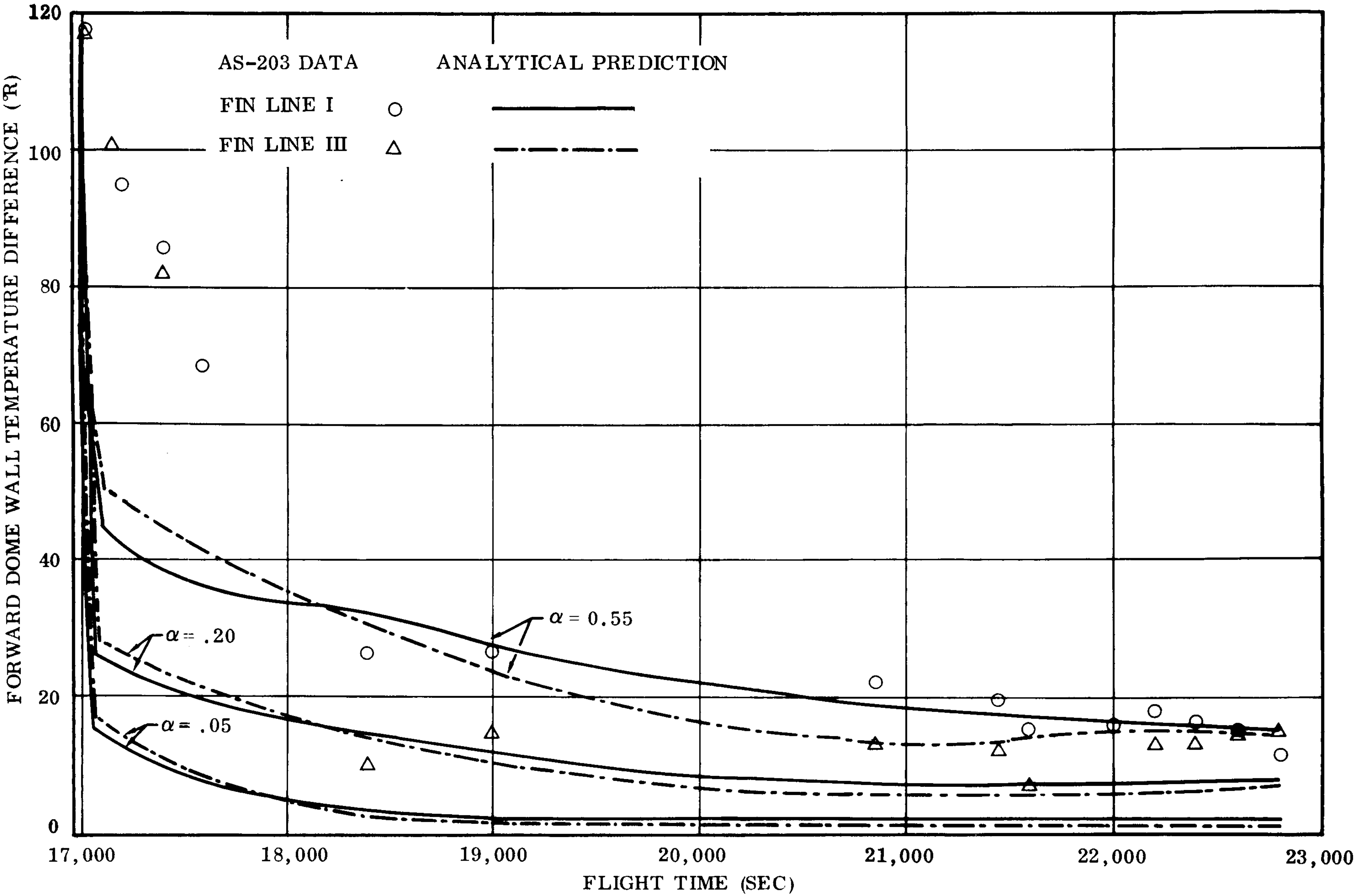

Figure 3-3. Forward Dome Wall Temperature Difference at STA 652.7 for the AS-203 Pressure Rise Experiment

One other modeling problem is apparent from a review of the experimental data in Figure 3-3. The temperature difference decay just prior to and immediately after the start of the closed tank pressure rise test (17140 seconds) is not properly predicted by the analytical model. The assumption was made in the thermal model for problem initial conditions that the temperature gradient across the tank dome wall was a straight line as shown as initial estimates in Figure 3-4. Due to the very rapid chilldown of the tank due to a tank venting blowdown and the low conductivity of the tank wall, this assumption was incorrect. It appears that the initial wall gradient may have been more nearly shaped like the approximation of Figure 3-4. A gradient of this type would explain the reason for the difference in slope of the temperature difference decay line between analysis and test.

The initial gradients which were assumed for the walls as input to the Convair Variable Boundary II Heat Conduction Program, P2162, (Ref. 2-9) were re-evaluated with a steady-state program which iterates until gradients are attained which support boundary conditions imposed on the problem. Boundary conditions imposed were external heat flux and internal conditions of fluid properties and sink temperatures. These internal wall conditions were measured temperature data at 16,700 sec representing conditions prior to the blowdowns at 16,723 and 17,023 sec. The steady-state temperature gradients at 16,700 seconds are shown for the ullage cylindrical section in Figure 3-4. Measured values of inside wall temperature at 16,920 seconds, as indicated by the earlier selection of initial gradients, were about 45°R. Thus, in the period from 16,700 sec to 16,920 sec, the profile in the wall changes from the indicated earlier straight profile to the curved profile indicated by dotted lines. This inner wall transient results from rapid wall cooling through forced convection during venting. It further accounts for the large initial temperature differences shown in Figure 3-3. These large differences decrease as venting ceases at 17,132 sec and the inner wall starts to increase in temperature at 17,500 sec. These transients were not originally adequately modeled with P2162 since stipulated inner boundary conditions were only free convection. The problem would have to be run in steps to account for these changes in conditions. However, modeling this phenomena during this short period is not considered important to overall long term heat flux results.

The results of the analysis for heating rates through the forward bulkhead are shown in Figure 3-5. The predicted heat flux for the cylindrical side wall sections is shown as a basis of comparison for the predicted magnitude of the forward dome heating. If the absorptivity of .05 had existed, the dome heating would have been almost insignificant. As indicated in Figure 3-5, for absorptivities investigated, the dome heat flux is always significantly less than the cylindrical section, although the dome surface area exceeds the dry side wall in this case by 18 percent. This fact is further demonstrated in Figure 3-6 where a heat flux comparison is made for the forward bulkhead, the ullage cylindrical section, and the liquid. Test data points from Reference 1-1 on Figure 3-5 correlate reasonably well with the cylindrical section

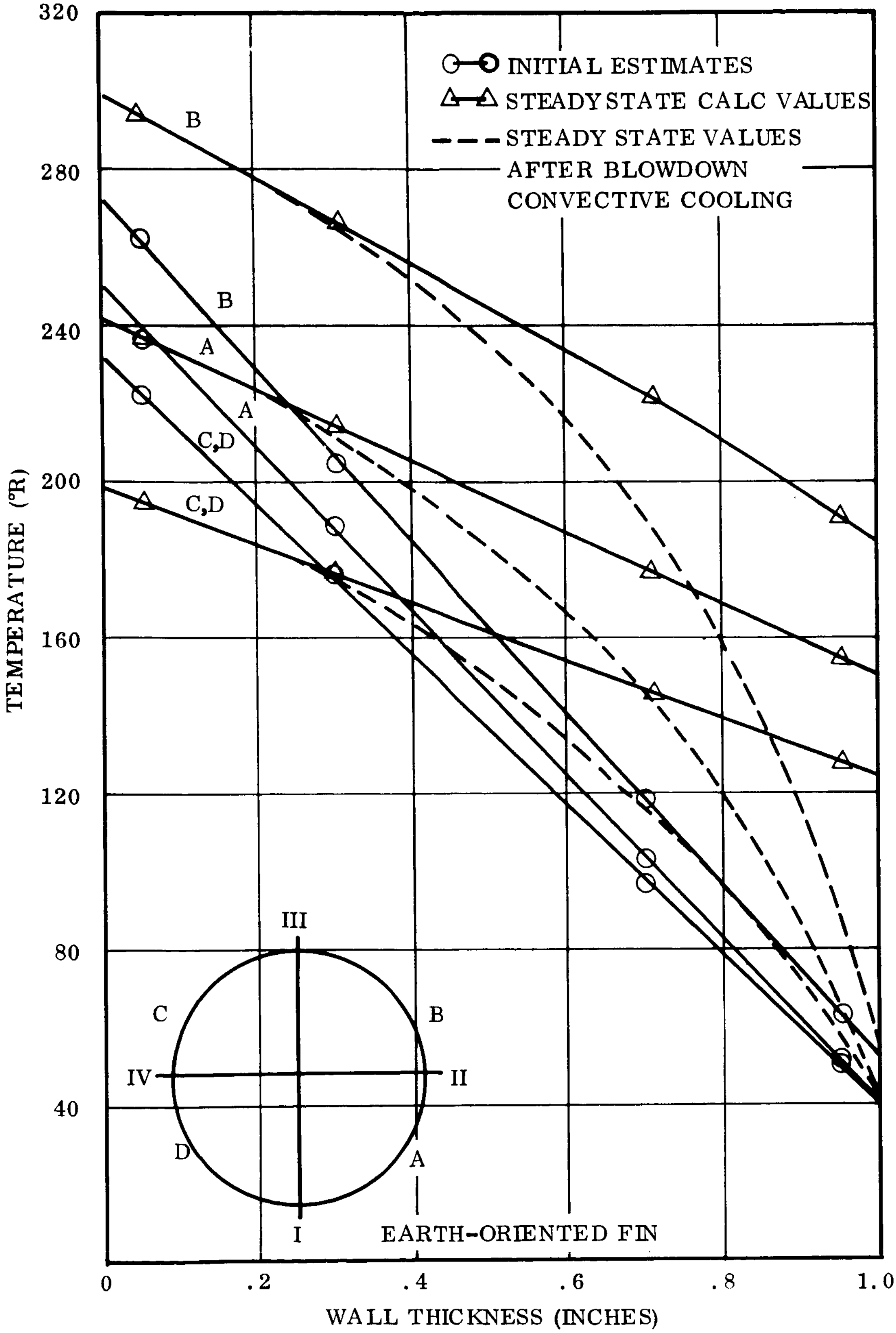

Figure 3-4. Wall Gradients for S-IVB Thermal Modeling

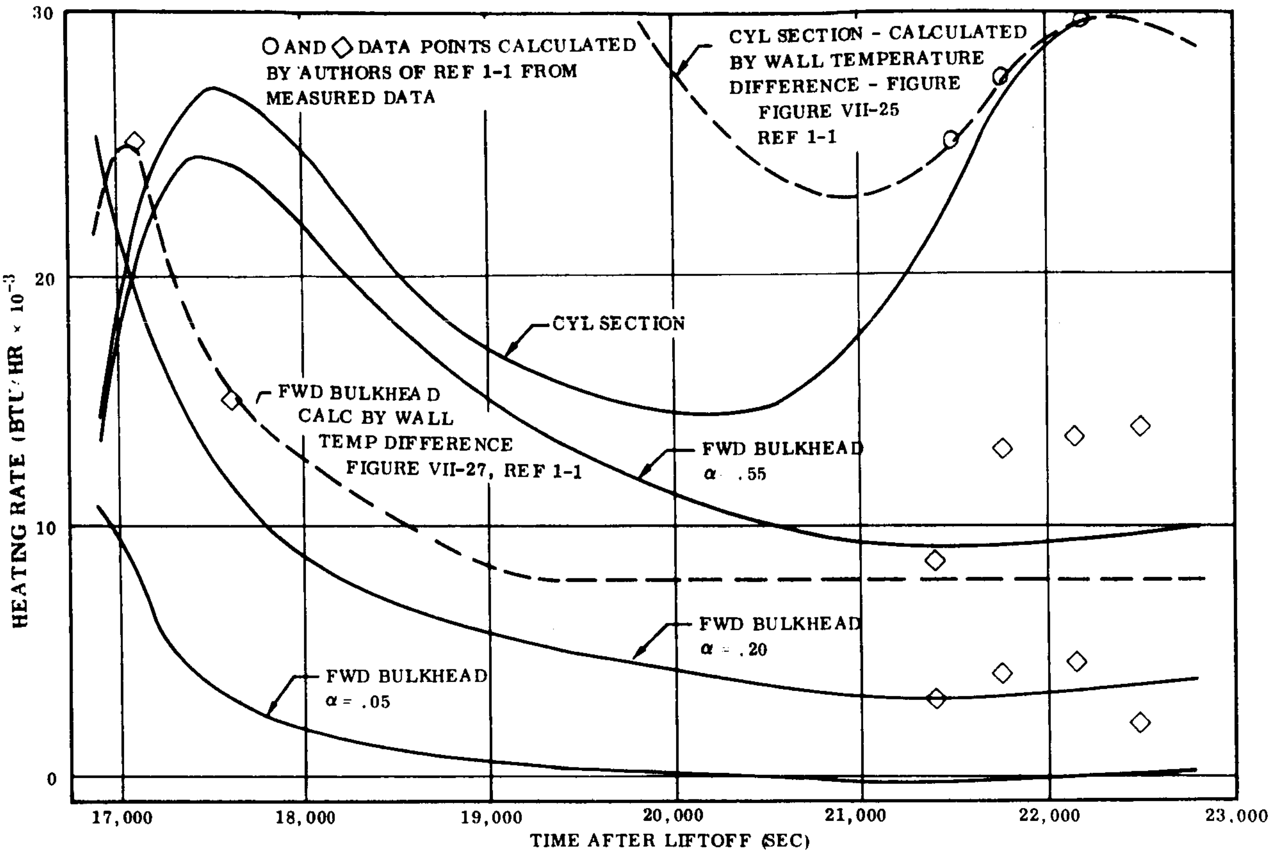

Figure 3-5. Comparison of Ullage Heating Rates for Two Absorptivities With AS-203 Data

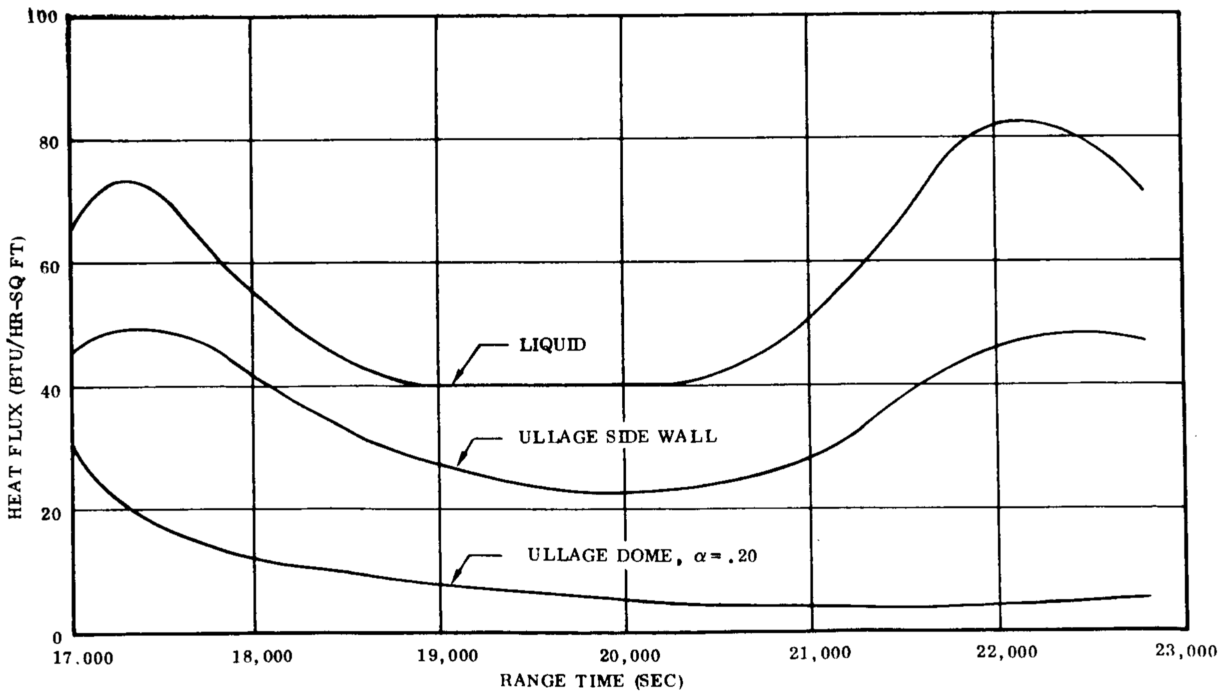

Figure 3-6. Heat Fluxes to Sections of AS-203 During Long Term Coast

prediction. Test data in the dome area confirms the absorptivity value is higher than .05. As the absorptivity on the forward dome increases, the forward bulkhead heating rates become a more significant contribution to ullage heating. From the pressure rise analysis discussed in Section 3.3 it appears ullage heating for the closed tank experiment should total about 49,000 BTU. The absorptivities of 0.05 and 0.55 gave respectively 41,000 and 61,000 BTU for ullage heating. The negative heating flux in Figure 3-5 and the inability to match the temperature differences in this area with $\alpha = .05$ lend support to a value of absorptivity near 0.20. As expected the prediction with α equal 0.20 falls between the previous predictions. It is significant that predictions with an absorptivity of .20 more closely matches the heat flux calculated by wall temperature difference than the other values for dome absorptivity. The wide scatter in the test data indicates the uncertainty of the exact behavior after 20,000 sec. A significant point is that for either .05 or .20 for α, the 3,000 or 7,000 BTU/hr flux is still a minor portion, less than 25 percent, of total ullage heating.

The heating rates to the liquid and gas are calculated in the thermodynamic program REPORTER (Ref. 3-6). The heating rates are input to the program as a function of axial location and the program calculates liquid and ullage heating. These heating rates are presented in Figure 3-7 for the ullage where a comparison can be made with the results reported in Reference 1-1. There, two approaches were used in an evaluation of the heating rates, one an evaluation of heating rates through changes in ullage fluid properties, and the other a calculation using measured wall temperature differences and an assumed thermal conductivity. The authors of Reference 1-1 prefer their results on change of fluid properties since it is in agreement with continuous vent flow and the thermal conductivity in the temperature difference method is probably higher than used. The comparison of these two methods with Convair predicted results suggests better agreement for the ullage during the fourth orbit with the wall temperature difference method, however, the phase angle of the cyclic nature of the data is not matched. Nonetheless, the most recent prediction using a dome α of 0.20 is preferred.

For liquid heating, predicted results are compared with test data in Figure 3-8. Predicted results again compare more favorably with the heating rate determined from the wall temperature difference method. Investigators in Reference 1-2 report a heat input of 79,000 BTU/hr to the liquid using wall temperature difference and 69,000 BTU/hr plus 47,000 BTU/hr boil-off using fluid properties. The Convair predicted value is only 52,000 BTU/hr input to the liquid, a value somewhat lower than the other investigators; nonetheless this value is sufficient heating to match the pressure profiles.

3.2 PRESSURE RISE RATE.

The existence of a valid model for thermal analysis and substantial results are prerequisite to the ability to predict the pressure rise rate. Other than defining hot spots and maximum temperatures, the thermal analysis is primarily responsible for

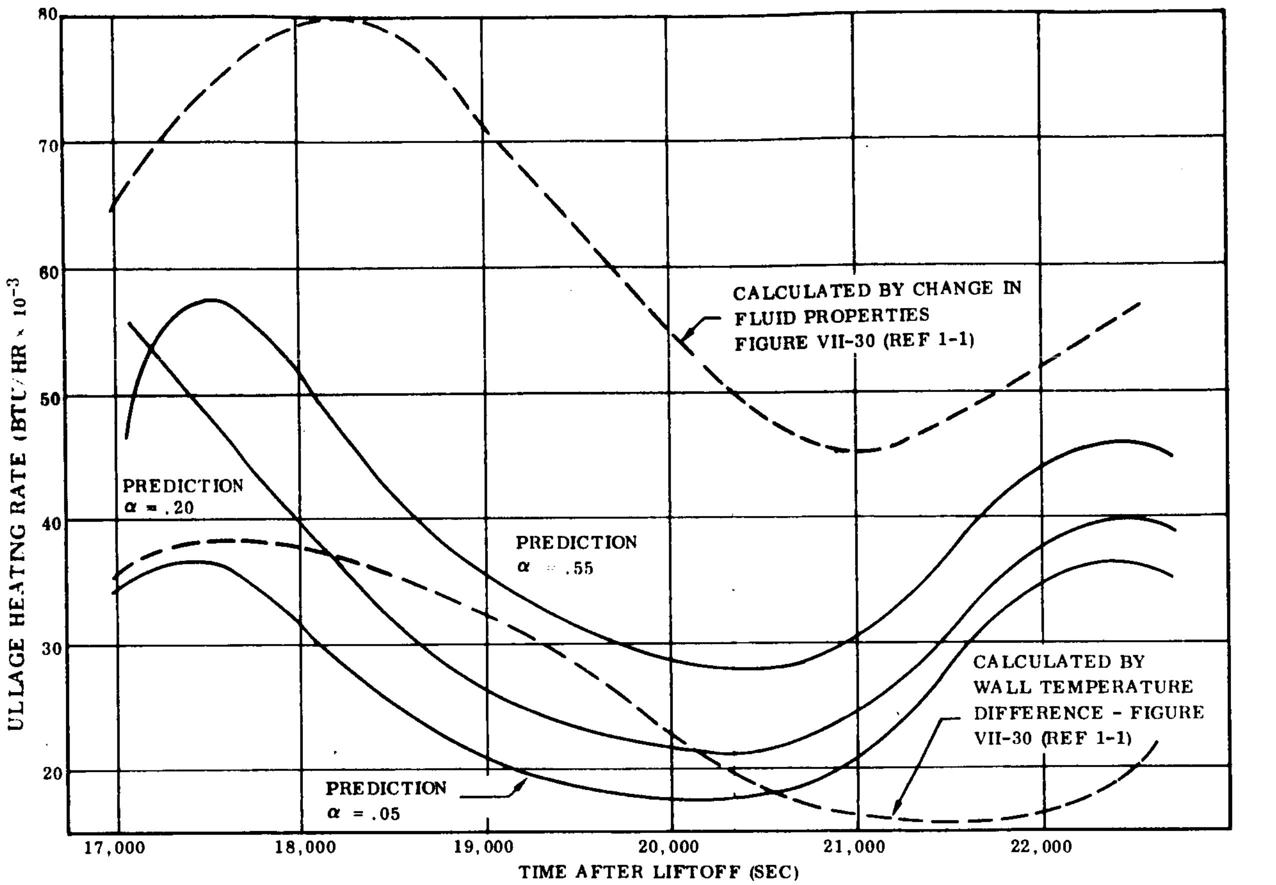

Figure 3-7. Comparison of Ullage Heating Rate With Calculated Values From AS-203 Data

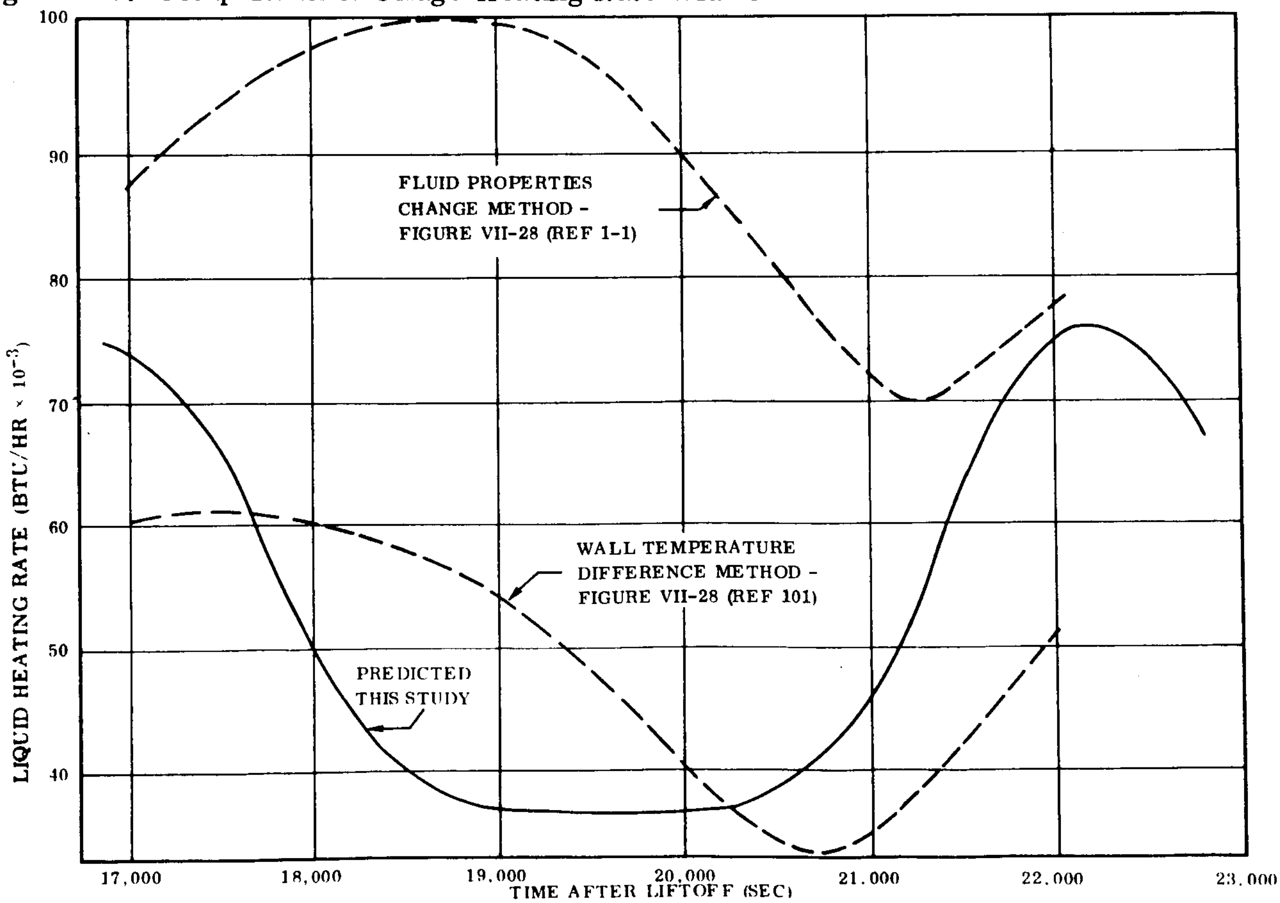

Figure 3-8. Comparison of Liquid Heating Rate With Measured AS-203 Data

an adequate model of the thermodynamic state of the fluid. A study of the pressure rise in the locked-up S-IVB - AS-203 tank during the range time of 17,100 to 28,000 seconds was completed. The results for the two programs used, P3542 (Ref. 2-5) and REPORTER (Ref. 3-6) are presented in Figure 3-9. Results indicate the important effect of the emissivity value for the forward dome. The results of the modeling are considered excellent.

Program REPORTER is a First Law thermodynamics analysis with a capacity for analysis of a 10 node problem permitting stratification in the ullage because of different axial heating rates; however, the use of a single node problem with one liquid and one ullage node has been found to give similar results for pressure rise rate to the multinode configuration. In the interest of economy, the single node analysis has been used.

The liquid thermodynamic states determined with REPORTER were independent of absorptivity on the forward bulkhead. The liquid in all instances remained subcooled during the entire simulation with no evaporation occurring. This is not entirely in agreement with previous investigators.

The differences in ullage heating due to different dome absorptivities resulted in different pressure rise rates. These rates are compared in Figure 3-9 with the pressure history of the AS-203 flight for the period of the closed tank experiment. These cases indeed bracket the test data. If boil-off occurred and was not accounted for in REPORTER, inclusion of boil-off would increase the low absorptivity prediction toward the flight data. It is noteworthy that the degree of subcooled liquid, 5.7°R below the saturated conditions for final test data pressure, indicates increasing liquid heat flux two-fold would not result in a prediction of boil-off with program REPORTER. Thus, to expect a contribution from evaporation with this model is unacceptable and the contribution of boil-off must be added outside the program. This difficulty with boil-off contribution has been experienced elsewhere in models which fail to adequately model stratification.

The analysis of the long term pressure rise during coast with the program P3542 developed by Epstein (Ref. 2-5) provides insight into the various contributions to pressure rise. Again, the significance of ullage heating cannot be over emphasized. Nonetheless the modeling with P3542 could at this point be improved only slightly with extra effort expended in matching predicted ullage heat flux with that input to the ullage gas. As indicated earlier, matching the predicted heat flux which leaves the inner tank wall with the desired heat flux calculated in P3542 is a cut-and-try process. The resistance and heat sink capability of the wall enter into the problem.

The modification to P3542 which permits monitoring energy input to the ullage and liquid for each time step and the summation of energy input provides information to evaluate program sensitivity to ullage heating. The predicted or desired heat input is compared in Figure 3-10 with the achieved heat input for two cases run with P3542.

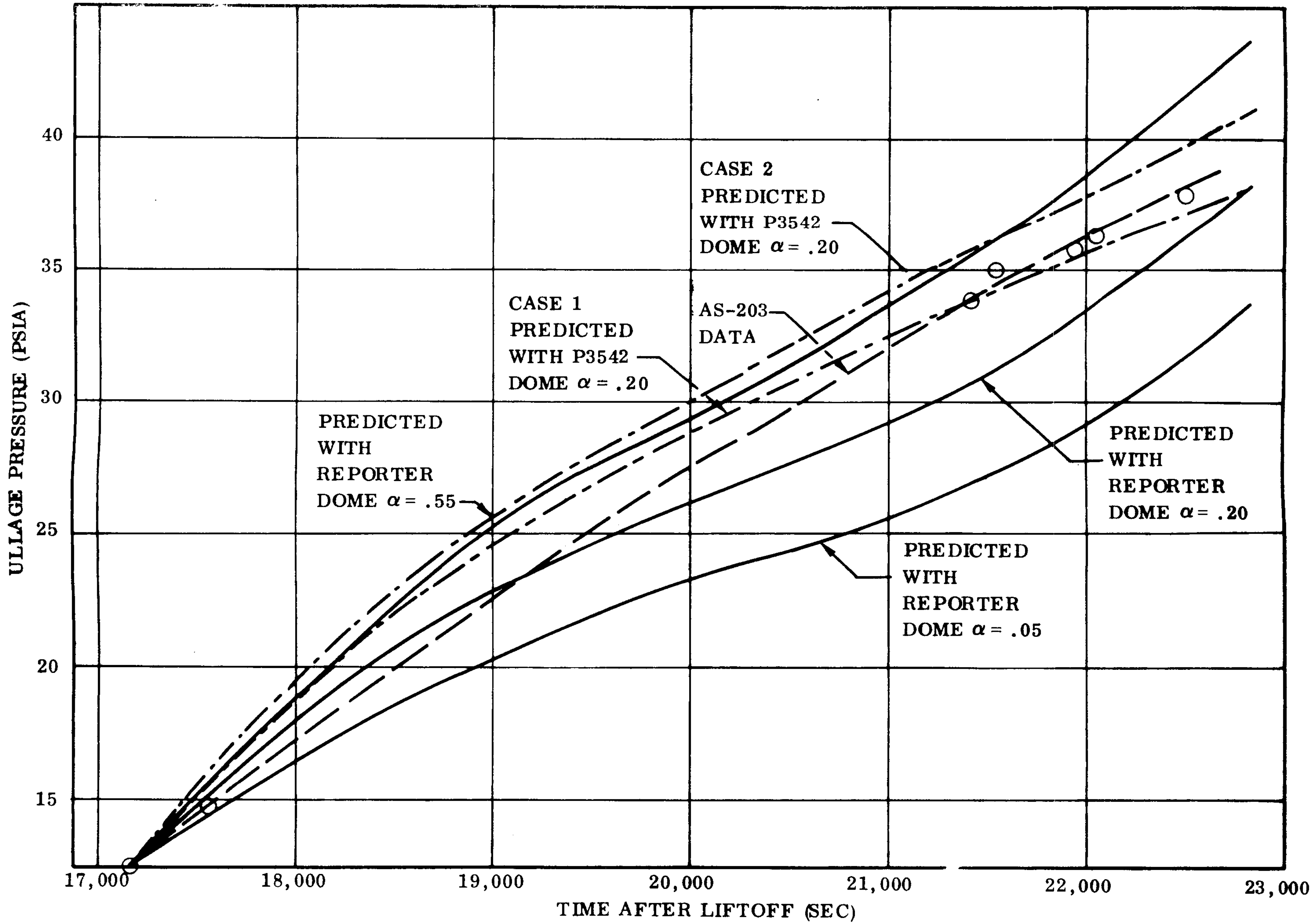

Figure 3-9. Comparison of Predicted Pressures With AS-203 Pressure History During Long Term Coast

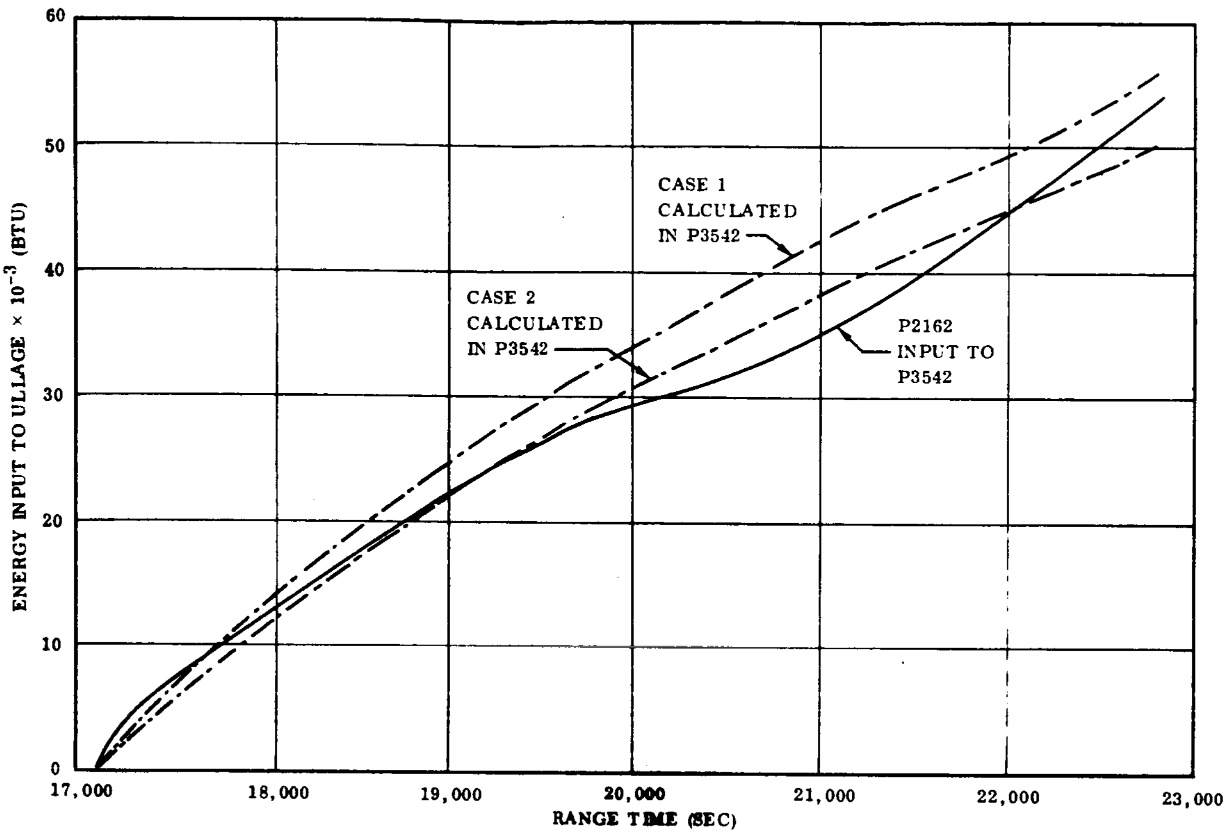

Figure 3-10. Comparison of Propellant Heating Rates Predicted With P2162 and Those Achieved in P3542

The desired heat input to the ullage was 53,700 BTU from P2162 for the period of lock-up. Case 1 with P3542 with 50,160 BTU input resulted in a pressure rise to 38.1 psia while Case 2 with 55,800 BTU resulted in a rise to 41.1 psia, both from 12.5 psia in 5700 seconds. This sensitivity to heat input suggests the required accuracy for heat input must be better than 5 percent if pressure rise rate is to fall within 1 psia during this type of coast phase. The Case 1 and 2 heat fluxes in Figure 3-10 resulted in the Case 1 and 2 pressure curves of Figure 3-9. The absence of AS-203 test data in the region 18,000-21,000 seconds and the backward extrapolation of the later data suggest the flight data curve may be higher than indicated. The Case 1 correlation in Figure 3-9 based wholly on predicted data is gratifying.

Another significant factor in the analysis with these two programs is the results for evaporation or boil-off. Program REPORTER predicted zero boil-off while P3542 predicted 32 and 36 lbs respectively for the two cases above. These latter values are significantly lower than those given in earlier studies where in excess of 200 lbs was reported.

In conclusion, the results of pressure rise rate are satisfactorily predicted with both REPORTER and P3542 within a desirable accuracy range. Both programs are equally dependent on good data for ullage heating, probably requiring 5 percent accuracy, while both are inadequate relating to effects of liquid stratification. The model by Epstein, P3542, only partially recognizes the boil-off contribution. Modifications to P3542 to monitor ullage heating are believed to aid significantly in the analysis of data.

4

DEPRESSURIZATION AND LIQUID LEVEL RISE

A depressurization or vent down of a cryogenic tank in orbit remains a realistic requirement, although recent zero-gravity vent systems have lessened this technology requirement somewhat. Nonetheless, current vehicles are vented down from an initial settled propellant condition. The phenomena of liquid level rise and liquid carryover are of interest to those defining propellant requirements. Photographic coverage of AS-203 did not indicate significant liquid level rise, but did show liquid globule dynamics. There is a requirement to define liquid globule behavior in the ullage. There is a requirement to define liquid interface behavior at higher vent down rates and the bulk liquid dynamics underlying the interface response.

The behavior of the liquid interface is analyzed with three models in this section. The first portrays gross bulk boiling, a second develops boundary layer vapor bubbles due to boiling, while a third examines liquid level rise resulting from a solution to overall bubble dynamics in a settled liquid. The models are presented in order of increasing complexity. The latter has broad application to problems of bubble motion in low gravity environments.

4.1 AS-203 DATA ANALYSES

During a rapid venting operation, boiling phenomena will have a significant influence on the dynamic and thermodynamic behavior of a propellant. There are two potential problems associated with venting a propellant tank under conditions of reduced gravity. These are:

1. Loss of propellant by boilover due to liquid level rise.

2. Loss of propellant from dynamics of liquid globules in the venting vapor.

This section describes the main findings of the AS-203 data analyses pertaining to the rapid depressurizations of the fuel tank.

Three rapid depressurizations of the liquid hydrogen (LH_2) tank were performed during the orbital flight of the S-IVB - AS-203 stage. The first was conducted through the continuous vent system (CV) and occurred 55 seconds after J-2 engine cutoff. The second and third blowdowns were through the non-propulsive vent system (NPV) and occurred during the third orbit of flight.

For the first depressurization, 19,000 lb of LH_2 were present in the tank. Because of the previous boost flight, the LH_2 was settled in the bottom of the tank approximately six inches below the baffle. The pressure was decreased from 30 psia to 22 psia in 170 sec during which 60 lbs of hydrogen vapor were vented. To determine the liquid level rise, temperature and liquid-vapor sensors in the vicinity of the initial liquid level were examined.

Temperature sensors C0345, CO346, and CO347 (see Figure 4-1) were plotted against time during the first blowdown and are shown in Figure 4-2. Also given are the heights (Δh) of these sensors from the settled liquid-vapor interface (S-IVB Sta. 443.5) at J-2 engine cutoff. The instrumentation indicates that 17 sec after engine cutoff CO346 and CO 347 become wetted for about 20 seconds. Because of the short wetting period, it appears that a slosh wave was generated at J-2 engine cutoff. On the down-cycle of the slosh wave, CO345 indicated dry for 30 seconds, CO346 dried for 60 seconds, and CO347 remained dry during the remainder of the first blowdown. On the second up-cycle of the slosh wave CO345 indicated wet for the remainder of the tracking period and CO346 indicated wet for 20 seconds. On the second down-cycle, CO346 showed dry for the remainder of the first depressurization. Since CO346 and CO347 remained dry during the latter portion of the first rapid blowdown, we can conclude that no significant liquid level rise due to vapor entrainment was present during this depressurization. From Figure 4-2 it is noted that the liquid was subcooled (temperature of 39.3°R or saturation pressure of 22.5 psia) at the start of first depressurization, therefore one would not expect bulk boiling as the pressure decreased from 30 to 22 psia.

Liquid-vapor sensor NO52 which was at the same station as temperature sensor CO347 indicated the same wetting and drying behavior as CO347. Measurement NO52 was the only liquid-vapor sensor that appeared to operate correctly, since it agreed with measurements of CO347. Sensor NO52 was a variable resistance type sensor similar to those used on the Centaur vehicle. The other liquid-vapor sensors seemed to trap liquid once they became wet.

During the third orbit, the second rapid depressurization was conducted through the NPV system with 16,300 lbs of LH_2 remaining aboard. Since the tanks had been operating with continuous venting prior to this blowdown, both the liquid and the ullage were at saturation temperature throughout, and the liquid was settled in the bottom of the tank. The pressure was decreased from 19.5 psia to 13.8 psia in 180 seconds, and 360 lbs of hydrogen vapor were vented. The television camera film, temperature sensors, and liquid-vapor sensors were examined to establish the magnitude of liquid level rise for this venting period.

The TV camera at the top of the tank recorded a white fog forming above the liquid level at the beginning of the venting operation. This fog reached the top of the tank 1-1/4 minutes later and prevented visually locating the liquid level during the depressurization. Temperature sensors CO345, CO346, and CO347 were plotted against time during the second rapid blowdown and are shown in Figure 4-3. Since both the liquid and ullage were saturated, temperature sensors were not effective in distinguishing liquid from vapor.

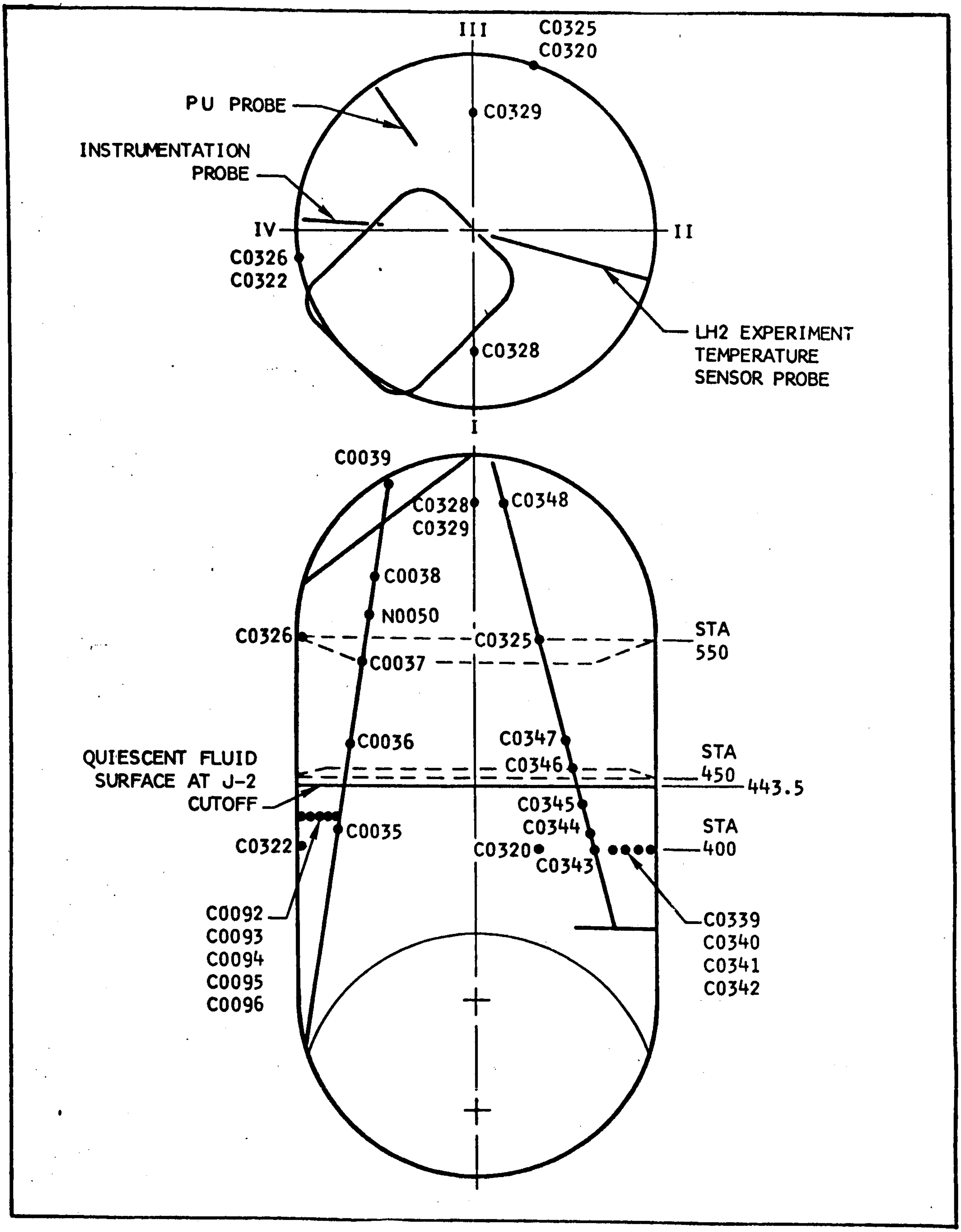

Figure 4-1. LH_2 Temperature Sensor Location in S-IVB Tank

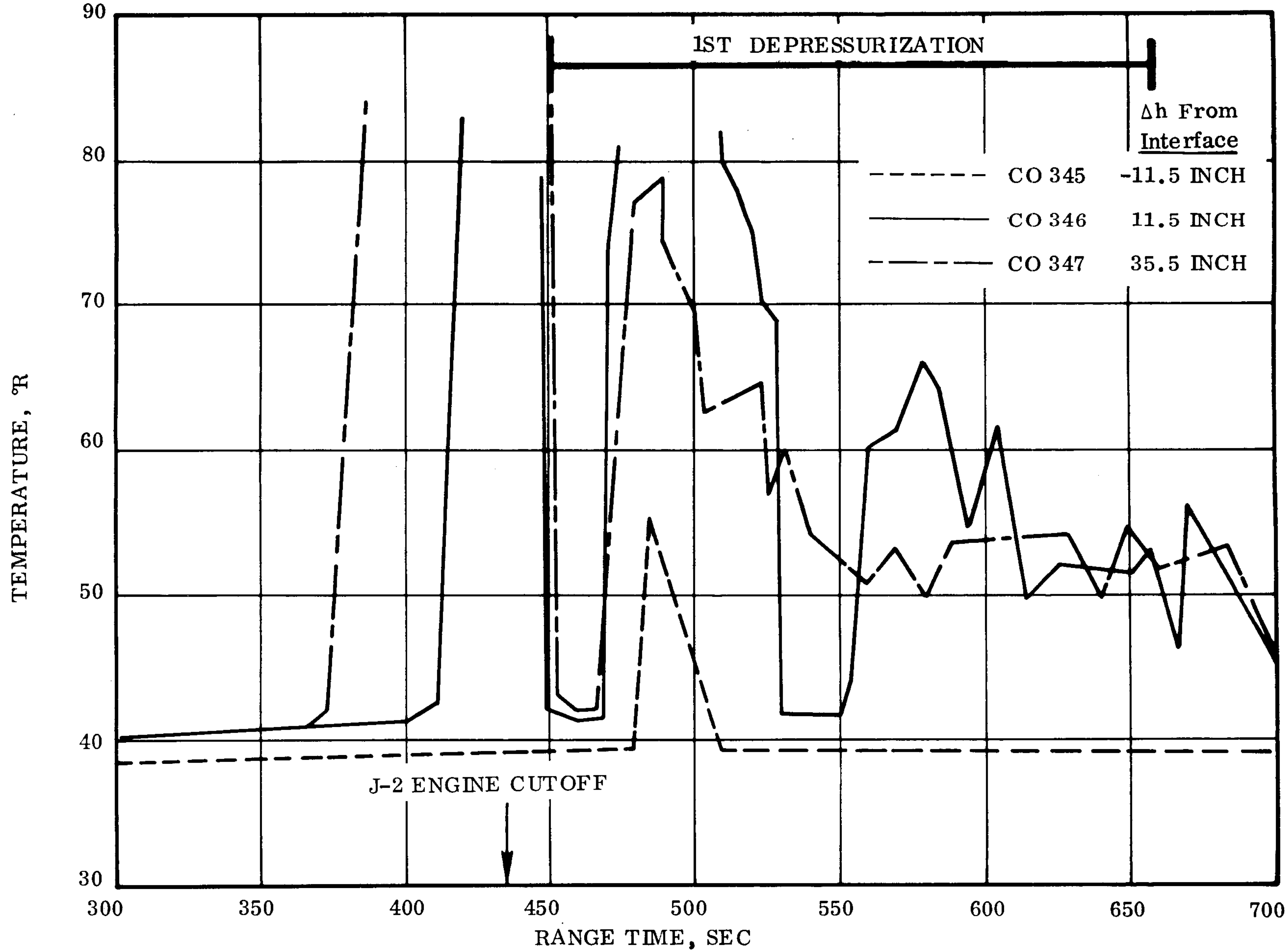

Figure 4-2. Temperature Vs Range Time During First Depressurization For Temperature Sensors in Vicinity of Initial Liquid Level

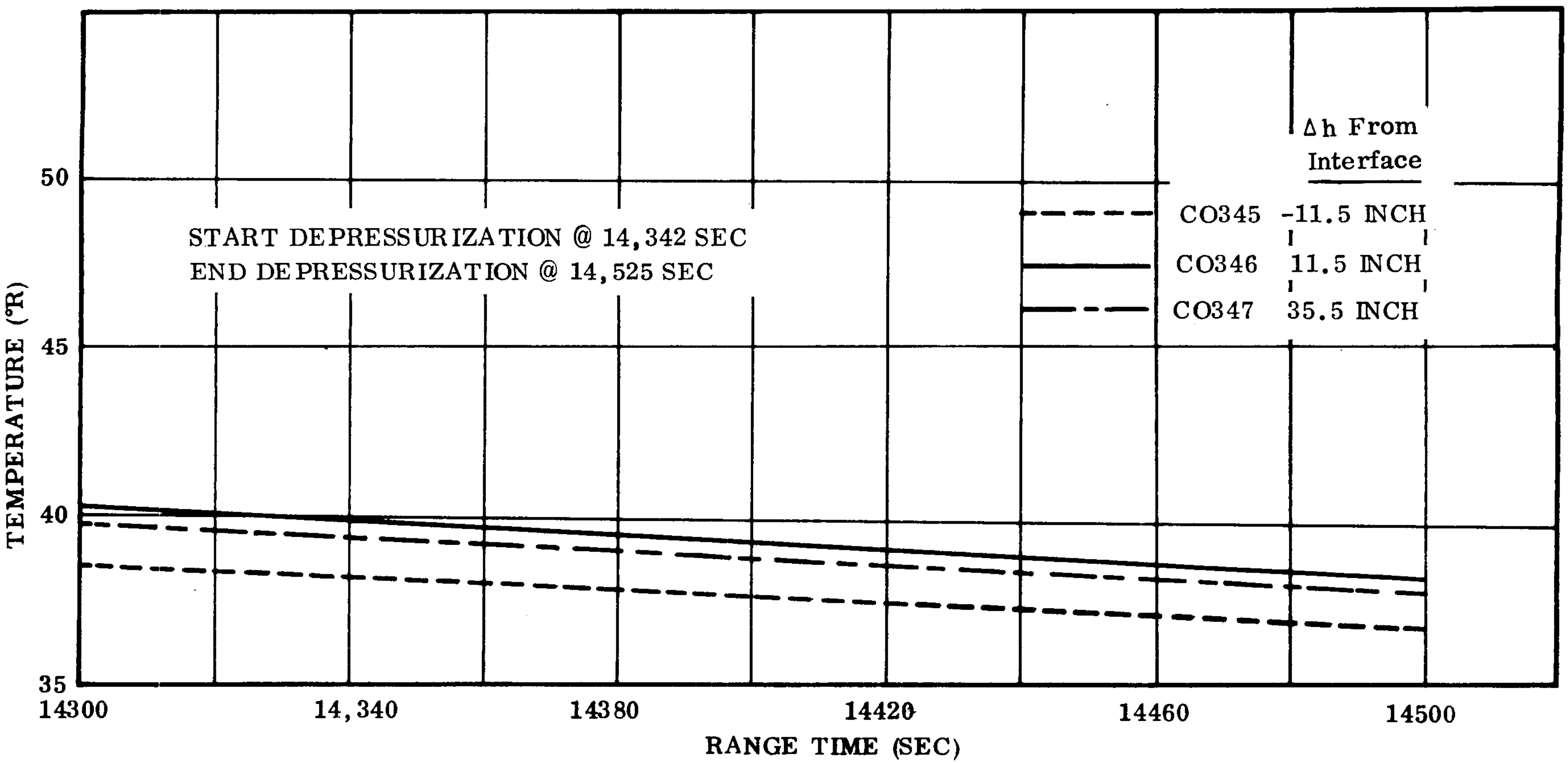

Figure 4-3. Temperature Versus Range Time During Second Depressurization For Temperature Sensors in Vicinity of Initial Liquid Level

It would have been more advantageous to run a pressure rise test prior to this depressurization rather than to operate the CV system. Locking up the tank would have set up stratification in the ullage and would have made temperature sensors more effective in distinguishing liquid from vapor as was demonstrated with the first depressurization in Figure 4-2.

Liquid-vapor sensor NO52 which was 35.5 inches above the initial liquid level is shown plotted in Figure 4-4 for the second blowdown. The output of NO52 has been erroneously processed and presented in degrees Rankine instead of volts. However, the use of the output to indicate wet or dry appears valid. The blowdown was initiated at 14, 342 seconds and 40 seconds later N052 became wet and continued to intermittently wet and dry during the remainder of the venting sequence. After termination of the venting operation at 14,525 seconds, this sensor continued to alternately wet and dry with decreasing frequency. Since earlier observations indicated NO52 was the only liquid-vapor sensor operating correctly, the data from this sensor suggest most of the liquid level rise was due to sloshing and not to vapor entrainment caused by boiling.

Figure 4-4. Response of Liquid-Vapor Sensor N)52 During Second Depressurization

The third rapid depressurization test consisted of two venting cycles spaced 200 seconds apart. For the first cycle, the pressure was reduced from 17 psia to 13 psia in 90 seconds, and 150 lbs of hydrogen vapor were vented. During the second cycle, the pressure was reduced from 14.4 psia to 11.9 psia in 100 seconds, and 160 lbs of vapor were vented. The results of the third blowdown are quite similar to those of the second. Fog formation and saturated conditions again prevented determining the position of the liquid level. The results of liquid-vapor sensor NO52 are shown plotted in Figure 4-5 and 4-6 for the third venting sequence. The first step of the two-step blowdown was initiated at 16,730 seconds and about 50 seconds later, NO52 became wet for approximately 180 seconds; thereafter, NO52 alternately dried and wetted before, during, and after the second step of the blowdown. This observed wetting-drying cycle could have been caused by globules in the ullage or a low level slosh wave. A slosh wave could have resulted from the change in acceleration level caused by the NPV system. However, slosh period would be 40 seconds or greater for the acceleration level at this range time which is higher than the observed wetting period of 15 seconds. Globules were observed to be present from photographic coverage.

As previously mentioned, a second potential problem during a rapid depressurization is globule dynamics in the ullage. Near the end of the second blowdown, nearly spherical liquid globules ranging in size from one to six inches were observed flowing past the TV lens toward the vent with velocities of about 1.5 ft/sec. During the third depressurization large, irregular shaped globules appeared and floated towards the TV camera. These liquid globules appeared to be several times larger than those observed in the second blowdown. However, the globules did not appear to constitute a substantial liquid loss.

The sizes of the observed globules were considerably greater than a globule which could have been entrained by the drag of the vented vapor under prevailing fluid conditions. The larger observed sizes could possibly have been the result of ejection at the liquid-vapor interface by rapid surface boiling or break-up of a slosh wave. Coalescence of smaller globules in the ullage could also account for the observed larger sizes. Part of the wetting and drying of liquid-vapor sensor NO52 reported in Figure 4-4 through 4-6 may be attributed to liquid globules intermittently hitting this sensor. Future analyses of this boiling phenomena is required to examine possible formation mechanisms and subsequent motion of the liquid globules.

Since the quality meter did not perform satisfactorily, it was not possible to determine the amount of liquid lost through the vent systems (Ref. 1-1). However, temperature measurements upstream of the CV and NPV orifices indicated that superheated vapor was vented during most of the rapid blowdowns. Some liquid was lost due to entrainment, but this appeared to be minimal. No liquid appeared to be lost due to liquid level rise due to boiling.

Boiling studies were conducted to develop analytical models to determine: (a) liquid level rise, (b) maximum depressurization rate, and (c) maximum quantity of vapor that can be vented before liquid boilover occurs. Since the magnitude of liquid level rise due to vapor entrainment could not be determined from the AS-203 experiment, no valid boiling correlations can be made for this flight.

Liquid level rise caused by boiling constitutes a potential problem area for space vehicles utilizing cryogens. The level of a liquid cryogen boiling in a tank increases due to the presence of vapor bubbles entrained in the liquid. The amount of vapor

Figure 4-5. Response of Liquid-Vapor Sensor NO52 During Initial Part of Third Depressurization

entrainment is enhanced in a low-gravity environment when a decrease in buoyancy force results in a reduction in bubble rise velocity; longer bubble residence times in the liquid occur. The liquid level rise problem is particularly serious during pressure relief venting of a tank containing saturated liquid wherein large quantities of vapor can be generated from boiling caused by the pressure reduction.

A model for prediction of liquid level rise due to boiling is desirable for design purposes to preclude liquid boilover during a venting operation. Further, it is desirable to predict the maximum venting rate that can be scheduled for a rapid

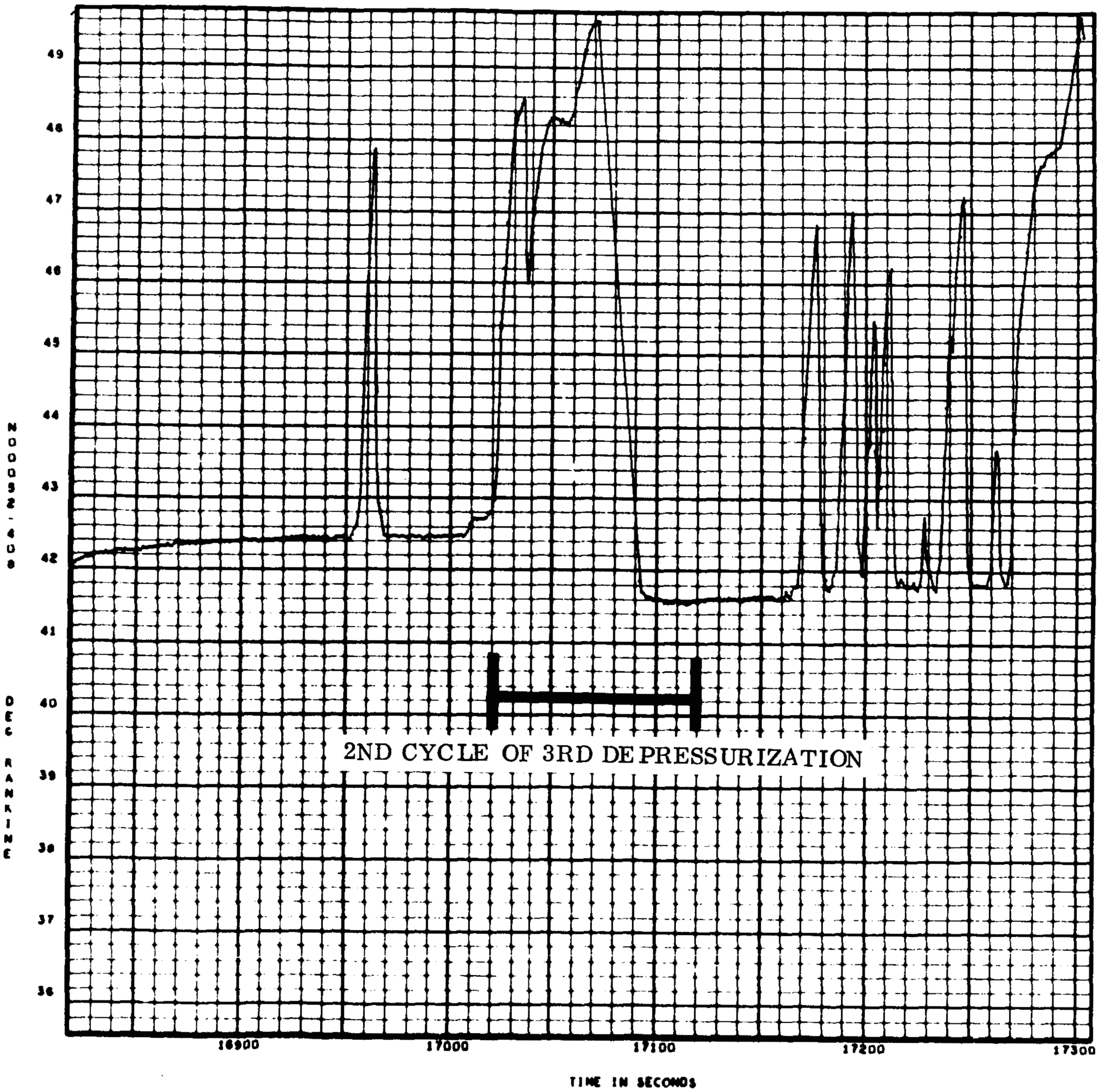

Figure 4-6. Response of Liquid-Vapor Sensor NO52 During Final Part of Third Depressurization

blowdown of a cryogenic tank. To date, there is no quantitative data of level rise during venting in a low-gravity environment. A successful design of a cryogenic tank incorporating pressure relief venting depends on the availability of such information. However, before experiments are conducted, it is desirable to have analytical tools available to predict liquid level rise during a venting operation. The development of these tools is the purpose of this study.

A purely analytical approach to the problem of liquid level rise will be employed here. The model employs the basic equations of motion and heat transfer. At the present time, there are few analytical investigations of liquid level rise (Ref. 4-1, 4-2, 4-3, 4-4). This is because the unknowns involved are rather difficult to describe analytically. These unknowns include determining the amount of energy that goes into vapor production and quantity of vapor that remains entrained in the liquid during a venting operation. The first unknown involves describing bubble nucleation, growth, and departure at a solid surface and liquid-vapor interface, while the second entails describing the motion, interaction, and coalescence of individual bubbles in a liquid. Also, there are problems related to determining the relative importance of nucleation at a solid surface, liquid-vapor interface, and impurities in the liquid bulk. The above problems which previous investigators have neglected or simplified in their liquid level models are further examined in this study.

This parametric model is concerned with indicating the possible magnitude of liquid level rise under certain simplifying assumptions. Equations are derived to determine the quantity of liquid mass evaporated allowing for saturation pressure change, liquid superheat, and wall heat transfer. From the evaporated mass, equations are developed to predict liquid level rise in terms of a boiling mass residency parameter, β. This parameter describes the amount of vapor that remains entrained in the liquid and is related to the nucleation process, motion and interaction of bubbles. For large magnitudes of entrained vapor, significant liquid level rise is predicted.

4.2 ANALYTICAL MODEL FOR BULK LIQUID

Consider a cylindrical tank of height H that is initially filled with liquid to a height h_o. The entire liquid remains saturated and settled in the bottom of the tank during the course of a venting operation in which the saturation pressure decreases. The reduction in mass of saturated liquid by evaporation and the subsequent liquid rise due to vapor entrainment are to be determined for different levels of pressure reduction. Also, estimates of the effects of liquid superheat and wall heat transfer are determined.

4.2.1 <u>LEVEL RISE DUE TO PRESSURE REDUCTION</u>. The quantity of liquid mass evaporated by boiling due to a saturation pressure reduction can be determined from an energy balance on a saturated liquid given as

$$\lambda dm = mC_s \, dT \qquad (4-1)$$

where heat transfer, liquid superheat, and variable properties have been neglected. Integrating equation 4-1 between initial and final states yields

$$\frac{m_f}{m_o} = \exp\left[\frac{C_s}{\lambda}(T_{s_f} - T_{s_o})\right] \tag{4-2}$$

$$\Delta h_\ell = h_o\left\{\exp\left[\frac{C_s}{\lambda}(T_{s_f} - T_{s_o})\right] - 1\right\} \tag{4-3}$$

This change in liquid height in equation 4-3 assumes no vapor entrainment.

If a fraction β of vapor generated over the reduction in pressure remains entrained in a settled liquid, the increase in liquid height due to bubble displacement is given

$$\Delta h_V = \frac{\beta(m_o - m_f)}{\rho_V A_c} \tag{4-4}$$

where β has been assumed to remain constant over the duration of a venting operation. This is an approximation due to the unsteady nature of the nucleation process, location of nucleation, and bubble motion in the liquid. Analyses in Section 4.4 examines these interactions. For now, however, β will be assumed to represent some average quantity of vapor entrained in the liquid during the time interval of a vent cycle. From the summation of the Δh_ℓ due to vaporization and the Δh_V due to vapor entrainment, change in saturation pressure and vapor entrainment is given by

$$\frac{h}{h_o} = \frac{m_f}{m_o} + \beta\frac{\rho_\ell}{\rho_V} - \beta\frac{\rho_\ell}{\rho_V}\frac{m_f}{m_o}$$

$$= \exp\left[\frac{C_s}{\lambda}\left(\frac{dT}{dP}\right)\Delta P\right] + \beta\frac{\rho_\ell}{\rho_V}\left\{1 - \exp\left[\frac{C_s}{\lambda}\left(\frac{\overline{dT}}{dP}\right)\Delta P\right]\right\} \tag{4-5}$$

where an average slope of the saturated liquid-vapor pressure curve, dT/dP, has been employed, and $\Delta P = P - P_o$.

Calculations which have been performed utilizing equation 4-5 are presented in Figure 4-7. Average liquid hydrogen properties were used over a pressure range of 10-50 psia.

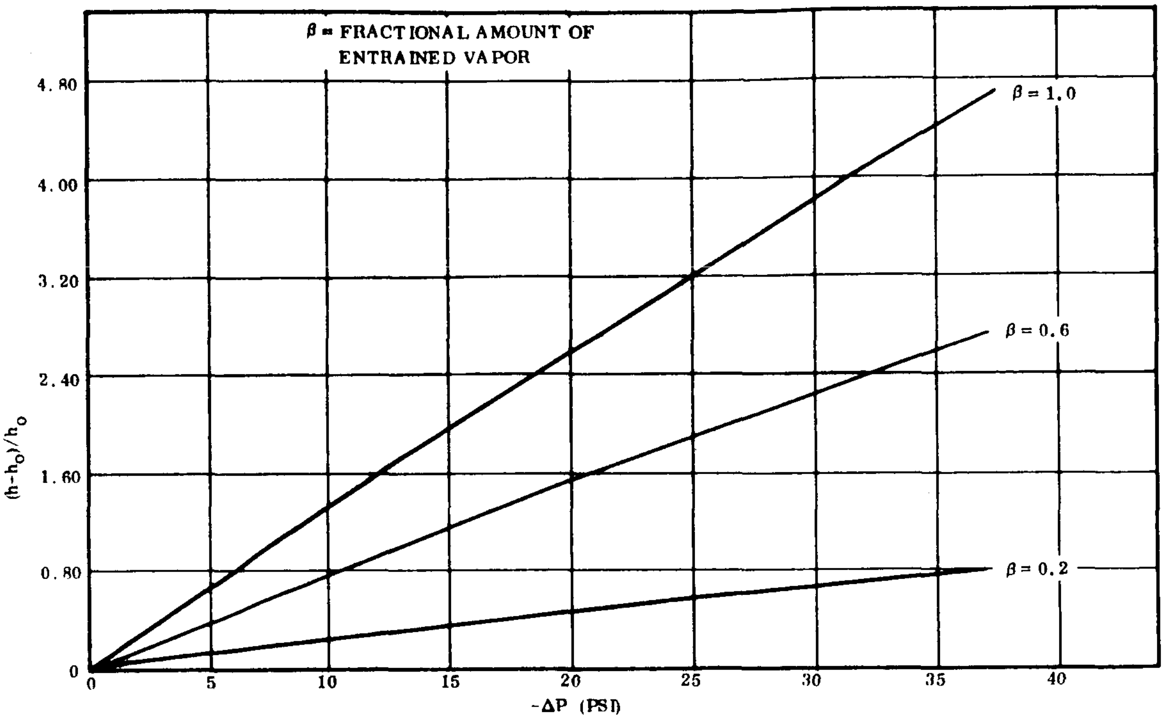

Figure 4-7. Relative Liquid Level Rise Versus Pressure Reduction

It is noted in Figure 4-7 that potentially serious liquid level rise problems can occur for high pressure reductions, depending on the quantity of entrained vapor. For example, for a pressure reduction of 26 psi where 60 per cent of the vapor generated remains entrained, the liquid level rise would be twice the initial fill level.

To determine the maximum allowable pressure reduction for venting a tank of height H initially filled to a level h_o, without liquid reaching the top of the tank, Equation 4-5 is solved for ΔP_{max} corresponding to $h = H$ to yield

$$\Delta P_{max} = \frac{\lambda}{C_s} \frac{dP}{dT} \ln\left[1 - \left(\frac{H}{h_o} - 1\right)\left(\frac{1}{\beta(\rho_\ell / \rho_v) - 1}\right) \right] \qquad (4\text{-}6)$$

Calculated results using Equation 4-6 with LH_2 properties are presented in Figure 4-8. This figure shows that the magnitude of pressure relief during a one cycle blowdown may be small depending on the fill level and quantity of entrained vapor. It is not unlikely that multiple vent cycles would have to be employed to reach a required pressure reduction if β were near one.

It should be noted here that two conservative assumptions were made in this model. These are:

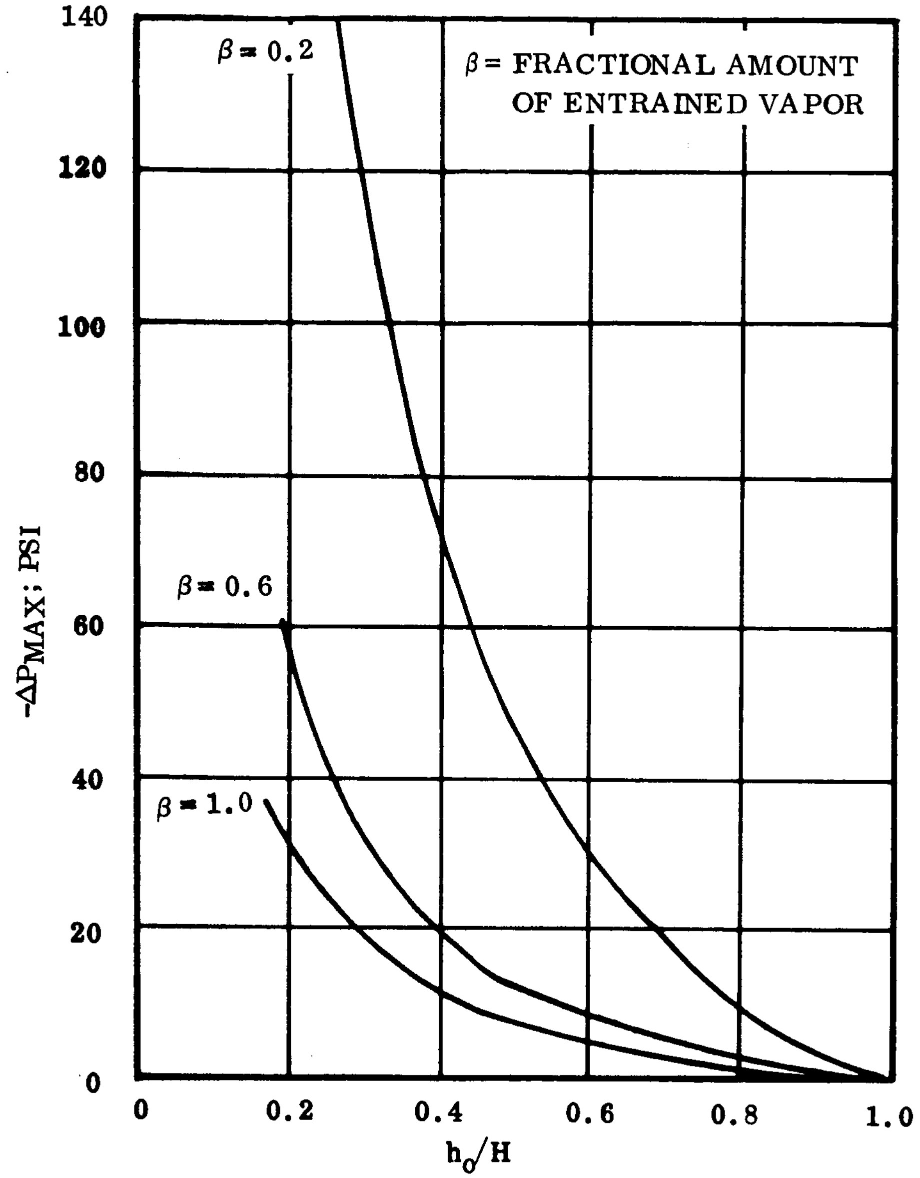

Figure 4-8. Maximum Pressure Drop Relationship For Fractional Fill Levels

1. That all the heat input into the tank is absorbed in vapor generation.

2. That the fraction of vapor specified by β which is generated in the liquid remains entrained.

From the analysis of the S-IVB vent-downs during the AS-203 flight (Section 4.1) it is believed that both of these assumptions are overly conservative and place severe restrictions on venting a propellant tank as noted from the $\beta = 1$ curves of Figures 4-7 and 4-8. Both of these assumptions must be examined to predict their quantitative importance.

4.2.2 EFFECTS OF LIQUID SUPERHEAT. Before boiling occurs in the bulk liquid or at the wall, the liquid temperature must rise above the saturation pressure by an amount proportional to the surface tension forces on the bubble surface. Thus the degree of superheat required is dependent on liquid properties, operating pressure, and geometry of the nucleation site. To account for the energy which can be absorbed in liquid superheat, Equation 4-1 is modified as

$$- m'C_s \Delta T_i + \lambda dm = mC_s\, dT \tag{4-7}$$

where m' is the superheated mass. Dividing through by m and integrating Equation 4-7 between initial and final states corresponding to a saturation temperature change yields for the final liquid mass

$$\frac{m_f}{m_o} = \exp\left[\frac{C_s}{\lambda} (\Delta T_s + \psi \Delta T_i) \right] \tag{4-8}$$

where $\psi \equiv m'/m$ is assumed constant, $\Delta T_s = T_f - T_o$, $\Delta T_i = T_{Superheat} - T_o$. Equation 4-8 relates how liquid superheat reduces the amount of evaporation since part of the energy released due to a saturation pressure reduction is absorbed in superheating the liquid. Similar to the derivation of Equation 4-5, the liquid level rise due to pressure reduction with superheat effects included is given as

$$\frac{h}{h_o} = \exp\left[\frac{C_s}{\lambda} (\Delta T_s + \psi \Delta T_i) \right] + \beta \frac{\rho_\ell}{\rho_v} \left\{ 1 - \exp\left[\frac{C_s}{\lambda} (\Delta T_s + \psi \Delta T_i) \right] \right\} \tag{4-9}$$

To determine the magnitude of superheat that a liquid can sustain before boiling, the following expression developed in Reference 4-5 for a bubble growing in a solid cavity will be used. Experimental values of superheat which are required for wall nucleation are less than the theory for cavities suggest. They are also considerably less than would be required for nucleation in the pure liquid where sites are not present.

$$\Delta T_i \simeq \frac{R_v T_s^2}{J \lambda} \; \frac{2\sigma}{r P_\ell} \tag{4-10}$$

Using saturated LH_2 properties corresponding to a pressure of one atmosphere and a cavity radius of 10^{-4} inch which is typical for most surfaces, the amount of superheat is determined to be 0.116°R. This result is consistent with the values measured in Reference 4-4. Using this value of superheat in Equation 4-9 and assuming all the liquid is superheated ($\lambda = 1$) results in a 12 per cent reduction in level rise for a 1°R reduction in saturation temperature and $\beta = 0.6$. It should be noted that a 2.5°R superheat was required to initiate boiling of LH_2 in Reference 4-6 which employed a different surface material and preparation than that of Reference 4-4. This indicates that surface effects can be important. If this higher value of superheat is attainable for LH_2 and nucleation at a solid surface is the main contributor to vapor production, then, superheat effects can become very significant as a factor in delaying and reducing LH_2 level rise.

4.2.3 INFLUENCE OF WALL HEAT TRANSFER. Heat transfer through the walls of a cryogenic tank containing saturated liquid is another mechanism for vapor generation. To account for wall heat transfer, the energy equation for a saturated liquid is given

$$\delta Q_w + \lambda dm = mC_s dT \tag{4-11}$$

Dividing through by m, approximating

$$\frac{\delta Q_w}{m} \simeq \frac{\delta Q_w}{m_o} \exp\left[\frac{C_s}{\lambda} \Delta T_s\right] \tag{4-12}$$

from the use of Equation 4-1 and integrating Equation 4-11 between initial and final states for constant heat transfer results in

$$\frac{m_f}{m_o} = \exp\left\{\frac{1}{\lambda}\left[C_s \Delta T_s - \frac{\Delta Q_w}{m_o} \exp\left(\frac{C_s \Delta T_s}{\lambda}\right)\right]\right\} \tag{4-13}$$

Equation 4-13 shows how wall heat transfer results in increased vapor production. As derived previously, the liquid level rise due to pressure reduction with constant wall heat transfer is given as

$$\frac{h}{h_o} = \exp\left\{\frac{1}{\lambda}\left[C_s \Delta T_s - \frac{\Delta Q_w}{m_o} \exp\left(\frac{C_s \Delta T_s}{\lambda}\right)\right]\right\}$$

$$+ \beta \frac{\rho_\ell}{\rho_v}\left\{1 - \exp\left[\frac{C_s}{\lambda} \Delta T_s - \frac{\Delta Q_w}{\lambda m_o} \exp\left(\frac{C_s \Delta T_s}{\lambda}\right)\right]\right\} \tag{4-14}$$

Using the following values in Equation 4-14 which are representative of the third orbit, first vent-down of the S-IVB LH_2 tank during the AS-203 flight

$\dot{Q}_w$	$= 25$ BTU/sec	m_o	$= 16,300\ lb_m$
$\Delta\Theta$	$= 180$ sec	ΔQ_w	$\simeq 4500$ BTU

results in a 11 percent increase in level rise due to wall heat transfer for a change in saturation temperature of 1°R and $\beta = 0.6$. For heating rates near the value used here and larger saturation temperature changes, the influence of wall heat transfer on level rise becomes negligible as compared to pressure reductions by venting.

4.2.4 CONSIDERATION OF BOTH SUPERHEAT AND WALL HEAT TRANSFER.

From the analysis presented in the previous two sections, the influence on a saturated liquid of both liquid superheat and wall heat transfer can be accounted for by consideration of the energy balance

$$+ \delta Q_W - m'C_s \, \Delta T_s + \lambda dm = mC_s \, dT \tag{4-15}$$

Dividing through by m, using the approximation given in Equation 4-12, and integrating between initial and final states yields

$$\frac{m_f}{m_o} = \exp\left\{ \frac{1}{\lambda}\left[C_s \, \Delta T_s + \psi C_s \, \Delta T_i - \frac{\Delta Q_W}{m_o} \exp\left(\frac{C_s \; T_s}{\lambda} \right) \right] \right\} \tag{4-16}$$

Equation 4-16 indicates how liquid superheat and wall heat transfer oppose each other in terms of vapor production. The liquid level rise due to saturation temperature change with liquid superheat and wall heat transfer included is determined to be

$$\frac{h}{h_o} = \exp\left\{ \frac{1}{\lambda}\left[C_s \Delta T_s - \psi C_s \Delta T_i - \frac{\Delta Q_W}{m_o} \exp\left(\frac{C_s \Delta T_s}{\lambda} \right) \right] \right\}$$

$$+ \beta \frac{\rho_\ell}{\rho_v} \left\{ 1 - \exp\left[\frac{C_s \; T_s}{\lambda} - \frac{\psi C_s \; T_i}{\lambda} + \frac{\Delta Q_W}{\lambda m_o} \exp\left(\frac{C_s \Delta T_s}{\lambda} \right) \right] \right\} \tag{4-17}$$

Substituting the values used for superheat and wall heat transfer used in Sections 4.2.1.2 and 4.2.1.3 results in a 1 percent reduction in LH_2 level rise for a saturation temperature change of 1°R. This results from opposing effects due to the 12 percent reduction from superheat and 11 percent increase caused by wall heat transfer. Therefore, from the results determined here, the effects of superheat and wall heat transfer on LH_2 level rise are negligible compared to saturation pressure reductions.

In this analyses on liquid level rise, the quantity of entrained vapor was left as an unknown parameter and has been assumed to remain constant with time during the period of a venting cycle. To remove these shortcomings, further study of the basic phenomena involved in a venting process is required. These phenomena include bubble nucleation, growth, rise, interaction, and coalescence, which are discussed in Section 4.4. Also, the relative importance of nucleation at a surface, liquid-vapor interface, and in the liquid bulk must be examined.

After the above time-dependent bubble phenomena have been resolved, the unsteady ·ture of liquid level rise can be examined. From the determination of bubble size and spatial distributions as a function of time during a vent-down, the rate of liquid rise can be determined for various vent flow rates. Maximum vent rate and quantity of vented vapor can then be determined before boilover occurs for various fill levels and gravity levels.

4.3 BOUNDARY LAYER MODEL FOR LIQUID LEVEL RISE

An analytical model is developed to predict the rise in tank liquid level due to bubbles entrained in the boundary layer during a venting process. This model compliments the previous development with the assumption that the major boiling phenomena occurs at the wall rather than the interface or within the bulk. The model presented results from a solution for the boundary layer thickness and volume as a function of time. A steady state boundary layer solution is used with an additional constraint of a mass balance on the boundary layer. The development and application of this model is presented in the following sections.

4.3.1 DESCRIPTION OF BOUNDARY LAYER ANALYTICAL MODEL. Pressure relief venting of a cryogenic tank containing saturated liquid causes preferential boiling along the walls of the container and at the liquid-vapor interface. The bubbles generated by boiling along the walls will have a certain rise velocity depending on their size and the environmental acceleration level. Because of the rise velocities of bubbles and continuous depressurization of saturated liquid, vapor will continuously be leaving the liquid at the interface and forming along the tank walls. It is the purpose of the model developed here to determine the quantity of vapor entering and leaving the bulk liquid and the boundary layer so that the amount of entrained vapor and subsequent liquid level rise can be found.

Because a buoyancy force acts on vapor bubbles generated at the tank wall and imparts a certain rise velocity to them, a two-phase boundary layer exists at the tank wall which will grow until it reaches equilibrium. Certain characteristics of the boundary layer are beyond the scope of this model and must be obtained elsewhere from specialized models, experimental determination, or engineering judgment. These include the boundary layer quality, relative velocity between liquid and vapor, profile shapes, and bubble sizes in the boundary layer. The sizes of the bubbles must be ascertained to predict the bubble velocities. The spacing of the bubbles in the boundary layer must be known or assumed in order to predict the boundary layer characteristics.

Although it is not possible to calculate the spacing and the bubble diameters directly, some estimates can be made from qualitative considerations. The saturated liquid in the tank is evaporated at a certain rate depending on the depressurization rate. Most of the vaporization which occurs other than at the interface results in small bubbles created along the tank walls. Since the acceleration level will be low and the bubbles are small, these bubbles will have low velocities in the direction of the acceleration vector. The period of time that a bubble exists in the vicinity of another bubble provides a good opportunity for bubble coalescence or formation of vapor bundles. As bubbles coalesce, their velocities increase, since the bubble velocity is proportional to the square root of the bubble diameter. The larger bubbles, moving at higher velocities than the smaller bubbles, will coalesce with smaller bubbles that they encounter. These considerations suggest that the bubbles in the boundary layer will probably be very large. The bubbles will be spaced a certain distance apart. Experimental evidence (Ref. 4-7 and movie) indicates that a bubble rising in a fluid in a gravity field behind another bubble will catch up and coalesce with the first bubble if the initial spacing of the bubbles is too small. Hence, closely spaced bubbles in the boundary layer will coalesce.

Based on the above qualitative considerations, the following assumptions will be made concerning the bubble spacing and size distribution in the boundary layer:

1. All bubbles at any given axial height along the boundary layer are equal in diameter.

2. There is only one bubble at any given point extending from the tank wall to the edge of the two phase region. This is shown in Figure 4-9.

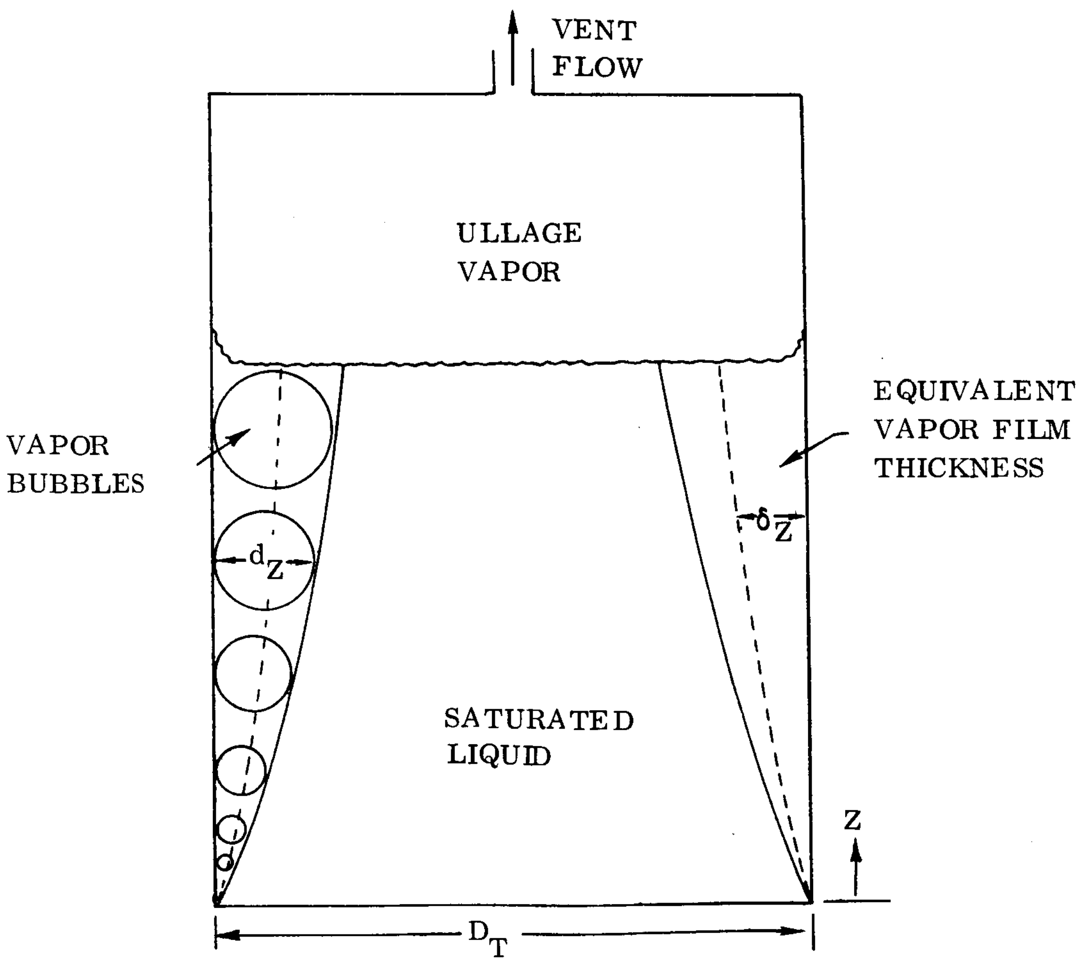

Figure 4-9. Bubble Boundary Layer Model

3. The bubbles are assumed to be spaced as a function of bubble diameter.

Bubble spacings factors, S_{ℓ_Z} and S_{v_Z} which are functions of tank height, are defined as the number of bubble diameters defining the space between bubble peripheries.

From a local mass balance on the vapor in the boundary layer, the shape of the boundary layer can be determined. For mathematical convenience, it is assumed that a) there are no temperature gradients in the boundary layer, and b) the liquid velocity in the boundary layer is negligible. Also, for the purpose of this analysis, it is assumed that at equivalent vapor film exists instead of discrete bubbles. At any given point in the boundary layer, the boundary layer thickness which is also equal to the bubble diameter at that point will be proportional to the vapor film thickness.

Referring to Figure 4-10, we can determine a relationship between bubble diameter and equivalent film thickness by equating the volumes occupied by bubbles of a given spacing

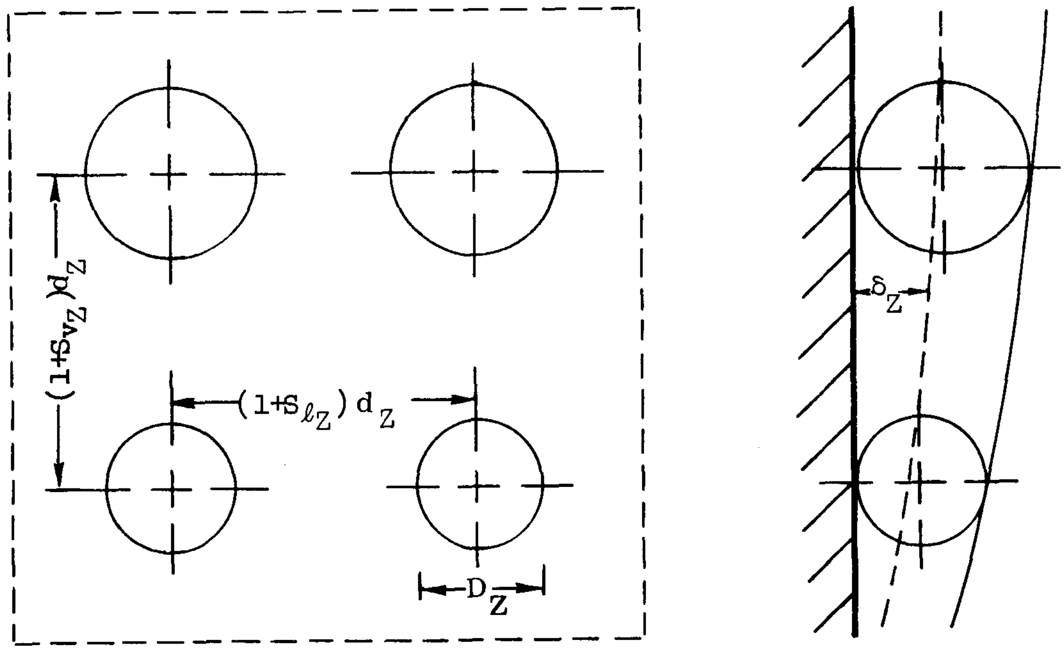

Figure 4-10. Bubble Geometric Spacing Factors

and a vapor film. This is given as

$$\frac{\pi d_Z^3}{6} = (1 + S_{\ell_Z})\, d_Z\, (1 + S_{v_Z})\, d_Z\, \delta_Z$$

or

$$\delta_Z = \frac{\pi}{6} \frac{d_Z}{(1 + S_{\ell_Z})\,(1 + S_{v_Z})} \qquad (4\text{-}18)$$

The following equation for bubble velocities which has been shown (Ref. 4-8) to be good for bubble Reynolds numbers greater than 5000 will be used to determine the local film velocity

$$u_Z = 0.73 \left[(\rho_\ell - \rho_v) g \, d_Z / \rho_\ell \right]^{1/2} \tag{4-19}$$

The time dependent mass balance on a differential element of the vapor film includes an input term due to boundary layer vapor velocity and due to bulk evaporation, an output term at the upper boundary, and a growth or accumulation term, individual terms are indicated in Figure 4-11.

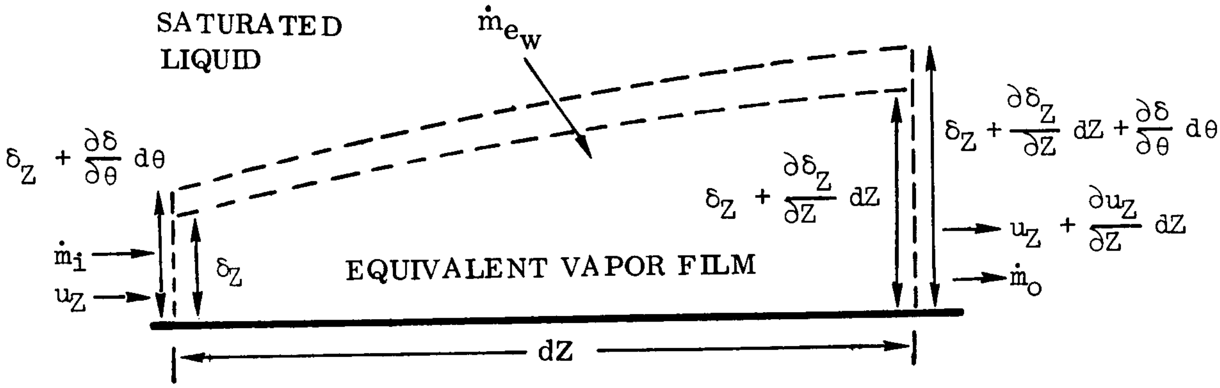

Figure 4-11. Mass Balance for Differential Film Layer Section for Unsteady State Boundary Layer

$$\pi D_T \rho_v u_Z \left[\delta_Z + \frac{1}{2} \frac{\partial \delta_Z}{\partial \theta} d\theta \right] d\theta + \dot{m}_{e_W} d\theta - \pi D_T \rho_v \left[u + \frac{\partial u_Z}{\partial_Z} dZ \right]$$

$$\times \left[\delta + \frac{\partial \delta_Z}{\partial Z} dZ + \frac{1}{2} \frac{\partial \delta_Z}{\partial \theta} d\theta + \frac{1}{2} \frac{\partial^2 \delta_Z}{\partial Z \partial \theta} dZ \, d\theta \right] d\theta$$

$$= \pi D_T \rho_v \left[\frac{\partial \delta_Z}{\partial \theta} d\theta \, dZ + \frac{1}{2} \frac{\partial^2 \delta_Z}{\partial Z \partial \theta} d\theta \, dZ \right] \tag{4-20}$$

Simplifying and neglecting higher order differentials,

$$\frac{\dot{m}_e}{\rho_v \pi D_T} - \left[u_Z \frac{\partial \delta_Z}{\partial Z} dZ + \delta_Z \frac{\partial u_Z}{\partial Z} dZ \right] = \frac{\partial \delta_Z}{\partial \theta} dZ \tag{4-21}$$

Equation 4-21 is not readily amenable to solution; it is convenient to decouple the time dependent growth term and consider the shape of the boundary layer as a function of height only. The time-dependent growth term is small in comparison to the flow terms. The growth term can be treated within the analytical model as a restriction imposed on the solution in a later step by the mass balance of the boundary layer. Thus

$$\rho_v \pi D_T \left[u_Z \frac{d\delta_Z}{dZ} + \delta_Z \frac{du_Z}{dZ} dZ \right] = \dot{m}_{e_W} \tag{4-22}$$

The rate of saturated liquid evaporation in the boundary layer incremental distance dZ due to the change in saturation temperature of the bulk fluid is given as

$$\dot{m}_e = - \frac{C_s \rho_\ell \pi D_T (D_T/4 - \delta_Z)}{\lambda} \frac{dT}{d\theta} \tag{4-23}$$

where the boiling cross sectional area is defined as $\pi D_T^2/4 - \pi D_T \delta_Z$.

To determine the amount of liquid mass evaporated in the boundary layer as compared with interface evaporation, we define a quantity ϵ which is the fraction of evaporated mass that forms along the walls, that is

$$\epsilon \equiv \frac{\dot{m}_{e_W}}{\dot{m}_e} \tag{4-24}$$

With the evaporation occurring along the walls of the container and at the liquid vapor interface, one approach is to say that the relative importance of nucleation at the walls versus the liquid-vapor interface is given to a first approximation by a ratio of wall area S_W to the interfacial area

$$\epsilon \sim \frac{S_W}{S_W + (\pi D_T^2/4)} \tag{4-25}$$

A more accurate approach is to use the bubble surface area output by program EVOLVE (Ref. 4-9), as the preferred ratio is interfacial areas rather than wall area.

From the use of Equations 4-23 and 4-24, Equation 4-22 becomes

$$\delta_Z \frac{du_Z}{dZ} + u_Z \frac{d\delta_Z}{dZ} = - \frac{\epsilon C_S \rho_\ell}{\rho_v \lambda} \left[\frac{D_T}{4} - \delta_Z \right] \left[\frac{dT}{dP} \right] \frac{dP}{d\theta} \tag{4-26}$$

where the slope (dT/dP) of the saturated vapor-pressure curve has been employed.

The variation of film thickness with position along the wall is given by simultaneous solution of Equations 4-18, 4-19 and 4-26. Rearranging Equation 4-18

$$dZ = \frac{6}{\pi}(1 + S_{\ell})(1 + S_V)\,\delta_Z$$

and substituting into Equation 4-19 yields

$$u_Z = 0.73 \left[\frac{6\,(1 + S_{\ell})\,(1 + S_V)\,(\rho_{\ell} - \rho_V)\,g\,\delta_Z}{\pi\,\rho_{\ell}} \right]^{1/2} \tag{4-27}$$

$$\frac{du_Z}{dZ} = \frac{0.73}{2} \left[\frac{6\,(1 + S_{\ell})\,(1 + S_V)\,(\rho_{\ell} - \rho_V)\,g}{\pi\,\rho_{\ell}} \right]^{1/2} \delta_Z^{-1/2}\,\frac{d\delta_Z}{dZ} \tag{4-28}$$

Substituting (4-27) and (4-28) into (4-26) gives

$$\left(\frac{3}{2}\right)\left(0.73\right)\left[\frac{6\,(1 + S_{\ell})\,(1 + S_V)\,(\rho_{\ell} - \rho_V)\,g}{\pi\,\rho_{\ell}} \right]^{1/2} \delta_Z^{1/2}\,\frac{d\delta_Z}{dZ}$$

$$= -\frac{\epsilon\,C_S\,\rho_{\ell}}{\rho_V\,\lambda}\left[\frac{D_T}{4} - \delta_Z\right]\left[\frac{dT}{dP}\right]\frac{dP}{d\theta} \tag{4-29}$$

Defining the following

$$K_1 \equiv \frac{3}{2}\cdot 0.73 \left[\frac{6\,(1 + S_V)\,(1 + S_{\ell})\,(\rho_{\ell} - \rho_V)\,g}{\pi\,\rho_{\ell}} \right]^{1/2} \tag{4-30}$$

$$K_2 \equiv -\frac{\epsilon\,C_S\,\rho_{\ell}}{\rho_V\,\lambda}\left[\frac{dT}{dP}\right]\frac{dP}{dt} \tag{4-31}$$

and

$$K_3 \equiv \frac{K_2}{K_1} \tag{4-32}$$

Equation 4-29 can be written as

$$\frac{\delta_Z^{1/2}\,d\,\delta_Z}{(D_T/4 - \delta_Z)} = K_3\,dZ \tag{4-33}$$

Equation 4-33 can be integrated by making the following substitutions

$$\delta_Z = y^2 \qquad \text{and} \qquad d\delta_Z = 2y\, dy$$

which gives

$$\int_o^y \frac{y^2\, dy}{D_T - 4y^2} = \frac{K_3}{8} \int_o^Z dZ \tag{4-34}$$

This integral can be evaluated from a table of integrals to be

$$-\frac{y}{4} + \frac{\sqrt{D_T}}{8} \tanh^{-1}\left[\frac{2y}{\sqrt{D_T}}\right] = \frac{K_3}{8} Z \tag{4-35}$$

Expanding $\tanh^{-1}$ in a series

$$\tanh^{-1} 2\left[\frac{\delta_Z}{D_T}\right]^{1/2} = 2\left[\frac{\delta_Z}{D_T}\right]^{1/2} + \frac{2^3}{3}\left[\frac{\delta_Z}{D_T}\right]^{3/2} + \frac{2^5}{5}\left[\frac{\delta_Z}{D_T}\right]^{5/2}$$

$$+ \frac{2^7}{7}\left[\frac{\delta_Z}{D_T}\right]^{7/2} + \frac{2^9}{9}\left[\frac{\delta_Z}{D_T}\right]^{9/2} + \cdots\cdots$$

higher order terms after the first five are less than one percent significant for boundary layers less than one foot in the S-IVB.

Equation 4-35 reduces to

$$Z = \frac{8}{K_3}\left[\frac{\delta^{3/2}}{3\, D_T} + \frac{2^2\, \delta^{5/2}}{5\, D_T^2} + \frac{2^4\, \delta^{7/2}}{7\, D_T^3} + \frac{2^6\, \delta^{9/2}}{9\, D_T^4} + \cdots\right] \tag{4-36}$$

The volume occupied by the vapor film boundary layer can be found from

$$V_{BL} = \pi D_T \int_o^h \delta_Z\, dZ = \pi D_T \int_o^{\delta(h)} \delta_Z \frac{dZ}{d\delta_Z} d\delta_Z \tag{4-37}$$

Substituting Equation 4-36 into 4-37 and evaluating gives

$$V_{BL} = \frac{8\pi}{K_3}\left[\frac{\delta(h)^{5/2}}{5} + \frac{2^2\,\delta(h)^{7/2}}{7\,D_T} + \frac{2^4\,\delta(h)^{9/2}}{9\,D_T^2} + \frac{2^6\,\delta(h)^{11/2}}{11\,D_T^3}\cdots\right] \tag{4-38}$$

From Equation 4-36 above, it is apparent that the implicit expression for δ as a function of Z is not time dependent. Similarily, the boundary layer volume, Equation 4-37, is not time time dependent. It is observed that the only free constant in this equation is K_3. By iterating with Equation 4-36 and a conservation of mass relation Equation 4-39, which utilizes variables δ_Z at the interface and V_{BL}, one can obtain a growing boundary layer. The assumption here is that the boundary layer shape is characterized only by K_3, and is in the form of Equation 4-36. The mass balance on the boundary layer of Figure 4-12 is

$$\rho_v\, d\,V_{BL} - (\rho_v\, u_Z\, \delta_Z)_{Z=h}\,\pi\, D_T\, d\theta + dm_{e_w} = 0 \tag{4-39}$$

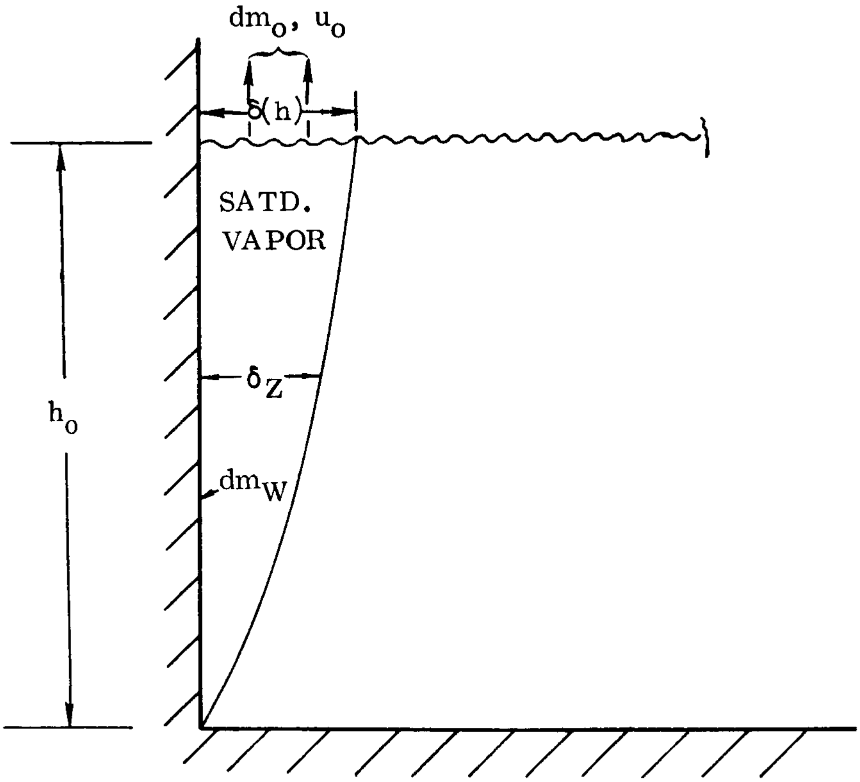

Figure 4-12. Mass Conservation in the Boundary Layer

wh··h can also be written as

$$\rho\,\frac{dV_{BL}}{d\theta} = \pi\, D_T\,(\rho_v\, u_Z\, \delta_Z)_{Z=h} - \frac{\epsilon\, m_\ell\, C_S}{\lambda}\left[\frac{dT}{dP}\right]\frac{dP}{d\theta} \tag{4-40}$$

Using Equations 4-27 and 4-36 with Z=h, this equation becomes

$$\frac{dV_{BL}}{dt} = - \frac{\epsilon m_{\ell} C_S}{\rho_v \lambda} \left[\frac{dT}{dP}\right] \frac{dP}{dt} + (0.73)\, \pi D_T \left[\frac{6(1+S_{\ell})(1+S_v)(\rho_{\ell} - \rho_v)\, g}{\pi \rho_{\ell}}\right]^{1/2} \delta_h^{3/2} \tag{4-41}$$

from which the time rate of change of liquid level height can be found from

$$\frac{dh}{dt} = \frac{1}{\pi D_T (D_T/4 - \delta_Z)_{Z=h}} \frac{dV_{BL}}{dt} \tag{4-42}$$

To determine the change of liquid level height from Equation 4-42, the depressurization rate (dP/dt) due to tank venting must be determined. The depressurization rate can be found from a mass balance on the tank. The change in vapor mass in the tank due to liquid evaporation and vent outflow is given as

$$dm_g = dm_e - \dot{m}_v \,\delta t \tag{4-43}$$

The vapor-mass in the tank can be related to the tank pressure by the equation of state

$$m_g = \frac{PV}{Z\,RT}$$

from which the change in vapor mass for negligible change in ullage volume is given as

$$\frac{dm_T}{m_g} = \frac{dP}{P} - \frac{dT}{T} = \frac{dP}{P} - \frac{1}{T}\left[\frac{dT}{dP}\right] dP \tag{4-44}$$

Substituting Equation 4-44 and the change in mass due to liquid evaporation in Equation 4-43 gives

$$m_g \left[\frac{dP}{P} - \frac{1}{T}\left(\frac{dT}{dP}\right) dP\right] = - \frac{m_{\ell} C_S}{\lambda} \left(\frac{dT}{dP}\right) dP - \dot{m}_v \,\delta t$$

which can be solved for the depressurization rate

$$\frac{dP}{dt} = \frac{- \dot{m}_v}{\frac{m_{\ell} C_S}{\lambda} \left[\frac{dT}{dP}\right] + m_g \left[\frac{1}{P} - \frac{1}{T}\left(\frac{dT}{dP}\right)\right]} \tag{4-45}$$

From the substitution of Equation 4-45 into Equation 4-41 and then into Equation 4-42, the rate of change of liquid level rise can be determined.

Another variable of interest is the mass remaining in the boundary layer as a function of time. From Equation 4-38 above and from Equation 4-2, the ratio of final to initial liquid mass is determined

$$\frac{m_{\ell f}}{m_{\ell_o}} = \exp\left[\frac{C_S \Delta T_S}{\lambda}\right] \tag{4-46}$$

This gives the quantity of saturated liquid mass evaporated due to saturation temperature change; the fraction of mass evaporated that remains entrained in the boundary layer at any time is defined as β where

$$\beta = \frac{V_{BL}\,\rho_V}{m_{\ell_o}\left[1 - \exp\frac{C_S \Delta T_S}{\lambda}\right]} \tag{4-47}$$

4.3.2 PARAMETRIC ANALYSIS. This model has been programmed for the CDC 6400 and the FORTRAN code, LIQLEV, is presented as Appendix B. A parametric analysis of the important variables defined in the previous section was undertaken. The results explore the range of variables anticipated for an upper stage experiencing a g-level of approximately 3×10^{-4} g's. Bubble residency time is affected by this g-level. The program is, by necessity, restricted to a defined geometric configuration. The S-IVB hydrogen tank, 21.67 ft in diameter, with an initial liquid height of 14.4 ft representative of AS-203 orbital conditions was selected.

The fraction of evaporated mass feeding the boundary layer, ϵ, was varied from .4 to .8 at three discrete levels. A fourth level consisted of an input function, $\epsilon = f(\theta)$, from EVOLVE with ϵ starting at zero and reaching a steady state value of .60 at 180 seconds, see Figure 4-22. The boiling area is defined to include all vapor interfacial area, either bulk interface or bubble interface. Vent rate was varied from 1.1 to 3.3 lbs/sec. Bubble spacing factors of 1.0, 2.0, and 4.0 were used. In all cases the tank was initially saturated at 19.5 psia and was vented down to 13.8 psia. This nominally required 280 seconds.

As anticipated, for a given volume of vapor generated in the boundary layer, i.e. 5490 cu ft at final tank conditions, only a small fraction remained in the boundary layer. This amount is lower as bulk interfacial boiling increases at lower values of ϵ. This phenomena is illustrated for dimensionless liquid interface rise, $\Delta h/h_o$ in

Figure 4-13. The boundary layer has nearly reached steady-state conditions for the prescribed vent rate, thus these values reflect the maximum liquid level rise expected for these conditions, independent of venting duration. The film thickness is correspondingly larger with higher values of ϵ.

The effect of the venting rate, the primary variable in this process, is shown in Figure 4-14 with the corresponding $dP/d\theta$ for these vent rates. The lowest vent rate selected, 1.1 lb/sec resulted in a steady state boundary layer with a maximum increase in liquid level of less than one foot. The vent rate for AS-203 was 2.2 lb/sec and steady state conditions were being approached at 280 seconds. For higher vent rates, correspondingly higher liquid levels were defined. The film thickness was also determined for the various vent rates. The above comments on steady-state obtain; results are presented in Figure 4-15.

The effect of bubble spacing is more difficult to picture. Since the mass evaporated is constant for a given depressurization rate, the larger bubbles which form have a shorter residency in the boundary layer and result in less overall liquid level rise. Unfortunately, no data was available from AS-203 to confirm this variable selection, thus a spacing of 1.0 was used in most of the parametric study. Effects of this parameter are presented in Figure 4-16.

The results of Program EVOLVE show this parameter to be characteristically less than 1.0. Increasing S_v and S_ℓ makes bubbles larger which should rise faster with lower residence time. This results in small boundary layer volume, i.e. less vapor hold-up. A glance at the analytical formulation shows that doubling the spacing has the same overall effect as doubling the g-level. One of course would calculate larger bubble diameters for the same boundary layer thickness for higher S_v and S_ℓ.

Two design variables which may be specified for the venting process are rate of pressure decay and g-level for the operation. In Figure 4-17, the resultant liquid level increase for a tank of AS-203 proportions is presented. At larger values of time, the boundary layer approaches steady state and ceases to grow. Indeed, the predicted liquid level rise in 280 seconds for AS-203 does not appear to cause a problem. The relationship between g-level and the dimensionless height variable is presented in Figure 4-18. It can be stated that the liquid level rise is not a strong function of g-level.

4.4 BUBBLE DYNAMICS MODEL FOR LOW-G

The phenomena of liquid level rise can only be approached with some degree of sophistication when the behavior of the bubble population can be modeled. Convair recognized the need for an analytical model to describe bubble behavior in low-g and developed a computer model solely under the 1968 company funded IRAD program (Ref. 4-9). This model considers the buoyant and drag forces acting on the bubble in the various Reynolds number regimes. The fluid temperature gradients also result

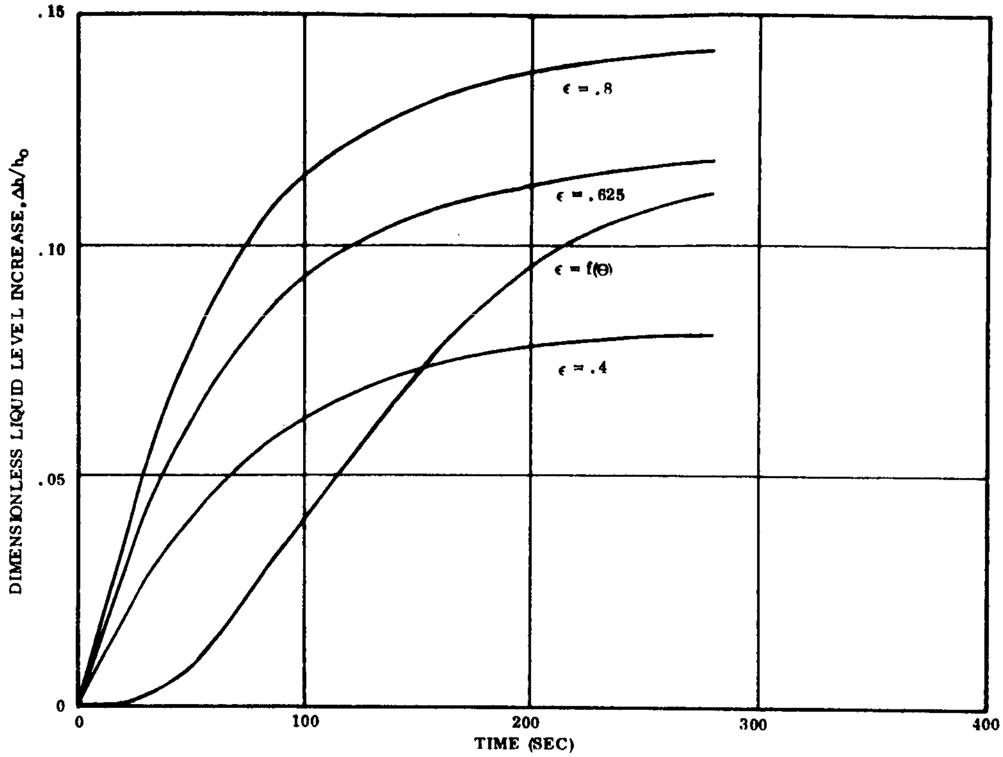

Figure 4-13. Dimensionless Liquid Level Increase With Time for a Range of ϵ Values

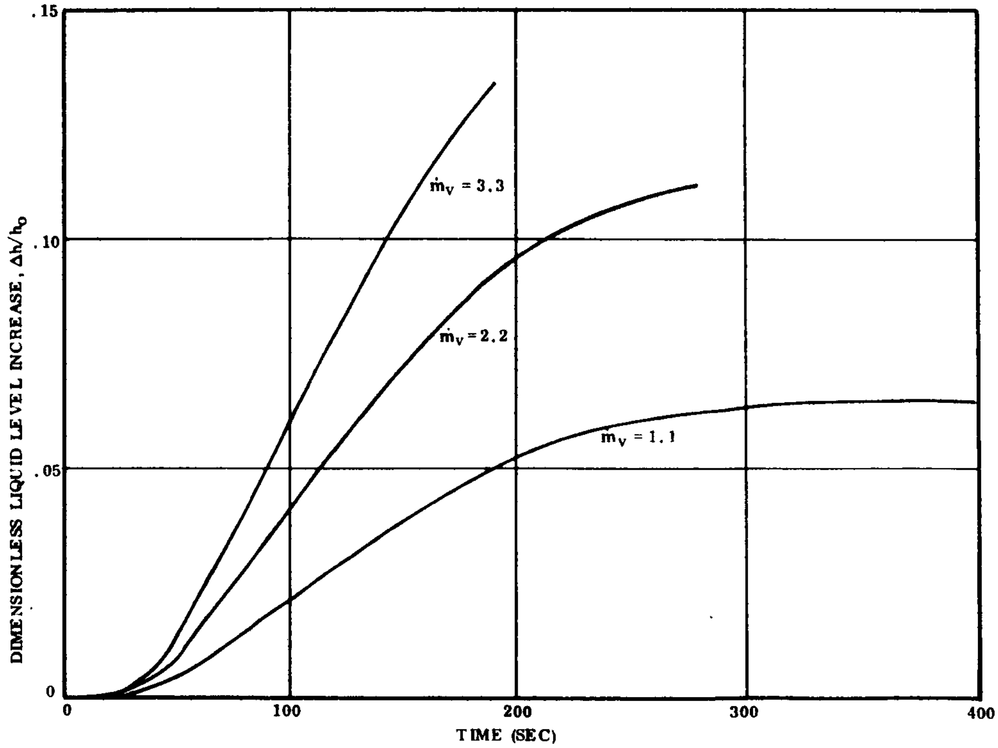

Figure 4-14. Dimensionless Liquid Level Increase With Time for Various Vent Rates

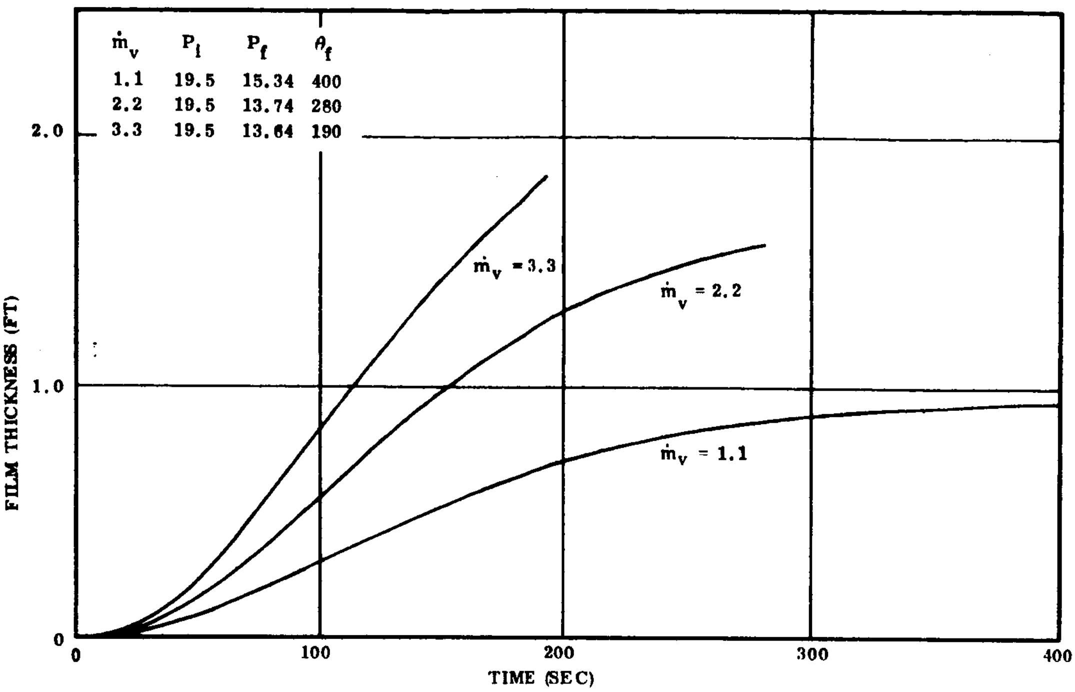

Figure 4-15. Film Thickness Variation With Time for Various Vent Rates

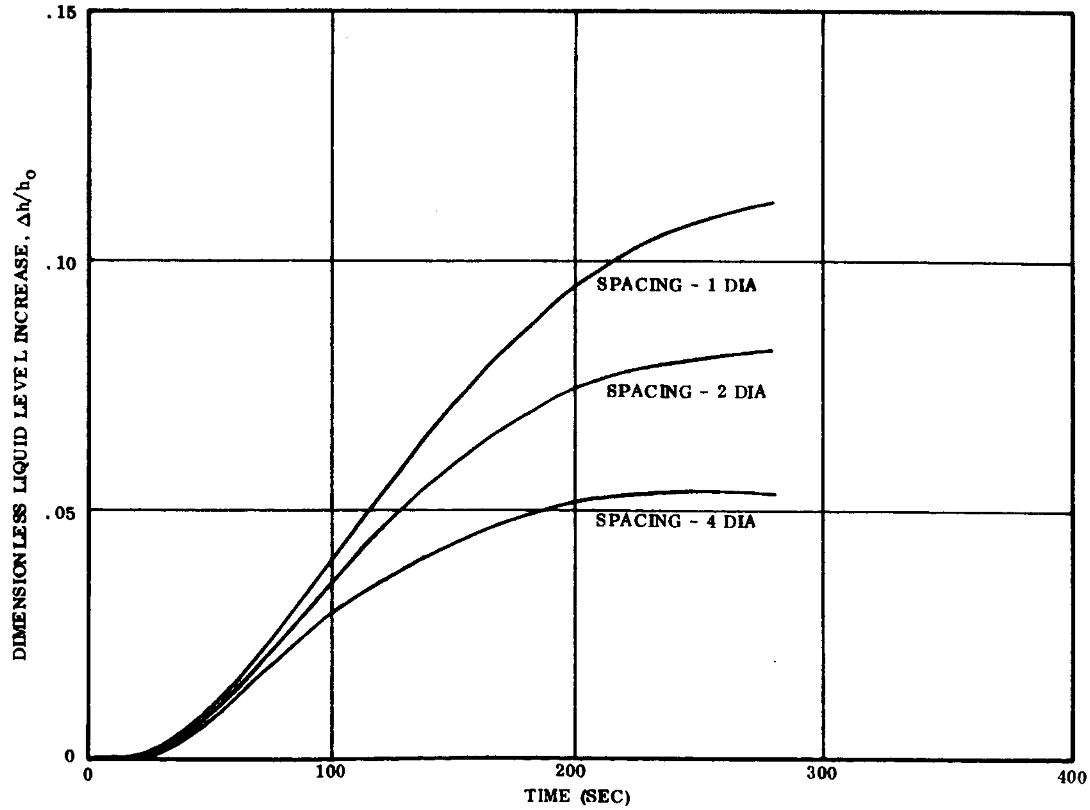

Figure 4-16. Dimensionless Liquid Level Increase With Time for Various Bubble Spacings

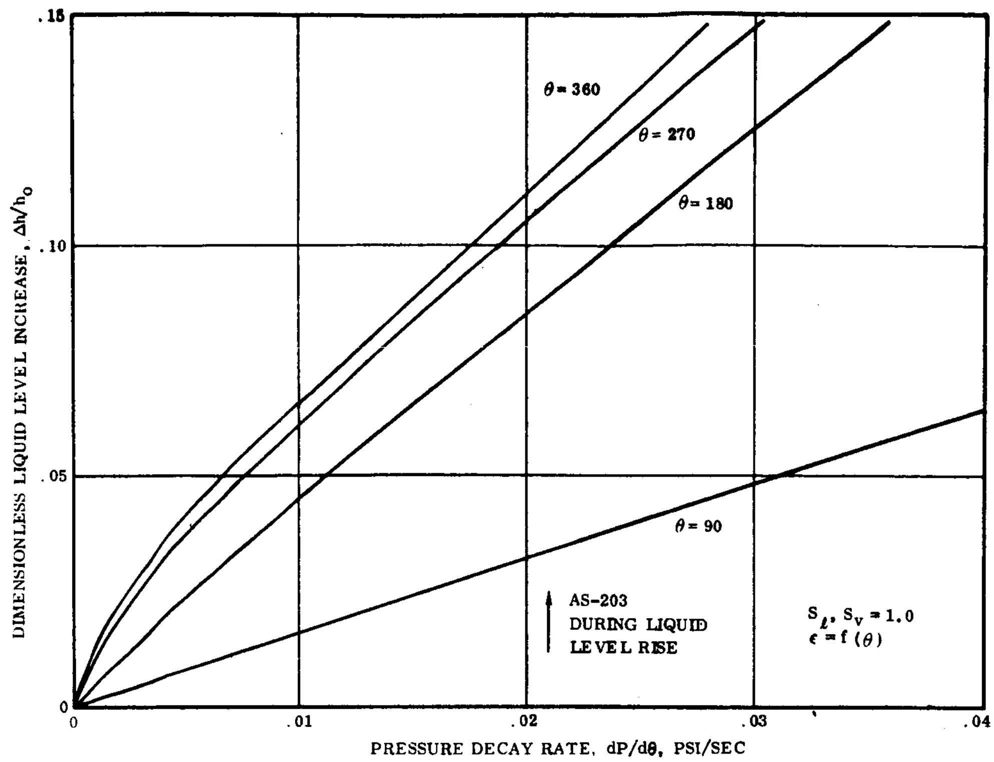

Figure 4-17. Dimensionless Liquid Level Increase Dependence on Pressure Decay Rate

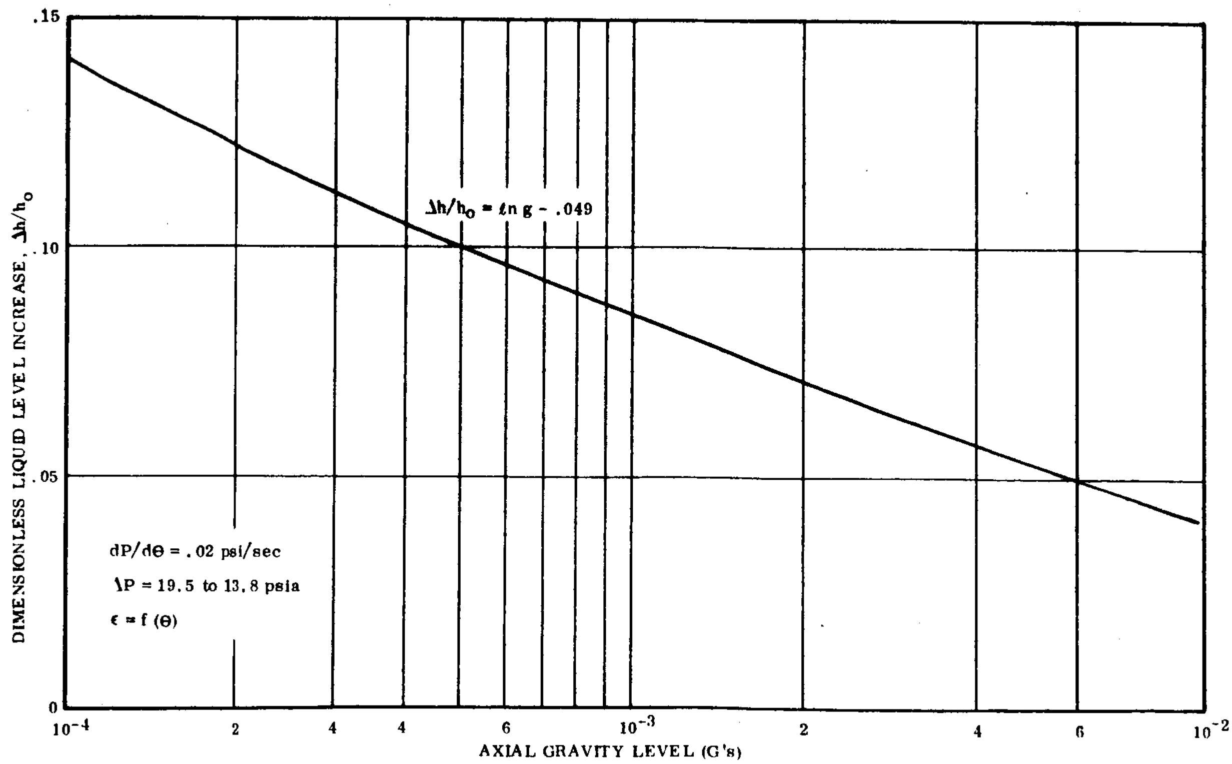

Figure 4-18. Dimensionless Liquid Level Increase Dependence on g-Level

in surface tension forces acting on the bubble. The resultant bubble motion from these forces in a finite medium is considered. Interaction between bubbles, agglomeration, and bubble wake effects are considered.

4.4.1 ANALYTICAL MODEL. Heat transfer to the propellant is defined by the liquid level, its orientation, and energy transport mechanisms at the tank wall. The latter necessitates a specification of boiling parameters, e.g. number of sites, radius of each site, and frequency of production at each site.

The propellant moments of inertia and the liquid location are determined by the spatial distribution of voids, heat transfer and void generation, surface orientation, and pressure transient of the tank contents. Additional requirements for void distribution description are generated by propellant venting and outflow problems, e.g. vapor entrainment.

A computer program has been developed to give rigorous definition of the previously mentioned variables. The resulting computer program (EVOLVE) describes the temporal and spatial evolution of a bubble society. The CDC 6400 code, developed under company funds, is listed in Appendix C. The phenomenological considerations which are embodied in the program are

1. Bubble generation with time and spatial dependent radii and frequencies.

2. Kinematics and energetics of a single bubble moving in temperature and inertial acceleration fields in three dimensions.

3. Time and spatial dependent temperature and inertial acceleration fields.

4. The effect of wake behind a bubble on following bubbles.

5. Bubble agglomeration.

6. Slip or no-slip interaction with tank walls.

7. Interaction of a single bubble with porous walls (screens).

8. Vaporization (2 ways).

   a. Nucleate boiling as mentioned.

   b. "Bulk" boiling due to change in state of liquid (pressure decay) - this vapor generation is divided between the liquid-ullage interface and the existing bubble population in proportion to relative surface areas.

9. Liquid energy conservation, outflow, and level determination.

10. Convective heat transfer to liquid phase which is dependent on liquid level.

The program is designed to consider populations of up to 1,000 bubbles, three dimensional transport, bubble dependent surface orientation (not necessarily normal to inertial acceleration vector), and time dependent ullage pressure history. Analytical treatments of the above phenomena which are incorporated in the program are described in the following sections.

4.4.1.1 Single Bubble Dynamics. The motion of a bubble moving in a liquid with noncolinear gravitational and temperature fields is considered by summing the body and surface forces acting on the bubble, neglecting the bubble inertia.

$$\vec{F}^{B} + \vec{F}^{ST} + \vec{F}^{D} = 0 \tag{4-48}$$

$\vec{F}^{B}$ ≡ buoyant force

$\vec{F}^{ST}$ ≡ surface tension force resulting from liquid temperature gradient

$\vec{F}^{D}$ ≡ liquid-bubble momentum exchange (drag)

The equation of motion for a bubble, neglecting inertia (implies terminal velocity), is written as the difference form of the time integral of velocity

$$\delta \vec{x} = \bar{\vec{v}}_B \, \delta t \tag{4-49}$$

$\delta \vec{x}$ ≡ vector change in position

$\bar{\vec{v}}_B$ ≡ average velocity

δt ≡ time increment

The buoyant force is given (for nearly spherical bubbles)

$$\vec{F}^{B} = \left[\frac{4}{3} \pi R_B^3 g (\rho_\ell - \rho_g) \right] \hat{e}_g \tag{4-50}$$

Consideration of the effect of a surface tension gradient on bubble motion requires conceptual investigation of the principles of interfacial phenomena. The interface is a thin film which is elastic but not plastic (it may not flow), Reference 4-10, for no circulation within the bubble. The bubble is treated as an inertialess void. The normal traction, therefore, establishes the surface topology and has no accelerative effect on the bubble. A confined liquid segment, on the other hand, would have an induced pressure gradient corresponding to the surface tension gradient and would cause the liquid to flow. The tangential tractions will accelerate the bubble since the interfacial surface cannot flow. The result for an axially symmetric surface is given by Reference 4-11 as

$$\vec{F}^{ST} = -\iint \Delta \underline{\underline{T}} \cdot \vec{n}_T \, dS \equiv \text{acceleration due to surface effects} \tag{4-51}$$

$\Delta \underline{\underline{T}} \equiv$ net surface traction tensor

$\vec{n}_T \equiv$ unit tangent vector to surface

For an axially symmetric surface and surface tension gradient

$$\Delta \underline{\underline{T}} \cdot \vec{n}_T = (\vec{\nabla}\sigma \cdot \vec{n}_T)\, \vec{n}_T \tag{4-52}$$

For small changes in bubble radius with polar angle

$$\Delta \underline{\underline{T}} \cdot \vec{n}_T \simeq \left[\frac{\partial \sigma}{\partial R_B} \left(\frac{1}{R_B} \frac{\partial R_B}{\partial \theta} \right) + \frac{1}{R_B} \frac{\partial \sigma}{\partial \theta} \right] \vec{n}_\theta \tag{4-53}$$

The bubble radius for an axial symmetric bubble is given by the balance of normal surface traction forces across the bubble surface, this is constant since the surface is not growing,

$$\frac{\sigma}{R_B} = \frac{\sigma_o}{R_{B_o}} = \text{constant} \tag{4-54}$$

which defines the bubble radius or topology. For an axial temperature field

$$\sigma = \sigma_o + R_B \cos\theta \frac{\partial \sigma}{\partial T} \frac{\partial T}{\partial Z} \tag{4-55}$$

$$\frac{\partial \sigma}{\partial R} = \cos\theta \frac{\partial \sigma}{\partial T} \frac{\partial T}{\partial Z} \tag{4-56}$$

From equation 4-54

$$\frac{1}{R_B} \frac{\partial R_B}{\partial \theta} = \frac{R_{B_o}}{\sigma_o R_B} \frac{\partial \sigma}{\partial \theta} \tag{4-57}$$

Equation 4-53 becomes

$$\Delta_{\underline{\underline{T}}} \cdot \vec{n}_T \cong \frac{1}{R_B} \frac{\partial \sigma}{\partial \theta} \left[\cos\theta \frac{\partial \sigma}{\partial T} \frac{\partial T}{\partial Z} \frac{R_{B_o}}{\sigma_o} + 1 \right] \vec{n}_\theta \tag{4-58}$$

From symmetry, only the axial component of force survives

$$F_Z^{ST} = \iint (\nabla\sigma \cdot \vec{n}_T) \sin\theta \, ds \tag{4-59}$$

$$\frac{1}{R_B} \frac{\partial \sigma}{\partial \theta} \cong - \sin\theta \frac{\partial \sigma}{\partial T} \frac{\partial T}{\partial Z} \tag{4-60}$$

$$F_Z^{ST} = - 2\pi \int_0^\pi R_{B_o}^2 \sin^3\theta \frac{\partial \sigma}{\partial Z} \left[\cos\theta \frac{\partial \sigma}{\partial T} \frac{\partial T}{\partial Z} \frac{R_{B_o}}{\sigma_o} + 1 \right] d\theta \tag{4-61}$$

To first order, equation 4-61 yields,

$$F_Z^{ST} = - \frac{8\pi}{3} \frac{\partial \sigma}{\partial T} \frac{\partial T}{\partial Z} R_{B_o}^2 \tag{4-62}$$

Equation 4-62 is for a nearly spherical gas volume with a single surface (bubble). The vector form of (4-62) is

$$\vec{F}^{ST} = - \frac{8\pi}{3} \frac{\partial \sigma}{\partial T} R_{B_o}^2 \vec{\nabla} T \tag{4-64}$$

The drag force is given by

$$\vec{F}_D = - C_D \rho_\ell \frac{v_B^2}{2} (\pi R_B^2) \hat{e}_v \tag{4-64}$$

The velocity vector direction is given by the vector sum of forces (equation 4-48),

$$\hat{e}_v = \frac{\{\vec{F}^{ST} + \vec{F}^B\}}{|\vec{F}^{ST} + \vec{F}^B|} \tag{4-65}$$

In order to define the drag coefficient, it is necessary to review the kinematics of bubble drag. Three regions of interest are considered

I Spherical Particle
II Nearly Spherical Particle
III Deformable Body and the Transition Region

Region I is commonly known as Stokes drag region for spheres; the Reynolds number interface for Regions I and II occurs at Re $\approx$ 2, Reference 4-12. Region II is for nearly spherical particles and is the same functional relationship as Region I with different constants. The Reynolds number interface for Regions II and III is a function of fluid parameters and is defined by the intersection of the drag function in Region II with the functional relationship in Region III. Typical values of Re at the intersection are 80-400. The evaluation of the region separation and functional dependences in each region are based on extensive study and comparison of data contained in References 4-8 and 4-12. Considerable scatter and conflict in data preclude a more definitive evaluation. In Regions I and II, the drag coefficient is a simple function of Reynolds No.

$$C_D = a\ Re^n \tag{4-66}$$

The velocity is defined by

$$v_B = \left[\frac{\mu_\ell}{2R_B\rho_\ell}\right]\left[-\frac{64R_B^2\rho_\ell\frac{\partial\sigma}{\partial T}(\vec{\nabla}T\cdot\hat{e}_v)}{3\ a\ \mu_\ell^2}+\frac{32\ R_B^2\ \rho_\ell g(\rho_\ell-\rho_g)(\hat{e}_g\cdot\hat{e}_v)}{3\ a\ \mu_\ell^2}\right]^{\frac{1}{2+n}} \tag{4-67}$$

The value for "a" of 24 provides reasonable data correlation for Region I, with n = -1. For Region II, a = 19.7 and n = -.725 are appropriate.

Region III is associated with the onset and growth of surface deformation due to tangential shear stresses. The region embodies both the initial oblate deformation and the final "hemispherical cap" configuration. The drag coefficient is a function of the ratio of accelerative forces ($\vec{F}^B + \vec{F}^{ST}$) to normal surface tension traction; for only buoyant forces, this is the Eötvös or Bond number.

$$N_E \equiv \frac{3\ |\ \vec{F}^B + \vec{F}^{ST}\ |}{\pi\ R_B\ \sigma} \tag{4-68}$$

$$C_D = C_\infty\ (1 - e^{-\lambda N_E}) \tag{4-69}$$

The exponential relaxation of equation 4-69 accommodates the transition to the totally deformed hemispherical cap state. Values of $C_\infty = 2.64$ and $\lambda = 0.13$ were found to give the best correlation with References 4-8 and 4-12. Using n = 0 and a = C_D in equation 4-67, the velocity is prescribed for Region III.

In Region III, the acceleration due to surface tension gradient (temperature field) is reduced because the topological deformation alters the surface integral and traction in equation 4-51 and introduces anisotropic components. However, this force is only important in low-g buoyancy situations; therefore, the alteration for region dependence is neglected.

The effect of finite medium on the velocity is approximately treated by considering the mass conservation equation of the liquid surrounding the bubble in the limited region. The increased relative velocity around the bubble increases the drag and results in a reduced velocity for the bubble in the confined region.

$$\frac{v_{B_A}}{v_{B_\infty}} = \left[1 - \left(\frac{R_B}{R_T}\right)^2\right] \quad (4\text{-}70)$$

where R_T defines a finite radius region. Reference 4-8 shows that this result is approximately correct (it is obviously self consistent). The velocity, actually, falls off somewhat faster for bubbles in region III. For a medium containing many bubbles, the velocity is defined by

$$v_{B_A} \cong v_{B_\infty} (1 - \alpha) \quad (4\text{-}71)$$

where α is the local area fraction of bubbles.

4.4.1.2 Bubble Energy Equation for a Single Bubble. Thermodynamic evolution of a bubble is described by a differential form of the first law energy equation. The gaseous phase inside the bubble is considered to be saturated at the pressure corresponding to the external pressure plus the surface traction. Energy transport (heat and/or mass transfer) between the bubble and liquid phase is considered.

$$0 = m_2 u_2 - m_1 u_1 + \delta m_c \bar{h}_T + \delta m_Q \bar{h}_T - \delta m_V \bar{h}_T + \delta (Pv) \quad (4\text{-}72)$$

for time 1 to time 2, where,

$$\bar{h}_T \equiv \begin{cases} \bar{h}_g \sim \delta m_c < 0,\ \delta m_Q < 0,\ \delta m_V > 0 \\ \bar{h}_{fg} \sim \delta m_c > 0,\ \delta m_Q > 0, \delta m_V < 0 \end{cases}$$

Continuity of bubble mass yields

$$m_2 - m_1 = \delta m_V - \delta m_Q - \delta m_c \quad (4\text{-}73)$$

It is assumed that the bubble remains at saturated gas conditions.

4.4.1.3 Wake Effects. In the study of bubble populations, the velocity field behind a bubble (wake) must be considered in the velocity prescription of bubbles traveling in succession. As an approximate approach, a superposition of wake velocities which interfere with a particular bubble is used. This is quite reasonable for moderately dense populations because the wake relaxes as $(x/d)^{-2/3}$ for axisymmetric bubbles.

The velocity of bubble "i" is given by

$$\vec{v}_B^{\,i} = \vec{v}_{BA}^{\,i} + \sum_{j \neq i} \langle \vec{v}_w^{\,ji} \rangle$$

where

$\vec{v}_w^{ji}$ ≡ wake velocity which interacts with bubble "i" from bubble "j"

The velocity field in the wake of axisymmetric bodies is expressed by a vector representation of the wake velocity

$$\vec{v}_w^{ji} = f_1^{ji} \, \vec{v}_{B_A}^{j} + f_2^{ji} \left[\frac{\vec{R}_{ji}}{|\vec{R}_{ji}|} - \frac{(\vec{R}_{ji} \cdot \vec{V}_{B_A}^{j})}{|\vec{R}_{ji}| \, |\vec{V}_{B_A}^{j}|} \vec{v}_{B_A}^{j} \right] \tag{4-75}$$

where

$\vec{R}_{ji} \equiv \vec{x}^{j} - \vec{x}^{i}$ ≡ relative vector coordinate of bubble (j) with respect to bubble (i)

$\vec{x}$ ≡ position vector of bubble

f_1^{ji} ≡ functional dependence of axial velocity in wake on the relative distance $|\vec{R}_{ji}|$

f_2^{ji} ≡ functional dependence of radial velocity in wake on the relative distance $|\vec{R}_{ji}|$

The terms axial and radial are defined by the velocity vector of the lead bubble (j).

The velocity field behind a single body with axial symmetry has been investigated, Reference 4-13, for turbulent wakes. The consideration of only turbulent wakes is reasonable since laminar wakes occur only for very small bubbles or low velocities where wakes are not important; also, the laminar wake is similar to a turbulent wake in its attentuation, $(x/d)^{-1}$, References 4-10 and 4-14.

The functions f_1^{ji} and f_2^{ji} are

$$f_1^{ji} = |\vec{v}_{B_A}^{j}| \left[0.202 \, C^{-0.8} \right] \left[\frac{C_D \, \pi \, R_B^{j2}}{x_{ji}^2} \right] \left[1 - \eta_{ji}^{3/2} \right]^2 \tag{4-76}$$

$$f_2^{ji} = |\vec{v}_{B_A}^{j}| \left[0.0825 \, C^{-1.067} \right] \left[\frac{C_D \, \pi \, R_B^{j2}}{x_{ji}^2} \right]^{2/3} \eta_{ji} \left[1 - \eta_{ji}^{3/2} \right]^2 \tag{4-77}$$

where

$$x_{ji} \equiv \frac{\vec{R}_{ji} \cdot \vec{V}_{B_A}^{j}}{|\vec{v}_{B_A}^{j}|} \tag{4-78}$$

≡ projection of relative position vector on velocity direction of lead bubble

$$\eta_{ji} \equiv \left| \vec{R}_{ji} - x_{ji} \vec{v}^{\,j}_{B_A} \right| \Big/ b$$ $\equiv$ normalized projection of relative position vector on the direction normal to velocity of the lead bubble (4-79)

$$b \equiv 1.222\, C^{-0.267} \left(C_D \pi R_B^{j2} x_{ji} \right)^{1/3} \tag{4-80}$$

The constant "C" is determined by experimental correlation. A value of C = 0.288 was obtained using data in Reference 4-15.

4.4.1.4 <u>Agglomeration and Tank Wall Interaction.</u> Inter-bubble agglomeration (coalescence) and bubble, liquid-ullage surface coalescence is represented by two equations

$$\left| \vec{R}_{ji} \right| \le \left(R_B^i + R_B^j \right) + \delta_{IMP} \tag{4-81}$$

δ_{IMP} $\equiv$ impact parameter for bubble collisions

$$\left| \vec{R}_{is} \right| \le R_B^i + \delta_{IMP}^s \tag{4-82}$$

δ_{IMP}^s $\equiv$ impact parameter for bubble-surface collision

$\vec{R}_{is}$ $\equiv$ vector from bubble center normal to liquid-ullage surface

Equations 4-81 and 4-82 define conditions for agglomeration to occur; for inter-bubble collision, the resulting bubble is positioned at the center of mass of the two original bubbles. Observation of coalescence indicates that

$$\delta_{IMP}^s = \delta_{IMP} = 0$$

Bubble collisions with the confining walls of the tank result in one of two possible situations: free slip, no slip.

$$\text{Free Slip} \sim \vec{v}_B \cdot \vec{n} \Big|_{WALL} = v_{B_n} \Big|_{WALL} = 0$$

$$\text{No Slip} \sim \vec{v}_B \Big|_{WALL} = 0$$

In the first situation, the bubble hits the wall and travels along a geodesic of the surface; for the second situation, the bubble strikes the wall and remains at the point of impact.

Another consideration is that the wall may be porous and the bubble could possibly escape; this is determined by the relation of the normal force of bubble at the container wall to the surface tension retardation force provided by the wall pores. If the normal force is greater than the combined surface tension forces of all involved pores, then the bubble "escapes" and is lost forever; if the normal force is less, the bubble is retained.

4.4.1.5 Vaporization. There are two mechanisms for vapor generation: nucleate boiling, and "bulk" boiling. For nucleate boiling, the site, the time dependent initial radius, and the time dependent frequency of production are input to the program. The mass of vapor produced is subtracted from the liquid phase and a new bubble is born.

Boiling which is the result of change in thermodynamic state of the liquid (bulk), e.g., pressure decay and convective heat transfer, is added to the existing voids, including the ullage space, in proportion to liquid-gas interfacial areas.

$$\delta m_V^i = \frac{C_A(4\pi R_B^{i2})\,\delta m_{LV}}{\left[A_s + 4\, C_A\, C_{DEG} \sum_j (\pi R_B^{j2})\right]} \tag{4-83}$$

where

δm_{LV} = liquid phase mass change due to vaporization

A_s = liquid-ullage interface area

δm_V^i = mass addition to i^{th} bubble

C_A ≡ arbitrary weighting factor

C_{DEG} ≡ degeneracy factor for considering only a sector

The parameter C_A permits alteration in the partitioning of vapor production between bubbles and the ullage space. The degeneracy factor is an antifact which represents an axisymmetric container and void distribution as a degenerate sector of the cross section. In other words, only the evolution of voids in one degenerate sector need be considered if all forces obey the same symmetry rules as the container and the voids do not out grow this sector. The program uses C_{DEG} to keep track of gas, liquid phase and volume changes to insure the satisfaction of conversation requirements.

$$C_{DEG} = \frac{2\pi}{\text{SECTOR ANGLE (RADIANS)}} \equiv \text{INTEGER QUANTITY} \tag{4-84}$$

Observations of boiling due to pressure reduction indicate that existing voids increase appreciably in size and that some new nucleation sites appear on the walls; however, there is no evidence that new bubbles are created internal to the liquid phase providing that no incipients are present, e.g. gases in solution, solid particles, and other contaminants. The latter could be input as additional nucleation sites.

4.4.1.6 Liquid Energy Conservation and Level Determination. The liquid phase energy conservation is defined by a differential first law energy equation. The pressure history is a given function of time (input).

$$\delta Q_{\ell} = m_{\ell_2} u_{\ell_2} - m_{\ell_1} u_{\ell_1} + \bar{h}_{\ell}\, \delta m_o + \bar{h}_{fg}\, \delta m_{LV} \qquad (4\text{-}85)$$

where

δQ_{ℓ} ≡ convective or conductive heat transfer to liquid (input per unit liquid height)

$\delta m_o = \delta m_{FO} - \delta m_c - \delta m_Q$

Mass conservation yields,

$$m_{\ell_2} - m_{\ell_1} = \delta m_o + \delta m_{LV} \qquad (4\text{-}86)$$

Because of the arbitrary surface angle (function of time) and the various axisymmetric tank configurations, the liquid level is calculated every time step by an iterative method. The convective or conductive heat transfer to the liquid is input per unit liquid height; therefore the program explicitly calculates the feedback effect of changing heat input with liquid level.

4.4.2 DEMONSTRATION PROBLEM FOR S-IVB LIQUID LEVEL RISE. As an illustration of the program EVOLVE, a problem was chosen which simulates the S-IVB liquid hydrogen tank in the settled condition at $\sim 3 \times 10^{-4}$ g. The problem simulates depressurization at 14,342 seconds in the AS-203 experiment. The tank was despresurized at the rate of 1.9 psi/min from 19.5 psia. The initial propellant mass was 16,300 lb_m. Thirteen sites were distributed between four radial planes and the bottom center of the tank; each site producing a one-inch diameter bubble per second.

Figure 4-19 illustrates the effects of agglomeration and wakes on the number of bubbles existing at any time; at the end of 30 seconds, there are nearly twice as many bubbles with wake interactions as there are without wakes. The reason is that the bubbles are drawn away from the site by the additional velocity increment inhibiting agglomeration; in some cases, however, the opposite effect could occur. The effect of agglomeration is shown by the difference in the number produced and the number present (the ratio 390:30 for a case without wakes).

Figures 4-20 and 4-21 depict a particular radial plane with three sites plus the site at the origin after an elapsed time of 30 seconds, for cases of wake and no wake interactions, respectively.

With the problem solution known to 30 seconds for the 180 second blow down, it was apparent that a symmetrical solution was developing which could be approximated by considering only a corner bubble site with thirteen sites spaced around the tank perimeter. The solution to this problem with wakes, which are considered important, was continued for a set-up with a degeneration factor of 13. This approach neglects the interactions at the five feet generation site location on the same radii, however, this effect is of minor significance. It is, nonetheless, important to represent 13 sites versus 1 site because of the important effects of void areas which affect bubble velocity and liquid level rise, which in turn causes longer travel before the

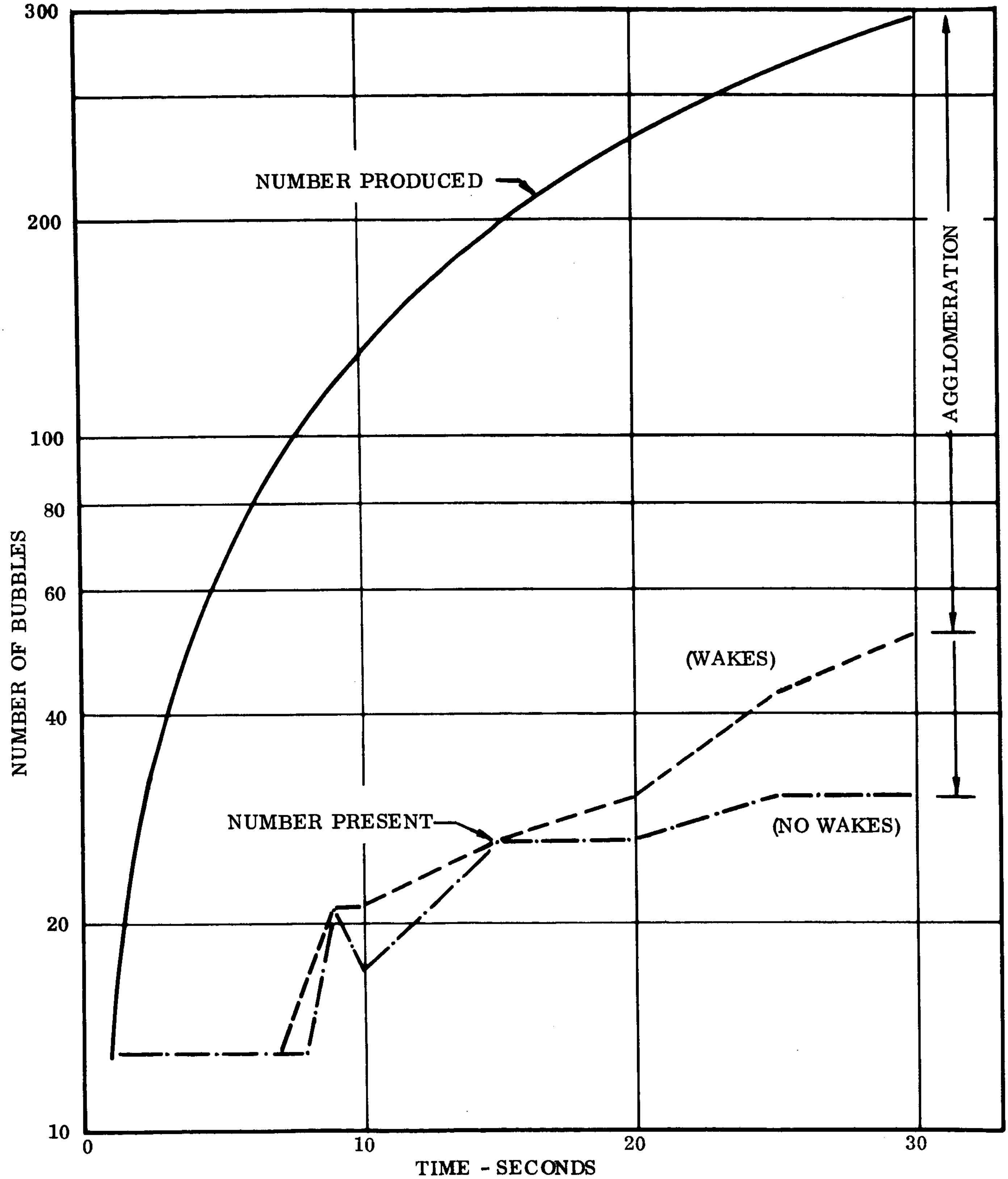

Figure 4-19. Bubble Population Produced Compared to Number Existing After Agglomeration for Wake and No Wake Cases as a Time-Dependent Function

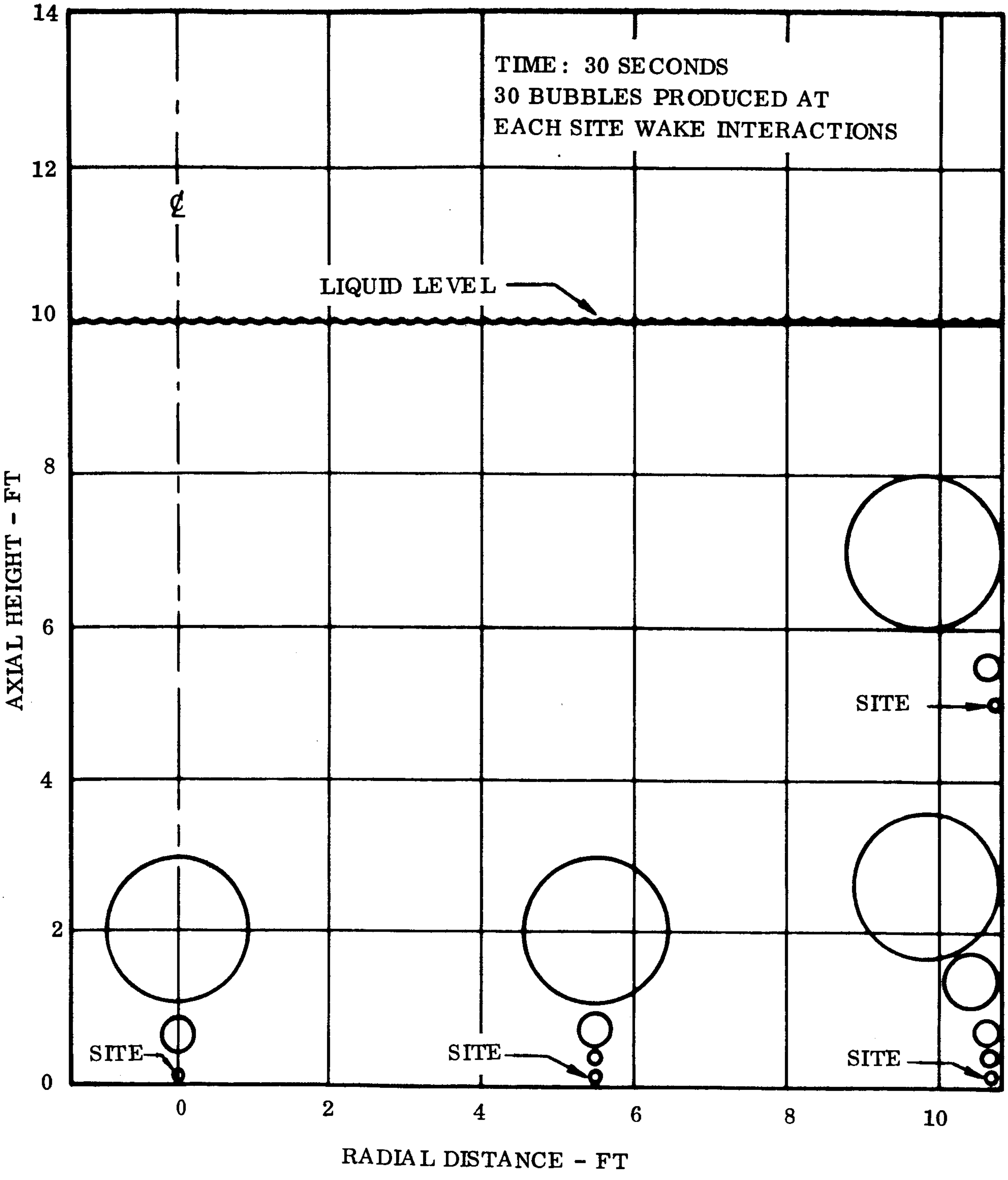

Figure 4-20. Bubble Distribution After 30 Seconds in a Typical Radial Plane of S-IVB For Wake Interaction Case

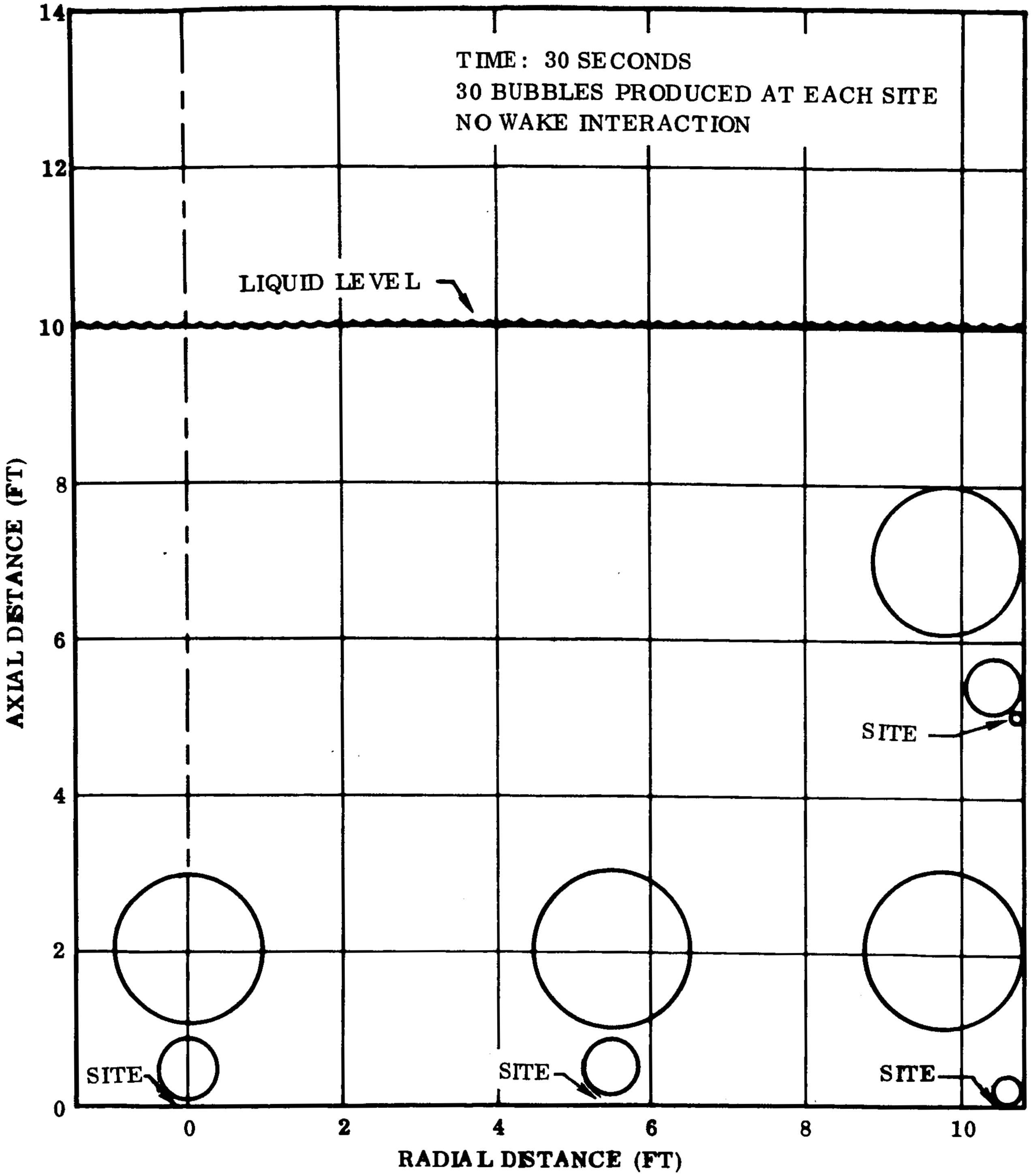

Figure 4-21. Bubble Distribution After 30 Seconds in a Typical Radial Plane of S-IVB for No Wake Interaction Case

bubble breaks the surface. It is quite interesting that agglomeration for the entire period limits the bubble population to only 143 bubbles, while a total of 1560 were generated. The bubble population growth rate is depicted in Figure 4-22; it is noted agglomeration results in only 117 bubbles (9 per site) at problem end time of 122.4 seconds. The calculation interval for this study was 0.2 second with a one-inch bubble generated on the tank bottom each second.

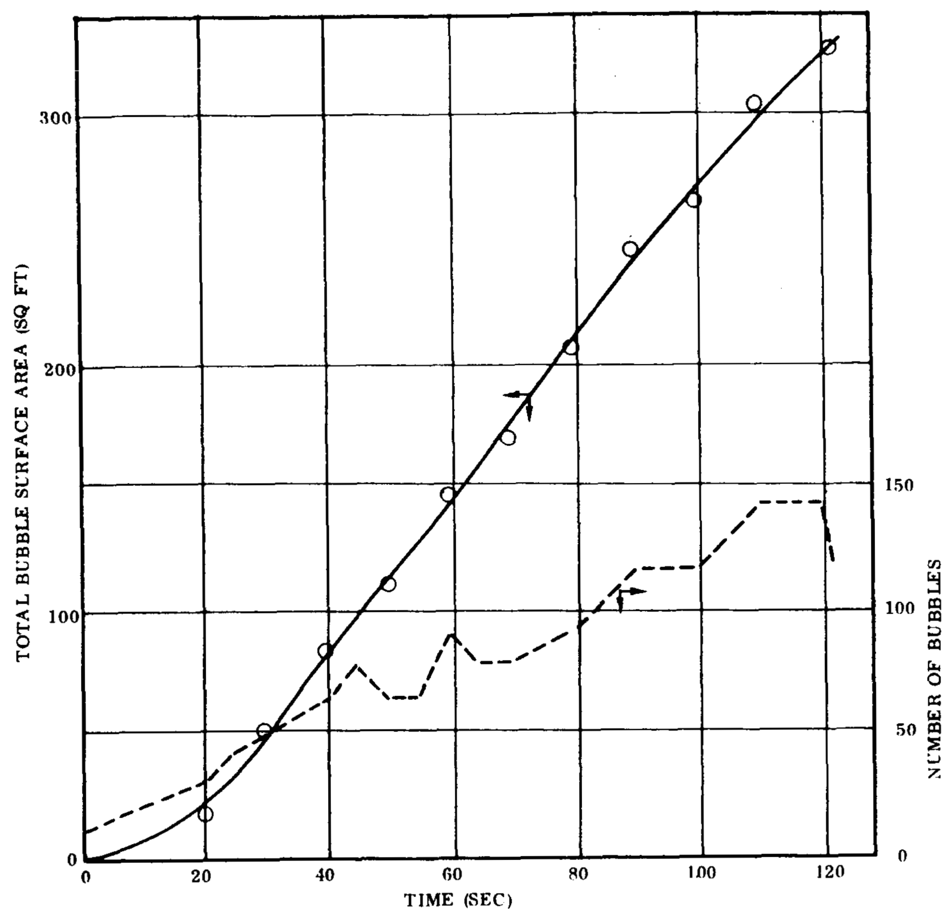

Figure 4-22. Bubble Population and Areas for S-IVB Simulation

For this solution of the AS-203 blowdown, all liquid/vapor surfaces, i.e. interface and bubbles were weighted equal for their vaporization potential. A parameter permits weighting the above two surfaces differently. It was indicated earlier that a preferred ratio of bubble generation sites may be based on bubble surface area rather than wall area. Such a parameter can be generated from the bubble surface area curve presented in Figure 4-22. The shape of this curve is influenced by agglomeration as well as void fraction and bubble velocity. It is shown that in the 120 second period, for the parameters assigned, no bubbles broke the surface. It is estimated some cyclic steady state condition might develop after a period of several minutes.

These results can be related to the liquid level rise problem by means of the volume of bubbles entrapped at any time. The volume history entrapped for the thirteen sites assumed for this problem is presented in Figure 4-23. The liquid level rise for the

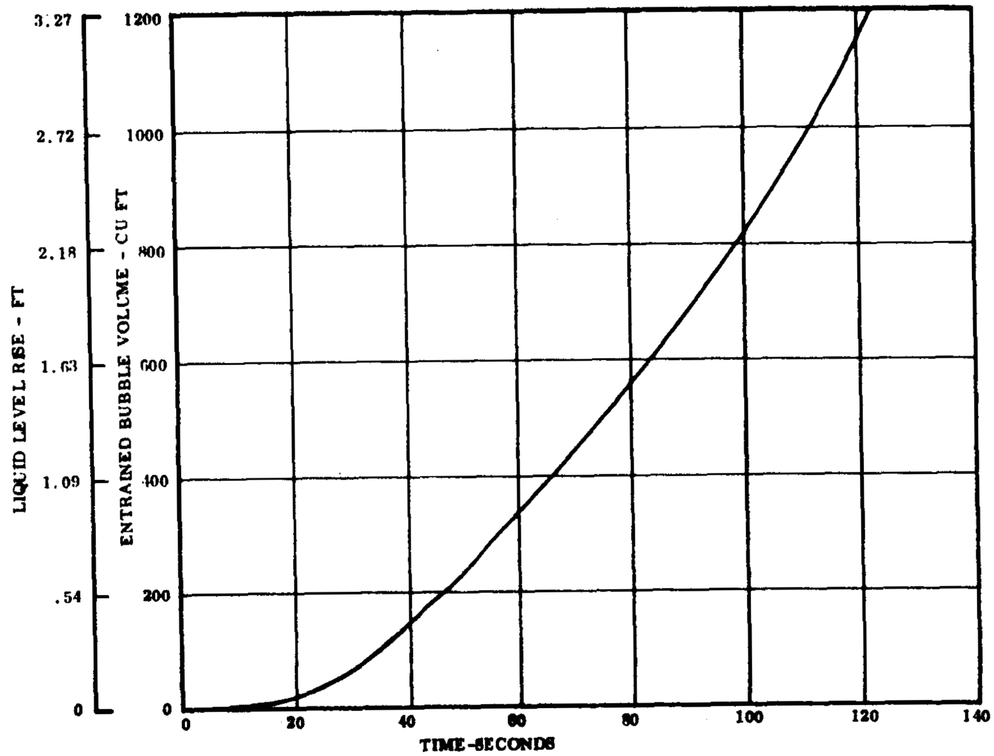

Figure 4-23. Liquid Level Rise and Entrained Volume for S-IVB Simulation

S-IVB - AS-203 vehicle is also presented. It appears this may approach a worse case analysis, since an assumption of a larger number of generation sites would result in less bubble interference due to void fraction ultimately resulting in bubbles which would rise faster and depart the liquid surface at an earlier time. The computer program EVOLVE computes bubble velocity with Equation 4-67; for $Re > 5000$, the increase in velocity is proportional to the square root of the radius; however, a decrease in velocity occurs due to local area fraction proportional to bubble radius squared, Equation 4-73. To illustrate this further, the diameter and velocity of the uppermost bubble is presented versus time in Figure 4-24. Recall that with bubbles of this size, a total of thirteen at the same tank height, the void fraction effect is a strong factor in decreasing bubble velocity.

It is illustrative to consider the population of bubbles at any given time in the tank generated by a single representative site. The print cycle period of ten seconds disclosed a range of 2 to 11 bubbles present per generation site. It is relatively

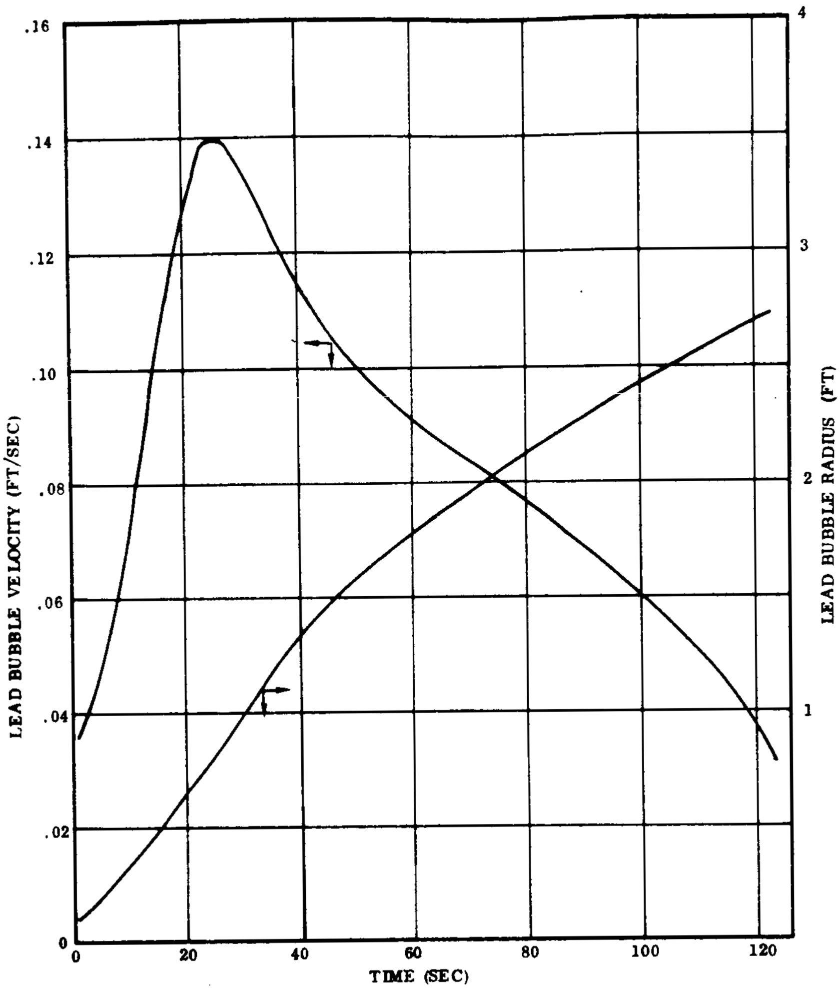

Figure 4-24. Lead Bubble Characteristics for S-IVB Simulation

simple to trace the upward trajectory of the first bubble; however, later bubbles move faster within its wake and agglomerate making bubble identification difficult. The overview of this population is presented in Figure 4-25 with the approach to the rising liquid surface indicated. It is estimated the upper bubble will break the surface prior to 180 seconds resulting in a liquid level collapse of several feet. Formulation of the problem with generation rate, number of sites, and degeneracy (scaling) factor of thirteen resulted in an impossible geometric configuration within confines of the S-IVB which limits 13 bubbles around the perimeter to approximately 2.09 feet radius. Agglomeration in a lateral direction, not accounted for in a degenerate solution, would have modified the results if 13 physical sites had been used. In summary, the above problem gives representative results which are conservative while demonstrating the potential of the computer model. Parametric tradeoffs would include increasing generation sites and rates to increase total bubble area and bubble velocities while reducing individual bubble sizes. A more random generation pattern would also result in higher velocities by resulting in an overall reduced void fraction.

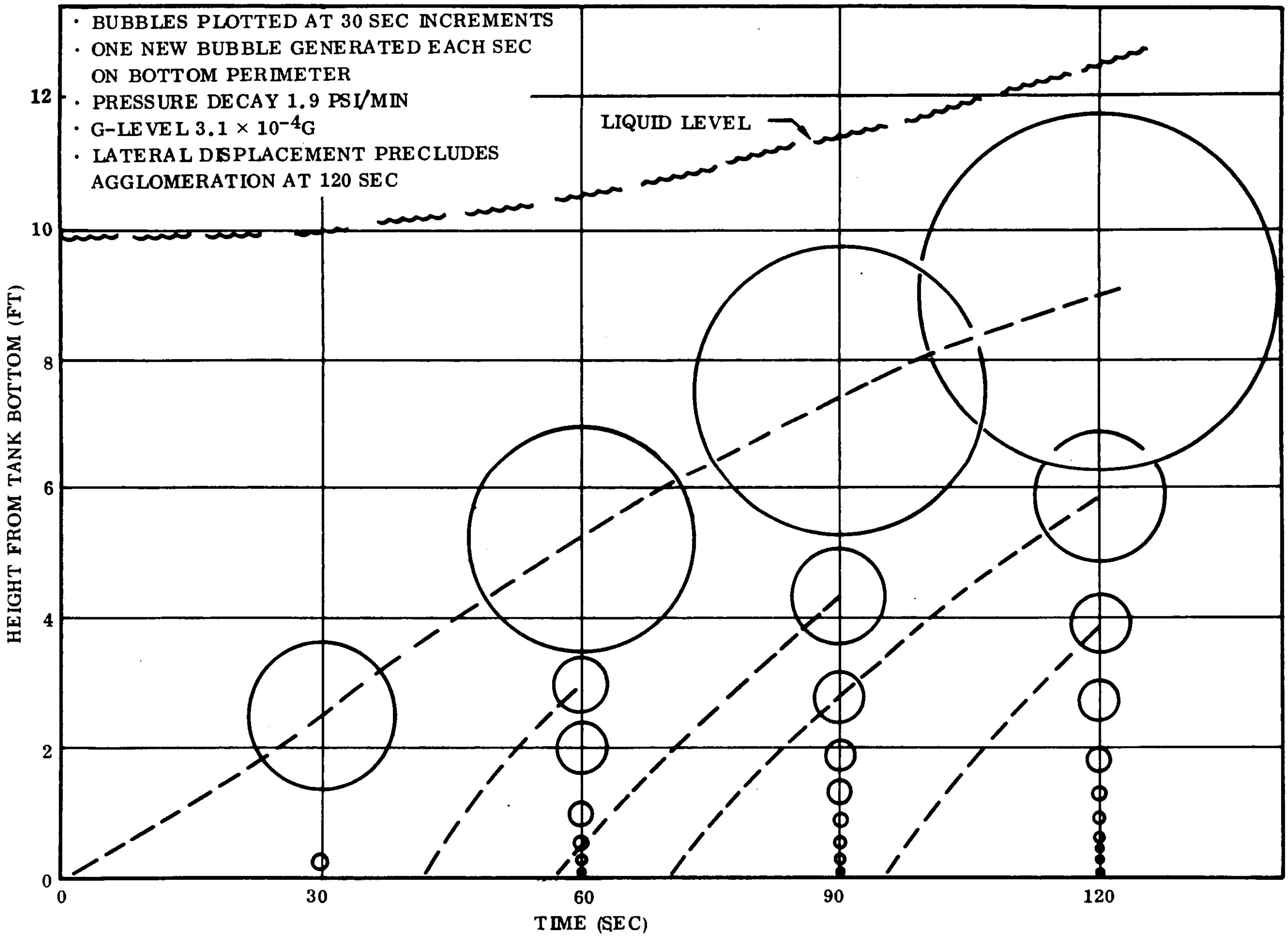

Figure 4-25. Important Effects of Bubble Agglomeration and Void Fraction in Finite Media Define Bubble Trajectories

4.5 LIQUID LEVEL RISE CONCLUSIONS AND RECOMMENDATIONS

The analtyical model LIQLEV developed for liquid level rise confirms the observed absence of level rise on AS-203. This model adequately determines the anticipated phenomena for parametric conditions other than AS-203. The model represents the growing boundary layer fed by evaporation of the saturated bulk and gives the steady state boundary layer conditions. A rapid vent down with less than approximately 20 percent ullage for the rates discussed here could result in liquid level rise to the vent. The analytical model should be used to define the particular case in question. This program can be used in conjunction with Program EVOLVE for the analysis of bubble phenomena resulting in liquid level rise. The gross analytical model, LIQLEV, is much more economical to use than Program EVOLVE, typical cases requiring less than one minute of CDC 6400 time. The analytical model represents a considerable improvement over earlier models given in the literature (Ref. 4-1 and 4-4). In particular, it considers the residence time of the bubble in the boundary layer as well as distributing the evaporative surface between the bulk liquid/ullage interface and the bubble interfacial area. The parametric studies conducted with this model are representative of the design information which can be acquired from the model.

The bubble dynamics program, EVOLVE, developed at Convair under company-funded research, supplements the above liquid level program. EVOLVE meticulously computes the dynamics of the bubbles in a low-g field considering wake effects and agglomerations. These latter two effects have been shown to be important in defining the bubble population, residence time, and surface area/volume ratio for the entrained gas. Recent program verification with one-g test data in Freon 11 lends confidence to the model. A pressing need exists for verification of this model with low gravity bubble dynamic data. The model will serve as a valuable tool for analysis of robtial propellant behavior including experiments. All potentials of Program EVOLVE have not been fully explored. Bubble phenomena in long term low-g storage is a major factor in predicting heat transfer and pressure rise evaluation. A continuing program in this area of low-g bubble phenomena is required.

A phenomena which is not understood or predicted by either of the above programs is the interface break-up into globules in low-g. Forces which are negligible in one-g have been observed in AS-203 films to cause globules to be thrown into the ullage and possibly out through the vent systems. A study to define size and velocity of the globules as a function of forces and gravity level is required. The effects of the unbalanced thrusting from venting liquid may exceed the significance of the mass loss. An evaluation of interface forces such as sloshing and inertia forces related to emerging bubbles should be examined. A model should be formulated which would predict globule size and velocity as a function of interface disturbances or forces. It is recommended further analysis be conducted in this area to define this gravity-sensitive phenomena.

5

PROPELLANT CONTROL AND SETTLING ANALYSIS

Propellant control and settling analysis studies are based on an analysis of propellant sloshing dynamics. The sloshing dynamics are represented by an equivalent mechanical model obtained from the solution of the hydrodynamic equations (Reference 5-1). An ideal liquid is assumed, i.e., nonviscous, incompressible and irrotational flow. This model is combined with other dynamic elements of the vehicle to study the overall system propellant dynamic behavior. Effects such as stratification or thermally driven motions are not included in this portion of the study. The fundamental difficulty with this model is its assumption of perturbational fluid motion, while the low-g slosh condition is characterized by large displacements of the free liquid surface. The analysis has been divided in two areas; slosh model correlation with drop tower test results and simulation of the AS-203 propellant sloshing/vehicle dynamics.

5.1 PROPELLANT SLOSHING MATHEMATICAL MODEL

The mathematical model used in this analysis is based on the pendulum analogy to duplicate the forces and moments produced by the oscillating propellants. The total propellant mass is divided into two separate masses each treated individually. One mass, the reduced mass, is treated as being rigid; the remaining propellant mass, termed the slosh or pendulum mass, is free to oscillate. The reduced mass, its moment of inertia and center of gravity are used to calculate a new effective vehicle moment of inertia and center of gravity, (Figure 5-1). These values are then used in all subsequent vehicle slosh analyses. Forces and moments produced by propellant sloshing are coupled to the vehicle through the pendulum hinge point. The length of the pendulum is governed by the natural frequency of the oscillating propellants. All sloshing parameters are dependent on the propellant tank geometry and are functions of the undisturbed liquid level within the tank.

In reality an infinite number of slosh modes exists however in practice only one mode is usually considered. All energy pertaining to the propellant liquid is assumed contained in the first mode slosh mass. Splashing, geysering, or breakaway liquid is not accounted for. In addition low-g capillary effects are not included directly. The usual procedure, for low Bond number conditions where capillary effects are significant, is to superimpose the liquid level rise as approximated by the height of the meniscus on the results obtained from the mechanical propellant slosh analogy. This superposition is demonstrated in a later section.

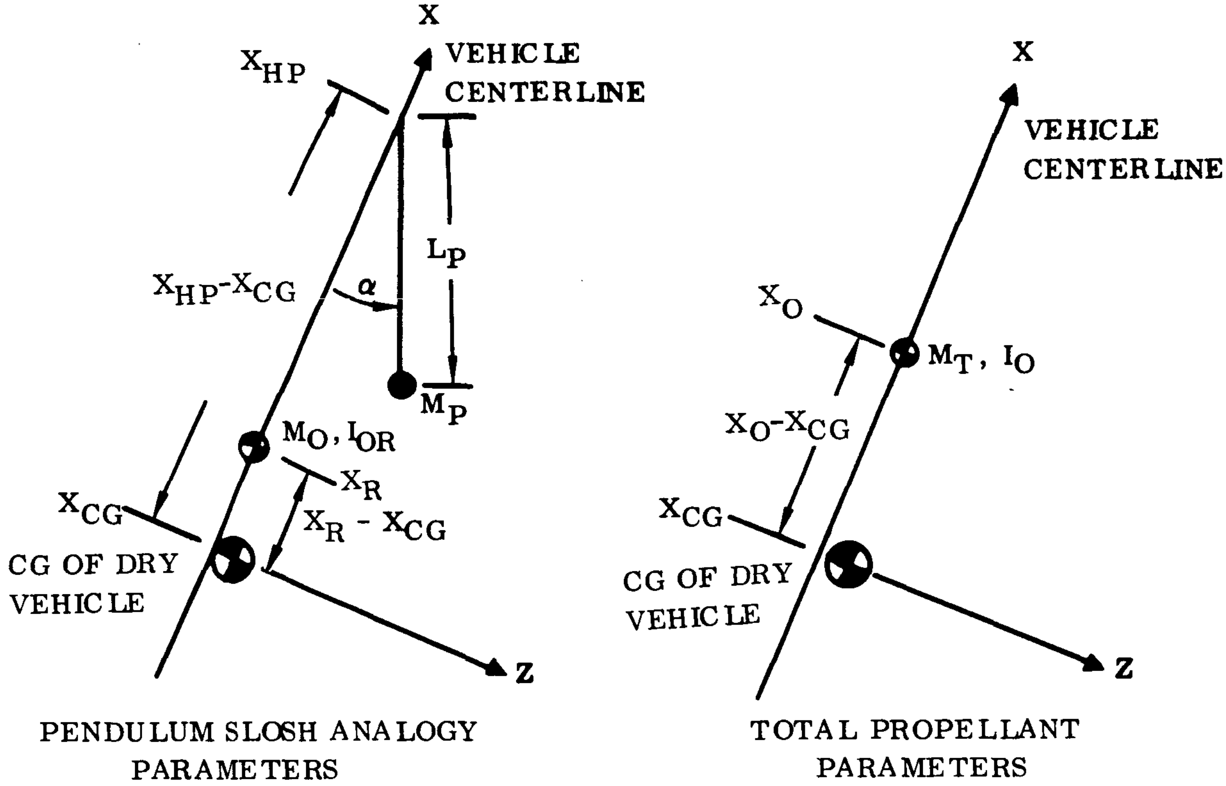

M_T	Total liquid propellant mass.
X_0	Station number of the center-of-gravity of total propellant mass (M_T).
I_R	Moment of inertia of total propellant mass (M_T) treated as a rigid settled mass about its center of gravity (X_0).
M_P	Sloshing propellant mass used as the pendulum mass in the pendulum analogy for first mode sloshing.
M_{P_2}	Sloshing propellant mass used as the pendulum mass in the pendulum analogy for second mode sloshing.
M_O	Reduced propellant mass, the total propellant mass less the first mode slosh mass. $M_O = M_T - M_P$. This mass is added to the vehicle dry weight (vehicle total weight less liquid propellant in the tank) and is treated as a rigid point mass at station X_R.
X_R	Station number of the center of gravity of reduced propellant mass (M_O).
I_{OR}	Moment of inertia of reduced propellant mass (M_O) about its center of gravity (X_R).
X_{HP}	Station number of the pendulum hinge point for first mode slosh.
L_P	Pendulum length used in the pendulum analogy for first mode sloshing.

Figure 5-1. Propellant Sloshing Parameters for Pendulum Slosh Analogy

5.1.1 S-IVB PROPELLANT SLOSHING PARAMETERS. Propellant sloshing parameters have been determined for the liquid oxygen and hydrogen tanks. Figures 5-2 and 5-3 illustrate these parameterss as a function of the propellant interface level. These parameters were obtained from a digital computer program, Ref. 5-2. All mass and moment of inertia parameters are based on an assumed propellant density. To reflect any change in density multiply these data by the ratio of the density change. Note that in both cases the second mode sloshing mass (Mp_2) is insignificant relative to that of the first mode. In addition to the slosh analogy parameters, the mass, center of gravity, and moment of inertia of the propellant treated as being rigid are also presented.

5.1.2 DROP TOWER MODEL PROPELLANT SLOSHING PARAMETERS. Propellant sloshing parameters for the six inch scale model fuel tank are presented in Figure 5-4. The propellant interface level is given in inches relative to the tank bottom. Note that above approximately 4 inches bottom effects are negligible as the slosh mass and pendulum length remain essentially constant until reaching the dome section of the tank forward end.

5.2 BAFFLE DAMPING MATHEMATICAL MODEL

The analytical slosh analysis treats the slosh baffle purely as an energy dissipation device. The propellant motion is not physically constrained. Instead kinetic energy is removed in accordance with the theoretical energy dissipation provided by the baffle. Under this condition the propellant slosh wave remains continuous and is limited in amplitude only as a function of the slosh energy.

The baffle damping expression for a ring baffle in an arbitrary tank with rotational symmetry is obtained from Reference 5-2. The theory is basically an extension of Miles (Reference 5-3) baffle damping equation to include tank bottom effects for any tank with rotational symmetry. The baffle drag coefficient is based on a curve fit to test results obtained from Reference 5-4. Energy losses due to damping are obtained as an instantaneous function of time. This is especially important for the low "g" slosh condition which is characterized by oscillations with long time periods. During coast phase flight the function of the baffle is to damp the liquid oscillations within a very few cycles. Under these conditions where more than 50 percent of the total energy dissipated can be dissipated over the first half cycle, the time averaging process can lead to serious errors in predicting liquid behavior.

The relationship between propellant slosh and energy dissipation is given by:

$$\frac{dE}{dt} = -C_\zeta \frac{|\alpha|^3}{\sqrt{\alpha_{MAX}}} \qquad (5\text{-}1)$$

where α_{MAX} represents the instantaneous maximum pendulum displacement as defined by the instantaneous slosh energy and C_ζ is the baffle energy dissipation

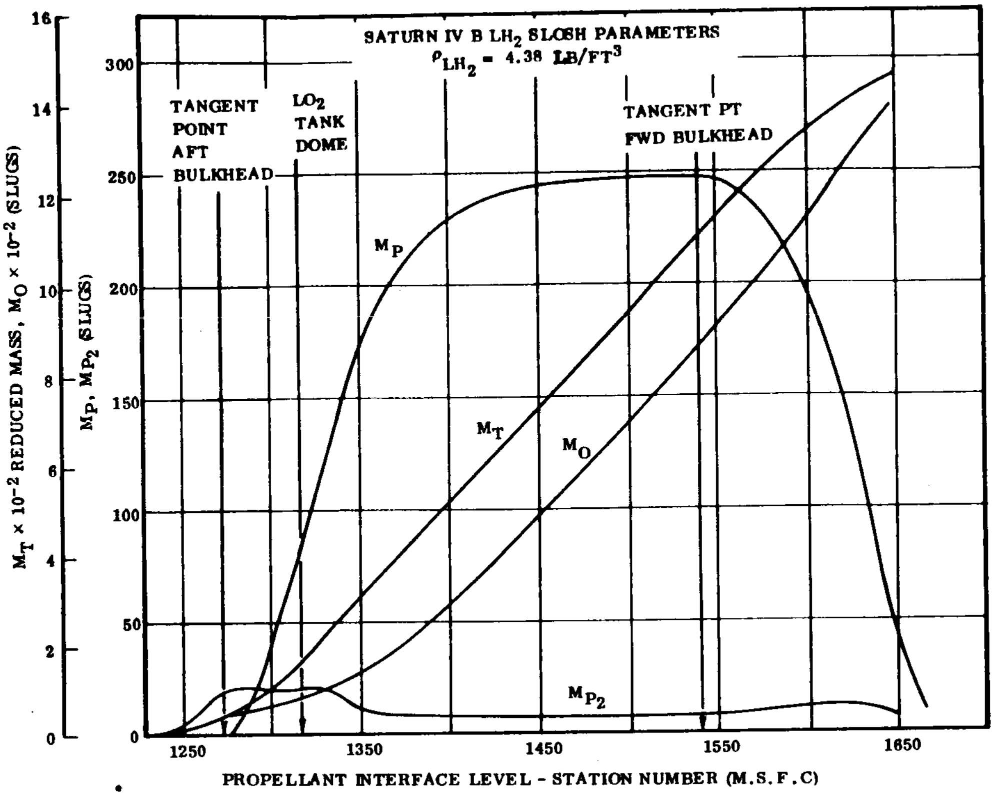

Figure 5-2a. S-IVB Fuel Tank Slosh Parameters as a Function of Propellant Interface Level

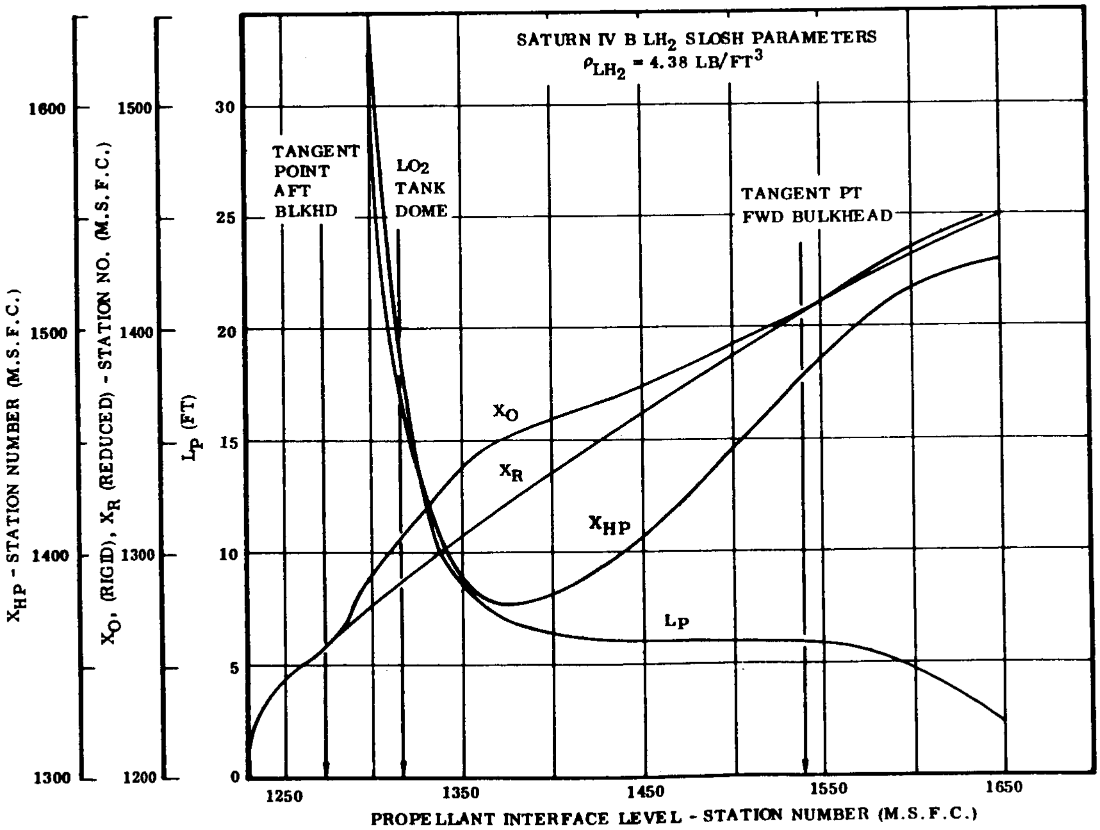

Figure 5-2b. S-IVB Fuel Tank Slosh Parameters as a Function of Propellant Interface Level

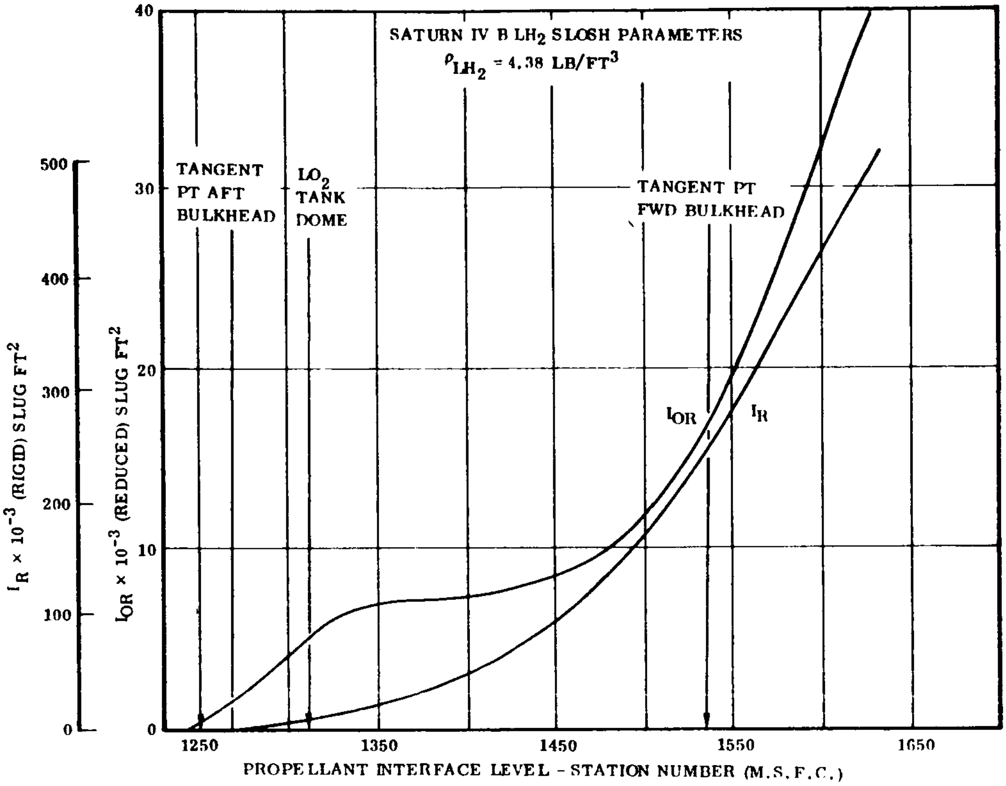

Figure 5-2c. S-IVB Fuel Tank Slosh Parameters as a Function of Propellant Interface Level

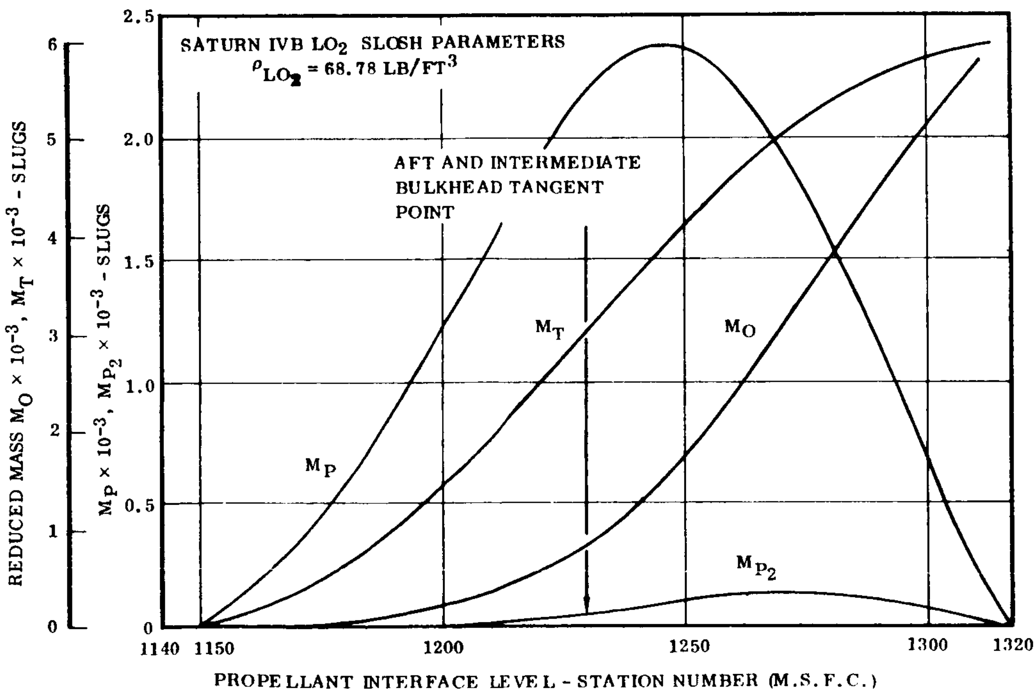

Figure 5-3a. S-IVB Oxidizer Tank Slosh Parameters as a Function of Propellant Interface Level

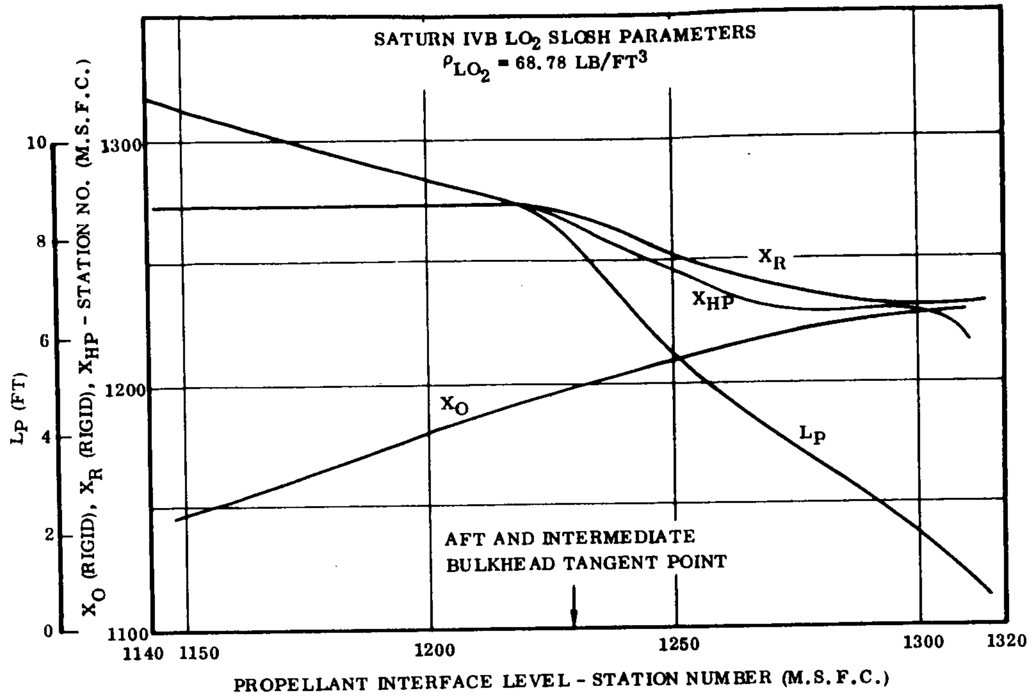

Figure 5-3b. S-IVB Oxidizer Tank Slosh Parameters as a Function of Propellant Interface Level

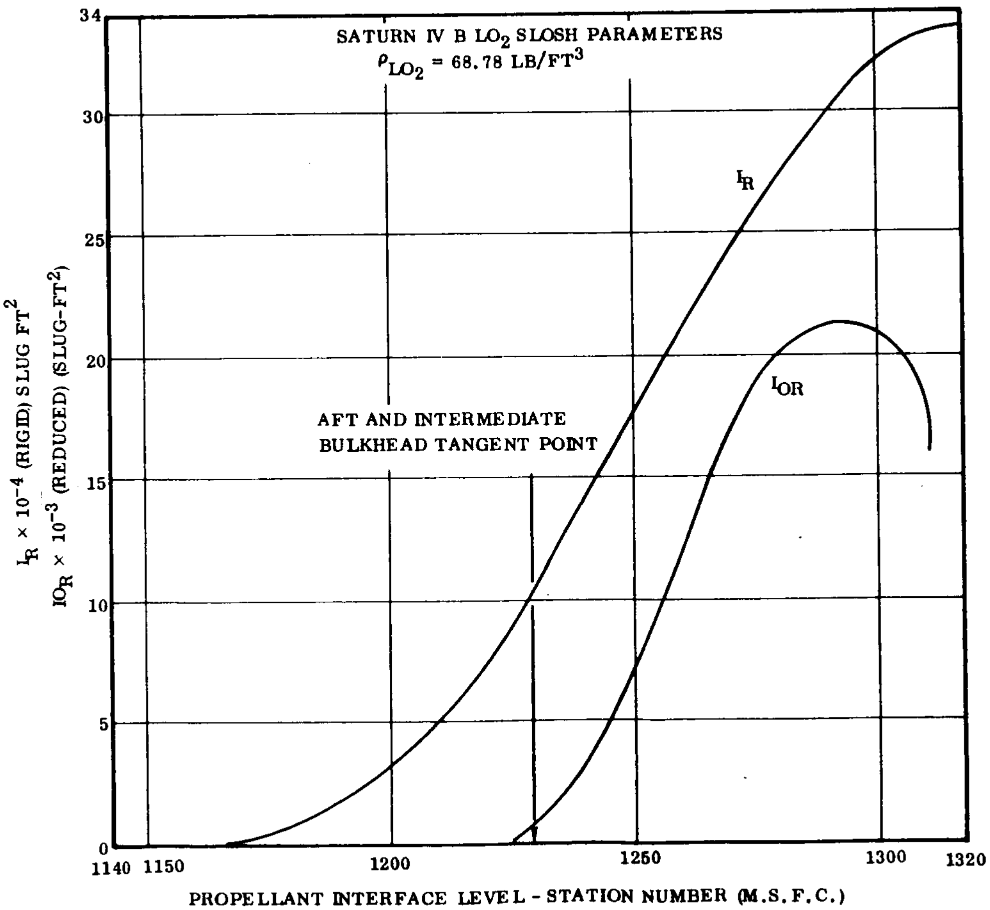

Figure 5-3c. S-IVB Oxidizer Tank Slosh Parameters as a Function of Propellant Interface Level

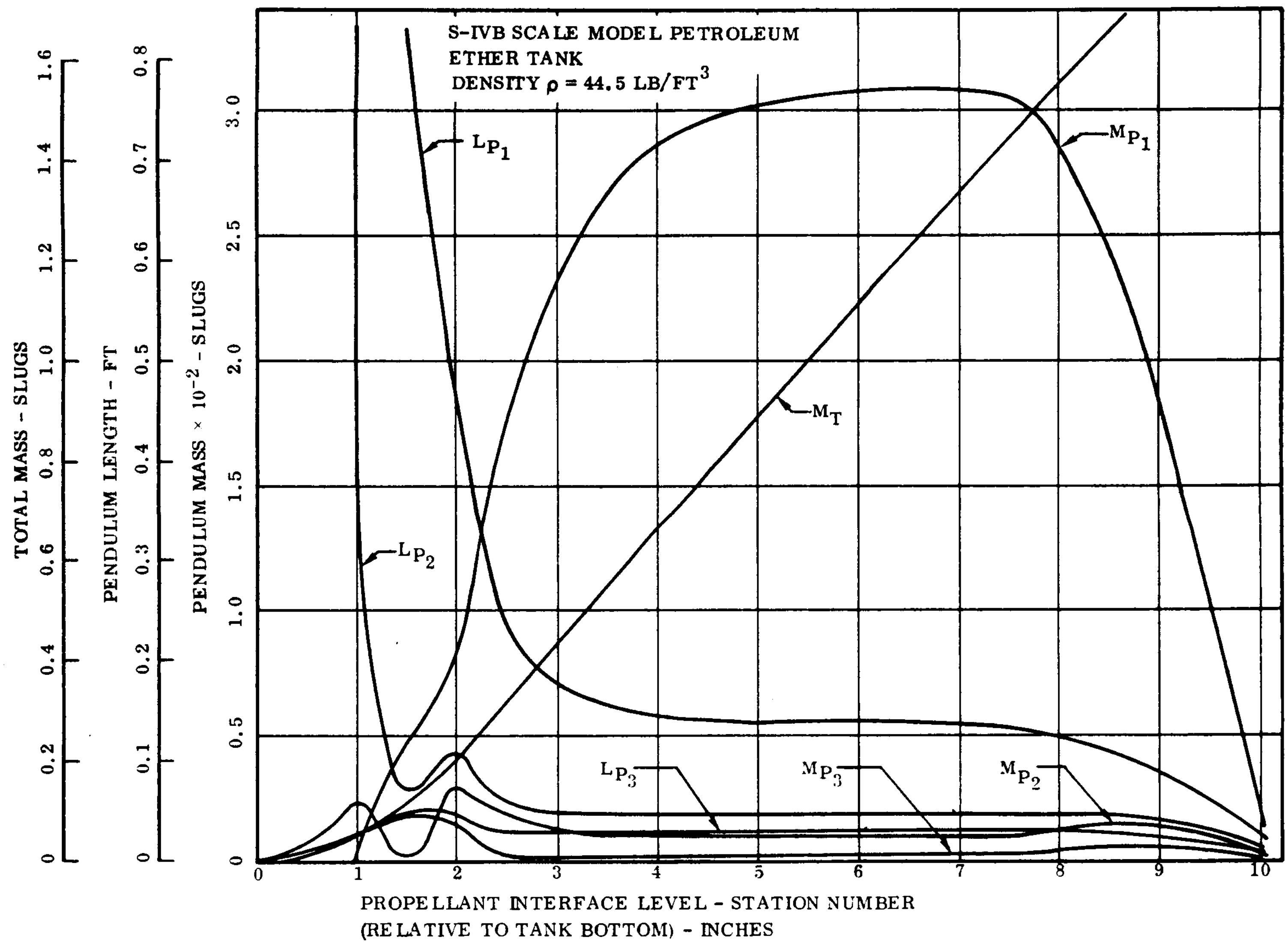

Figure 5-4. S-IVB Scale Model LH_2 Tank Slosh Parameters as a Function of Propellant Interface Level

constant. This energy dissipation constant is incorporated into the mechanical slosh analogy to simulate effective baffle damping. The proportionality constant for a given tank geometry is dependent on the baffle dimensions, location within the tank, and location relative to the undisturbed liquid level.

The derivation of the energy dissipation constant is based on the solution of the hydrodynamic equations. This constant is determined by integrating the vertical component of fluid velocity over the wetted baffle area. A fundamental assumption is that of perturbational fluid displacements. Based on this theoretical solution the baffle becomes ineffective when the quiescent liquid level is below that of the baffle. A similar condition exists for large amplitude motion even when the nominal liquid level is above the baffle. Under this condition the wetted portion of the baffle is a function of the slosh amplitude. Theoretical damping expressions when the baffle is allowed to become uncovered have been developed in References 5-5 and 5-6. These expressions unfortunately are based on averaging techniques making use of an effective baffle area over a complete slosh cycle.

These conditions do not exist during Centaur flight except perhaps during the first slosh cycle following main engine shutdown. However during the S-IVB AS-203 orbital experiment and the drop tower slosh tests the baffle is uncovered. Baffle damping for simulation of these cases assumed an effective baffle area based on expected slosh amplitudes. This assumption in effect results in an average energy dissipation. The baffle damping coefficient for both the full scale and drop tower model tank as a function of the quiescent liquid level is given in Figures 5-5 and 5-6 respectively.

5.3 DROP TOWER PROPELLANT SLOSHING ANALYSIS

The drop tower slosh data is valuable in that it enables a direct evaluation of the propellant slosh theoretical solution as applied to the low g condition. Analytical results of drop tower sloshing are based on simulation. Analytical data is compared with test data obtained from Reference 5-7 wherever possible. Unfortunately the actual test data available did not cover the complete range of test conditions. Under these circumstances questions regarding data reduction techniques and the validity of some of the reduced data have been unanswered with a corresponding reduction in confidence level. In any case the drop tower provides more complete quantitative propellant sloshing data than can be obtained from flight testing. Furthermore test conditions can be controlled to practically eliminate unknown disturbances often present in flight results. Every effort is made to correlate test data with theoretical results to point out the slosh model inaccuracies in this application.

A digital computer program was set up to simulate the drop tower propellant sloshing dynamics. The simulation uses the pendulum analogy to duplicate the sloshing dynamics, provision is included for three slosh modes. The pendulum slosh analogy

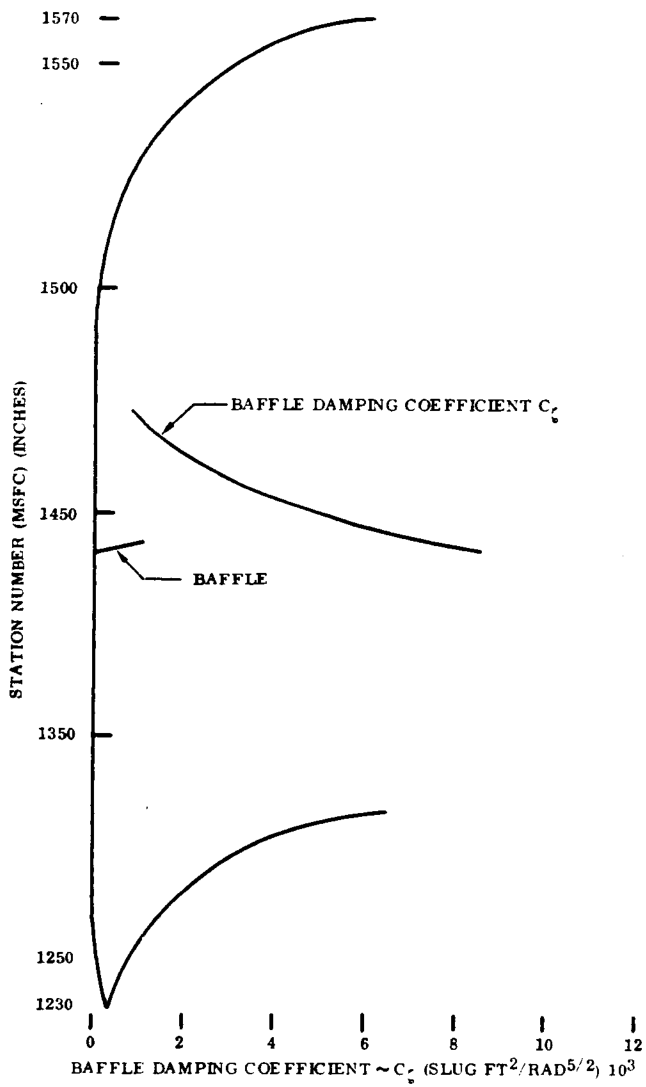

Figure 5-5. Baffle Damping Energy Dissipation Constant as a Function of Quiescent Liquid Level for S-IVB - AS-203 Vehicle

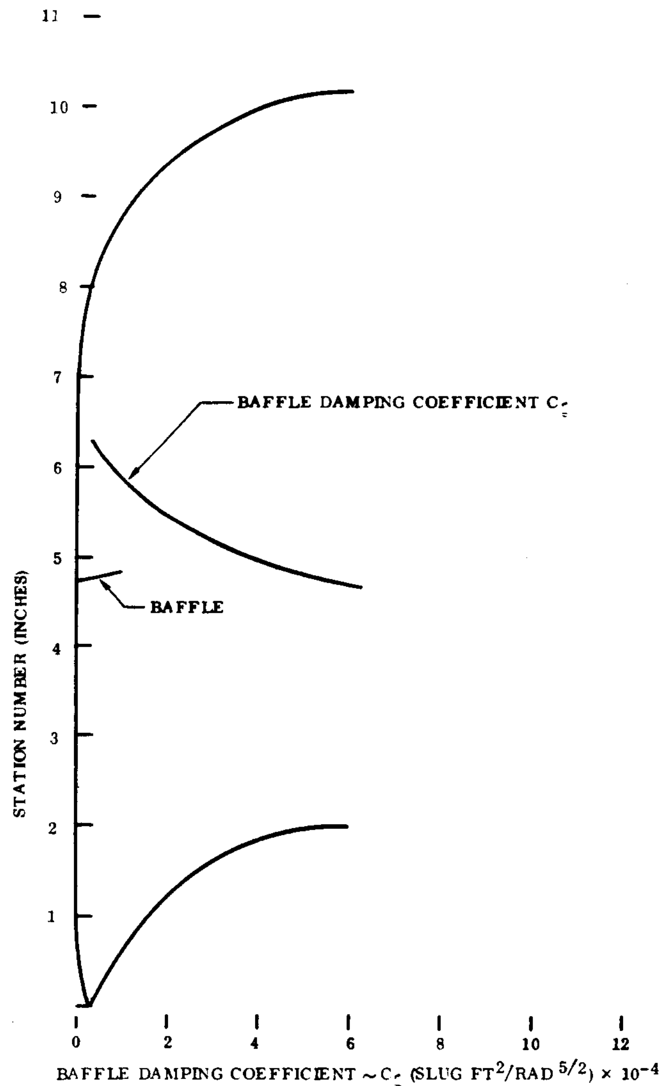

Figure 5-6. Baffle Damping Energy Dissipation Constant as a Function of Quiescent Liquid Level For S-IVB Drop Tower Model

parameters and the basic mathematical model are shown in Figure 5-7. Propellant inertia and pendulum hinge point parameters are not required since the model tank is assumed to have only one degree of freedom in the axial direction. The analytical procedure was the same as that employed in the actual model test. Sloshing was induced in a one "g" environment, then the acceleration reduced to a low level as defined by the Bond number. Data was obtained on propellant slosh wave amplitude, velocity and acceleration. This data enabled determination of the maximum liquid slosh amplitude, amplification factor, effective baffle damping coefficient, and slosh period as a function of Bond number and Froude number.

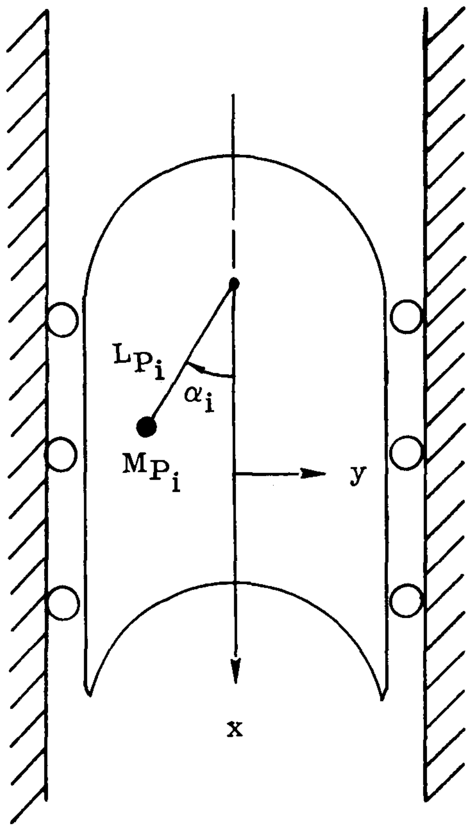

L_{P_i} Pendulum length used in the pendulum analogy for the i^{th} mode sloshing.

M_{P_i} Sloshing propellant mass used as the propellant mass in the pendulum analogy for i^{th} mode sloshing.

α_i Pendulum displacement angle for i^{th} mode sloshing.

Figure 5-7. Drop Tower Propellant Slosh Analogy Parameters

5.3.1 MAXIMUM LIQUID AMPLITUDE WITH CLEAN TANK CONFIGURATION (NO BAFFLES)

5.3.1.1 Analytical Results. A series of computer runs have been made simulating the drop tower slosh testing. Propellant sloshing is initiated under a one g condition, then the g-level is suddenly reduced to a low value as described by the Bond number. The maximum liquid amplitude plotted in dimensionless form is presented in Figure 5-8 as a function of the square root of the Froude number. The Froude number is calculated at initiation of the low "g" condition and is therefore a measure of the initial slosh kinetic energy. The upper curve represents the clean tank configuration, ie, no baffle damping. The lower curve, with points denoted by solid symbols, illustrates conditions including baffle damping. The data presented here does not include the liquid level rise produced by low g capillary effects.

Figure 5-9 illustrates the maximum liquid amplitude as a function of time for a typical simulation run. Since for analytical purposes the slosh wave is antisymmetric, this represents the amplitude of either the left or right side, the only difference being the sign of the amplitude. Figure 5-10 shows the propellant mode shapes for a large amplitude first mode slosh wave and the same wave superimposed on a low-g meniscus, as approximated by a sphere. Note that the new wave profile now appears distorted although in reality, it remains a first mode slosh wave.

5.3.1.2 Drop Tower Test Results. The maximum drop tower liquid amplitude data (Ref. 5-7) is presented in Figure 5-11 for comparison with analytical results shown in Figure 5-8. A comparison of the data for the clean tank configuration shows that for Froude numbers exceeding approximately 1.0, the predicted amplitude (Figure 5-8) exceeds that obtained from tests (Figure 5-11), conversely for Froude numbers less than 1.0 the amplitude is less than observed in tests. The broken line represents a smooth curve approximation to the maximum amplitude curve with low g capillary effects as approximated by the height of the meniscus subtracted out. The height of the meniscus as a function of Bond number was analytically determined based on the theory of Reference 5-8.

Figure 5-12 shows a typical amplitude versus time curve for both the left and right sides measured at the tank wall as obtained from test data. Basic slosh modes are evident during both the one g and subsequent low g periods. However because of the data scatter, which appears as "noise," filtering or smoothing is necessary to make maximum effective use of the data in correlating with analytical results. The slosh amplitude shows a relatively large steady state wave height after the drop during the low-g condition. This large bias appears to be characteristic of all available test data. The left side amplitude for this case has a bias of 1.3 inches at the point of maximum wave height and the right side 0.8 inches. This compares with a predicted meniscus height based on low g capillary effects of approximately 0.29 inches. Assuming that the theoretical meniscus (0.29 inches) does agree with unexcited test results in the transition to low-g, still a significantly greater rise (1.3 inches total) in the quiescent liquid level was observed for a test drop in the excited state than can be predicted analytically by conventional slosh theory. Because of the short test time duration, the new quiescent level cannot be examined for a sufficient period of time; however the observed quiescent level rise does appear to be decreasing with increasing time, indicative of a transient response.

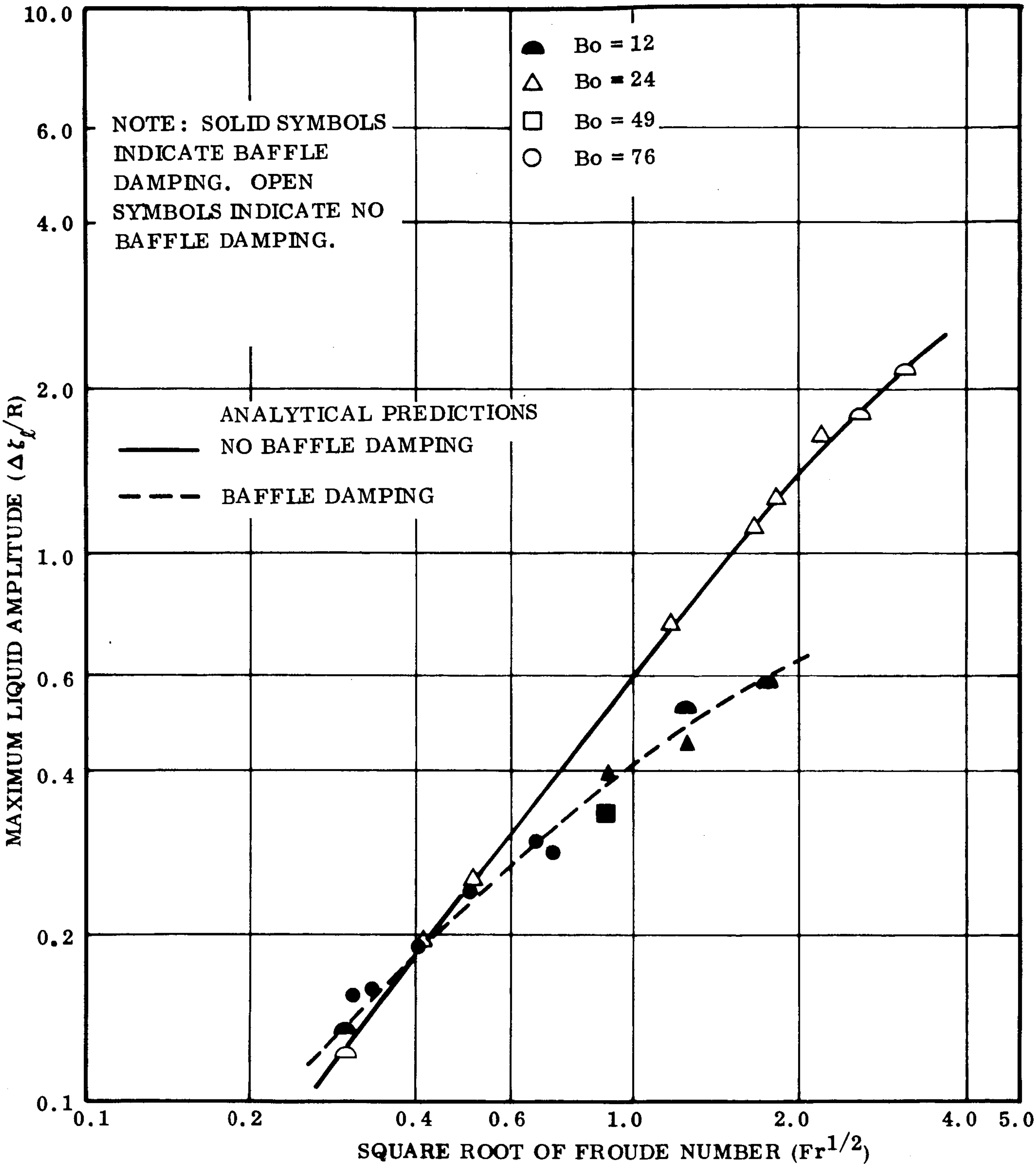

Figure 5-8. Maximum Liquid Slosh Amplitude Determined From Analytical Model for Several Bond Numbers

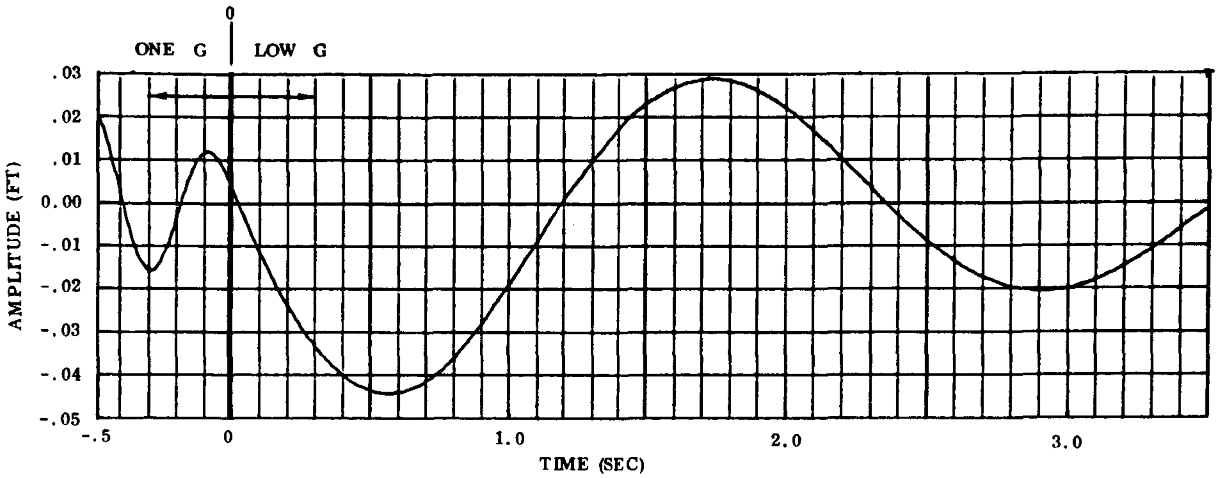

Figure 5-9. Liquid Amplitude History of a Typical Simulation Run

Table 5-1 presents a summary of the liquid level rise during the low g condition along with the analytically determined meniscus height for three tests on which data is available.

Table 5-1. Quiescent Liquid Level Rise Obtained From Drop Tower Test Results

Test No.	Bond No.	Quiescent Liquid Level Rise (Inches) Left Side	Right Side	Analytically Determined Meniscus Height
2F-41	76	1.3	0.80	0.29
2F-42	76		0.23	0.29
2F-49	95	0.70	0.25	0.22

Inspection of the drop tower film data shows that as the slosh wave passes through the equilibrium point it is highly curved in the shape of a meniscus. Figure 5-13 illustrates this for test 2F-14 at the second zero crossing. This observed "meniscus" height is the same as that shown on Figure 5-12 at 2.5 seconds. The curvature however appears in the plane of the slosh motion only and not in both planes as would a meniscus produced by low g capillary effects. In addition, liquid inertia effects due to the sudden reduction in axial acceleration should be manifested on both the pitch and yaw planes. The symmetry of the liquid interface profile suggests that the observed waveform does not represent a low-g surface perturbation. Unfortunately an insufficient number of data points was available and no attempt was made to correlate the quiescent liquid level rise with specific test conditions over and above that attributable to low-g capillary effects.

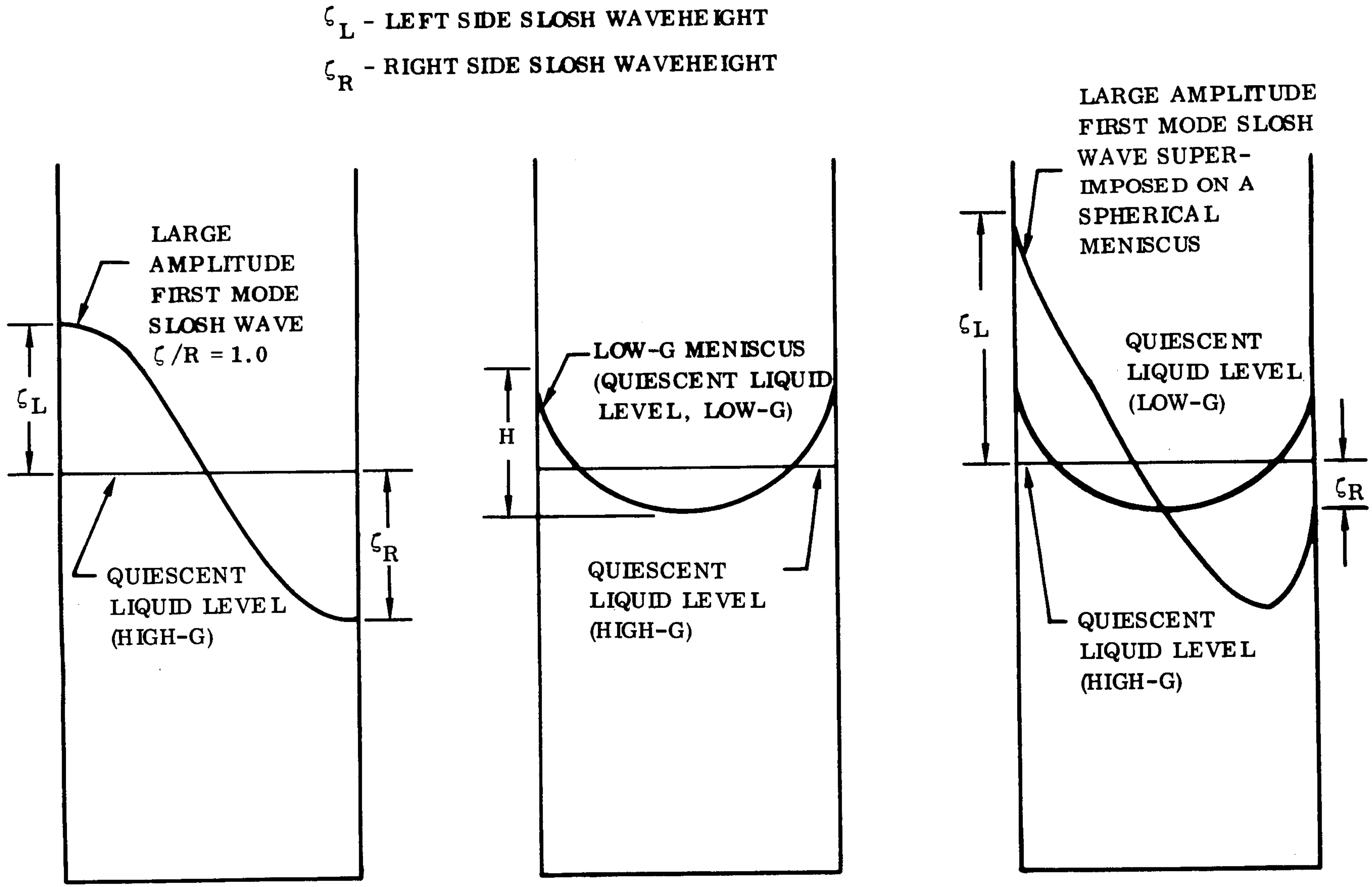

Figure 5-10. Propellant Slosh Liquid-Vapor Interface Profiles

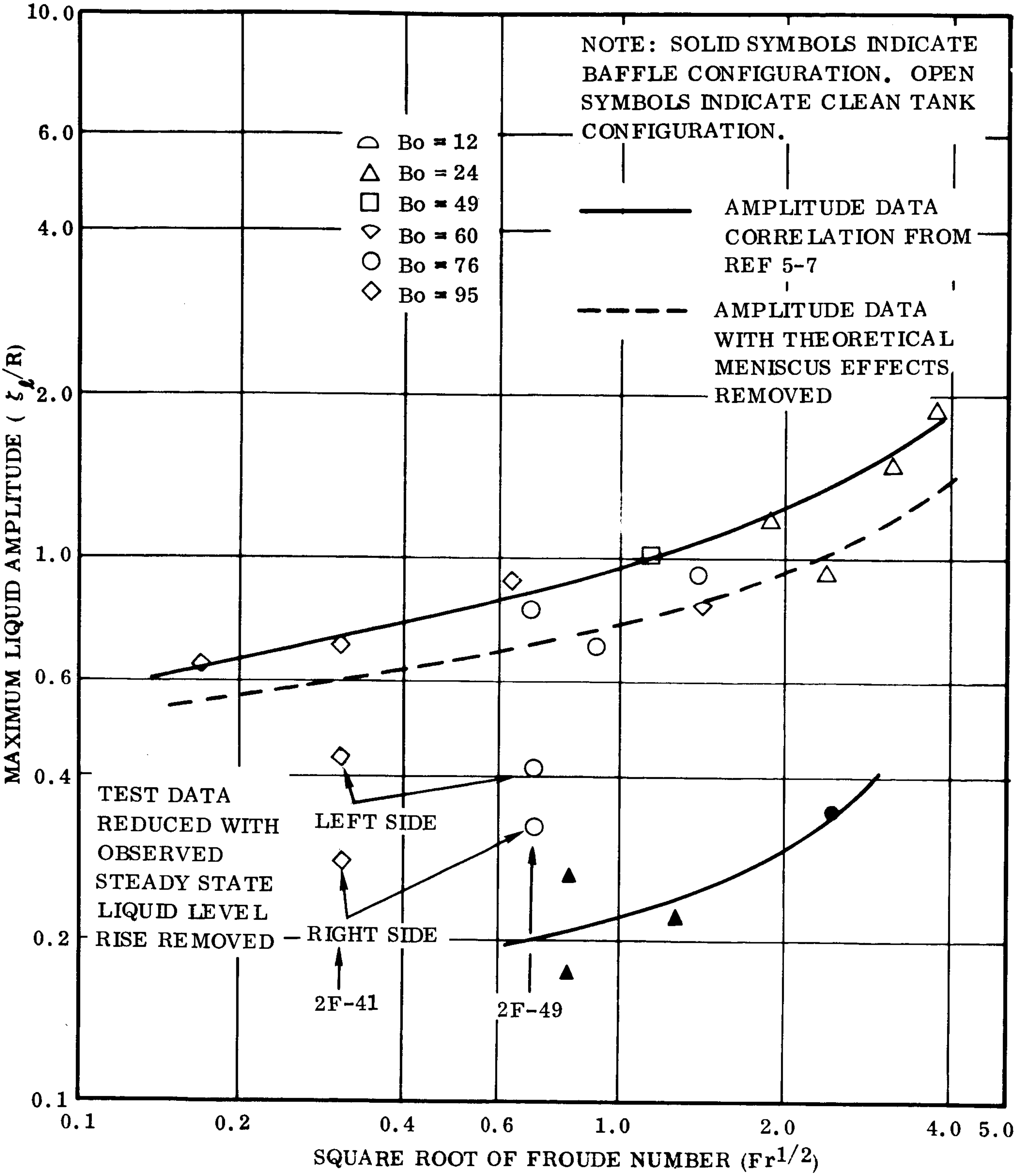

Figure 5-11. Drop Tower Test Data For Maximum Liquid Slosh Amplitude

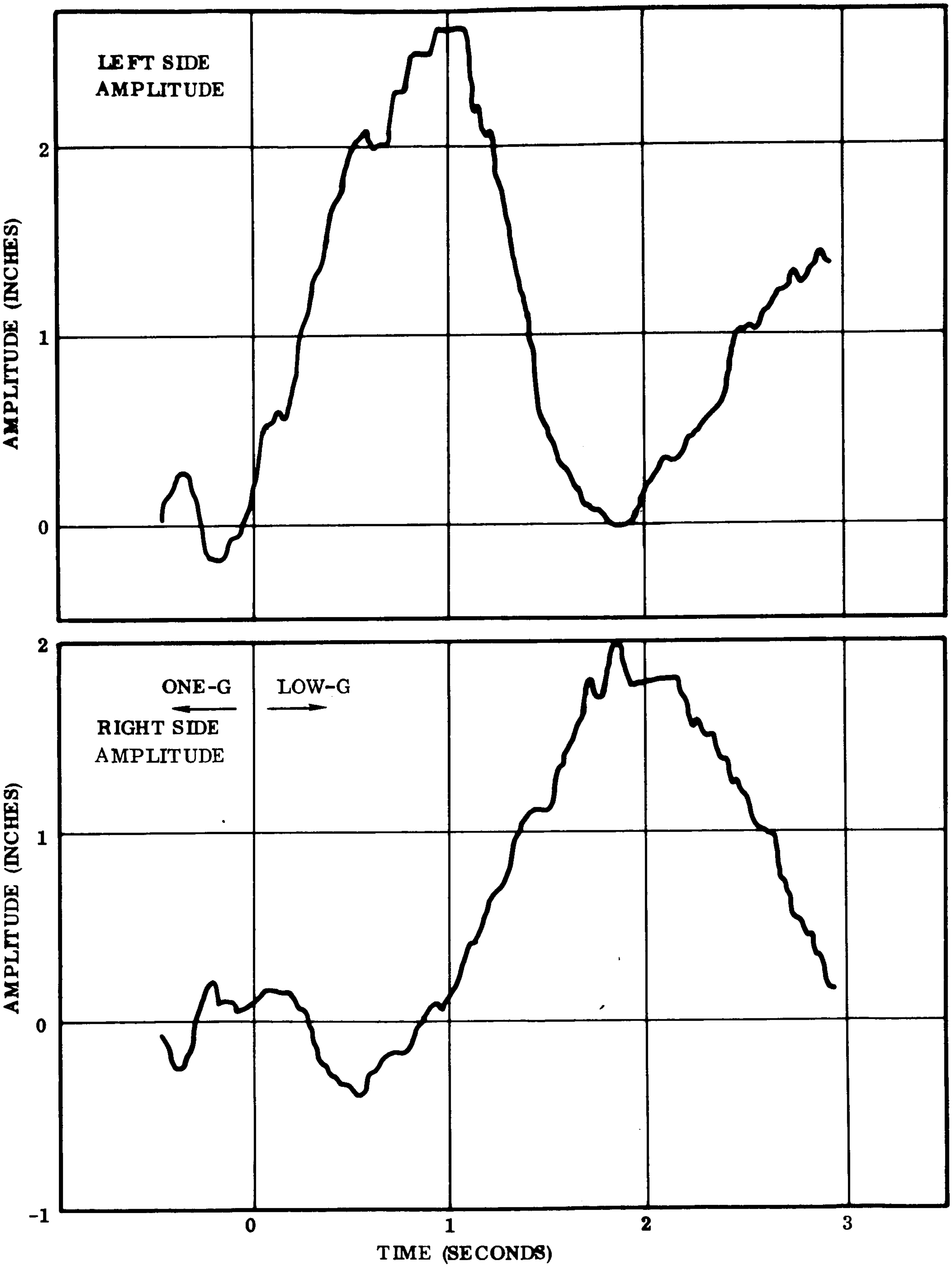

Figure 5-12. Drop Tower Slosh Test 2F-41 Slosh Amplitude History

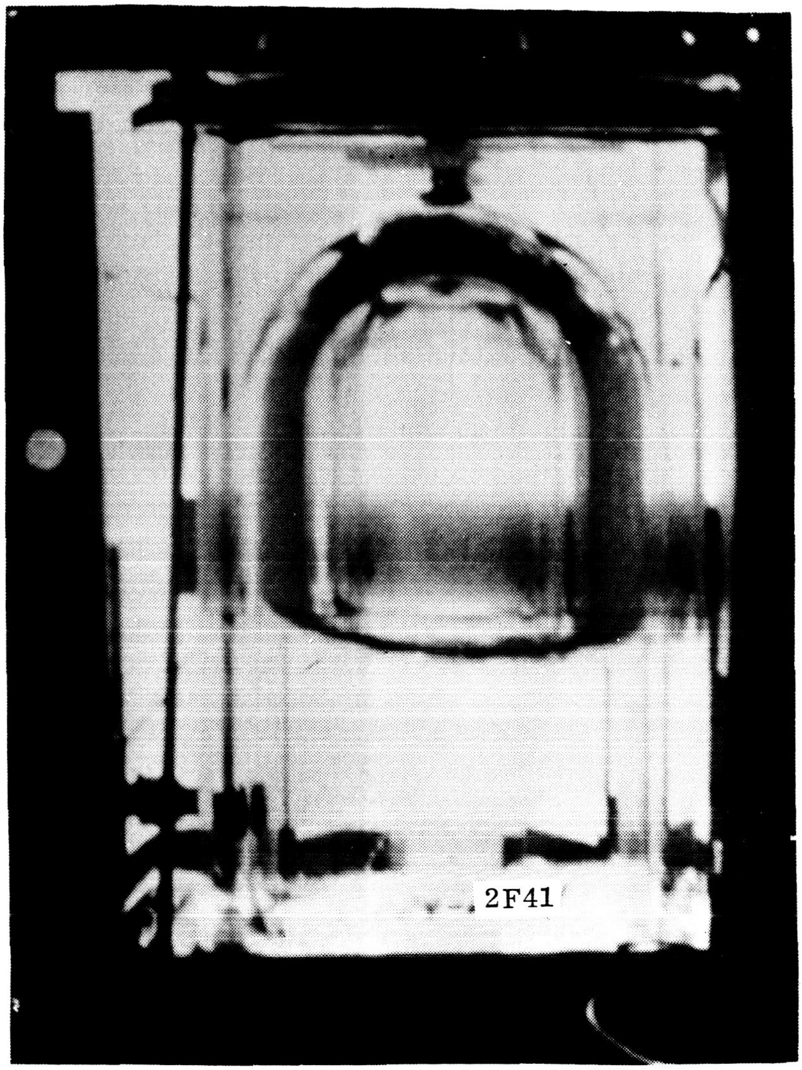

Figure 5-13. Liquid Vapor Profile Test 2F-41 at 2.5 Seconds

Removing this total bias from the available data and recomputing the maximum slosh liquid amplitude gives the four points plotted on Figure 5-11 below the broken line. Both the left and right side data points are given assuming the same Froude number. This modification brings the analytical data in closer agreement with test results, however, more test data points are required to improve on this correlation. Unfortunately, although requested, more data was not available. The magnitude of this exaggerated meniscus liquid level rise in any case remains an unanswered question requiring further study.

5.3.2 MAXIMUM LIQUID AMPLITUDE WITH BAFFLED TANK CONFIGURATION

5.3.2.1 Analytical and Test Results. Data points for the maximum liquid amplitude for the tank configured with the baffle are also presented on the figures discussed above. The vehicle configured with a baffle represents a more realistic condition compared to that without a baffle. Most liquid propellant space vehicles designed with a multiburn capability will require use of an antislosh device for propellant control because of the inherently low natural slosh damping. Here again an insufficient number of test data points is available for a thorough correlation of analytical and test results.

Conditions with the baffle are unique in that in the tank, the fluid motion is physically impeded by the baffle causing the fluid motion to be directed through the unbaffled portion of the liquid vapor interface. In this manner the baffle acts more as a slosh deflector confining propellant motion than as a baffle in the conventional sense. The slosh analytical model includes the effect of the baffle purely as an energy dissipation device. The propellant motion is not physically constrained. Kinetic energy is removed in accordance with the theoretical energy dissipation provided by the baffle.

The theoretical baffle damping is based on fluid drag in deflecting the liquid flow around the baffle. Under the low-g conditions being analyzed here the baffle is only wetted during a portion of the slosh cycle. The analytical solution has not been verified for this sustained condition. The results presented are based on an assumed effective baffle area based on expected slosh amplitudes. For this reason close correlation of propellant wave height at the tank wall for the test data and analytical results is not expected.

The maximum amplitude data (Figures 5-8 and 5-11) for this condition shows reasonable agreement with the slope of the two curves being similar. However, more analytical work remains to be done in correlating the analytically determined baffle damping with that observed in actual tests, in particular, the rate of energy dissipation when the baffle is only partially covered during a slosh cycle. An alternative, if more test data were available, would be to parameterize the baffle energy dissipation in an attempt to empirically fit the slosh test data.

5.3.3 AMPLIFICATION FACTOR. Another measure of liquid slosh amplitude entering a low g condition is obtained from the amplification factor. This is given by:

$$\frac{\zeta_h}{\zeta_\ell} = \left[\sin^2 \phi + \frac{a_h}{a_\ell} \cos^2 \phi\right]^{1/2} \qquad (5\text{-}2)$$

where ϕ is the instantaneous slosh phase angle when the acceleration level is reduced from a_h to a_ℓ and ζ_h is maximum slosh waveheight under the high-g condition and ζ_ℓ the maximum under the reduced-g condition. The amplification factor is based on energy considerations as measured by the maximum propellant waveheight . It is a measure of the maximum wave height under low g conditions based on initial energy conditions at the time of the g level change. Low-g capillary effects are not included. Theoretically for a slosh wave possessing mechanical energy only, this gives the maximum waveheight in the absence of damping.

5.3.3.1 Analytical Results. Figure 5-14 shows the theoretical amplification factor as a function of the cosine of the phase angle squared. Based on linear slosh theory, this is the ratio of the Froude number at the drop to the maximum Froude number prior to the drop assuming no damping. A family of curves is presented for the drop tower test conditions. Points on the curve have been obtained from analytical simulation or drop tower test condition runs for the clean tank configuration. The points designated by solid symbols represent the amplification factor including the slosh attenuation provided by baffle damping as obtained from analytical simulation runs. The difference between these solid points and the corresponding smooth curve is a measure of the baffle efficiency in reducing the slosh amplification factor. This analysis indicates that the baffle as analytically simulated for the drop tower test configuration effectively reduced the amplification factor.

5.3.3.2 Drop Tower Test Results. The amplification data presented in Reference 5-7 appears to have little or no correlation with the analytically determined amplification factor. However for a valid comparison the steady state liquid level rise must first be removed from this data since this effect is not included in the amplification factor. Under this condition the measured slosh amplification factor does not exceed the theoretical maximum value, ie, the amplification factor for a phase angle of zero. Figure 5-15 shows the theoretical solution and the three test data points available. Note points are both above and below the theoretical curve. This figure suggests an error may have occurred in the phase angle in fitting a linear function to the test amplitude data. Again an insufficient number of data points are available to make any definite conclusions.

5.4 S-IVB AS-203 SLOSH SIMULATION

Simulation of the propellant slosh during orbital flight includes the basic slosh model with a six degree of freedom rigid vehicle. The forces and moments produced by the on-off attitude control system is also included. Propellant sloshing analysis during orbital coast is treated in two phases. The first is concerned with settling of the transient motion produced by main engine cutoff. Once the propellant motion has been stabilized, it must be retained in that condition to permit propellant tank venting. The primary concern here is with dissipating the slosh energy upon entering the low thrust coast mode. During sustained orbital coast, propellant slosh perturbations are produced by settling thrust disturbances, propellant tank venting, reaction control motor firings, and vehicle attitude changes. The initial phase is characterized by large amplitude slosh waves while the coast mode is characterized by relatively low amplitude slosh waves. The available flight data during orbital coast is qualitative at best, but the TV camera does show very low amplitude slosh waves.

5.4.1 VEHICLE DYNAMIC MODEL. The dynamic model used for orbital coast is that of a six degree of freedom rigid vehicle with forces and moments produced by propellant motion represented by pendulums. The propellant slosh damping consists of a small linear component produced by fluid viscosity and in the liquid hydrogen tank a larger amplitude dependent term as a result of the baffle. The basic rigid body equations of motion with the addition of the propellant sloshing forces and

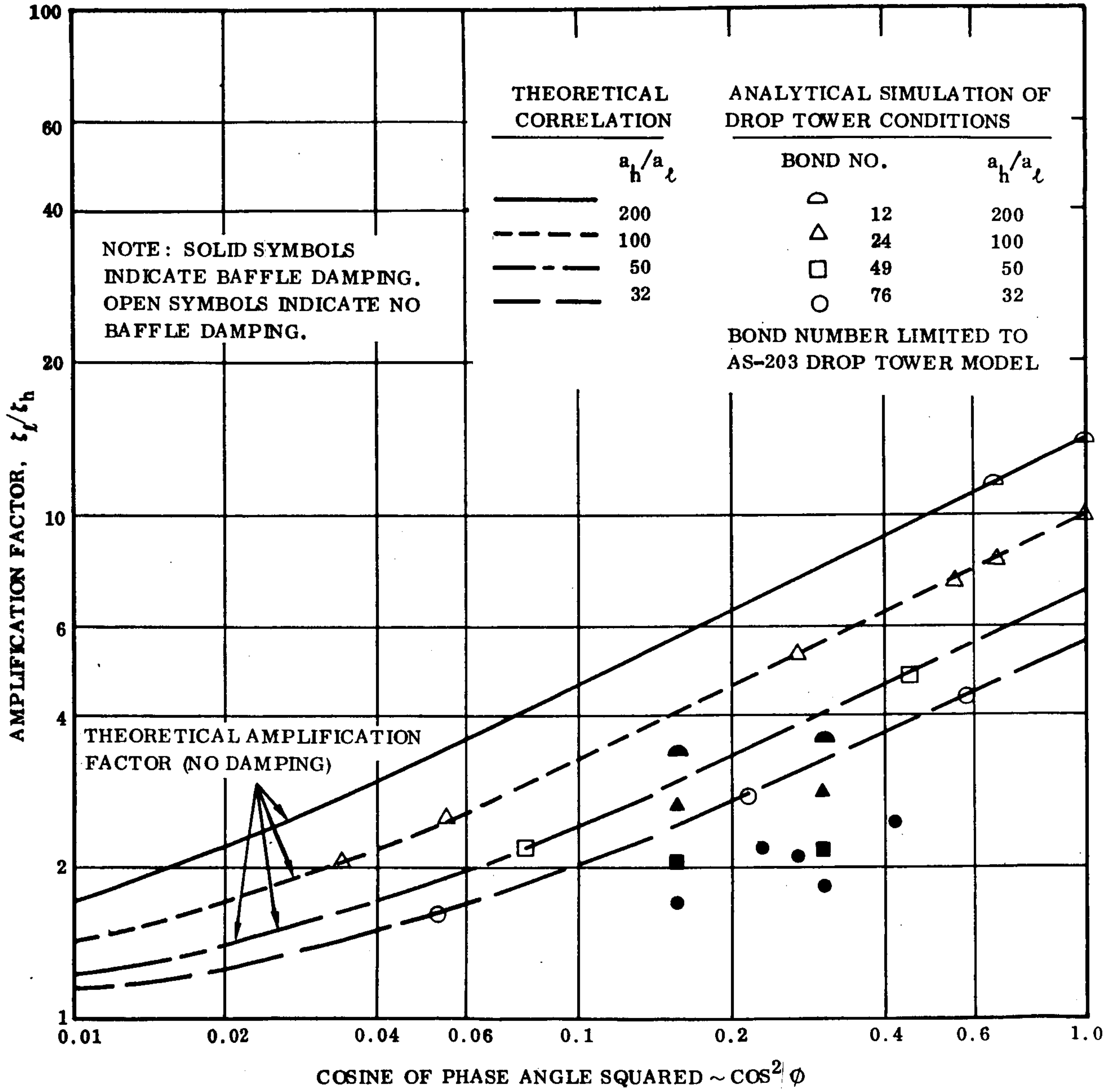

Figure 5-14. Comparison of Theoretical Slosh Amplification Factor With Simulation Result for No Baffle and Baffled Tank Configurations

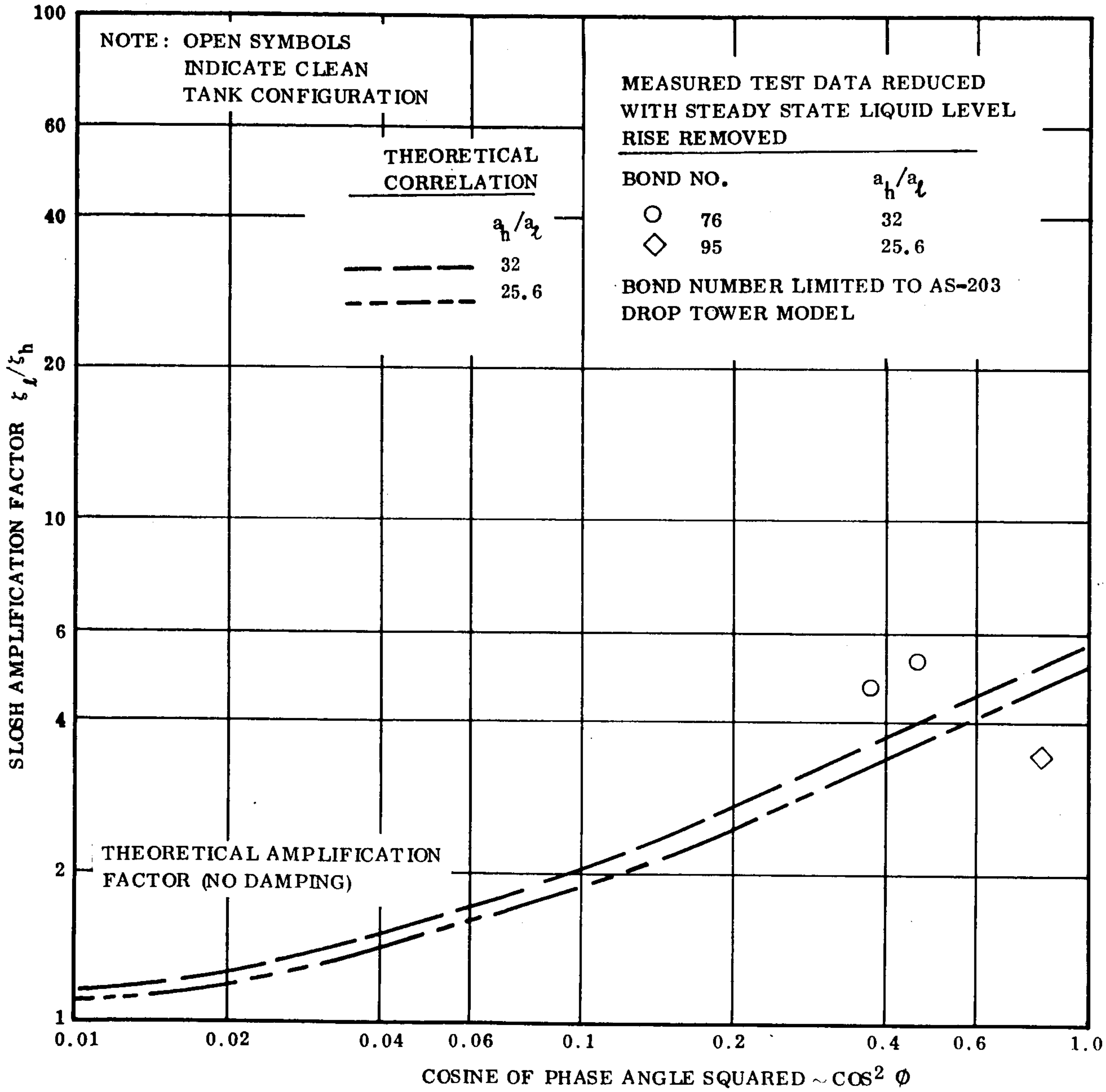

Figure 5-15. Comparison of Theoretical Amplitude Factor With Modified Drop Tower Test Results

moments are given below.

Force equations are:

$$F_x = A_x M_T \tag{5-3}$$

$$F_y = A_y M_o - A_x (M_{P0} \beta_0 + M_{PF} \beta_F) \tag{5-4}$$

$$F_z = A_z M_o - A_x (M_{P0} \alpha_0 + M_{PF} \alpha_F) \tag{5-5}$$

The equations of angular momentum are:

$$L = I_{xx_o} \dot{P} - I_{xy_o} \dot{Q} - I_{xz_o} \dot{R} + A_z M_o \Delta y_o - A_y M_o \Delta z_o \tag{5-6}$$

$$M = I_{yy_o} \dot{Q} - (I_{zz_o} - I_{xx_o}) PR + A_x (M_{P0} \ell_0 \alpha_0 + M_{PF} \ell_F \alpha_F)$$

$$+ A_x M_o \Delta z_o \tag{5-7}$$

$$N = I_{zz_o} \dot{R} + (I_{yy_o} - I_{xx_o}) PQ - A_x (M_{P0} \ell_0 \beta_0 + M_{PF} \ell_F \beta_F)$$

$$- A_x M_o \Delta y_o \tag{5-8}$$

The propellant sloshing equations are:

$$\ddot{\alpha}_F = - \frac{\dot{Q} (L_{PF} - \ell_F) + A_z}{L_{PF}} - \frac{A_x}{L_{PF}} \alpha_F - \frac{C_\zeta \dot{\alpha}_F}{M_{PF} L_{PF}^2 \sqrt{\alpha_{F_{MAX}}}} \left| \dot{\alpha}_F \right|$$

$$- 2\omega_F \zeta_F \dot{\alpha}_F \tag{5-9}$$

$$\ddot{\alpha}_0 = - \frac{\dot{Q} (L_{P0} - \ell_0) + A_z}{L_{P0}} - \frac{A_x}{L_{P0}} \alpha_0 - 2\omega_0 \dot{\alpha}_0 \left[\zeta_0 + \frac{C_{NL}}{\pi} \left| \alpha_{0_{MAX}} \right| \right] \tag{5-10}$$

$$\ddot{\beta}_F = \frac{\dot{R} (L_{PF} - \ell_F) - A_y}{L_{PF}} - \frac{A_x}{L_{PF}} \beta_F - \frac{C_\zeta \dot{\beta}_F}{M_{PF} L_{PF}^2 \sqrt{\beta_{F_{MAX}}}} \left| \dot{\beta}_F \right|$$

$$- 2\omega_F \zeta_F \dot{\beta}_F \tag{5-11}$$

$$\ddot{\beta}_0 = \frac{\dot{R}\,(L_{P0} - \ell_0) - A_y}{L_{P0}} - \frac{A_x}{L_{P0}}\,\beta_0 - 2\omega_0\,\dot{\beta}_0\left[\zeta_0 + \frac{C_{NL}}{\pi}\left|\beta_{0MAX}\right|\right] \qquad (5\text{-}12)$$

Figure 5-16 illustrates this model. A separate pendulum is used for each propellant tank in both pitch and yaw. Roll or rotary slosh is neglected with the vehicle assumed to rotate about the propellants.

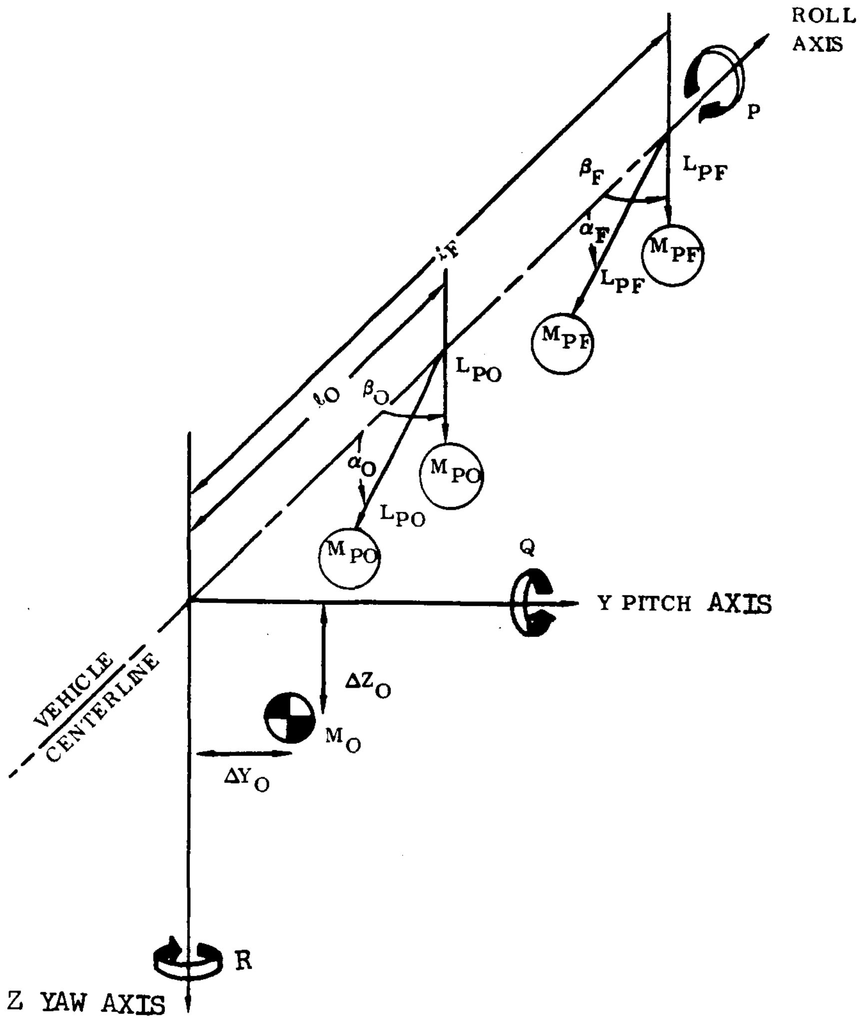

Figure 5-16. S-IVB Propellant Slosh Dynamic Model

The primary disturbance affecting propellant motion during sustained coast is produced by the reaction control motors in stabilizing the vehicle attitude along the desired reference attitude. Vehicle perturbations are produced by propellant tank vent disturbances and attitude maneuvering requirements. The attitude control system details have been obtained from Reference 5-9. The engine locations are shown in Figure 5-17 and the autopilot diagram as simulated in Figure 5-18. The engine thrust characteristics are approximated by a square pulse. The total impulse is preserved and effective thrust use and decay times are treated as pure

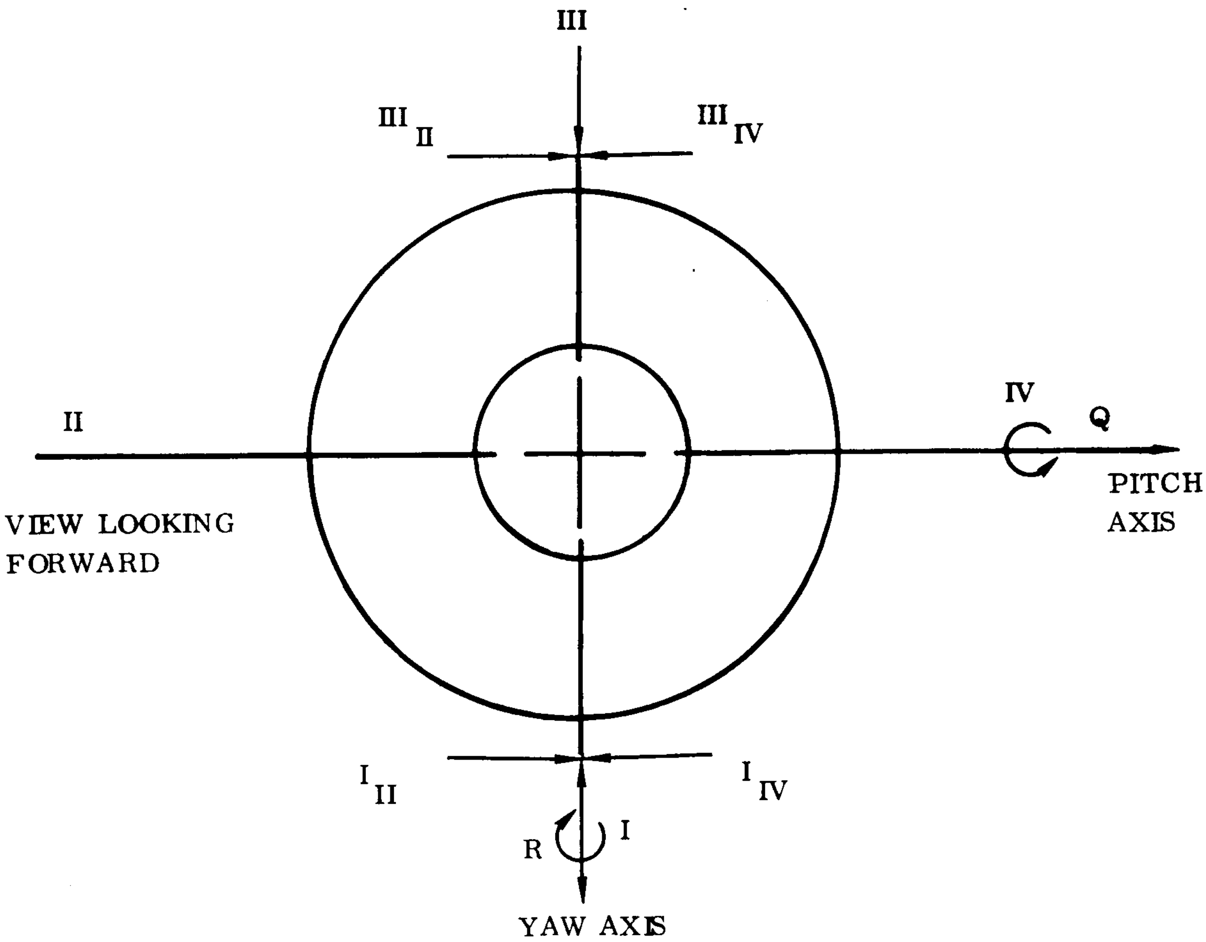

Figure 5-17. Saturn S-IVB Attitude Control System Engine Locations

time delays. The engine control is such that the engines are commanded on when the controlling error signal exceeds the ON limit and commanded OFF when the signal falls below the OFF threshold. The pitch axis operates independently using two engines for control. Yaw and roll control is provided by a set of four engines operating in a coupled mode. The necessary parameter values obtained from personal communication with MDAC are given in Table 5-2. The commanded vehicle attitude is along the local horizontal with the positive yaw axis pointed down. The guidance attitude command is updated once every second commanding an -0.068 deg/sec average pitch rate.

5.4.2 SIMULATION RESULTS. Figure 5-19 shows typical simulation results during LH_2 continuous venting. The condition simulated is during the first continuous vent period of the first orbit. The average axial thrust is 8.0 pounds which produces a 1.36×10^{-4} g axial acceleration. The Bond number is approximately 400

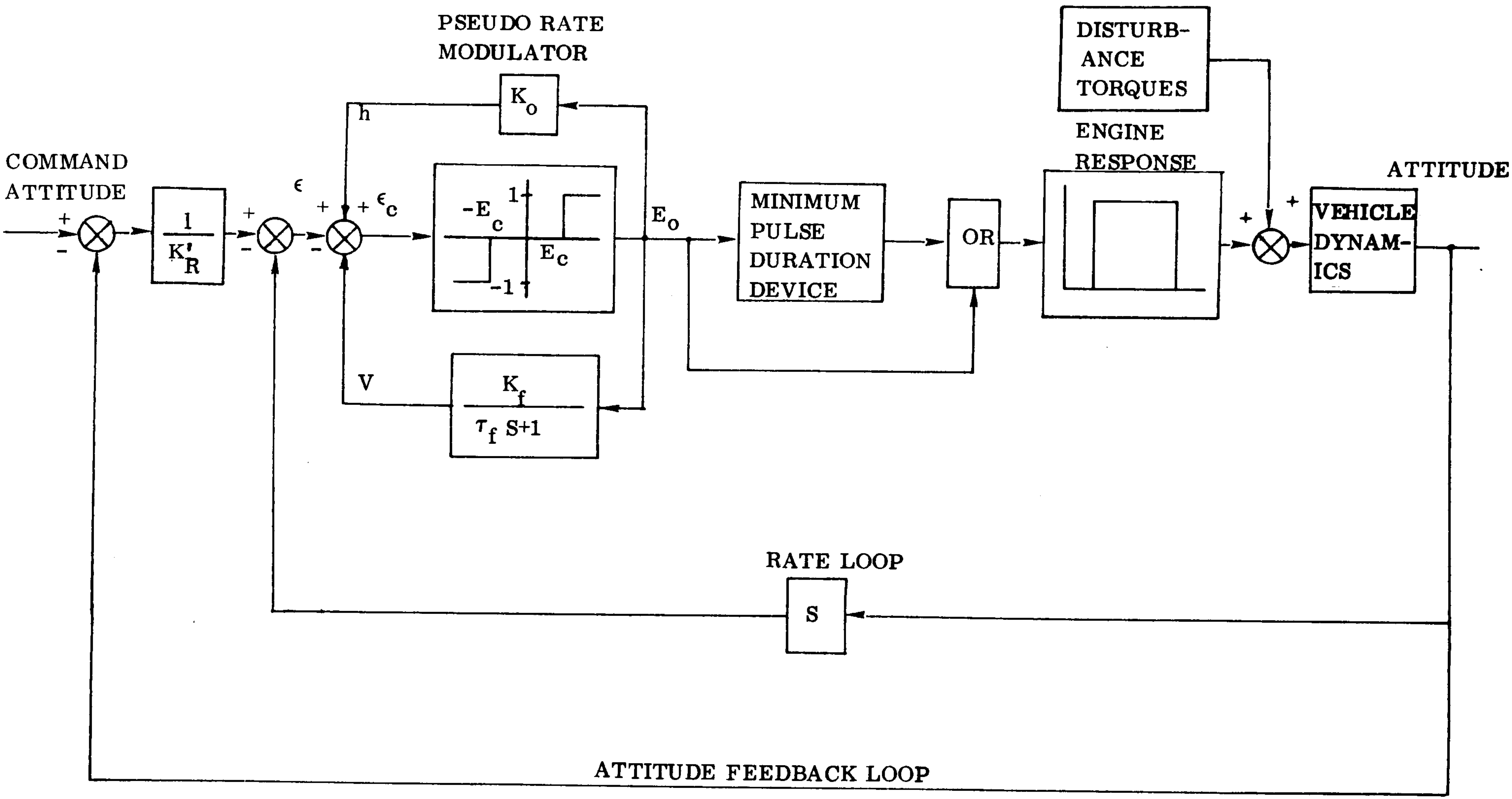

Figure 5-18. S-IVB Attitude Control System Autopilot Block Diagram

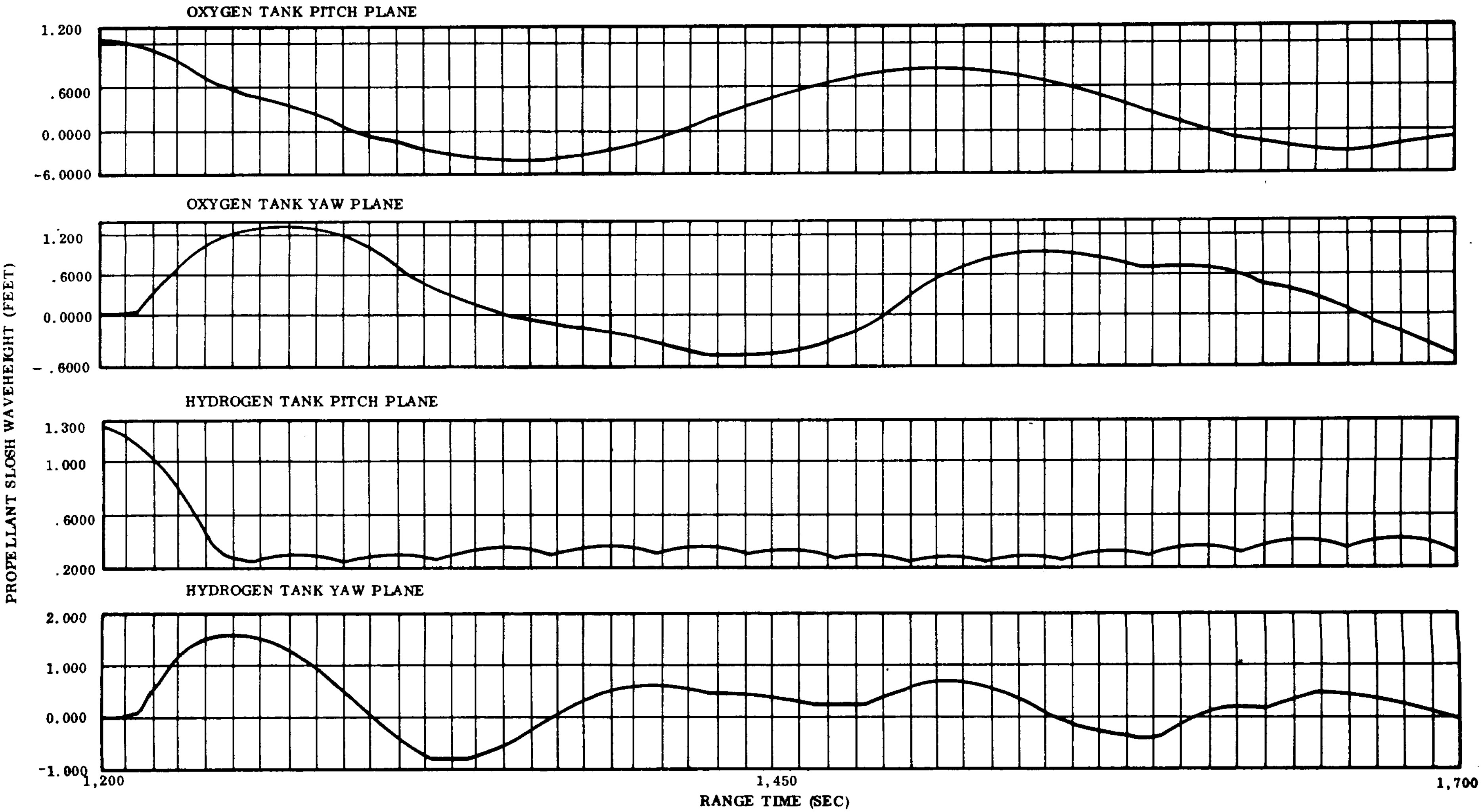

Figure 5-19. AS-203 Propellant Slosh Wave

Table 5-2. Saturn S-IVB AS-203 Coast Phase Attitude Control System Parameters

Parameter	Description	Value	Units
A/P Gain Ratio	K'_R	5.0	sec
Psuedo Rate Feedback Gain	$K_f E_o$	0.133	deg/sec
Pseudo Rate Feedback Constant	t_f	0.65	sec
Pseudo Rate Circuit Hysteresis	$K_o E_o$	0.0133	deg/sec
Rate Threshold	E_c	0.20	deg/sec
Attitude Control Motor Thrust		142	lbs
Equivalent Engine Rise Time		25	millisec
Equivalent Engine Decay Time		10	millisec
Guidance Pitch Over Cycle Time	Δt	1.0	sec

minimizing capillary effects. The undamped natural first mode slosh frequencies have a period of 305 seconds in the oxidizer tank and 234 seconds in the fuel tank. Propellant sloshing is initiated in each tank in the pitch plane only. The initial wave-height is 15 inches in each case; initial velocity is zero. In the LH_2 tank this amplitude just makes contact with the baffle. Two disturbances are present, one produced as a result of pitch plane steering commands. The second is produced by the continuous vent system; pitch and yaw disturbances are 3.3 ft-lb and -3.4 ft-lb respectively as obtained from flight data.

The propellant slosh amplitude data (Figure 5-19) shows a relatively insensitivity to both disturbances. The results show that in pitch both initial slosh waves decrease in amplitude with time. Because of the assumption of a slight amount of baffle damping LH_2 slosh damps out faster than LO_2 even though there is no contact with the baffle. This is an inaccuracy of the baffle damping model used. In yaw, where no initial slosh motion was assumed, a slosh wave is initiated in response to yaw control motor firings. Although neither of the disturbances are particularly significant, the larger of the two is produced by attitude control motor firings in response to the steering commands; this relegates the continuous vent disturbance to a minor role. The lateral attitude control disturbances directly excite propellant motion. Fortunately the reverse is not true. That is, the forces and moments produced by propellant sloshing are insufficient to cause attitude control system response.

Fuel sloshing in the pitch plane shows the effects of guidance system attitude commands on propellant behavior. Note that after the initial slosh transient has passed there is a 0.3 ft steady state slosh amplitude. A low amplitude oscillatory wave about this value can be seen. In addition a higher frequency (approximately 40 second period) component produced by attitude control motor firings in response to guidance commands can be seen. The time average lateral thrust of these firings is approximately 0.3 pound, this moves the net vehicle acceleration vector (axial plus lateral) 2 degrees off the longitudinal vehicle axis resulting in the 0.3 ft steady state waveheight. In order to keep this steady liquid level rise small the ratio of the average lateral to axial thrust should be minimized. This can be accomplished by reducing all disturbances and maneuvering requirements to a minimum. For example, during the low thrust Centaur orbital flight no laterally directed engines are used for pitch and yaw control.

Inspection of the AS-203 propellant slosh amplitude data shows that the LO_2 slosh is oscillating at its natural frequency. The LH_2 tank pitch sloshing shows in addition a cyclic response to attitude control motor firings. In the case of yaw the slosh wave is somewhat irregular and the frequency less obvious. The AS-203 flight represents an unusual situation in that the fuel slosh mass exceeds that of the oxidizer tank. For normal tanking conditions the LO_2 sloshing mass is an order of magnitude larger than the LH_2 counterpart. This is significant since when this condition exists the coupled system is driven by LO_2 propellant sloshing, with LH_2 beating in response. Although LO_2 is the driving function, by virtue of its large mass, usually LH_2 is of greatest interest as a result of the greater boiloff and venting considerations.

5.4.3 SUMMARY OF SIMULATION RESULTS. Analytical results are based on simulation of AS-203 orbital flight during LH_2 continuous venting, range time of 1200 seconds. Unfortunately there is no quantitative propellant amplitude flight data with which to compare simulation results directly. Under this condition verification of simulation results is qualitative at best. The propellant slosh amplitude data shows the perturbations produced by vehicle disturbances are insufficient to excite the propellants. This is true even in the oxidizer tank which does not contain a baffle. Slosh perturbations produced by attitude control motor firings are clearly evident and point out the need to keep vehicle disturbances at a minimum. In addition the forces and moments produced by propellant slosh were insufficient to cause coupling through the attitude control system.

The results show that no coupled frequencies exist and that after the initial transient has passed the propellants oscillate at their natural frequencies. These results are in agreement with those presented in Reference 5-10 and point out the usefulness and applicability of the analytical slosh analysis.

5.5 SIMULATIONS WITH MARKER AND CELL MODEL

The Marker and Cell (MAC) method of solution for fluid dynamic problems originated at Los Alamos and has been developed for application to low-g problems under Convair research funds (Ref. 5-11, 5-12, 5-13). A brief description of the program as it currently exists at Convair is given below. Applications to sloshing, settling, and propellant stratification are typical phenomena which can be simulated. In a second phase to this study contract, extensive modifications are being made to the MAC method to include surface tension and two-fluid simulation capability. Under that phase of the study, the complete code will be delivered to the NASA/MSFC.

The MAC method is a numerical technique used to solve the full Navier-Stokes equations for a viscous incompressible fluid. These equations are coupled with the energy equation through the Boussinesq approximation to account for buoyancy effects due to density gradients. An initial value problem is then created by specifying the initial fluid velocities and temperatures and the velocities and temperatures around the boundaries of the system. When the differential equations are differenced, a two dimensional spacial mesh is created that may be visualized as covering the fluid system. The fluid passes through the mesh in increments corresponding to the velocities and time steps of the difference equations. In order to graphically depict the fluid motion, "marker particles" are placed in the cells of the mesh and moved with the velocities of the cells in which they reside at a particular time. The program stores the coordinates of all particles on tape for each time step, and this tape is then processed by data display equipment. This equipment plots a point on microfilm at the coordinates of each particle, and the resulting series of plots shows how the fluid configuration progresses in time. In addition to the particle plots, velocity vector plots and temperature and pressure contour plots are available that completely describe the fluid motion. When a series of these plots are placed together a motion picture is made that is analogous to viewing an actual experiment.

5.5.1 SLOSHING SIMULATION MECHANICS. Since the AS-203 data on slosh is available only from an above camera view and because of the large tank size, it was decided to investigate MAC slosh modeling using drop tower data. The test series recorded on film in the MSFC tower provides good visual data for simulation. Details of the experimental conditions were provided in a recent paper (Ref. 5-7).

The MAC simulation was performed for a six-inch diameter by ten inches high container filled to four inches with petroleum ether. A flat bottom cylinder was assumed. The actual physical situation modeled is a lateral acceleration setting up an initial slosh wave followed by a low-g drop period of approximately 4 seconds at constant accelerations within the range of 0.008 to 0.0313 g. Difficulties were encountered in the simulation of the initial accelerations setting up the wave motion at one-g prior to the drop. Wave motion was initiated by either initial displacement of the interface resulting in a potential energy source or initial fluid motion or acceleration imparting kinetic energy prior to the drop. The following methods were evaluated and compared after a few time steps.

A. The fluid was given an initial distorted interface at time zero resembling the zero velocity position after one-quarter cycle.

B. The fluid with a flat interface was given an initial velocity at time zero in a lateral direction.

C. The fluid was given an initial lateral acceleration at time zero which was cut-off at drop time.

D. The fluid was given an initial positive lateral acceleration at time zero followed by an equal magnitude and duration negative acceleration, both prior to drop.

In all of the above methods, secondary wave motion occurred at the interface and moved from the high amplitude liquid side to the low. This secondary wave motion was not observed in the drop tower film data prior to drop because of its low level. Interface disturbances observed in the analysis of movie data for Test 2F-41 when g-level dropped from 1.0 to 0.0313 were not relatable to the surface motion predicted with MAC. The single lateral acceleration, C above, appears most suitable for initiating the slosh wave.

The results of a MAC simulation of the drop tower data is presented in Figure 5-20 to illustrate the difficulties with interface motion. The small sloshing wave perturbation in this case was started with the fluid given an initial velocity at time zero simulating the side motion of the container in the one-g environment. At time .3 seconds, the g-level is reduced from 1-g to .0313-g for the remainder of the run. The input variables were a 13 $\times$ 20 mesh of size .05 ft with 630 particles. The kinematic viscosity of the fluid is 3.37×10^{-6} ft^2/sec. It is concluded that numerical instabilities occur in the interface cells due to high velocities gradients, low viscosity, and the absence of surface tension. Similar observations have been reported by Daly (Ref. 5-14) in his investigation of Rayleigh-Taylor instabilities with the marker-and-cell method. In the illustration 5-20, the interface is distorted prior to the drop time of .3 seconds, these instabilities are then magnified in the low-g environment. It is observed that the main slosh wave is significantly magnified in the low-g environment. Modifications now in progress under the continuation of this contract to incorporate surface tension in the MAC method will considerably enhance the predictive reliability of this procedure for sloshing.

5.5.2 <u>SETTLING DEMONSTRATION MODEL</u>. The Marker and Cell method has application in several areas of thermodynamic and fluid dynamic investigation. A sample problem was developed under Convair research funds to illustrate a possible settling experiment for the S-IVB configuration from an unsettled liquid situation. The results of this sample case are presented in Figure 5-21. A mesh of 21 $\times$ 36 cells of one ft by one ft model the S-IVB fuel tank. Nine particles are placed in each cell full of liquid. A pressure of 35 psia is applied uniformly to the interface.

Commencing at time zero and remaining constant, a settling force of 1.35 g is applied vertically along with a .01 lateral force. The presentation duration of Figure 5-21

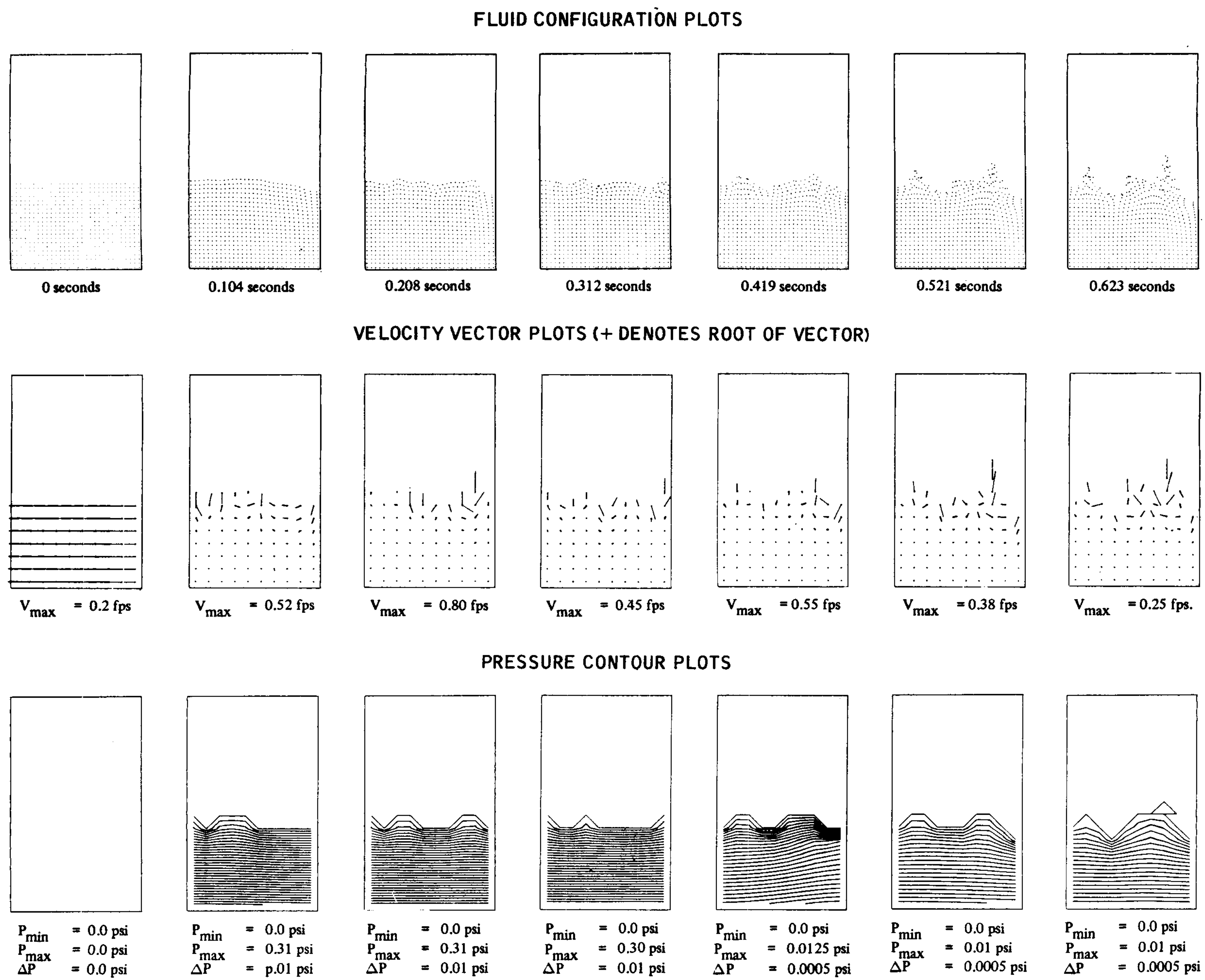

Figure 5-20. Sloshing Simulation With MAC for Scale Model S-IVB in a Drop Tower Test

represents 0.909 seconds real time. The scaling factor for velocity vectors can be determined from the values indicated for the maximum vector. With a constant ullage pressure of 35 psia, pressure isobars are shown with P_{min} at the top of the tank and P_{max} at the tank bottom. This example indicates the potential of this method for modeling orbital fluid behavior. Excessive running time is a program limitation for analysis of fluid dynamics after the initial fluid mass impinges on the opposite end of the tank. Fluid velocities are very high requiring small time steps; moreover accurate fluid resolution after this time requires selection of an initially very fine mesh with the inherent higher cost. A motion picture presentation running two minutes depicting this experimental simulation has been produced.

5.5.3 STRATIFICATION/DESTRATIFICATION MODELING. Another feature of the MAC method which indicates potential for low-g modeling is the stratification or destratification of fluids. A free convection study has been performed in a liquid hydrogen tank in a 10^{-3} g field to show the potential for tankage with complex boundary conditions. In this case, the fluid is initially at 35°R with the side walls kept at 369°R. A penetration resulted in a hot spot at 600°R on the left wall while the bottom bulkhead was kept at 166°R. Mesh size was 0.2 ft for a 13 × 19 mesh with 464 particles used. The temperature and velocity contours are shown in Figure 5-22. The initial temperature contour plots show the development of a heated fluid layer along the sidewalls and bottom. This causes convection patterns as shown in the velocity vector plots. These patterns are strongly influenced by the presence of the baffles which deflect the hot fluid toward the middle of the tank. The temperature contours on the lower left side show the presence of the high heat flux penetration and it can be seen that the fluid velocity on this side is greater than on the right. In addition to the two major vortices in the lower part of the tank, there are two above the baffles. The temperature contours show gradual heating of the bulk fluid due to mixing until at about 35 seconds there is no longer any distinct unheated liquid. At this time what appears to be a numerical instability can be seen in the downward moving fluid adjacent to the heated fluid layer. This is probably caused by the high velocity gradients and low viscosity. Increasing the viscosity or decreasing the mesh size would help to reduce this instability, however, another differencing scheme should also be considered.

The simulation of the AS-203 stratification during the long-term coast phase was examined; however the planned computer budget did not permit the extensive investigation which would have been required in developing the modeling of that stratification phenomena.

5.5.4 MARKER AND CELL MERITS. The MAC method shows significant benefits as a tool for the analysis of fluid behavior in low-g. The ability to simulate several aspects of drop tower testing have been demonstrated (Ref. 5-12). The introduction of surface tension into the model will qualify the model for further analysis of various aspects of interface behavior in low-g. Specifically, sloshing and settling studies should be continued after the inclusion of surface tension is completed. The potentials of this tool for destratification analysis with the simulation of internal mixing with a pump should be further pursued.

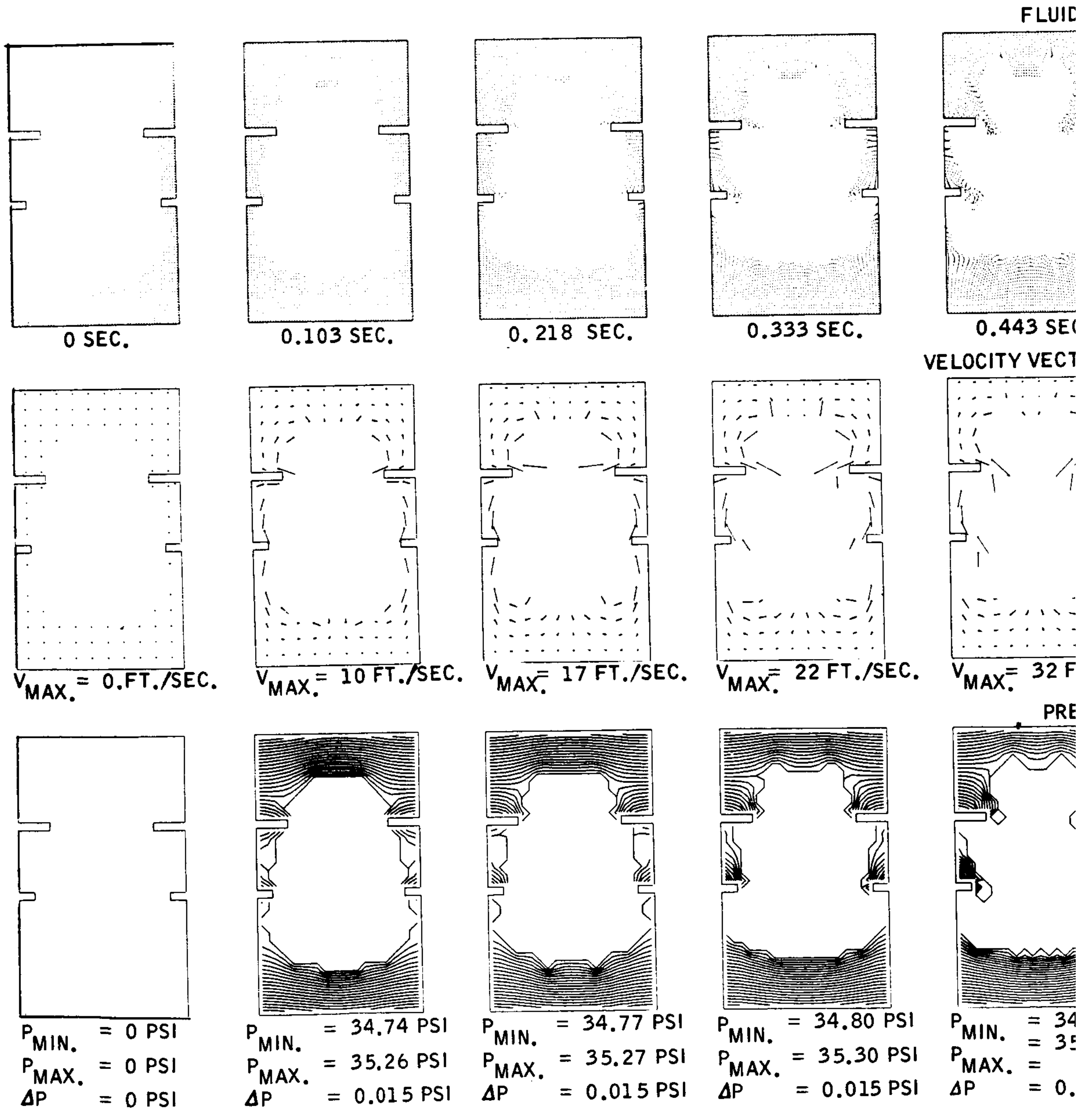

Figure 5-21. Fluid Simulation Study on S-IVB I

FOLD-OUT #1

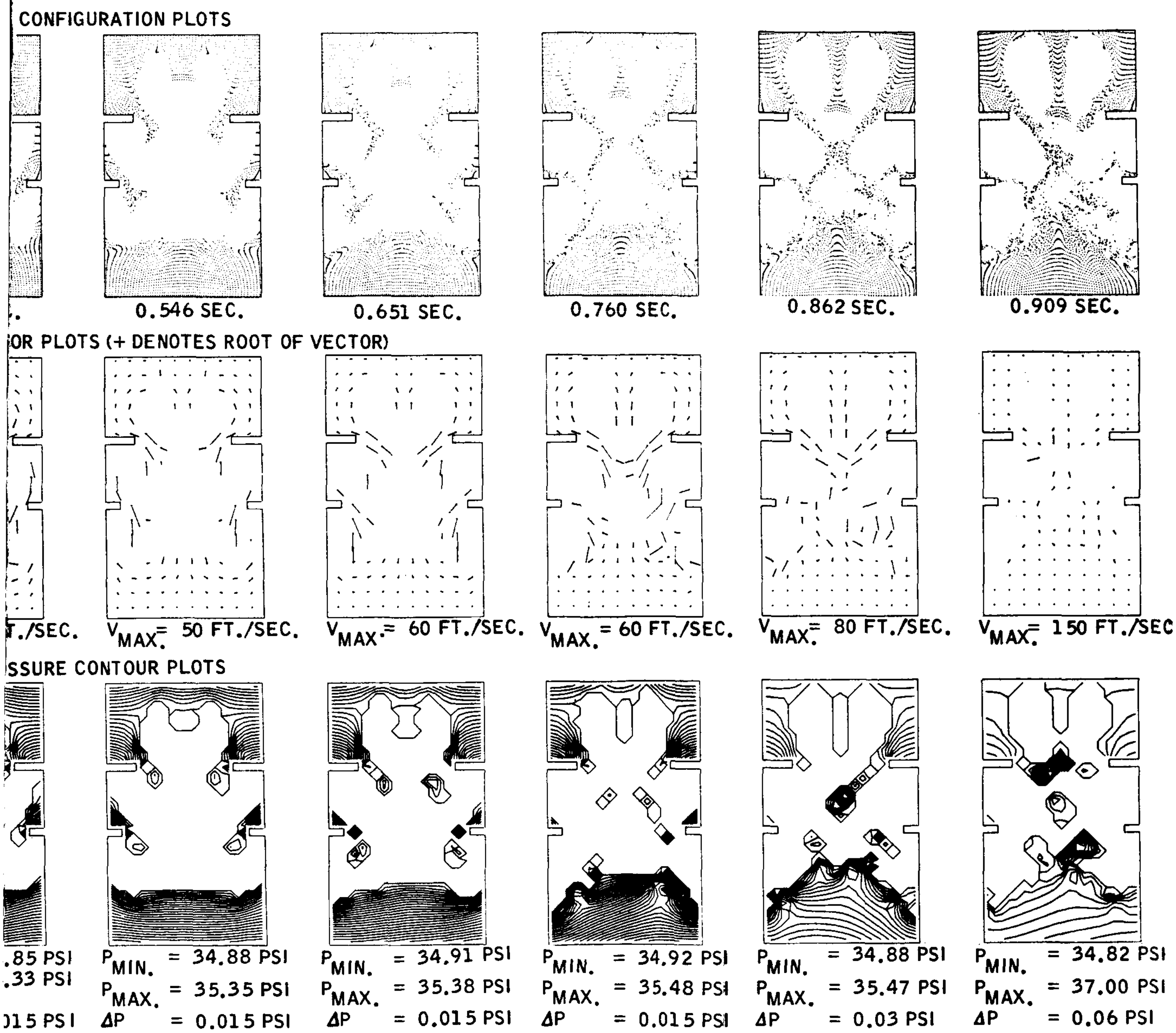

iquid Hydrogen Tank During Engine Restart in Orbit

FOLD-OUT #2

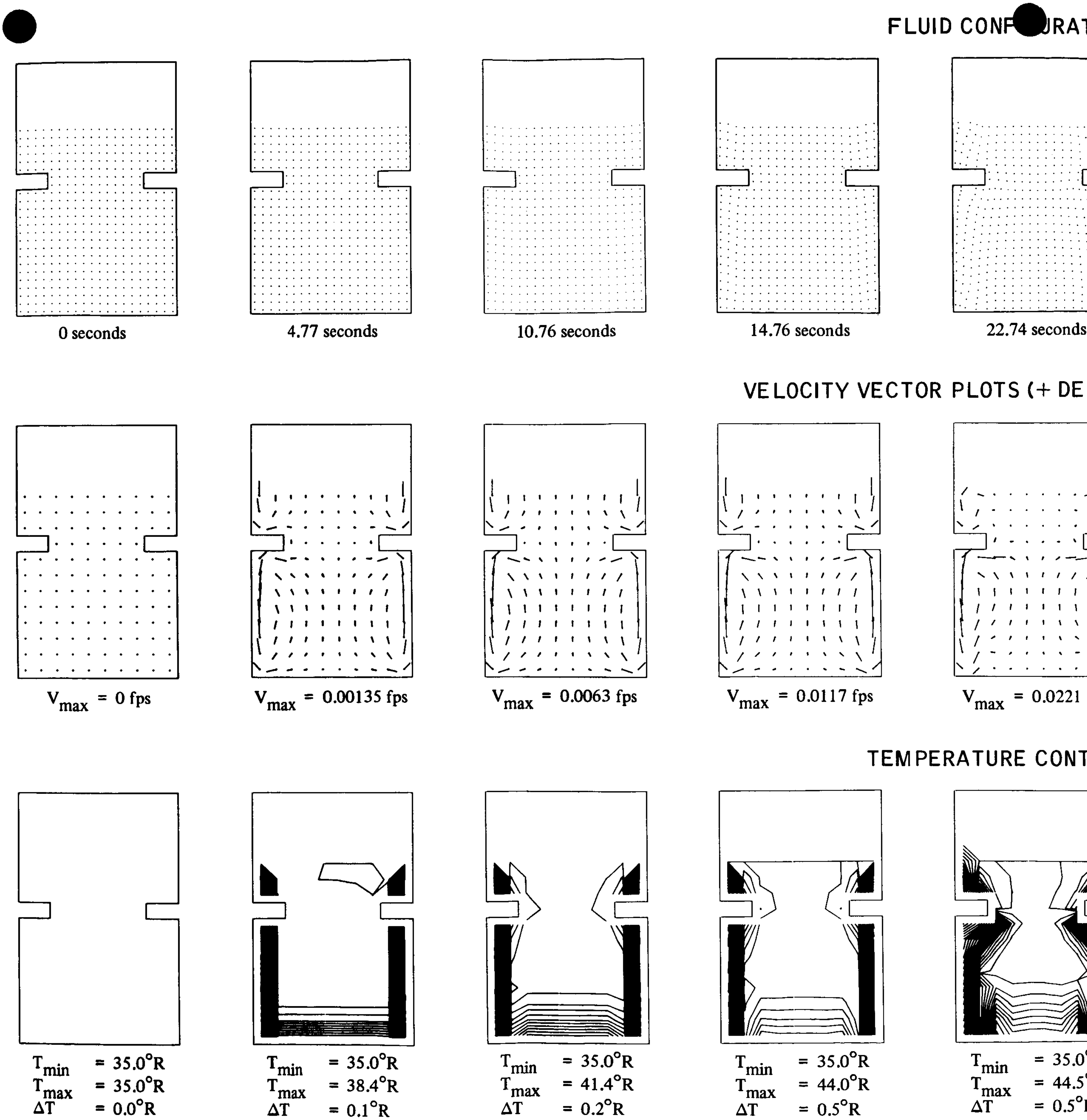

Figure 5-22. Stratification From Combi

FOLD-OUT # 1

ION LOTS

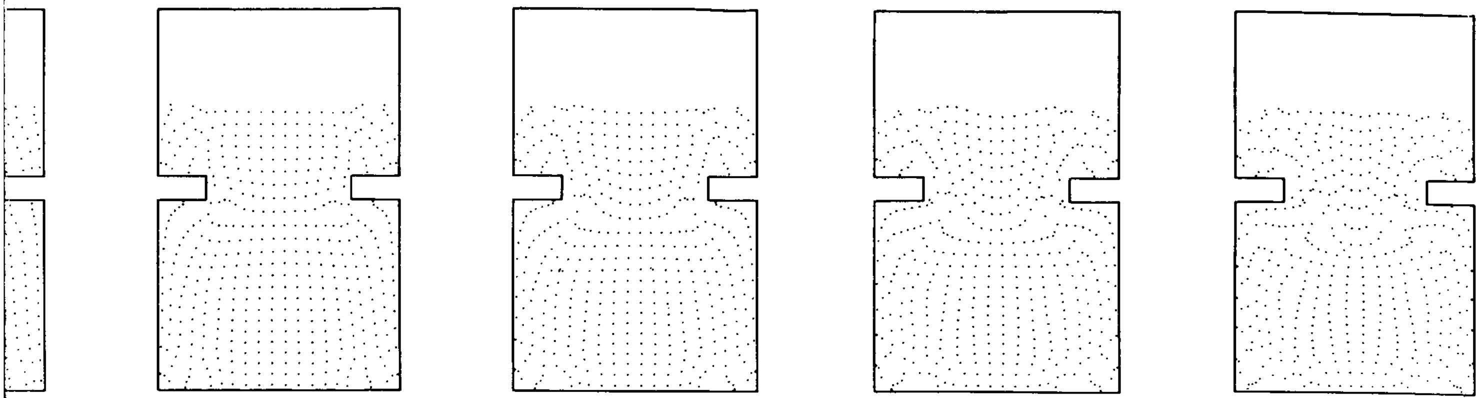

29.73 seconds | 34.72 seconds | 39.71 seconds | 45.69 seconds

NOTES ROOT OF VECTOR)

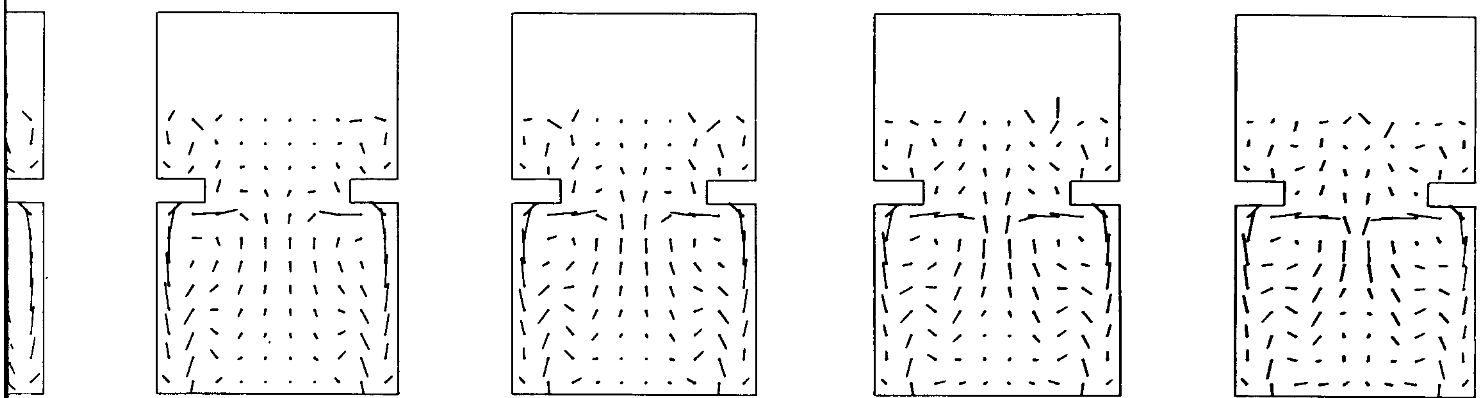

ps

V_{max} = 0.0316 fps | V_{max} = 0.0329 fps | V_{max} = 0.0333 fps | V_{max} = 0.0340 fps

OUR PLOTS

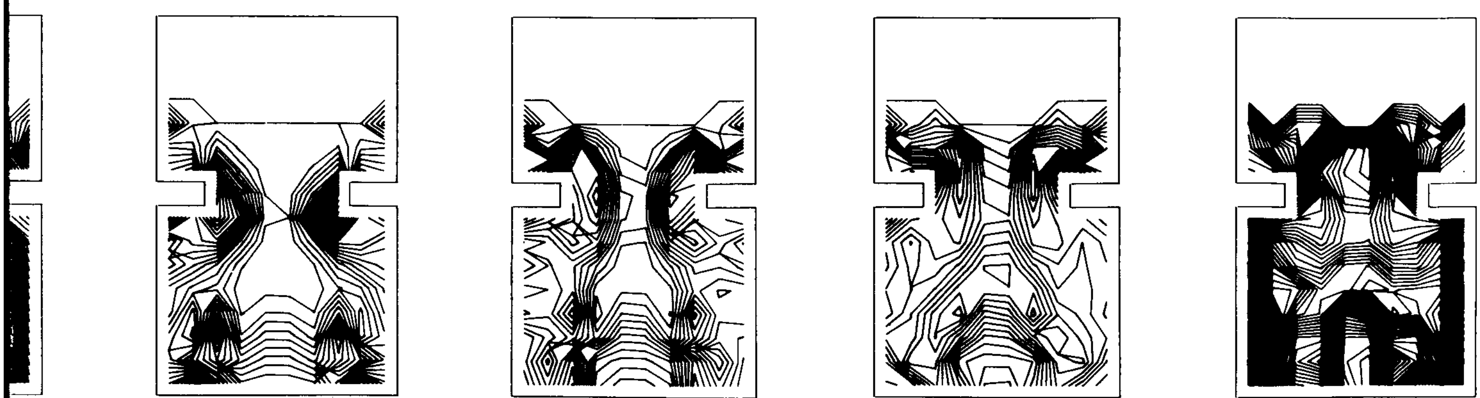

R
R

T_{min} = 35.0°R	T_{min} = 35.0°R	T_{min} = 35.0°R	T_{min} = 35.0°R
T_{max} = 45.0°R	T_{max} = 41.5°R	T_{max} = 41.5°R	T_{max} = 42.8°R
ΔT = 0.5°R	ΔT = 0.5°R	ΔT = 0.5°R	ΔT = 0.2°R

ned Sidewall and Bottom Heating

FOLD-OUT #2

6

CONCLUSIONS AND RECOMMENDATIONS

1. The PRISM model used in Section 2 indicates adequately the energy and mass contributions during the repressurization process. This model is highly suited to a parametric analysis of energy contributions including recirculation flow. The AS-203 data can be represented by this model with judicious selection of empirical constants. The S-II Pressurization model was analyzed to determine its suitability to repressurization analysis; from the disparity with AS-203, it was concluded that the influence of recirculation flow on the ullage pressure behavior is significant.

   The analysis of chilldown flow merits further analysis. This requirement will reoccur in the design of engine chilldown sequences for all vehicles with orbital restart requirements. Although a recent contract (Reference 6-1) resulted in a chilldown computer model, this model lacks the flexibility for analyzing lines where thermal mass varies with length. A program is required in which flow rate and thermal mass are input and outlet quality is defined. The interaction of this recirculation flow with the bulk liquid and then apparent interaction with the ullage should be further analyzed.

2. Convair computer codes for propellant heating were found to be adequate for the analysis of AS-203 orbital heating during the long term coast. Large differences were determined between the heating for the four individual vehicle quadrants; this should be accounted for in all thermal analyses. The heating rate to the dome was higher than originally assessed, the absorptivity of the forward dome exterior had probably deteriorated from .05 to .20. The latter value fit thermal predictions best. This deterioration should be avoided on future flights by proper insulating techniques. Thermal energy predictions agreed more closely with AS-203 rates predicted by wall temperature difference than with changes in fluid properties. Evaporation was probably less than 50 lbs during the long term coast period.

   The ullage heating should be predicted within five percent to attain reasonably accurate pressure rise rates. Both the S-II Pressurization program and REPORTER closely predict pressure rise rate when furnished with good ullage heating data. Although settled propellant coast pressure rise prediction capability has been verified within this study, unsettled propellant behavior should be further considered and models verified for extended long term coast.

3. The AS-203 data was reviewed and indicated no serious problems with liquid level rise for vent rates of 2.2 lb_m/sec with the propellant initially settled. Parametric studies with three analytical models confirmed these results. A model which states all sensible heat goes to boil-off is unreliable and overly conservative. A pre-design model developed on the basis of boiling in the boundary layer affords reasonable results for liquid level rise parametric data. A bubble dynamics model confirms the above pre-design model and indicates good potential for the study of bubble behavior in low-gravity environments. In the analysis of liquid level rise, significant factors are wake effects on bubble velocities, agglomeration, and void faction effects on bubble velocities. A related area to liquid level rise is the break-up of the interface into globules which float in the ullage. This was observed on AS-203 but the mechanism providing this large amount of energy to the globules was not identifiable.

The behavior of bubbles in temperature fields in low gravity environments will define the propellant ullage configuration for design specification. Ullage growth due to bubble agglomeration from localized heat leaks should be analyzed. The program EVOLVE provides a useful tool to perform this analysis. The fluid configuration also interacts with propellant heating and the pressure rise evaluation. These areas merit extended analyses before design proceeds on new stages with long coast periods. An analytical study is called for on interface break-up during changes in g-level and during vent downs. An examination of interfacial forces and the interaction of emerging bubbles is required. The location of the propellant and the ability to control this location are important considerations in vehicle design.

4. Liquid propellant slosh analysis is based on an analytical solution to the hydrodynamic equations of motion. Drop tower testing of a 6-inch scale model S-IVB afforded more detailed data for analysis than the AS-203 coverage; however both were simulated with the slosh model. The correlation of maximum liquid amplitude with Froude number between the slosh model and drop tower data shows under prediction below a Froude number of one and over prediction at higher Froude numbers. Differences shown between theoretical amplification factor and observed model data are an indication of baffle efficiency. Transient meniscus effects complicate the analysis of sloshing in drop tower tests, in addition the meniscus is larger than theoretically predicted. The most serious discrepancy between analytical and test results however exists in the modeling of propellant slosh with partially uncovered baffles.

Time averaging of propellant slosh energy losses in low-g can result in serious errors in predicting fluid behavior. Mathematical modeling under these slosh conditions is not well established. Further analytical development and correlation with test data is necessary. Possibly curve fitting test results with current slosh baffle damping parameters would prove useful.

Simulation of S-IVB sustained coast shows that the reaction control motors are the single most important disturbance. It is therefore necessary to minimize vehicle maneuvering requirements and keep disturbances at a minimum. No coupled frequencies were observed in simulating S-IVB flight conditions; the propellants oscillated at their natural frequencies. The results of this study are in qualitative agreement with actual AS-203 results and confirm the utility and applicability of the sloshing model used.

5. The Marker-and-Cell model has broad applicability in the analysis of fluid behavior in low-g. In slosh simulation some difficulty was encountered in setting up initial conditions. Fluid simulation of sloshing can be improved with the addition of surface tension to the model. Applicability of the model to sloshing, settling, and stratification are demonstrated. Additional analysis is required in wave amplification analysis as related to propellant control devices such as baffles and deflectors. It is also recommended that further efforts be made to simulate other available low-g data with this theoretical model to define and confirm the applicability to orbital low-gravity simulation.

7

REFERENCES

1-1 Anon.: Evaluation of AS-203 Low Gravity Orbital Experiment. Chrysler Corp. Report BB-3.4.3-S-101, Contract NAS8-4016, January 1967.

1-2 Anon.: Saturn S-IVB-203 Stage Flight Evaluation Report, Volume II. Douglas Report SM-46988, October 1966.

1-3 Anon.: Results of the Second Saturn 1B Launch Vehicle Test Flight AS-203. NASA/MSFC, Report MPR-SAT-FE-66-12, September 1966 (Conf.)

2-1 Anon.: Design Guide for Pressurization System Evaluation. Vol. I, Report 2334, Contract NAS7-169, September 1962.

2-2 Wulff, W. and Schipma, P.: Design Guide for Pressurized Gas Systems. Illinois Institute of Technology Research Institute Report IITRI-C6070-20, NAS7-388, June 1967.

2-3 Anderson, J. E.; Scott, O. L.; Brady, H. F.: Advanced Pressurization Systems for Cryogenic Propellants. NASA CR-54467, Contract NAS3-2574, January 1967.

2-4 Thompson, J. F. and Nein, M. E.: Prediction of Propellant Tank Pressurization Requirements by Dimensional Analysis. NASA TN D-3451, NASA/MSFC, June 1966.

2-5 Epstein, M.; et al: Fortran Program for the Analysis of a Single Propellant Tank Pressurization System. Rocketdyne Report R-5725, June 1964.

2-6 Schilling, R. J.: AC-8 Second BPS Fuel Tank Pressure Simulation. Convair Computer Program 3995, March 1966.

2-7 Armfield, L. E.: Space Vehicle Radiant Energy Program (SAINT NERO). Convair Report GDC-ERR-AN-929, November 1966.

2-8 Dummer, R. S. and Breckenridge, W. T., Jr.: Radiation Configuration Factors Program (CONFAC). Convair Report ERR-AN-224, February 1963.

2-9 O'Neill, R. F.; Worscheck, G. A.; and Kramer, J. L.: Variable Boundary II Heat Conduction Program. Contract NAS3-8711, Convair Report GDC-BTD67-004, August 1967.

3-1 Walburn, A. B. and Bradshaw, R. D.: Development of Analytical Methods for Predicting Residual Cryogenic Propellant Behavior in Orbital Vehicles, Interim Report. Contract NAS8-20165, Convair Report GDC-DDB66-011, October 1966.

3-2 Walburn, A. B.; Evans, E. A.; and Ball, W.: Development of Analytical Methods for Predicting Residual Cryogenic Propellant Behavior in Orbital Vehicles, Final Report. Contract NAS8-20165, Convair Report GDC-DDB67-003, November 1967.

3-3 Haussler, Jonathan B.: Saturn AS-203 Postflight Trajectory. NASA TMX-53534, November 1966.

3-4 Pearson, B. Douglas Jr. and Neel, Carr B.: Albedo and Earth Radiation Measurements From OSO-II. Paper 67-330, AIAA Thermophysics Specialist Conference, New Orleans, Louisiana, April 17-22, 1967.

3-5 Lemke, L. C.: Radiative Surface Property Degradation as a Result of Salt Atmosphere Exposure. AIAA Paper 66-141, 3rd Aerospace Sciences Meeting, New York, January 1966.

3-6 Walburn, A. B., and Evans, E. A.: Residual Propellant Orbital Thermodynamics Program (REPORTER) Version A. Convair Report GDC-DDB67-004, Contract NAS8-20165, November, 1967.

4-1 Adelberg, M.: Level of a Boiling Liquid in a Low-Gravity Environment. J of Spacecraft and Rockets, 5, No. 1, 108, 1968.

4-2 McGrew, J. L., and Larkin, B. K.: Cryogenic Liquid Experiments in Orbit, Vol. II. NASA CR-652, December 1966.

4-3 Swalley, F. E., Platt, G. K., Hastings, L. J., Saturn V Low Gravity Fluid Mechanic Problems and Their Investigation by Full-Scale Orbital Experiment. Proceedings of Symposium on Fluid Mechanics and Heat Transfer Under Low Gravity, Palo Alto, California, June 1965.

4-4 Fredreckson, G. O., Schweikle, J. D.: Thermo and Hydrodynamic Experiment Research Module in Orbit, Final Report, Contract NAS8-1053, DAC-60594, March 1967.

4-5 Rohsenow, W. M., and Choi, H.: Heat, Mass, and Momentum Transfer. P. 217, Prentice-Hall, Inc. (1961).

4-6 Shirley, J. E.: Final Report for the General Dynamics/Astronautics Zero-G Program Covering the Period from May 1960 through March 1962. Convair Report FY62-0031, NAS8-2664, August 1962.

4-7 Siegel, R. and Keshock, E. G.: Nucleate and Film Boiling in Reduced Gravity From Horizontal and Vertical Wires. NASA TR R-216, February 1965.

4-8 Harmathy, T. Z.: Velocity of Large Drops and Bubbles in Media of Infinite or Restricted Extent. AIChE J, 6, 281-8, 1960.

4-9 Evans, E. A., et al: Thermodynamic and Fluid Mechanic Studies of Cryogenic Propellants, Chapter 3, Convair Report GDC-ERR-1333, December 1968.

4-10 Landau, L. D. and Lifshitz, E. M.: Fluid Mechanics, Addison Wesley, 1959.

4-11 Aris, R.: Vectors, Tensors and the Basic Equations of Fluid Mechanics, Prentice-Hall, Inc., 1962.

4-12 Peebles, F. N. and Garber, J. H.: Studies on Motion of Gas Bubbles in Liquids, Chemical Engineering Progress, Volume 49, No. 2, February 1953.

4-13 Swain, L. M.: On the Turbulent Wake Behind a Body of Revolution, Proc. Royal Society London, Series A, Vol. 125, p 647, 1929.

4-14 Schlichting, H.: Boundary Layer Theory, McGraw-Hill, Inc. 1960.

4-15 Gibson, C. H., Chen, C. C., and Lin, S. C.: Measurements of Turbulent Velocity and Temperature Fluctuations in the Wake of a Sphere, Journal of AIAA, Vol. 6, No. 4, p 642, April 1968.

5-1 Lomen, D. O.: Liquid Propellant Sloshing in Mobil Tanks of Arbitrary Shape, NASA CR 222, April 1965.

5-2 Lomen, D. O.: Analysis of Fluid Sloshing. GDC-DDE66-018, June 1966.

5-3 Miles, J. W.: Ring Damping of Free Surface Oscillations in a Circular Tank. Journal of Applied Mechanics, PP 274-276, June 1958.

5-4 Keulegan, G. H. and Carpenter, L. H.: Forces on Cylinders and Plates in an Oscillating Fluid. Journal of Research of the National Bureau of Standards, Vol. 60, No. 5, May 1958.

5-5 Lomen, D. O.: Elastic, Non-Linear, and Damping Considerations for Sloshing in Tanks of Arbitrary Shape. GDC-ERR-AN-802, December 1965.

5-6 Bauer, H. F.: The Damping Factor Provided by Flat Annular Ring Baffles for Free Fluid Surface Oscillations. NASA-MTP-AERO-62-81, November 1962.

5-7 Toole, L. E. and Hastings, L. J.: An Experimental Study of the Behavior of a Sloshing Liquid Subjected to a Sudden Reduction in Acceleration. NASA TM-X-53755, August 1968.

5-8 Satterlee, H. M. and Reynolds, W. C.: The Dynamics of the Free Liquid Surface in Cylindrical Containers Under Strong Capillary and Weak Gravity Conditions. Stanford University Technical Report LG-2, May 1964.

5-9 Anon: Astroionics Systems Handbook, Saturn Launch Vehicles. August 1965.

5-10 Buchanan, H. J. and Bugg, F. M.: Orbital Investigation of Propellant Dynamics in a Large Rocket Booster. NASA Technical Note, NASA TN D-3968, May 1967.

5-11 Bradshaw, R. D.; Kneisel, K. M., et al: Thermodynamic Studies of Cryogenic Propellant Management. Convair Report GDC-ERR-AN-1144, December 1967.

5-12 Bradshaw, R. D.; Kneisel, K. M., et al: Thermodynamic and Fluid Mechanic Studies of Cryogenic Propellants. Convair Report GDC-ERR-1333, December 1968.

5-13 Welch, J. E., et al: The MAC Method, A Computing Technique for Solving Viscous, Incompressible, Transient Fluid-Flow Problems Involving Free Surfaces. Los Alamos Scientific Laboratory, Report LA-3425, November 1965.

5-14 Daly, B. J.: A Numerical Study of the Effect of Surface Tension on Interface Stability. Los Alamos Scientific Laboratory, Report LA-DC-9991, 1968.

6-1 Anon.: A Study of Cryogenic Container Thermodynamics During Propellant Transfer - Volume III, Transfer Line Thermodynamic Analysis, Lockheed Missiles and Space Company Report K-14-67-3, NAS8-20362, November 1967.

APPENDIX A

PRISM PROGRAM

This program is designed to predict pressurization system requirements and pressure histories for the Centaur and S-IVB vehicles. The full capability of the program is indicated by the input, nomenclature and program listings given below. Some program options were not used as evidenced by the sample input case shown at the end of the program listing. The input is explained following the listing.

The problem was inputted in three phases. In the first phase, helium addition and ambient heating were included. In the second phase recirculation begins. In the third, helium addition is not included while ambient heating and recirculation continue.

Card 1 of the input gives the constant data indicated on page A-3. Helium bottle data is not included since the helium flow rate, temperature and pressure are input as a function of time.

Card 2 gives indicators for heat input. Three heating segments each will be input with heating values. The heat transfer options in the program are not used since the data obtainable from these calculations was already available from the Variable-Boundary II Heat Conduction Program (P 2162). The sixth, seventh and eighth data fields indicate whether recirculation, multilayer walls and helium flow rates inputs are to be used.

Cards 3, 4, and 5 give the stations for each of the 3 heating segments.

Card 6 indicates the heat table entries will be 14 for Table 1.

The next 14 cards (7-20) give the heating rate for 14 time values for segment 1.

Cards (21-50) give heating tables for nodes 2 and 5.

Card 51 gives the number of recirculation values to be inputted. The next five cards give that number of recirculation flow rates. This is followed by the Δh between the liquid entering the recirculation system and the fluid exiting the recirculation system and reentering the tank. The times corresponding to these flow rates and enthalpy changes are then listed in order.

The next table (Card 67-73) for helium pressurant inflow gives 9 entires of flowrate, followed by 9 entries of temperature entering the tank and 9 time values.

Card 74 begins the case data which is specified by "namelist." Following the title card is series of case data values giving the initial ullage pressure, temperature, mass of liquid and saturation pressure.

The case data is followed by phase data indicating whether recirculation, helium addition, liquid outflow, venting, interfacial heat transfer tank wall vaporization, or ullage heating directly by the recirculation flow occurs. Also given are the gravity level, the initial time and time step and the allowable integration errors. Phase data is given for all three phases separately.

Three cases are then inputted in addition to the initial case outlined. The case data and phase data are repeated completely for each case with appropriate changes made corresponding to each case.

Central processer time used for the four runs in Figures 2-6 and 2-7 was 34 sec.

LISTING OF PRISM INPUT
(P3995)

1.1 CONSTANT DATA - FORMAT (8E10.5)

AL = Area of Liquid - Gas Interface, ft^2

CP = Approx. Const. Pressure Specific Heat of Propellant Vapor, Btu/lb ^oR

CV = Approx. Const. Volume Specific Heat of Propellant Vapor, Btu/lb ^oR

CPHE = Const. Pressure Specific Heat of Helium Vapor, Btu/lb^oR

CVHE = Const. Volume Specific Heat of Helium Vapor, Btu/lb ^oR

HFG = Heat of Vaporization of Propellant, Btu/lb

CL = Specific Heat of Liquid Propellant , BTU/lb^oR

RHE = Gas Constant of Helium,

VBTL = Volume of Helium Bottle, in^3

MBTL = Mass (Weight) of Helium Bottle, lb

CBTL = Specific Heat of Helium Bottle, Btu/lb ^oR

ABTL = Helium Bottle Area For Heat Transfer From Bottle to Helium, ft^2

2.1 INDICATORS FOR HEAT INPUT- FORMAT(10 I2)

NQSEGS = No. of Segments (or Nodes) of tank heating to be Inputted

NQWTBS = No. of Tank Heating Tables

NCWTBS = No. of Tank Wall Specific Heat Tables

NNERØ = No. of Sets of St. Nero Heating Tables

NRETRØ = 0 or Blank for no Retromaneuver Data
Positive Interger For Input of Retromaneuver Data

IRECIR = 1 or 0,Recirculation Flow, 0 if Omitted

MLTIWL = 1 or 0,Multiple Material Wall or Multitemp Wall
0 if Single Thickness

IBURP = 1 or 0, 1 - Inputting Helium Bottle Flow Rate
0 - No Helium Bottle

2.2 HEATING SEGMENTS (NODES) - FORMAT (5I2, 7E10.2) - Repeat

IQW = Heating Table Flag

ICW = Tank Wall Heating and specific heat flag.

IFLUX = Flag to indicate whether heating rate or heat flux is being input 0 - Rate
1 - Flux

IAW = Tank Side Wall Area Flag

INERØ = St. Nero Heating Table Flag (will not handle upper dome type radiation)

STØPS = Station of Top of Heating Segment - from top

SBØTS = Station of Bottom of Heating Segment - from top

QW = Segment Heating Rate (or Flux)

TW = Segment Wall Temperature

MW = Segment Wall Mass

EMISS = Emissivity for Reradiation to Space From Segment Wall Area

FAW = Ratio of Segment Area to Tank Wall Area Between (ST4P) and (SBØTS)

Also (if ICW = 0 with Format E 10.5):

CW = Specific Heat of Wall Segment

Note: If IQW. 6TO, QW may be left blank, also if ICW. LT. 0 TW, MW, and EMISS may be omitted.

If FAW is left blank, program sets it equal to 1.0

2.3 HEATING RATE TABLES - FORMAT (2I2, 6X, E10.2/(2E10.2)) - REPEAT NQWTBS

NQ = No. of Pairs of Entries in Heating Table

NQTB = Heating Table No. (must be LT. 6)

DTQ = Bias Added to (TIME) prior to Loock-up in Table

TBTQ = Time Entries in Tank Heating Table, Second

TBQ = Heating Rate (or Flux) Entries in Heating Table, Btu/sec

2.4 SPECIFIC HEAT TABLE - FORMAT (2I2/(2E10.2)) - Repeat NCWTBS TIMES

NCW = No. of Pairs of Entries in Heating Table

NCWTB = Specific Heat Table No. (Must be LT. 4)

TBTCW = Temperature Entries

TBCW = Specific Heat

2.5 ST NERO HEATING RATE INPUT - FORMAT (2I2, 6X, 3E10.2) and (F10.2, 10X, 4F10.3)

2.6 RETROMANEUVER DATA

2.7 RECIRCULATION TABLE

NRE	=	No. of entries Recirculation Table (Maximum 50)
XRECIR	=	Recirculation Flow Rate, LB/SEC
XDELH	=	Recirc ΔH, BTU/LBM
RETIME	=	Time of entry
NHE	=	Number of entries, Helium pressurization table
HEFLOW	=	Helium flow rate, LB/SEC
HETMP	=	Helium temperature at inlet, °R
TBURP	=	Time of entry

3.1 CASE TITLE CARD - FORMAT (8A10)

HEAD

3.2 CASE DATA - FORMAT SPECIFIED BY 'NAME LIST" (Good for every phase run or initialized values

P, PU	=	Total tank pressure, psia
PHE	=	Initial ullage temperature, °R
TU	=	Initial ullage temperature, °R
TW	=	Initial wall temperatures (supercede TW in 2.2), °R
TBTL	=	Initial temperature of Helium Bottle and Helium in Bottle, °R
PBTL	=	Initial pressure of Helium in GH, PSIA
XML	=	Initial mass of liquid, lbs
PSATL	=	Initial vapor pressure of liquid, PSIA
ISAVE	=	Flat = 1 for normal initialization = 2 for reinitialization to previously saved conditions = 3 to use conditions at end of previous phase as initial conditions for next phase
NVENT, XPVENT, XMVENT	=	No. of entries and vectors containing table of vent flow rate versus pressure

4.1 PHASE TITLE CARD - FORMAT (80H)

4.2 PHASE DATA - FORMAT SPECIFIED BY "NAMELIST"

CD	=	Burp Orifice Discharge Coefficient
AØTØT	=	Burp Orifice Area "Seen" By He Bottle, in^2
AØFUEL AØGAS	=	Burp Orifice Area "Seen" by Ullage, in^2 (2 names for same variable)
CØNTLG CONQLG	=	Constant Multiplied to Rate of Heat Transfer From Gas to Liquid (usually = 1.0)
CØNTV	=	Constant to specify vent temperature, $T_{vent} = T_u + CONTV*(T_u - T_{liq})$
DEADWT	=	Dead weight of vehicle (for acceleration calcu)
WRATIØ	=	Ratio of Total Liquid Propellants to Liquid in Tank Under Study
TIME	=	Initial Time (This is updated during phase and equals TIMEF at End of Phase)
TIMEF	=	Final Time of Phase
DTIME	=	Initial Stepsize (changed in DIFE3 to Satisfy Error Tolerances)
DTTØL	=	Time Allowance in Specifying Boil-off
EPSP	=	Allowable Relative Error in Pressure Iteration
EPSR	=	Allowable Relative Error in Integration
EPSA	=	Allowable Absolute Error in Integration
HAMS	=	Heat Transfer Parameter in Spray Calculations
HBTL	=	Helium Bottle Heat Transfer Coefficient, Btu/hr-ft^2-^oR
HEUSE	=	Helium (Constant) Usage Rate, lbs/sec
IFLØW	=	Venting Flag = 1 Vent - but V/V initially closed = 2 Vent - but V/V initially open = 3 No venting - vent rate initially set = 0. = 4 Call subroutine VENT = 5 No venting - vent rate set = 0 each time.
G	=	G LEVEL = (g/g_o)
MDØTFF	=	Vent valve flow rate at P=PFFLØW and T = 45^oR, lbs/sec
MDØTRS	=	Vent valve reseat flow rate, lbs/sec
MPRESET	=	Vent Valve Reseat Pressure, psia

PCRACK = Vent valve cracking pressure, psia

PFFLØW = Vent valve full-flow, pressure, psia

MDØTL = Liquid outflow rate (constant), lbs/sec

NEXT = Flag = 1 to return for input beginning at 1.1 at end of phase
= 2 to return for input beginning at 2.1 at end of phase
= 3 to return for input beginning at 3.1 at end of phase
= 4 to return for input beginning at 4.1 at end of phase
= 5 to stop at end of phase

PCQLH2 / FQLIQ — Fraction of liquid heating which goes to heating liquid, remainder goes to boil-off, this parameter is calculated in Prog. if CONQBO > 0.

TM = Vector of integrated quantities

NQS = Number of Heating Sections - Supercedes NQS (= NQSEGS) in 2.1

DTQ = Heating Table Time Bias, Seconds

QBP = Boost pump Heating Rate, Btu/sec

QWG = Rate of Heat Transfer From Walls to Ullage, Btu/sec (Not used if NWSTO)

QWL = Rate of Heat Transfer From Walls to Liquid, Btu/sec

TIMES = Time Bias in Spray Calculations, seconds

X = Quality of spray flow

F = Total Vehicle Thrust, Pounds

DTQSW = Same as DTQ(1)

RRATE = Vehicle Roll Rate (Relative to St Nero Input), Degrees/sec

QW = Wall Heating Rate, Supersedes QW in 2. 2, Btu/sec or Btu/sec-ft^2

PVARYØ = Pressure at which bump orifice area is set to zero, psia

DPVARY = Delta-Pressure (Below PVARYØ) at which orifice area begins to be restricted.

CONSAT = Constant to specify pressure at which liquid boil-off occurs
= 1.0 for B/O at partial pressure of vapor
= 0.0 for B/O at tank pressure

ISAVE = Save Flag = 1 To not save initial conditions of phase
= 2 To save initial conditions of phase for initial conditions of future case

DISPRAY	= Flag	= 1 To perform spray calculations during phase = 2 To not perform spray calculation during phase
ICPV	= Flag	≤0 Do not call subroutine CPVENT >0 Call constant pressure venting subroutine in CPVENT. Must also set IFLØW = 5
CØNQSP	= Constant to specify LOX tank standpipe heat transfer.	
IRETRO	= Flag	≤ 0 Do not call subroutine RETRO during phase > 0 Call subroutine RETRO during phase
XMPULL	= Liquid mass remaining in tank when gas pull-through occurs during retromaneuver, pounds	
IPLØT	=	≤ 0 No plots = 1 Save points for plots = 2 Save points for plots and generates plots at end of phase
NPLØT	= Identifies variables to be plotted	
CONFAC	= Fraction of energy to liquid due to recirculation	
TNVNT	= Vent temperature	
KBURP	= Flag for helium addition,	0 -No Helium 1 - Helium Added
CØNBRP	= Constant between 0. and 1.0. If 1.0 as maximum heat transfer occurs due to burp. If 0.0 no vapor is formed due to burp.	
CØNQBØ	= Constant between 0.0 and 1.0 determine fraction of Helium added to sensible heat of liquid. 0.0 for Helium added to the top of the tank. 1.0 for Helium added at the bottom and bubbled up through the fluid.	
KRECIRC	= Recirculation flag - set to 1 to start recirculation	
CONFAC	= Constant 1.0 means all recirculation flow condenses before it reaches the ullage, 0.0 means all recirculation flow reaches the ullage with no energy transfer to the liquid.	

DL DØ AT AC FRICTN GAM LINE MFØ MC MFT AFI KBUG AE FMIN	Variables for Improved Centaur Venting Subroutine

PROGRAM LISTING FOR PRISM

```
RUN(S,,,,,,,,,1)
SET(0)
LGO.
R
      PROGRAM PRISM (INPUT, TAPE5=INPUT, OUTPUT, TAPE6=OUTPUT, TAPE48)
C
C               CENTAUR TANK PRESSURE SIMULATION PROGRAM
C
      DIMENSION TM(99),HEAD(8),AWLL(2),TMSAVE(99)
      REAL    MDOTL ,MDOTBP,MDOTE ,MDOTV ,MDOTG ,MDOTHE,MDOTFF,MDOTS ,
     *        MDOTSO,MBTL  ,MDOTET,MDOTRS,LEFF  ,MW
      REAL   MDOTE3
      COMMON /CMAIN/
     *        AOTOT ,AOGAS ,AL    ,AWLL  ,ABTL  ,
     *        CD    ,CV    ,CP    ,CVHE  ,CPHE  ,CL    ,CHTL  ,
     *        CONQLG,CONTV ,CONSAT,CONQSP,
     *        DEADWT,DTIME ,DTTOL ,DPVARY,
     *        EPSP  ,EPSR  ,EPSA  ,F     ,FQLIQ ,FMDOTS,G     ,
     *        HFG   ,HAMS  ,HEUSE ,HBTL  ,HW    ,HL    ,
     *        IFLOW ,IFLOW1,ISPRAY,I1    ,I2    ,ICPV  ,ISAVE ,LEFF ,
     *        MDOTL ,MDOTBP,MDOTE ,MDOTV ,MDOTG ,MDOTHE,MDOTFF,MDOTS ,
     *        MDOTSO,MBTL  ,MDOTET,MDOTRS,NTDOT ,
     *        P     ,PBTL  ,PCRACK,PRESET,PFFLOW,PR    ,P1    ,PINV  ,
     *        PVARYO,PMAX  ,PMIN  ,PCON  ,
     *        QGS   ,QBHE  ,QBP   ,QWL   ,QWG   ,QGL   ,
     *        RHOL  ,RHOG  ,RHE   ,
     *        SV    ,SVSAT ,SVVNT ,SLL   ,SIGN  ,STOP  ,SVLIQ ,
     *        TU    ,TU1   ,TSAT  ,TVNT  ,TIMES ,TMES2 ,TIME1 ,
     *        UG    ,UGSAT ,UGVNT ,
     *        VTOT  ,VL    ,VU    ,VU1   ,VBTL  ,
     *        WRATIO,X
      COMMON /HEAT/
     *        NQS   ,IQW(30) , ICW(30) ,IFLUX(30) ,IAW(30) ,EMISS(30),
     *       STOPS(30) ,SBOTS(30) ,QW(30) ,TW(50) ,MW(30) ,CW(30) ,
     *        FAW(30) ,ATOP(30) ,AW(30) ,NQW(5) ,TBTQ(30,5),TBQ(30,5),
     *        NCW(3) ,TBTCW(30,3) ,TBCW(30,3) ,DTQ(5),
     *        NAW(2)  ,TBSA(90,2)  ,TBA(90,2)
      COMMON /TABLE/
     *        NPG,NTG,TBPG(9)   ,TBTG(9,50),TBSV(9,50),TBUG(9,50),
     *        NSAT ,XPSAT(10)   ,XTSAT(10) ,XSVSAT(10) ,XUGSAT(10),
     *        XHFG(10) ,XSVLIQ(10) ,NVOL ,TBHVOL(110),TBVOL 110),
     *        NVENT,XPVENT(10) ,XMVENT(10),NS ,XTIMES(20) ,XMDOTS(20)
     *,       TBTKW(10,3) ,TBKW(10,3) ,NKW(3)
      COMMON /CVENT/DL    ,DO    ,AT    ,AC    ,FRICTN,GAM   ,LINE  ,
     *        MO    ,MC    ,MT    ,AI    ,PTO   ,PTS   ,POO   ,POS   ,
     *        FPO   ,FPT   ,PCO   ,PIO   ,AE    ,KBUG  ,ME    ,ISP   ,
     *        PCS   ,DPENT ,PTANK ,IFIRST,IPRINT,FMIN
      COMMON /S4HEAT/
     *        MLTIWL  ,MATL(7,12),NSLICE(12),THICK(7,12),WD 3)
C
      COMMON /S4MAIN/
     *       XRECIR(50),XDELH(50) ,RETIME(50),RECIRC     ,DELH      ,
     *       NRE        ,CONFAC     ,IRECIR     ,TBI        ,MDOTE3    ,
     *       KRECIR     ,QLREC      ,MDOTC
```

```
C
      COMMON/BURP/
     *        IBURP      ,NHE        ,HEFLO (50),HETMP(50) ,TBURP (50),
     *        KBURP      ,PHE
      COMMON /CNERO/ NNERO,NSETS,NSET(2),INERO(30),RRATE
      COMMON /CTEMP/ CONBRP,CONQBO,SBOT
      COMMON /CPLOT/ IPLOT, NPLOT(8)
      COMMON /CTEMP1/ IRETRO,XMPULL
      COMMON /CTEMP2/ PSAT,MDOTE2,PVLIQ,QV,QVL,QVG,PVAP
      COMMON /CDIFE/ IERROR,NOFE
      REAL MC     ,MO     ,MT     ,LINE   ,ISP    ,ME     ,MFO    ,MFT
      REAL  MDOTC
      EQUIVALENCE (AOFUEL,AOGAS),(PCQLH2,FQLIQ),(DTQSW,DTQ(1)),(PU,P),
     *            (MO,MFO),(MT,MFT),(AI,AFI),(CONQLG,CONTLG)
      EXTERNAL DERIV,CNTRL
C
      NAMELIST /CASE/ P    ,PU     ,TU     ,PSATL ,TBTL   ,PBTL   ,XML    ,
     *        TW     ,PR     ,TMES2 ,FMDOTS,ISAVE ,PHE    ,
     *        NS     ,XTIMES,XMDOTS,NVENT ,XPVENT,XMVENT,IFTB
C
      NAMELIST /PHASE/ CD ,AOTOT ,AOFUEL,CONTLG,CONTV ,DEADWT,DTTOL ,
     *        DTIME ,EPSP  ,EPSR  ,EPSA  ,HAMS  ,HBTL  ,HEUSE ,IFLOW ,
     *        MDOTL ,MDOTFF,NEXT  ,PCQLH2,PRESET,PCRACK,PFFLOW,TM    ,
     *        NQS   ,DTQ   ,QBP   ,QWG   ,QWL   ,TIME  ,TIMEF ,TIMES ,
     *        WRATIO,X     ,AOGAS ,FQLIQ ,F     ,DTQSW ,RRATE ,QW    ,
     *        PVARYO,DPVARY,CONSAT,ISAVE ,ISPRAY,ICPV  ,MDOTRS,CONQLG,
     *        CONQSP,CONBRP,CONQBO,IPLOT ,NPLOT ,TVNT  ,IRETRO,XMPULL,
     *        DL    ,DO    ,AT    ,AC    ,FRICTN,GAM   ,LINE  ,MFO   ,
     *        MC    ,MFT   ,AFI   ,KBUG  ,AE    ,AI    ,FMIN  ,IMIX
     *       ,G     ,CONFAC,TBI   ,KRECIR,KBURP ,DTHE
C
      DO 10 I=1,NPG
   10 TBPG(I) = 1./TBPG(I)
      PMINP = 1./PMAX
      PMAX = 1./PMIN
      PMIN = PMINP
      IPRINT = 1
      CONBRP = 1.0
      XMPULL = 1.E+10
C
   20 READ (5,30) AL,CP,CV,CPHE,CVHE,HFG,CL,RHE,
     *            VBTL,MBTL,CBTL,ABTL
   30 FORMAT (8E10.5)
C
   40 READ (5,185) NQSEGS,NQWTBS,NCWTBS,NNERO,NRETRO,IRECIR, MLTIWL
     *            ,IBURP
      IF (NQSEGS.LE.0) GO TO 90
      NQS = NQSEGS
      NSETS = 0
      DO 80 I=1,NQS
      READ (5,160) IQW(I),ICW(I),IFLUX(I),IAW(I),INERO(I),STOPS(I),
     *             SBOTS(I),QW(I),TW(I),MW(I),EMISS(I),FAW(I)
      IF (ICW(I).EQ.0) READ (5,30) CW(I)
      K = IAW(I)
```

```
      CALL TABL (STOPS(I),ATOP(I),TBSA(1,K),TBA(1,K),1,1,1,NAW(K),IB)
      CALL TABL (SBOTS(I),ABOT   ,TBSA(1,K),TBA(1,K),1,1,1,NAW(K),IB)
      AW(I) = ATOP(I) - ABOT
      IF (AW(I).LE.0.0) AW(I) = -AW(I) + 1.E-50
      IF (FAW(I).LE.0.0) FAW(I)=1.0
      IF (IFLUX(I).GT.0) FAW(I) = FAW(I)*AW(I)
      IF (IQW(I).EQ.0) QW(I) = QW(I)*FAW(I)
      IF (INERO(I).LE.0) GO TO 80
      IF (NSETS.EQ.0) GO TO 70
      DO 60 J=1,NSETS
   60 IF (IQW(I).EQ.NSET(J)) GO TO 80
   70 NSETS = NSETS + 1
      NSET(NSETS) = IQW(I)
   80 CONTINUE
C
   90 IF (NQWTBS.LE.0) GO TO 110
      DO 100 I=1,NQWTBS
      READ (5,170) NQ,NQTB,DTQ(NQTB),(TBTQ(J,NQTB),TBQ(J,NQTB),J=1,NQ)
  100 NQW(NQTB) = NQ
C
  110 IF (NCWTBS.LE.0) GO TO 130
      DO 120 I=1,NCWTBS
      READ (5,180) NC,NCWTB,(TBTCW(J,NCWTB),TBCW(J,NCWTB),J=1,NC)
  120 NCW(NCWTB) = NC
C
  130 IF (NNERO.GT.0) CALL NEROIN
      IF (IRECIR .LE. 0) GO TO 140
      READ (5,185) NRE
      READ (5,190) (XRECIR(I),I=1,NRE)
      READ (5,190) (XDELH (I),I=1,NRE)
      READ (5,190) (RETIME(I),I=1,NRE)
C
  140 IF(IBURP .LE. 0) GO TO 150
      READ (5,185) NHE
      READ (5,190) (HEFLO(I),I=1,NHE)
      READ (5,190) (HETMP(I),I=1,NHE)
      READ (5,190) (TBURP(I),I=1,NHE)
C
  150 IF (MLTIWL .LE.0) GO TO 200
      DO 155 I=1,NQS
      IF (ICW(I) .LT. 0) GO TO 155
      READ (5,185) NSLICE(I)
      K = NSLICE(I)
      DO 153 L =1,K
  153 READ (5,195) MATL(L,I),THICK(L,I)
      THICK(L,I) = THICK(L,I)/12.
  155 CONTINUE
      READ (5,190) (WD(I),I=1,3)
C
      IF (NRETRO.GT.0) CALL RETIN
C
  160 FORMAT (5I2,7E10.2)
  170 FORMAT (2I2,6X,E10.2/(2E10.2))
  180 FORMAT (2I2/(2E10.2))
```

```
  185 FORMAT (10I2)
  190 FORMAT (8E10.4)
  195 FORMAT (I10, E10.4)
C
C *** INPUT OF DATA FOR CASE
C
  200 READ (5,210) HEAD
      WRITE (6,220) HEAD
  210 FORMAT (8A10)
  220 FORMAT (1H1,24X,32H S-IV H TANK PRESSURE SIMULATION / 1H0,8A10/)
C
      READ (5,CASE)
C
      GO TO (250,230,245), ISAVE
  230 PU=PUSAVE
      TU=TUSAVE
      DO 240 I=1,NTDOT
  240 TM(I) = TMSAVE(I)
  245 ISAVE=1
      GO TO 270
C
  250 PINV = 1./(P - PHE)
      CALL DTABL2 (TU,PINV,UG,THPG(1),1,NPG,1,1,IB,TBTG(1,1),TBUG(1,1),
     *                                          9,9,NTG)
      CALL DTABL2 (TU,PINV,SV,THPG(1),1,NPG,1,1,IB,TBTG(1,1),TBSV(1,1),
     *                                          9,9,NTG)
      CALL TAPL (PSATL,TL,XPSAT(1),XTSAT(1),1,1,1,NSAT,IB)
      CALL TAPL (TL,SVLIQ,XTSAT(1),XSVLIQ(1),1,1,1,NSAT,IB)
      VU = VTOT - XML*SVLIQ
      XMG = VU/SV
      XMHE = PHE*VU*144./RHE/TU
      TM(1) = XMG*UG + XMHE*CVHE*TU
      TM(2) = XMG
      TM(3) = XMHE
      TM(4) = XML
      TM(5) = TL
      TM(6) = 0.0
      IF (IBURP .GT. 0) GO TO 255
      TM(7) = PBTL*VBTL/RHE/TBTL/12.
      TM(8) = TBTL
      TM(9) = TBTL
      TM(10) = 0.0
  255 NTDOT = 10
      IF (NQS.LE.0) GO TO 265
      IF(MLTIWL .GT. 0) GO TO 265
      DO 260 I=1,NQS
      IF (ICW(I).LT.0) GO TO 260
      NTDOT = NTDOT + 1
      TM(NTDOT) = TW(I)
  260 CONTINUE
  265 IF (NSETS.LE.0) GO TO 270
      NTDOT = NTDOT + 1
      TM(NTDOT) = 0.0
  270 NEXT = 4
```

```
      IERROR = 1
C
C *** INPUT OF DATA FOR PHASE
C
  280 READ (5,290)
      WRITE (6,290)
  290 FORMAT(80H   DUMMY FORMAT FOR INPUT OF TITLE
     *                                                         )
C
      READ (5,PHASE)
C
      IFIRST = 1
      TIME1 = TIME
      IF (IFLOW.NE.3) GO TO 300
      MDOTV = 0.0
      MDOTG = 0.0
      MDOTHE = 0.0
  300 IF (ISPRAY.NE.2) GO TO 305
      QGS = 0.0
      MDOTS = 0.0
      MDOTSC = 0.0
  305 IF (IMIX.LE.0) GO TO 310
      CALL MIX (TIME,TIMEF,TM)
      IMIX=0
      GO TO 350
  310 GO TO (340,320), ISAVE
  320 PUSAVE=PU
      TUSAVE=TU
      DO 330 I=1,NTDOT
  330 TMSAVE(I) = TM(I)
      ISAVE=1
C
  340 CALL DIFE3 (DERIV,CNTRL,NTDOT,-1,EPSR,EPSA,TIME,TM,DTIME,TIMEF)
C
      GO TO (350,370,370),IERROR
  350 IF (IPLOT.GT.1) CALL PLOT (TIME,TM)
      GO TO 380
  360 READ (5,PHASE)
  370 IF (NEXT.EQ.4) GO TO 360
  380 GO TO (20,40,200,280,390),NEXT
  390 STOP
      END
      SUBROUTINE DIFE3 (DERIW,CNTRL,N,M,EPSR,EPSA,X,Y,H,XE)
C
C
C     THIS SUBROUTINE INTEGRATES A SYSTEM OF FIRST ORDER ORDINARY
C     DIFFERENTIAL-EQUATIONS. TO PERFORM A SINGLE STEP OF INTEGRATION,
C     IT USES THE SUBROUTINE *DIFE1*, WHICH USES THE RUNGE-KUTTA-MERSON
C     METHOD, AND PROVIDES AN ESTIMATE OF THE LOCAL TRUNCATION ERROR
C     BASED ON THIS ERROR,THE SUBROUTINE ADJUSTS THE STEPSIZE SUCH
C     THAT THE TOLERANCES ARE SATISFIED.
C
C     ARGUMENTS..
C
```

```
C          DERIW       =  DUMMY-NAME FOR SUBROUTINE FOR COMPUTING THE
C                         DERIVATIVES
C          CNTRL       =  DUMMY-NAME FOR SUBROUTINE FOR PRINTING THE RESULTS
C          N           =  NUMBER OF EQUATIONS IN THE SYSTEM
C          M           =  NUMBER OF STEPS BETWEEN TWO CONSECUTIVE EXITS TO
C                         SUBROUTINE CNTRL
C          EPSR        =  VARIABLE SPECIFYING MAXIMUM ALLOWABLE RELATIVE
C                         ERROR(IF NEGATIVE OR ZERO-STEPSIZE IS NOT CHANGED)
C          EPSA        =  VARIABLE SPECIFYING MAXIMUM ALLOWABLE ABSOLUTE
C                         ERROR
C          X           =  INDEPENDENT VARIABLE
C          Y           =  DEPENDENT VARIABLES (VECTOR)
C          H           =  STEP SIZE (POSITIVE OR NEGATIVE)
C          XE          =  FINAL VALUE OF INDEPENDENT VARIABLE
C
C
      COMMON /CDIFE/ IERROR,NOFE
      DIMENSION Y(1),YL(50),ERR(50),YDOT(50)
      EXTERNAL  DERIW,CNTRL
C
      CALL DERIW (X,Y,YDOT)
      CALL CNTRL (X,Y,YDOT,0.0)
C
C     TEST WHETHER BACKWARD OR FORWARD INTEGRATION
C     TEST IF INITIAL GUESS OF STEPSIZE HAS CORRECT SIGN
C
      IF (H) 350,290,10
   10 IF (XE-X) 330,310,30
   30 MPR = IABS(M)
C
C     STARTING THE INTEGRATION
C
   70 CALL DIFE1 (DERIW,N,0.0,X,Y,ERR)
C
C     BEGIN SEQUENCE OF INTEGRATION
C
   80 DO 260 IPR=1,MPR
      INC = 1
      DO 90 I=1,N
   90 YL(I) = Y(I)
  100 CALL DIFE1 (DERIW,N,H,X,Y,ERR)
      IF (EPSR) 230,230,110
C
C     DETERMINATION OF THE MAXIMUM RELATIVE OR ABSOLUTE INTEGRATION
C     ERROR,NOFE DESIGNATES EQUATION WITH LARGEST ERROR
C
  110 GO TO (115,190,400),IERROR
  115 ERRM = 0.
      DO 120 I=1,N
      ERRA = ABS(ERR(I)) /((ABS(Y(I)) + ABS(Y(I)-YL(I)))*EPSR + EPSA)
      IF (ERRM.GE.ERRA) GO TO 120
      ERRM = ERRA
      NOFE = I
  120 CONTINUE
```

```
C
C     TEST IF STEPSIZE IS APPROPRIATE TO PRESCRIBED MAXIMUM TRUNCATION
C     ERROR. (BEFORE INCREASING THE STEPSIZE THE PROGRAM CHECKS WHETHER
C     THE STEPSIZE WAS DECREASED IN THE PRECEDING STEP. THIS AVOIDS AN
C     UNWANTED DECREASE-INCREASE-DECREASE LOOP. THE PARAMETER INC IS
C     USED IN THIS TEST.)
C
      IF (ERRM.GT.1.0 ) GO TO 190
      IF (ERRM.GE..01 ) GO TO 230
      GO TO (130,230), INC
  130 IF (XE-X) 270,280,160
  160 H = 2.*H
      GO TO 100
C
  190 H = H/2.
      IERROR = 1
      INC = 2
      IF (H) 370,370,100
C
C     TEST IF X GREATER THAN UPPER END OF INTEGRATION-INTERVAL
C
  230 IF (XE-X) 270,280,260
  260 CONTINUE
C
C     SUBROUTINE CNTRL IS CALLED AFTER EVERY M COMPLETED INTEGRATIONS
C
      CALL DERIW (X,Y,YDOT)
      CALL CNTRL (X,Y,YDOT,H)
      GO TO 80
C
C     FINAL INTEGRATION STEP-STEPSIZE IS DETERMINED SO THAT ENDPOINT
C     OF INTEGRATION-INTERVAL WILL BE HIT
C
  270 CALL DIFE1 (DERIW,N,XE-H-X,X,Y,ERR)
  280 CALL DERIW (X,Y,YDOT)
      CALL CNTRL (X,Y,YDOT,H)
      RETURN
C
  290 WRITE (6,300)
  300 FORMAT (49HPROGRAM-ERROR, INITIAL GUESS OF STEPSIZE WAS ZERO)
      RETURN
  310 WRITE (6,320)
  320 FORMAT (73HPROGRAM-ERROR, INITIAL AND END-VALUE OF INTEGRATION-INT
     1ERVAL ARE THE SAME)
      RETURN
  330 WRITE (6,340)
  340 FORMAT (63HPROGRAM-ERROR, POSITIVE STEPSIZE BUT X-END SMALLER THAN
     1 X-BEGIN)
      RETURN
  350 WRITE (6,360)
  360 FORMAT (31HPROGRAM-ERROR,NEGATIVE STEPSIZE )
      RETURN
  370 WRITE (6,380)
  380 FORMAT (39HPROGRAM ERROR, STEPSIZE REDUCED TO ZERO)
```

```
  400 RETURN
      END
      SUBROUTINE DIFE1 (DERIW,N,H,X,Y,ERR)
C
C
C     THIS SUBROUTINE PERFORMS ONE STEP OF INTEGRATION BY THE
C     MERSONS MODIFIED RUNGE-KUTTA METHOD. IT USES FIVE SUBSTITUTIONS
C     INTO THE DIFFERENTIAL-EQUATIONS AND GIVES AN ESTIMATE OF THE
C     LOCAL TRUNCATION ERROR, WHICH CAN BE USED FOR THE ADJUSTMENT
C     OF THE STEP-SIZE
C
C        DERIW     = DUMMY-NAME FOR SUBROUTINE FOR THE EVALUATION
C                    OF THE RIGHT HAND SIDES OF THE DIFF.-EQUATIONS
C          N       = NUMBER OF THE EQUATIONS IN THE SYSTEM
C          H       = STEPSIZE
C          X       = INDEPENDENT VARIABLE
C         Y(I)     = DEPENDENT VARIABLE
C        ERR(I)    = LOCAL TRUNCATION ERROR
C
C     THE COMPUTED VALUES OF X AND Y ARE SAVED IN DOUBLE-PRECISION
C     FOR THE USE AS INITIAL-VALUES IN THE NEXT STEP
C
C     EACH TIME WHEN A NEW INTEGRATION SEQUENCE IS STARTED, THE
C     SUBROUTINE MUST BE CALLED WITH H=0 AND THE INITIAL-VALUES OF X AND
C     Y(I).
C
C     THE SUBROUTINE TESTS IF THE VALUE OF H IS THE SAME AS IN THE
C     PREVIOUS STEP
C
C        IF YES.. IT COMPUTES THE NEW STEP WITH THE X AND Y-VALUES
C                 AT THE END OF THE LAST STEP
C
C        IF NO..  IT COMPUTES THE NEW STEP WITH THE X AND Y-VALUES
C                 AT THE BEGINNING OF THE LAST STEP
C
C     TO REDUCE THE ROUND-OFF ERROR,DOUBLE -PRECISION IS USED IN
C     INCREMENTING THE DEPENDENT AND THE INDEPENDENT VARIABLES
C
C
      COMMON /CDIFE/ IERROR,NOFE
      DIMENSION Y(1),ERR(1),YY(50),P1(50),P3(50),P4(50),P5(50),
     1          YLDP(50),YZDP(50)
      DOUBLE PRECISION XLDP,YLDP,YZDP,DUDP,HDP,XZDP
      EXTERNAL DERIW
C
      IF (H) 10,20,10
   10 IF (H-H0) 40,60,40
C
C *** STORE INITIAL X AND Y
C
   20 XLDP=DBLE(X)
      DO 30 I=1,N
   30 YLDP(I)=DBLE(Y(I))
      H0 = 0.0
```

```
      RETURN
C
C *** RESTORE X AND Y
C
   40 DO 50 I=1,N
   50 Y(I)=SNGL (YLDP(I))
      X = SNGL(XLDP)
      H0 = H
      H2 = H/2.
      H3 = H/3.
      H6 = H/6.
      H8 = H/8.
      H15= H/15.
      HDP = DBLE(H)
      GO TO 80
   60 DO 70 I=1,N
   70 YLDP(I)=YZDP(I)
      XLDP=XZDP
C
C *** PERFORM ACTUAL INTEGRATION
C
   80 CALL DERIW (X,Y,P1)
      GO TO (85,135,135),IERROR
   85 DO 90 I=1,N
   90 YY(I) = Y(I) + P1(I)*H3
      XX=X + H3
      CALL DERIW (XX,YY,P3)
      GO TO (95,135,135),IERROR
   95 DO 100 I=1,N
  100 YY(I) = Y(I) + (P1(I)+P3(I))*H6
      CALL DERIW (XX,YY,P3)
      GO TO (105,135,135),IERROR
  105 DO 110 I=1,N
      P3(I) = P3(I)*3.
  110 YY(I) = Y(I) + (P1(I)+P3(I))*H8
      XX = X + H2
      CALL DERIW (XX,YY,P4)
      GO TO (115,135,135),IERROR
  115 DO 120 I=1,N
      P4(I) = P4(I) * 4.
  120 YY(I) = Y(I) + (P1(I)-P3(I)+P4(I))*H2
      XX = X+H
      CALL DERIW (XX,YY,P5)
      GO TO (125,135,135),IERROR
  125 DO 130 I=1,N
C
C *** INCREMENT DEPENDENT AND INDEPENDENT VARIABLES
C
      YZDP(I) = YLDP(I) + DBLE((P1(I) + P4(I) + P5(I))*H6)
      Y(I) = SNGL (YZDP(I))
  130 ERR(I) = (P1(I) - P3(I) + P4(I) - (P3(I) + P5(I))/2.) * H15
      XZDP = XLDP + HDP
      X = SNGL (XZDP)
  135 RETURN
```

```
      END                                                                DIF1103
      SUBROUTINE DERIV (TIME,TM,TMDOT)
C
      DIMENSION TM(99),TMDOT(99),AWLL(2)
      REAL    MDOTL ,MDOTBP,MDOTE ,MDOTV ,MDOTG ,MDOTHE,MDOTFF,MDOTS ,
     *        MDOTSO,MBTL  ,MDOTET,MDOTRS,LEFF  ,MW    ,MDOTC ,MDOTE2
      REAL MDOTLT
      REAL  MDOTE3
      COMMON /CMAIN/
     *        AOTOT ,AOGAS ,AL    ,AWLL  ,ABTL  ,
     *        CD    ,CV    ,CP    ,CVHE  ,CPHE  ,CL    ,CBTL  ,
     *        CONQLG,CONTV ,CONSAT,CONQSP,
     *        DEADWT,DTIME ,DTTOL ,DPVARY,
     *        EPSP  ,EPSR  ,EPSA  ,F     ,FQLIQ ,FMDOTS,G     ,
     *        HFG   ,HAMS  ,HEUSE ,HBTL  ,HW    ,HL    ,
     *        IFLOW ,IFLOW1,ISPRAY,I1    ,I2    ,ICPV  ,ISAVE ,LEFF ,
     *        MDOTL ,MDOTBP,MDOTE ,MDOTV ,MDOTG ,MDOTHE,MDOTFF,MDOTS ,
     *        MDOTSO,MBTL  ,MDOTET,MDOTRS,NTDOT ,
     *        P     ,PBTL  ,PCRACK,PRESET,PFFLOW,PR    ,P1    ,PINV  ,
     *        PVARYO,PMAX  ,PMIN  ,PCON  ,
     *        QGS   ,QBHE  ,QBP   ,QWL   ,QWG   ,QGL   ,
     *        RHOL  ,RHOG  ,RHE   ,
     *        SV    ,SVSAT ,SVVNT ,SLL   ,SIGN  ,STOP  ,SVLIQ ,
     *        TU    ,TU1   ,TSAT  ,TVNT  ,TIMES ,TMES2 ,TIME1 ,
     *        UG    ,UGSAT ,UGVNT ,
     *        VTOT  ,VL    ,VU    ,VU1   ,VBTL  ,
     *        WRATIO,X
      COMMON /HEAT/
     *        NQS   ,IQW(30) , ICW(30) ,IFLUX(30) ,IAW(30) ,EMISS(30),
     *       STOPS(30) ,SBOTS(30) ,QW(30) ,TW(50) ,MW(30) ,CW(30) ,
     *        FAW(30) ,ATOP(30) ,AW(30) ,NQW(5) ,TBTQ(30,5),TBQ(30,5),
     *        NCW(3) ,TBTCW(30,3) ,TBCW(30,3) ,DTQ(5),
     *        NAW(2)  ,TBSA(90,2)  ,TBA(90,2)
      COMMON /TABLE/
     *        NPG,NTG,TBPG(9)  ,TBTG(9,50),TBSV(9,50),TBUG(9,50),
     *        NSAT ,XPSAT(10)  ,XTSAT(10) ,XSVSAT(10) ,XUGSAT(10),
     *        XHFG(10) ,XSVLIQ(10) ,NVOL ,TBHVOL(110),TBVOL(110),
     *        NVENT,XPVENT(10) ,XMVENT(10),NS ,XTIMES(20) ,XMDOTS(20)
     *,       TBTKW(10,3) ,TBKW(10,3) ,NKW(3)
      COMMON /S4HEAT/
     *        MLTIWL  ,MATL(7,12),NSLICE(12),THICK(7,12),WD(3)
C
      COMMON /S4MAIN/
     *       XRECIR(50),XDELH(50) ,RETIME(50),RECIRC     ,DELH       ,
     *       NRE        ,CONFAC     ,IRECIR     ,TBI        ,MDOTE3     ,
     *       KRECIR     ,QLREC      ,MDOTC
C
      COMMON/BURP/
     *       IBURP      ,NHE        ,HEFLO (50),HETMP(50) ,TBURP (50),
     *       KBURP      ,PHE
C
      COMMON /CNERO/ NNERO,NSETS,NSET(2),INERO(30),RRATE
      COMMON /CTEMP/ CONBRP,CONQBO,SBOT
      COMMON /CTEMP1/ IRETRO,XMPULL
```

```
      COMMON /CTEMP2/ PSAT,MDOTE2,PVLIQ,QV,QVL,QVG,PVAP
      COMMON /CDIFE/ IERROR,NOFE
C
C *** MISCELLANEOUS INITIALIZATION
C
      IF (TIME.GE.TIME1) GO TO 10
      PINV = P1
      TU = TU1
      IFLOW = IFLOW1
   10 TIME1 = TIME
      CALL TABL (TM(5),SVLIQ,XTSAT(1),XSVLIQ(1),1,1,1,NSAT,IB)
      VL = TM(4)*SVLIQ
      VU = VTOT - VL
      RHOG = (TM(2) + TM(3))/VU
C
C *** ITERATION FOR ULLAGE PRESSURE AND TEMPERATURE
C
      I1 = I1 + 1
   20 I2 = I2 + 1
      IF (I2/I1.GT.200) GO TO 950
      IF (PINV.GT.PMAX.OR.PINV.LT.PMIN) GO TO 900
      CALL DTABL2 (TU,PINV,UG,TBPG(1),1,NPG,1,1,IB,TBTG(1,1),TBUG(1,1),
     *                                              9,9,NTG)
      CALL DTABL2 (TU,PINV,SV,TBPG(1),1,NPG,1,1,IB,TBTG(1,1),TBSV(1,1),
     *                                              9,9,NTG)
      VUP = TM(2)*SV
      TUP = TU
      TU = TU + (TM(1) - TM(2)*UG - TM(3)*CVHE*TU)/(TM(2)*CV+TM(3)*CVHE)
      PINV = PINV*(TUP/TU)*(VU/VUP)
      IF (ABS(TUP-TU).GT.EPSP*TU.OR.ABS(VUP-VU).GT.EPSP*VU) GO TO 20
C
      CALL DTABL2 (TU,PINV,UG,TBPG(1),1,NPG,1,1,IB,TBTG(1,1),TBUG(1,1),
     *                                              9,9,NTG)
      CALL DTABL2 (TU,PINV,SV,TBPG(1),1,NPG,1,1,IB,TBTG(1,1),TBSV(1,1),
     *                                              9,9,NTG)
      PVAP = 1./PINV
      PHE = TM(3)*RHE*TU/VU/144.
      P = PVAP + PHE
      PSAT = P - CONSAT*PHE
      CALL TABL (PSAT,TSAT ,XPSAT(1),XTSAT(1) ,1,1,1,NSAT,IB)
      CALL TABL (TM(5),PVLIQ ,XTSAT(1),XPSAT(1),1,1,1,NSAT,IB)
      CALL TABL (PVLIQ,HFG  ,XPSAT(1),XHFG(1)  ,1,1,1,NSAT,IB)
      CALL TABL (PVLIQ,SVSAT,XPSAT(1),XSVSAT(1),1,1,1,NSAT,IB)
      CALL TABL (PVLIQ,UGSAT,XPSAT(1),XUGSAT(1),1,1,1,NSAT,IB)
      CALL TABL (PVAP ,TSAT2,XPSAT(1),XTSAT(1) ,1,1,1,NSAT,IB)
      PCON = PVLIQ*144./778.
      HGSAT = UGSAT + PCON*SVSAT
C
C *** EVALUATION OF LIQUID BOIL-OFF AND VAPOR CONDENSATION RATES
C
      IF (TM(5).LE.TSAT) GO TO 30
      MDOTE = TM(4)*CL*(TM(5)-TSAT)/HFG/DTTOL
      GO TO 40
   30 MDOTE = 0.0
```

```
C
   40 IF (TU.GE.TSAT2) GO TO 50
      MDOTC = TM(2)*CV*(TSAT2-TU)/HFG/DTTOL
      GO TO 60
   50 MDOTC = 0.0
C
C *** EVALUATION OF VENTING RATE
C
   60 GO TO (80,90,150,70,140), IFLOW
   70 CALL VENT (TM,TMDOT)
      GO TO (80,90,120,150,125), IFLOW
   80 IF (P.LT.PCRACK) GO TO 140
      IFLOW = 2
   90 IF (P.LE.PRESET) GO TO 130
      TVNT = TU + CONTV*(TU - TSAT)
      IF (NVENT.LE.0) GO TO 100
      CALL TABL (P,MDOTV,XPVENT(1),XMVENT(1),1,1,1,NVENT,IB)
      GO TO 120
  100 IF (P.GE.PFFLOW) GO TO 110
      MDOTV = (MDOTRS + (MDOTFF-MDOTRS)*(P - PRESET)/(PFFLOW - PRESET))
     *                                                     *SQRT(45./TVNT)
      GO TO 120
  110 MDOTV = MDOTFF*(P/PFFLOW)*SQRT(45./TVNT)
  120 MDOTG = MDOTV*TM(2)/(TM(2) + TM(3))
      MDOTHE = MDOTV - MDOTG
  125 CALL DTABL2 (TVNT,PINV,UGVNT,TBPG(1),1,NPG,1,1,IB,TBTG(1,1),
     *                                         TBUG(1,1),9,9,NTG)
      CALL DTABL2 (TVNT,PINV,SVVNT,TBPG(1),1,NPG,1,1,IB,TBTG(1,1),
     *                                         TBSV(1,1),9,9,NTG)
      GO TO 150
  130 IFLOW = 1
  140 MDOTV = 0.0
      MDOTG = 0.0
      MDOTHE = 0.0
C
C *** DETERMINATION OF RETROMANEUVER FLOW RATE
C
  150 IF (IRETRO.LE.0) GO TO 158
      IF (TM(4).LT.XMPULL) GO TO 154
      CALL RETRO (P,TU,MDOTL,F,1)
      GO TO 158
  154 CALL RETRO (P,TU,MDOTG,F,2)
      SVVNT = SV
      UGVNT = UG
      MDOTL = 0.
C
C *** INITIALIZATION FOR COMPUTATION OF HEAT INPUTS
C
  158 CALL TABL (VL,SLL,TBVOL(1),TBHVOL(1),1,1,1,NVOL,IB)
      IF (NQS.LE.0) GO TO 310
      DO 160 I=1,2
  160 CALL TABL (SLL,AWLL(I),TBSA(1,I),TBA(1,I),1,1,1,NAW(I),IB)
      LEFF = 1./(12./(SLL-STOP) + 1./21.6)
      NTUCT1 = 10
```

```
      QWG = 0.0
      QWL = 0.0
      IF (NSETS.LE.0) GO TO 200
      CALL STNERO (TIME,TM(NTDOT))
      TMDOT(NTDOT) = RRATE
C
C *** SUMMATION OF HEAT INPUTS TO PROPELLANTS FROM TANK WALLS
C
  200 DO 300 I=1,NQS
      IF (IQW(I).EQ.0) GO TO 260
      IF (INERO(I).GT.0) GO TO 260
      K = IQW(I)
      CALL TABL (TIME+DTQ(K),QW(I),TBTQ(1,K),TBQ(1,K),1,1,1,NQW(K),IB)
      QW(I) = QW(I)*FAW(I)
C
  260 K = IAW(I)
      PART = (ATOP(I) - AWLL(K))/AW(I)
      IF (PART.GT.1.0) PART=1.0
      IF (PART.LT.0.0) PART=0.0
      IF (ICW(I) .EQ. 2) GO TO 265
      GO TO 270
  265 QG = PART * QW(I)
      QL = QW(I) - QG
      GO TO 290
  270 IF (MLTIWL .LE. 0) GO TO 275
      CALL TIKWAL (TM,TMDOT,QG,QL,NTDOT1,LEFF,I,PART,TU)
      GO TO 290
  275 NTDOT = NTDOT1 + 1
      CALL FCONV (TM(NTDOT1),HW,LEFF,1)
      QG = PART*HW*FAW(I)*(TM(NTDOT1) - TU)/3600.
      QL = (1. - PART)*QW(I)
      QRERAD = PART*0.1714E-8*FAW(I)*EMISS(I)*TM(NTDOT1)**4/3600.
      IF (ICW(I).EQ.0) GO TO 280
      K = ICW(I)
      CALL TABL(TM(NTDOT1),CW(I),TBTCW(1,K),TBCW(1,K),1,1,1,NCW(K),IB)
  280 TMDOT(NTDOT1) = (QW(I) - QG - QL - QRERAD)/MW(I)/CW(I)
  290 QWG = QWG + QG
  300 QWL = QWL + QL
C
  310 CALL FCONV (TSAT,HL,21.6,2)
      QGL = CONQLG*HL*AL*(TU - TSAT)/3600.
C
C *** ESTIMATION OF HEAT TRANSFER TO SPRAY IN ULLAGE
C
      GO TO (320,360), ISPRAY
  320 CALL TABL(TIME-TMES2       ,MDOTS ,XTIMES(1),XMDOTS(1),1,1,1,NS,IB)
      CALL TABL(TIME-TMES2-TIMES,MDOTSO,XTIMES(1),XMDOTS(1),1,1,1,NS,IB)
      MDOTS = FMDOTS*MDOTS
      TERM = 1. - HAMS*(TU-TSAT)*TIMES/3600./2.14/HFG
      IF (TERM) 340,340,330
  330 MDOTSO = FMDOTS*MDOTSO*TERM**2.14
      GO TO 350
  340 MDOTSO = 0.0
  350 QGS = TM(6)*HAMS*(TU - TSAT)/3600.
```

```
  360 IF (IBURP .LE. 0) GO TO 361
C
C *** HELIUM ADDITION LOOK-UP
C
      IF (KBURP .LE. 0) GO TO 364
      CALL TABL (TIME+DTHE,MDOTBP,TBURP(1),HEFLO(1),1,1,1,NHE,IB)
      CALL TABL (TIME+DTHE,THEIN ,TBURP(1),HETMP(1),1,1,1,NHE,IB)
      PHEL = P - PVLIQ
      IF (PHEL .LT. 0.001*P) PHEL= 0.001*P
      PART = CONBRP * (RHE*TM(5)/PHEL/144.)/SVSAT
      MDOTE2 = MDOTBP * PART
      GO TO 364
C
C *** DERIVATIVES OF HELIUM BOTTLE CONDITIONS
C
  361 PBTL = 12.*TM(7)*RHE*TM(8)/VBTL
      DMDA = 0.210*CD*PBTL/SQRT(TM(8))
      AOVARY = AOGAS*(PVARYO-P)/DPVARY
      IF (AOVARY.LT.0.0) AOVARY=0.0
      IF (AOVARY.GT.AOGAS) AOVARY=AOGAS
C
      PHEL = P - PVLIQ
      IF (PHEL.LT.0.001*P) PHEL = 0.001*P
      PART = CONBRP*(RHE*TM(5)/PHEL/144.)/SVSAT
      AOVARY = AOVARY/(1. + PART)
C
      MDOTBP = DMDA*(AOTOT-AOGAS-AOVARY)
      QBHE = HBTL*ABTL*(TM(9)-TM(8))/3600.
      TMDOT(7) = -MDOTBP - HEUSE
      TMDOT(8) = (QBHE - MDOTBP*RHE*TM(8)/778.)/TM(7)/CVHE
      TMDOT(9) = -QBHE/MBTL/CBTL
C
      MDOTBP = DMDA*AOVARY
      MDOTE2 = MDOTBP*PART
      CALL HETEMP (MDOTBP,TM(8),CONQSP,SLL,THEIN)
C
C *** DERIVATIVES OF TANK CONDITIONS
C
  364 IF (CONQBO .LE. 0.0) GO TO 365
      DTLMAX = CONQBO*QWL**0.714/(SBOT-SLL)**0.857/G**0.286
      FQLIQ = (TSAT - TM(5))/DTLMAX
      IF (FQLIQ.LT.0.0) FQLIQ = 0.0
      IF (FQLIQ.GT.1.0) FQLIQ = 1.0
C
  365 IF (KRECIR .LE. 0) GO TO 370
      CALL TABL (TIME+TBI,RECIRC,RETIME(1),XRECIR(1),1,1,1,NRE,IB)
      CALL TABL (TIME+TBI,DELH  ,RETIME(1),XDELH (1),1,1,1,NRE,IB)
      QLREC = CONFAC*RECIRC*DELH
      MDOTE3 = (1.-CONFAC)*DELH/HFG
C
  370 MDOTET = MDOTE + QGS/HFG + X*MDOTS + (1.-FQLIQ)*QWL/HFG + MDOTE2
     *           + MDOTE3
      MDOTLT = MDOTL + MDOTET - MDOTC
C
```

```
      TMDOT(1) = QWG - QGL - QGS - MDOTLT*SVLIQ*P*144./778.
     *           + MDOTET*(UGSAT + PCON*SVSAT) + MDOTBP*CPHE*THEIN
     *           - MDOTG*(UGVNT + PCON*SVVNT) - MDOTHE*CPHE*TVNT
     *           - MDOTC*(UGSAT + PCON*SVSAT - HFG)
      IF (ICPV.GT.0) CALL CPVENT (TM,TMDOT)
      TMDOT(2) = MDOTET - MDOTG - MDOTC
      TMDOT(3) = MDOTBP - MDOTHE
      TMDOT(4) = -MDOTLT
      TMDOT(5) = (QWL + QGL + QBP + QGS + QLREC
     *           - MDOTET*HFG + MDOTC*CL*(TSAT - TM(5)))/TM(4)/CL
      TMDOT(6) = (1. - X)*(MDOTS - MDOTSO) - QGS/HFG
      TMDOT(10) = MDOTV
  800 RETURN
C
C *** STEPS TO ATTEMPT RECOVERY FROM UNSTABLE INTEGRATION OR ITERATION
C
  900 IF (P1.LT.PMIN.OR.P1.GT.PMAX) GO TO 950
      IERROR = 2
      GO TO 800
  950 IERROR = 3
      WRITE(6,902) IERROR,NOFE,TUP,TU,VUP,VU,EPSP,PINV,PMAX,PMIN,UG,SV,
     *   TM(2)
  902 FORMAT(*  IERROR=*I2,*  NOFE=*I3,*  TUP=*E13.6,*  TU=*E13.6,
     *     *  VUP=*E13.6,*  VU=*,E13.6,*  EPSP=*E13.6,/*  PINV=*
     *     E13.6,*  PMAX=*E13.6,*  PMIN=*E13.6,*  UG=*E13.6,
     *     *  SV=*E13.6,*  TM(2)=*E13.6)
      GO TO 800
      END
      SUBROUTINE CNTRL (TIME,TM,TMDOT,DTIME)
      DIMENSION TM(99),TMDOT(99),AWLL(2)
      REAL   MDOTL ,MDOTBP,MDOTE ,MDOTV ,MDOTG ,MDOTHE,MDOTFF,MDOTS ,
     *       MDOTSO,MBTL  ,MDOTET,MDOTRS,LEFF
      REAL  MDOTE3
      COMMON /CMAIN/
     *       AOTOT ,AOGAS ,AL    ,AWLL  ,ABTL  ,
     *       CD    ,CV    ,CP    ,CVHE  ,CPHE  ,CL    ,CBTL  ,
     *       CONQLG,CONTV ,CONSAT,CONQSP,
     *       DEADWT,DTIME ,DTTOL ,DPVARY,
     *       EPSP  ,EPSR  ,EPSA  ,F     ,FQLIQ ,FMDOTS,G     ,
     *       HFG   ,HAMS  ,HEUSE ,HBTL  ,HW    ,HL    ,
     *       IFLOW ,IFLOW1,ISPRAY,I1    ,I2    ,ICPV  ,ISAVE ,LEFF ,
     *       MDOTL ,MDOTBP,MDOTE ,MDOTV ,MDOTG ,MDOTHE,MDOTFF,MDOTS ,
     *       MDOTSO,MBTL  ,MDOTET,MDOTRS,NTDOT ,
     *       P     ,PBTL  ,PCRACK,PRESET,PFFLOW,PR    ,P1    ,PINV  ,
     *       PVARYO,PMAX  ,PMIN  ,PCON  ,
     *       QGS   ,QBHE  ,QBP   ,QWL   ,QWG   ,QGL   ,
     *       RHOL  ,RHOG  ,RHE   ,
     *       SV    ,SVSAT ,SVVNT ,SLL   ,SIGN  ,STOP  ,SVLIQ ,
     *       TU    ,TU1   ,TSAT  ,TVNT  ,TIMES ,TMES2 ,TIME1 ,
     *       UG    ,UGSAT ,UGVNT ,
     *       VTOT  ,VL    ,VU    ,VU1   ,VBTL  ,
     *       WRATIO,X
      COMMON /TABLE/
     *       NPG,NTG,TBPG(9)   ,TBTG(9,50),TBSV(9,50),TBUG(9,50),
```

```
     *        NSAT ,XPSAT(10)   ,XTSAT(10) ,XSVSAT(10) ,XUGSAT(10),
     *        XHFG(10) ,XSVLIQ(10) ,NVOL ,TBHVOL(110),TBVOL(110),
     *        NVENT,XPVENT(10) ,XMVENT(10),NS ,XTIMES(20) ,XMDOTS(20)
     *,       TBTKW(10,3) ,TBKW(10,3) ,NKW(3)
C
      COMMON /S4MAIN/
     *       XRECIR(50),XDELH(50) ,RETIME(50),RECIRC     ,DELH       ,
     *       NRE         ,CONFAC     ,IRECIR     ,TBI        ,MDOTE3     ,
     *       KRECIR      ,QLREC      ,MDOTC
C
      COMMON/BURP/
     *       IBURP       ,NHE        ,HEFLO (50),HETMP(50) ,TBURP (50),
     *       KBURP       ,PHE
      COMMON /CVENT/DL      ,DO     ,AT     ,AC     ,FRICTN,GAM    ,LINE   ,
     *        MO      ,MC     ,MT     ,AI     ,PTO    ,PTS    ,POO    ,POS    ,
     *        FPO     ,FPT    ,PCO    ,PIO    ,AE     ,KBUG   ,ME     ,ISP    ,
     *        PCS     ,DPENT ,PTANK ,IFIRST,IPRINT,FMIN
      COMMON /CPLOT/ IPLOT, NPLOT(8)
      COMMON /CTEMP2/ PSAT,MDOTE2,PVLIQ,QV,QVL,QVG,PVAP
      COMMON /CDIFE/ IERROR,NOFE
      REAL MC     ,MO     ,MT     ,LINE   ,ISP    ,ME
      REAL MDOTE2
      REAL  MDOTC
C
      I2 = (I2 + I1/2)/I1
      I1 = I1/5
      WRITE (6,10) I2,I1,NOFE,TIME,P,TU,TSAT,QWL,QWG,SLL,VU,PBTL,MDOTE,
     *             PVAP,PHE,UG,MDOTC,MDOTE2,MDOTE3,QLREC   ,
     *             (TM(I),I=1,10),(TMDOT(I),I=1,10)
C
      IF (NTDOT.GT.10) WRITE (6,20) (TM(I),I=11,NTDOT)
C
      GO TO (4,2),IPRINT
    2 WRITE (6,40) PCO,PCS,PIO,POO,PTO,DPENT,PTANK,F,ISP
C
    4 CALL DTABL2 (TU+0.5,PINV,UG2,TBPG(1),1,NPG,1,1,IB,TBTG(1,1),
     *                                               TBUG(1,1),9,9,NTG)
      CALL DTABL2 (TU+0.5,PINV,SV2,TBPG(1),1,NPG,1,1,IB,TBTG(1,1),
     *                                               TBSV(1,1),9,9,NTG)
      CP = ((UG2 - UG) + (PVAP*144./778.)*(SV2 - SV)) / 0.5
      CV = ( UG2 - UG ) / 0.5
C
      I1 = 0
      I2 = 0
      P1 = PINV
      TU1 = TU
      IFLOW1 = IFLOW
      IF (IPLOT.GT.0) CALL PLTSAVE (TIME,TM)
      RETURN
C
   10 FORMAT(///1X,I2,1H/,I1,1H/,I1,
     *        2X,4HTIME,5X,8HPRESSURE,5X,8HTEMP-ULL,5X,8HSAT-TEMP,
     *        5X,8HQ-LIQUID,7X,5HQ-ULL,4X,11HL/L STATION,5X,7HULL-VOL,
     *        5X,8HP-HE BTL,4X,9HMDOT-EVAP  / 10F13.5/
```

```
     *         18X,9HPRESS-VAP,4X,8HPRESS-HE,5X,5HU-VAP,8X,5HMDOTC,8X,
     *         6HMDOTE2,7X,6HMDOTE3,7X,9HQ-REC-LIQ  /13X,7F13.5//
     *         3X,10HULL-ENERGY,4X,9HMASS-FUEL,6X,7HMASS-HE,
     *         5X,8HMASS-LIQ,5X,8HTEMP-LIQ,3X,10HMASS-SPRAY,4X,9HHE IN BTL
     *         6X,7HTEMP-HE,5X,8HTEMP-BTL,3X,11HMASS VENTED/(10F13.5))
   20 FORMAT(13H0WALL TEMPS =,9F13.6/(10F13.6))
   40 FORMAT(/10X,3HPC0,10X,3HPCS,10X,3HPI0,10X,3HPO0,10X,3HPT0,
     *         8X,5HDPENT,8X,5HPTANK,12X,1HF,10X,3HISP/(10F13.6))
      END
      SUBROUTINE TIKWAL (TM,TMDOT,QG,QL,NTDOT1,LEFF,I,PART,TU)
      DIMENSION TM(99),TMDOT(99)
C
      COMMON /HEAT/
     *         NQS   ,IQW(30) , ICW(30) ,IFLUX(30) ,IAW(30) ,EMISS(30),
     *        STOPS(30) ,SBOTS(30) ,QW(30) ,TW(50) ,MW(30) ,CW(30) ,
     *         FAW(30) ,ATOP(30) ,AW(30) ,NQW(5) ,TBTQ(30,5),TBQ(30,5),
     *         NCW(3) ,TBTCW(30,3) ,TBCW(30,3) ,DTQ(5),
     *         NAW(2)  ,TBSA(90,2)  ,TBA(90,2)
      COMMON /TABLE/
     *         NPG,NTG,TBPG(9)  ,TBTG(9,50),TBSV(9,50),TBUG(9,50),
     *         NSAT ,XPSAT(10)  ,XTSAT(10) ,XSVSAT(10) ,XUGSAT(10),
     *         XHFG(10) ,XSVLIQ(10) ,NVOL ,TBHVOL(110),TBVOL(110),
     *         NVENT,XPVENT(10) ,XMVENT(10),NS ,XTIMES(20) ,XMDOTS(20)
     *,        TBTKW(10,3) ,TBKW(10,3) ,NKW(3)
      COMMON /S4HEAT/
     *         MLTIWL  ,MATL(7,12),NSLICE(12),THICK(7,12),WD(3)
C
C     THICK WALL HEAT FLOW -- STARTS WITH EXTERIOR SKIN SECTION
C
      K = NTDOT1 + 1
      QREAD = 0.1714E-8*AW(I)*EMISS(I)*TM(K)**4
      QIN = QW(I)*3600. - QRERAD
      J = 1
      L = 1
      CALL TABL (TM(K),WK1,TBTKW(1,J),TBKW(1,J),1,1,1,NKW(J),IB)
      M = MATL(L+1,I)
      CALL TABL (TM(K+1),WK2,TBTKW(1,M),TBKW(1,J),1,1,1,NKW(M),IB)
      R = (THICK(L,I)/WK1 + THICK(L+1,I)/WK2)/(2.* AW(I))
      QOUT = (TM(K)-TM(K+1))/R
      CALL TABL (TM(K),CPW , TBTCW(1,J),TBCW(1,J),1,1,1,NCW(J),IB)
      TMDOT(K) = (QIN - QOUT)/(AW(I)*THICK(L,I)*WD(J)*CPW)/3600.
C
C     INTERMEDIATE WALL SLICES --HEAT FLOW
C
      N= NSLICE(I) - 1
      DO 10 L=2,N
      K = K+1
      QIN = QOUT
      J = MATL(L,I)
      CALL TABL (TM(K),WK1,TBTKW(1,J),TBKW(1,J),1,1,1,NKW(J),IB)
      M = MATL(L+1,I)
      CALL TABL (TM(K+1),WK2,TBTKW(1,M),TBKW(1,J),1,1,1,NKW(M),IB)
      R = (THICK(L,I)/WK1 + THICK(L+1,I)/WK2)/(2.* AW(I))
      QOUT = (TM(K)-TM(K+1))/R
```

```
      CALL TABL (TM(K),CPW , TBTCW(1,J),TBCW(1,J),1,1,1,NCW(J),IB)
   10 TMDOT(K) = (QIN - QOUT)/(AW(I)*THICK(L,I)*WD(J)*CPW)/3600.
C
C     INTERIOR SECTION
C
      K=K+1
      L=L+1
      QIN = QOUT
      CALL FCONV (TM(K),HW,LEFF,1)
      J = MATL(L,I)
      CALL TABL (TM(K),WK1,TBTKW(1,J),TBKW(1,J),1,1,1,NKW(J),IB)
      R = (THICK(L,I)/WK1)/(2.* AW(I))
      RC = R      + 1./(HW*AW(I))
      QG = PART*(TM(K)-TU)/RC
      QL = (1.-PART)*(TM(K)-TM(5))/R
      QOUT = QG + QL
      CALL TABL (TM(K),CPW , TBTCW(1,J),TBCW(1,J),1,1,1,NCW(J),IB)
      TMDOT(K) = (QIN - QOUT)/(AW(I)*THICK(L,I)*WD(J)*CPW)/3600.
      NTDOT1 = K
      RETURN
      END
      SUBROUTINE FCONV (TSURF,HSURF,XL,IEQNS)
      DIMENSION AWLL(2)
      REAL   MDOTL ,MDOTBP,MDOTE ,MDOTV ,MDOTG ,MDOTHE,MDOTFF,MDOTS ,
     *       MDOTSO,MBTL  ,MDOTET,LEFF
      COMMON /CMAIN/
     *       AOTOT ,AOGAS ,AL    ,AWLL  ,ABTL  ,
     *       CD    ,CV    ,CP    ,CVHE  ,CPHE  ,CL    ,CBTL  ,
     *       CONQLG,CONTV ,CONSAT,CONQSP,
     *       DEADWT,DTIME ,DTTOL ,DPVARY,
     *       EPSP  ,EPSR  ,EPSA  ,F     ,FQLIQ ,FMDOTS,G     ,
     *       HFG   ,HAMS  ,HEUSE ,HBTL  ,HW    ,HL    ,
     *       IFLOW ,IFLOW1,ISPRAY,I1    ,I2    ,ICPV  ,ISAVE ,LEFF ,
     *       MDOTL ,MDOTBP,MDOTE ,MDOTV ,MDOTG ,MDOTHE,MDOTFF,MDOTS ,
     *       MDOTSO,MBTL  ,MDOTET,MDOTRS,NTDOT ,
     *       P     ,PBTL  ,PCRACK,PRESET,PFFLOW,PR    ,P1    ,PINV  ,
     *       PVARYO,PMAX  ,PMIN  ,PCON  ,
     *       QGS   ,QBHE  ,QBP   ,QWL   ,QWG   ,QGL   ,
     *       RHOL  ,RHOG  ,RHE   ,
     *       SV    ,SVSAT ,SVVNT ,SLL   ,SIGN  ,STOP  ,SVLIQ ,
     *       TU    ,TU1   ,TSAT  ,TVNT  ,TIMES ,TMES2 ,TIME1 ,
     *       UG    ,UGSAT ,UGVNT ,
     *       VTOT  ,VL    ,VU    ,VU1   ,VBTL  ,
     *       WRATIO,X
C
      TAVG = 0.5*(TU + TSURF)
      VISC = (4. + .22*TAVG)*.242E-3
      COND = (.06 + .0034*TAVG)*57.8E-3
      PR = CP*VISC/COND
      GRPR = PR*XL*(XL*RHOG*3600./VISC)**2*G*32.2*ABS(TSURF-TU)/TAVG
      GO TO (10,30), IEQNS
   10 IF (GRPR.GT.1.E+9) GO TO 20
      HSURF = 0.59*(COND/XL)*GRPR**.250
      RETURN
```

```
   20 HSURF = 0.13*(COND/XL)*GRPR**.333
      RETURN
   30 HSURF = 0.27*(COND/XL)*GRPR**.250
      RETURN
      END
      SUBROUTINE DUMMY (A,B,C,D,E)
C
C
      ENTRY NEROIN
      WRITE (6,100)
  100 FORMAT (1H0,*NNERO GT ZERO,SHOULD BE  ZERO*)
      RETURN
      ENTRY RETIN
      WRITE (6,200)
  200 FORMAT (1H0,* NRETRO GT ZERO,SHOULD BE ZERO*)
      RETURN
      ENTRY MIX
      WRITE (6,300)
  300 FORMAT (1H0,* IMIX GT ZERO,SHOULD BE ZERO*)
      RETURN
      ENTRY PLOT
      WRITE (6,400)
  400 FORMAT (1H0,* IPLOT GT ONE, SHOULD BE ONE*)
      RETURN
      ENTRY VENT
      WRITE (6,500)
  500 FORMAT (1H0,* IFLOW CAN NOT EQUAL FOUR IN THIS PROGRAM VERSION*)
      RETURN
      ENTRY RETRO
      WRITE (6,600)
  600 FORMAT (1H0,* IRETRO GT ZERO,SHOULD BE ZERO*)
      RETURN
      ENTRY STNERO
      WRITE (6,700)
  700 FORMAT (1H0,* NSETS GT ZERO, SHOULD BE ZERO*)
      RETURN
      ENTRY HETEMP
      WRITE (6,800)
  800 FORMAT (1H0,* SECTION OF PROGRAM ENTERED, SUBROUTINE HETEMP RQD*)
      RETURN
      END
      BLOCK DATA
C
      REAL    MDOTL ,MDOTBP,MDOTE ,MDOTV ,MDOTG ,MDOTHE,MDOTFF,MDOTS ,
     *        MDOTSO,MBTL  ,MDOTET,MDOTRS,LEFF
      DIMENSION AWLL(2)
      COMMON /CMAIN/
     *        AOTOT ,AOGAS ,AL    ,AWLL  ,ABTL  ,
     *        CD    ,CV    ,CP    ,CVHE  ,CPHE  ,CL    ,CBTL  ,
     *        CONQLG,CONTV ,CONSAT,CONQSP,
     *        DEADWT,DTIME ,DTTOL ,DPVARY,
     *        EPSP  ,EPSR  ,EPSA  ,F     ,FQLIQ ,FMDOTS,G     ,
     *        HFG   ,HAMS  ,HEUSE ,HBTL  ,HW    ,HL    ,
     *        IFLOW ,IFLOW1,ISPRAY,I1    ,I2    ,ICPV  ,ISAVE ,LEFF ,
```

```
     *         MDOTL  ,MDOTBP,MDOTE  ,MDOTV  ,MDOTG  ,MDOTHE,MDOTFF,MDOTS  ,
     *         MDOTSO,MBTL   ,MDOTET,MDOTRS,NTDOT ,
     *         P      ,PBTL   ,PCRACK,PRESET,PFFLOW,PR     ,P1     ,PINV   ,
     *         PVARYO,PMAX   ,PMIN   ,PCON   ,
     *         QGS    ,QBHE   ,QBP    ,QWL    ,QWG    ,QGL    ,
     *         RHOL   ,RHOG   ,RHE    ,
     *         SV     ,SVSAT  ,SVVNT  ,SLL    ,SIGN   ,STOP   ,SVLIQ  ,
     *         TU     ,TU1    ,TSAT   ,TVNT   ,TIMES  ,TMES2  ,TIME1  ,
     *         UG     ,UGSAT  ,UGVNT  ,
     *         VTOT   ,VL     ,VU     ,VU1    ,VBTL   ,
     *         WRATIO,X
      COMMON /HEAT/
     *         NQS    ,IQW(30) , ICW(30) ,IFLUX(30) ,IAW(30) ,EMISS(30),
     *       STOPS(30) ,SBOTS(30) ,QW(30) ,TW(50) ,MW(30) ,CW(30) ,
     *         FAW(30) ,ATOP(30) ,AW(30) ,NQW(5) ,TBTQ(30,5),TBQ(30,5),
     *         NCW(3) ,TBTCW(30,3) ,TBCW(30,3) ,DTQ(5),
     *         NAW(2)  ,TBSA(90,2)  ,TBA(90,2)
      COMMON /TABLE/
     *         NPG,NTG,TBPG(9)  ,TBTG(9,50),TBSV(9,50),TBUG(9,50),
     *         NSAT ,XPSAT(10)  ,XTSAT(10) ,XSVSAT(10) ,XUGSAT(10),
     *         XHFG(10) ,XSVLIQ(10) ,NVOL ,TBHVOL(110),TBVOL(110),
     *         NVENT,XPVENT(10) ,XMVENT(10),NS ,XTIMES(20) ,XMDOTS(20)
     *,        TBTKW(10,3) ,TBKW(10,3) ,NKW(3)
      COMMON /CPLOT/ IPLOT, NPLOT(8)
      COMMON /CTEMP/ CONBRP,CONQBO,SBOT
C
      DATA ISAVE,IFLOW,ISPRAY /1,1,2/
      DATA FMDOTS,PVARYO,DPVARY /1.,99.,1./
      DATA STOP, SBOT, VTOT / 0.5 ,437. ,10392.31 /
      DATA PMAX, PMIN, SIGN /100.,.01,1./
      DATA IPLOT,(NPLOT(I),I=1,8) /0,1,2,3,4,5,6,7,8/
C
      DATA NSAT  /  6/
      DATA (XPSAT(I),I=1,6)   /  10.0    ,  15.0    ,  20.0    ,  30.0    ,
     *         40.0   ,  50.0   /
      DATA (XTSAT(I),I=1,6)   /  34.260 ,  36.603 ,  38.436 ,  41.291 ,
     *         43.529 ,  45.400 /
      DATA (XSVSAT(I),I=1,6)  /  16.8879,  11.7299,   9.0293,   6.2031,
     *          4.7201,   3.7977/
      DATA (XUGSAT(I),I=1,6)  /  47.26   ,  49.37   ,  50.75   ,  52.34   ,
     *         53.03   ,  53.17   /
      DATA (XHFG(I),I=1,6)    / 193.53   , 191.55   , 189.23   , 184.10   ,
     *        178.58   , 172.81   /
      DATA (XSVLIQ(I),I=1,6)  /  0.2221 ,  0.2266 ,  0.2305 ,  0.2374 ,
     *         0.2437 ,  0.2498 /
C
      DATA  NS   / 13/
      DATA (XTIMES(I),I=1,13)  /-100.0    , -22.5    , -20.0    , -18.0    ,
     *        -16.0    , -14.0    , -12.0    , -10.0    ,  -8.0    ,  -6.0    ,
     *          0.0    ,   2.0    , 100.0    /
      DATA (XMDOTS(I),I=1,13)  /   0.0    ,    0.0    ,    0.18   ,    0.32   ,
     *           0.44   ,    0.51   ,    0.55   ,    0.58   ,    0.60   ,    0.61   ,
     *           0.61   ,    0.0    ,    0.0    /
C
```

```
      DATA NCW /5,6/
      DATA (TBTCW(I  ),I=1,5)/ 35. ,50. ,100.,250.,500./
      DATA (TBCW (I  ),I=1,5)/ .00095 , .0061 , .044 , .1548 , .220 /
C
      DATA (TBTCW(I),I=1,6)/ 25. , 100. , 200. , 300. , 400. , 500./
      DATA (TBCW(I) ,I=1,6)/.156 , .158 , .166 , .186 , .218 , .260/
C
      DATA NKW /6,6/
      DATA (TBTKW(I  ),I=1,6)/ 35.,50.,90.,175.,300.,500./
      DATA (TBKW (I  ),I=1,6)/ 94.,130.,163.,124.,115.,115./
C
      DATA (TBTKW(I  ),I=1,6)/ 20.,60.,100.,140.,200.,280./
      DATA ( TBKW(I  ),I=1,6)/ .01,.0185,.0275,.036,.0415,.0487/
C
      DATA  NQW(1) /24/
      DATA (TBTQ(I),I=1,24)  / -5262.0   ,-5022.0   ,-4782.0   ,-4422.0   ,
     *     -4062.0   ,-3402.0   ,-3222.0   ,-3162.0   ,-1062.0   ,-1002.0   ,
     *      -822.0   , -462.0   ,    0.0   ,  240.0   ,  480.0   ,  840.0   ,
     *      1200.0   , 1860.0   , 2040.0   , 2100.0   , 4200.0   , 4260.0   ,
     *      4800.0   , 5262.0   /
      DATA (TBQ(I),I=1,24)     /  12.50 ,  14.30 ,  14.80 ,  14.00 ,
     *        11.85 ,    5.60 ,    5.90 ,    1.00 ,    1.00 ,    6.65 ,
     *         6.20 ,    8.75 ,   12.50 ,   14.30 ,   14.80 ,   14.00 ,
     *        11.85 ,    5.60 ,    5.90 ,    1.00 ,    1.00 ,    6.65 ,
     *         6.20 ,    8.75 /
C
      DATA NAW /2,2/
C
      DATA (TBSA(I),I=1,2)   / 477.0    , 347.0    /
      DATA (TBSA(I),I=91,92)/ 437.0    ,  0.0     /
C
      DATA (TBA(I), I=1,2)   / 0.0      , 730.94   /
      DATA (TBA(I), I=91,92)/ 0.0      , 2473.88 /
      END
      BLOCK DATA
C
      COMMON /TABLE/
     *       NPG,NTG,TBPG(9)    ,TBTG(9,50),TBSV(9,50),TBUG(9,50),
     *       NSAT ,XPSAT(10)    ,XTSAT(10) ,XSVSAT(10) ,XUGSAT(10),
     *       XHFG(10) ,XSVLIQ(10) ,NVOL ,TBHVOL(110),TBVOL(110),
     *       NVENT,XPVENT(10) ,XMVENT(10),NS ,XTIMES(20) ,XMDOTS(20)
     *,      TBTKW(10,3) ,TBKW(10,3) ,NKW(3)
C
      DATA  NVOL /22/
      DATA (TBHVOL(I),I=1,22)/
     *      .5     ,   10.     ,   20.     ,   35.     ,   50.     ,   65.     ,
     *   80.     ,   95.     ,  115.     ,  130.     ,  200.     ,  270.     ,
     *  347.     ,  357.     ,  367.     ,  377.     ,  387.     ,  395.     ,
     *  407.     ,  417.     ,  427.     ,  437.     /
      DATA (TBVOL (I),I=1,22)/
     *10392.31  ,10371.43  ,10308.44  ,10140.53  , 9890.60  , 9577.46  ,
     * 9210.61  , 8808.15  , 8225.25  , 7768.47  , 5654.72  , 3540.98  ,
     * 1215.55  ,  937.66  ,  702.69  ,  447.54  ,  335.12  ,  244.61  ,
     *  128.63  ,   61.85  ,   32.68  ,    0.    /
```

```
C
      DATA  NPG   /  8/
      DATA  NTG   / 47/
C
      DATA  (TBPG(I),I=1,8)      /  15.0    ,  20.0    ,  30.0    ,  40.0    ,
     *      50.0    ,  60.0    ,  70.0    ,  80.0    /
C
      DATA  (TBTG(I),I=1,415,9)/  36.603 ,  38.0    ,  42.0    ,  46.0    ,
     *      50.0    ,  54.0    ,  58.0    ,  62.0    ,  66.0    ,  70.0    ,
     *      74.0    ,  78.0    ,  82.0    ,  86.0    ,  90.0    ,  96.0    ,
     *     102.0    , 108.0    , 114.0    , 120.0    , 126.0    , 132.0    ,
     *     138.0    , 144.0    , 150.0    , 158.0    , 166.0    , 174.0    ,
     *     182.0    , 190.0    , 220.0    , 240.0    , 260.0    , 280.0    ,
     *     300.0    , 320.0    , 340.0    , 360.0    , 380.0    , 400.0    ,
     *     420.0    , 440.0    , 460.0    , 480.0    , 500.0    , 520.0    ,
     *     540.0    /
      DATA  (TBSV(I),I=1,415,9)/  11.7299,  12.3162,  13.9239,  15.4747,
     *      16.9959,  18.4985,  19.9883,  21.4684,  22.9407,  24.4067,
     *      25.8675,  27.3238,  28.7764,  30.2256,  31.6721,  33.8372,
     *      35.9979,  38.1547,  40.3084,  42.4594,  44.6082,  46.7551,
     *      48.9003,  51.0440,  53.1865,  57.0415,  58.8949,  61.7469,
     *      64.5975,  67.4465,  78.1212,  85.2330,  92.3431,  99.4515,
     *     106.5580, 113.6633, 120.7682, 127.8721, 134.9733, 142.0754,
     *     149.1803, 156.2836, 163.3738, 170.4516, 177.5331, 184.6418,
     *     191.7834/
      DATA  (TBUG(I),I=1,415,9)/  49.37    ,  51.96    ,  58.77    ,  65.16    ,
     *      71.38    ,  77.52    ,  83.61    ,  89.68    ,  95.73    , 101.77    ,
     *     107.80    , 113.83    , 119.87    , 125.92    , 131.98    , 141.12    ,
     *     150.34    , 159.68    , 169.16    , 178.81    , 188.69    , 198.82    ,
     *     209.24    , 219.98    , 231.08    , 246.48    , 262.61    , 279.47    ,
     *     297.05    , 315.33    , 389.82    , 443.70    , 500.00    , 557.72    ,
     *     616.01    , 674.45    , 732.59    , 790.14    , 846.88    , 902.75    ,
     *     957.76    ,1011.93    ,1065.37    ,1118.19    ,1170.44    ,1222.26    ,
     *    1273.72    /
C
      DATA  (TBTG(I),I=2,416,9)/  38.436 ,  40.0    ,  42.0    ,  46.0    ,
     *      50.0    ,  54.0    ,  58.0    ,  62.0    ,  66.0    ,  70.0    ,
     *      74.0    ,  78.0    ,  82.0    ,  86.0    ,  90.0    ,  96.0    ,
     *     102.0    , 108.0    , 114.0    , 120.0    , 126.0    , 132.0    ,
     *     138.0    , 144.0    , 150.0    , 158.0    , 166.0    , 174.0    ,
     *     182.0    , 190.0    , 220.0    , 240.0    , 260.0    , 280.0    ,
     *     300.0    , 320.0    , 340.0    , 360.0    , 380.0    , 400.0    ,
     *     420.0    , 440.0    , 460.0    , 480.0    , 500.0    , 520.0    ,
     *     540.0    /
      DATA  (TBSV(I),I=2,416,9)/   9.0293,   9.5393,  10.1676,  11.3764,
     *      12.5487,  13.6998,  14.8366,  15.9628,  17.0810,  18.1925,
     *      19.2987,  20.4003,  21.4980,  22.5924,  23.6839,  25.3167,
     *      26.9448,  28.5692,  30.1904,  31.8089,  33.4252,  35.0395,
     *      36.6521,  38.2633,  39.8733,  42.0182,  44.1615,  46.3034,
     *      48.4441,  50.5831,  58.5959,  63.9333,  69.2689,  74.6028,
     *      79.9351,  85.2658,  90.5956,  95.9249, 101.2521, 106.5801,
     *     111.9098, 117.2380, 122.5563, 127.8654, 133.1772, 138.5089,
     *     143.8645/
      DATA  (TBUG(I),I=2,416,9)/  50.75    ,  53.73    ,  57.29    ,  63.96    ,
```

```
     *     70.34    ,  76.58   ,  82.75   ,  88.88   ,  94.98   , 101.07   ,
     *    107.15    , 113.22   , 119.29   , 125.36   , 131.46   , 140.64   ,
     *    149.89    , 159.26   , 168.77   , 178.45   , 188.35   , 198.50   ,
     *    208.93    , 219.70   , 230.81   , 246.23   , 262.37   , 279.24   ,
     *    296.83    , 315.13   , 389.65   , 443.55   , 499.86   , 557.59   ,
     *    615.89    , 674.34   , 732.49   , 790.05   , 846.79   , 902.67   ,
     *    957.68    ,1011.85   ,1065.30   ,1118.13   ,1170.38   ,1222.21   ,
     *   1273.67    /
C
      DATA (TBTG(I),I=3,417,9)/  41.291 ,  42.0    ,  44.0    ,  46.0    ,
     *     50.0     ,  54.0    ,  58.0    ,  62.0    ,  66.0    ,  70.0    ,
     *     74.0     ,  78.0    ,  82.0    ,  86.0    ,  90.0    ,  96.0    ,
     *    102.0     , 108.0    , 114.0    , 120.0    , 126.0    , 132.0    ,
     *    138.0     , 144.0    , 150.0    , 158.0    , 166.0    , 174.0    ,
     *    182.0     , 190.0    , 220.0    , 240.0    , 260.0    , 280.0    ,
     *    300.0     , 320.0    , 340.0    , 360.0    , 380.0    , 400.0    ,
     *    420.0     , 440.0    , 460.0    , 480.0    , 500.0    , 520.0    ,
     *    540.0     /
      DATA (TBSV(I),I=3,417,9)/   6.2031,   6.3707,   6.8244,   7.2584,
     *     8.0906,   8.8944,   9.6805,  10.4545,  11.2193,  11.9771,
     *    12.7290,  13.4762,  14.2193,  14.9590,  15.6957,  16.7962,
     *    17.8920,  18.9839,  20.0726,  21.1586,  22.2423,  23.3241,
     *    24.4042,  25.4829,  26.5603,  27.9952,  29.4284,  30.8602,
     *    32.2908,  33.7198,  39.0708,  42.6337,  46.1947,  49.7540,
     *    53.3116,  56.8678,  60.4231,  63.9778,  67.5310,  71.0844,
     *    74.6388,  78.1919,  81.7384,  85.2788,  88.8209,  92.3762,
     *    95.9472/
      DATA (TBUG(I),I=3,417,9)/  52.34   ,  53.82   ,  57.70   ,  61.32   ,
     *     68.12    ,  74.62   ,  80.97   ,  87.25   ,  93.47   ,  99.65   ,
     *    105.82    , 111.97   , 118.11   , 124.25   , 130.40   , 139.66   ,
     *    148.99    , 158.42   , 167.98   , 177.72   , 187.66   , 197.85   ,
     *    208.32    , 219.12   , 230.26   , 245.72   , 261.89   , 278.79   ,
     *    296.41    , 314.73   , 389.31   , 443.24   , 499.57   , 557.32   ,
     *    615.65    , 674.12   , 732.29   , 789.86   , 849.61   , 902.50   ,
     *    957.53    ,1011.71   ,1065.17   ,1118.00   ,1170.26   ,1222.09   ,
     *   1273.56    /
C
      DATA (TBTG(I),I=4,418,9)/  43.529 ,  46.0    ,  50.0    ,  54.0    ,
     *     58.0     ,  62.0    ,  66.0    ,  70.0    ,  74.0    ,  78.0    ,
     *     82.0     ,  86.0    ,  90.0    ,  96.0    , 102.0    , 108.0    ,
     *    114.0     , 120.0    , 126.0    , 132.0    , 138.0    , 144.0    ,
     *    150.0     , 158.0    , 166.0    , 174.0    , 182.0    , 190.0    ,
     *    200.0     , 210.0    , 220.0    , 240.0    , 260.0    , 280.0    ,
     *    300.0     , 320.0    , 340.0    , 360.0    , 380.0    , 400.0    ,
     *    420.0     , 440.0    , 460.0    , 480.0    , 500.0    , 520.0    ,
     *    540.0     /
      DATA (TBSV(I),I=4,418,9)/   4.7201,   5.1743,   5.8487,   6.4842,
     *     7.0978,   7.6973,   8.2865,   8.8680,   9.4433,  10.0136,
     *    10.5796,  11.1421,  11.7016,  12.5360,  13.3657,  14.1914,
     *    15.0139,  15.8337,  16.6512,  17.4667,  18.2805,  19.0929,
     *    19.9041,  20.9839,  22.0620,  23.1388,  24.2143,  25.2884,
     *    26.6297,  27.9696,  29.3085,  31.9841,  34.6578,  37.3297,
     *    40.0001,  42.6691,  45.3371,  48.0044,  50.6704,  53.3365,
     *    56.0033,  58.6690,  61.3297,  63.9858,  66.6432,  69.3100,
```

```
*        71.9883/
 DATA  (TBUG(I),I=4,418,9)/  53.03   ,  58.26   ,  65.69   ,  72.54   ,
*        79.12   ,  85.56   ,  91.91   ,  98.21   , 104.47   , 110.70   ,
*       116.92   , 123.13   , 129.34   , 138.69   , 148.09   , 157.58   ,
*       167.20   , 176.98   , 186.97   , 197.20   , 207.71   , 218.54   ,
*       229.72   , 245.21   , 261.41   , 278.34   , 295.99   , 314.33   ,
*       338.23   , 363.14   , 388.97   , 442.93   , 499.29   , 557.06   ,
*       615.41   , 673.89   , 732.08   , 789.67   , 846.43   , 902.34   ,
*       957.37   ,1011.56   ,1065.03   ,1117.87   ,1170.14   ,1221.98   ,
*      1273.45   /
C
 DATA  (TBTG(I),I=5,419,9)/  45.400  ,  46.0    ,  50.0    ,  54.0    ,
*        58.0    ,  62.0    ,  66.0    ,  70.0    ,  74.0    ,  78.0    ,
*        82.0    ,  86.0    ,  90.0    ,  96.0    , 102.0    , 108.0    ,
*       114.0    , 120.0    , 126.0    , 132.0    , 138.0    , 144.0    ,
*       150.0    , 158.0    , 166.0    , 174.0    , 182.0    , 190.0    ,
*       200.0    , 210.0    , 220.0    , 240.0    , 260.0    , 280.0    ,
*       300.0    , 320.0    , 340.0    , 360.0    , 380.0    , 400.0    ,
*       420.0    , 440.0    , 460.0    , 480.0    , 500.0    , 520.0    ,
*       540.0    /
 DATA  (TBSV(I),I=5,419,9)/    3.7977,    3.8957,    4.4908,    5.0312,
*         5.5442,    6.0404,    6.5252,    7.0015,    7.4712,    7.9356,
*         8.3956,    8.8519,    9.3051,    9.9800,   10.6501,   11.3161,
*        11.9789,   12.6390,   13.2967,   13.9525,   14.6065,   15.2591,
*        15.9105,   16.7773,   17.6424,   18.5061,   19.3686,   20.2297,
*        21.3047,   22.3785,   23.4512,   25.5945,   27.7357,   29.8752,
*        32.0132,   34.1498,   36.2854,   38.4204,   40.5542,   42.6879,
*        44.8221,   46.9553,   49.0846,   51.2101,   53.3364,   55.4703,
*        57.6131/
 DATA  (TBUG(I),I=5,419,9)/  53.17   ,  54.61   ,  63.00   ,  70.31   ,
*        77.18   ,  83.81   ,  90.32   ,  96.74   , 103.10   , 109.42   ,
*       115.72   , 122.00   , 128.28   , 137.70   , 147.18   , 156.73   ,
*       166.41   , 176.25   , 186.28   , 196.55   , 207.10   , 217.96   ,
*       229.17   , 244.70   , 260.93   , 277.90   , 295.57   , 313.93   ,
*       337.85   , 362.78   , 388.63   , 442.62   , 499.01   , 556.80   ,
*       615.17   , 673.67   , 731.87   , 789.48   , 846.26   , 902.17   ,
*       957.21   ,1011.41   ,1064.89   ,1117.74   ,1170.03   ,1221.87   ,
*      1273.34   /
C
 DATA  (TBTG(I),I=6,420,9)/  47.022  ,  50.0    ,  54.0    ,  58.0    ,
*        62.0    ,  66.0    ,  70.0    ,  74.0    ,  78.0    ,  82.0    ,
*        86.0    ,  90.0    ,  96.0    , 102.0    , 108.0    , 114.0    ,
*       120.0    , 126.0    , 132.0    , 138.0    , 144.0    , 150.0    ,
*       156.0    , 162.0    , 168.0    , 174.0    , 180.0    , 190.0    ,
*       200.0    , 210.0    , 220.0    , 240.0    , 260.0    , 280.0    ,
*       300.0    , 320.0    , 340.0    , 360.0    , 380.0    , 400.0    ,
*       420.0    , 440.0    , 460.0    , 480.0    , 500.0    , 520.0    ,
*       540.0    /
 DATA  (TBSV(I),I=6,420,9)/    3.1644,    3.5718,    4.0558,    4.5046,
*         4.9335,    5.3495,    5.7563,    6.1559,    6.5499,    6.9394,
*         7.3250,    7.7074,    8.2761,    8.8398,    9.3994,    9.9558,
*        10.5093,   11.0606,   11.6098,   12.1574,   12.7035,   13.2483,
*        13.7920,   14.3348,   14.8767,   15.4178,   15.9583,   16.8574,
*        17.7549,   18.6512,   19.5465,   21.3349,   23.1211,   24.9057,
```

```
     *        26.6887,  28.4704,  30.2512,  32.0312,  33.8101,  35.5889,
     *        37.3679,  39.1461,  40.9210,  42.6929,  44.4654,  46.2439,
     *        48.0296/
      DATA (TBUG(I),I=6,420,9)/  52.91  ,  59.96  ,  67.92  ,  75.14  ,
     *       82.01  ,  88.68  ,  95.23  , 101.71  , 108.12  , 114.50  ,
     *      120.86  , 127.20  , 136.71  , 146.26  , 155.89  , 165.62  ,
     *      175.51  , 185.59  , 195.90  , 206.49  , 217.39  , 228.62  ,
     *      240.23  , 252.23  , 264.64  , 277.45  , 290.66  , 313.52  ,
     *      337.47  , 362.42  , 388.29  , 442.32  , 498.73  , 556.55  ,
     *      614.93  , 673.44  , 731.66  , 789.28  , 846.08  , 902.00  ,
     *      957.06  ,1011.27  ,1064.75  ,1117.62  ,1169.91  ,1221.75  ,
     *     1273.23  /
C
      DATA (TBTG(I),I=7,421,9)/  48.464 ,  50.0   ,  54.0   ,  58.0   ,
     *       62.0   ,  66.0   ,  70.0   ,  74.0   ,  78.0   ,  82.0   ,
     *       86.0   ,  90.0   ,  96.0   , 102.0   , 108.0   , 114.0   ,
     *      120.0   , 126.0   , 132.0   , 138.0   , 144.0   , 150.0   ,
     *      156.0   , 162.0   , 168.0   , 174.0   , 180.0   , 190.0   ,
     *      200.0   , 210.0   , 220.0   , 240.0   , 260.0   , 280.0   ,
     *      300.0   , 320.0   , 340.0   , 360.0   , 380.0   , 400.0   ,
     *      420.0   , 440.0   , 460.0   , 480.0   , 500.0   , 520.0   ,
     *      540.0   /
      DATA (TBSV(I),I=7,421,9)/   2.7007,   2.8995,   3.3521,   3.7583,
     *         4.1408,   4.5085,   4.8660,   5.2159,   5.5599,   5.8991,
     *         6.2343,   6.5663,   7.0591,   7.5468,   8.0305,   8.5108,
     *         8.9883,   9.4635,   9.9366,  10.4081,  10.8781,  11.3469,
     *        11.8145,  12.2811,  12.7470,  13.2120,  13.6764,  14.4486,
     *        15.2194,  15.9889,  16.7575,  18.2923,  19.8251,  21.3561,
     *        22.8856,  24.4138,  25.9410,  27.4675,  28.9929,  30.5182,
     *        32.0436,  33.5682,  35.0900,  36.6092,  38.1289,  39.6535,
     *        41.1842/
      DATA (TBUG(I),I=7,421,9)/  52.35  ,  56.46  ,  65.32  ,  72.99  ,
     *       80.13  ,  87.00  ,  93.70  , 100.29  , 106.81  , 113.27  ,
     *      119.70  , 126.11  , 135.72  , 145.35  , 155.04  , 164.83  ,
     *      174.77  , 184.90  , 195.25  , 205.88  , 216.81  , 228.08  ,
     *      239.71  , 251.74  , 264.17  , 277.00  , 290.23  , 313.12  ,
     *      337.09  , 362.07  , 387.95  , 442.01  , 498.45  , 556.29  ,
     *      614.69  , 673.22  , 731.46  , 789.09  , 845.90  , 901.84  ,
     *      956.91  ,1011.13  ,1064.62  ,1117.49  ,1169.79  ,1221.64  ,
     *     1273.12  /
C
      DATA (TBTG(I),I=8,422,9)/  49.768 ,  50.0   ,  54.0   ,  58.0   ,
     *       62.0   ,  66.0   ,  70.0   ,  74.0   ,  78.0   ,  82.0   ,
     *       86.0   ,  90.0   ,  96.0   , 102.0   , 108.0   , 114.0   ,
     *      120.0   , 126.0   , 132.0   , 138.0   , 144.0   , 150.0   ,
     *      156.0   , 162.0   , 168.0   , 174.0   , 180.0   , 190.0   ,
     *      200.0   , 210.0   , 220.0   , 240.0   , 260.0   , 280.0   ,
     *      300.0   , 320.0   , 340.0   , 360.0   , 380.0   , 400.0   ,
     *      420.0   , 440.0   , 460.0   , 480.0   , 500.0   , 520.0   ,
     *      540.0   /
      DATA (TBSV(I),I=8,422,9)/   2.3452,   2.3747,   2.8169,   3.1950,
     *         3.5442,   3.8765,   4.1975,   4.5104,   4.8170,   5.1187,
     *         5.4162,   5.7104,   6.1464,   6.5772,   7.0039,   7.4272,
     *         7.8477,   8.2658,   8.6819,   9.0963,   9.5092,   9.9209,
```

```
     *        10.3315,  10.7410,  11.1498,  11.5578,  11.9651,  12.6422,
     *        13.3179,  13.9923,  14.6658,  16.0105,  17.3531,  18.6940,
     *        20.0333,  21.3713,  22.7084,  24.0447,  25.3801,  26.7152,
     *        28.0504,  29.3848,  30.7168,  32.0465,  33.3766,  34.7108,
     *        36.0503/
      DATA (TBUG(I),I=8,422,9)/  51.54   ,  52.26   ,  62.47   ,  70.71   ,
     *        78.18   ,  85.26   ,  92.13   ,  98.85   , 105.47   , 112.03   ,
     *       118.54   , 125.02   , 134.72   , 144.42   , 154.18   , 164.04   ,
     *       174.03   , 184.20   , 194.60   , 205.26   , 216.23   , 227.53   ,
     *       239.19   , 251.24   , 263.70   , 276.55   , 289.80   , 312.72   ,
     *       336.72   , 361.71   , 387.61   , 441.70   , 498.17   , 556.03   ,
     *       614.45   , 673.00   , 731.26   , 788.90   , 845.72   , 901.67   ,
     *       956.75   ,1010.98   ,1064.49   ,1117.37   ,1169.67   ,1221.53   ,
     *      1273.01   /
      END
R
     368.2      2.62      1.56      1.24      0.75     189.2      2.30     386.3

 3 3 0 0 0 1 0 1
 1 2 0 2 0      0.0     130.0       0.0       0.0       0.0       0.0       1.0
 2 2 0 2 0    130.0     240.0       0.0       0.0       0.0       0.0       1.0
 3 2 0 2 0    240.0     414.0       0.0       0.0       0.0       0.0       1.0
14 1
   5541.     .6600
   5551.     .7192
   5561.     .7902
   5571.     .7852
   5581.     .7925
   5591.     .7866
   5601.     .7755
   5611.     .7616
   5661.     .6972
   5711.     .6116
   5761.     .5577
   5811.     .4997
   5861.     .4430
   5911.     .3916
14 2
   5541.    3.6100
   5551.    3.8852
   5561.    4.1716
   5571.    4.1622
   5581.    4.2427
   5591.    4.2961
   5601.    4.3350
   5611.    4.3661
   5661.    4.3969
   5711.    4.5147
   5761.    4.4741
   5811.    4.5622
   5861.    4.5700
   5911.    4.4669
14 3
   5541.   13.200
```

```
   5551.   15.151
   5561.   16.686
   5571.   16.688
   5581.   17.298
   5591.   17.641
   5601.   18.145
   5611.   18.382
   5661.   19.784
   5711.   21.116
   5761.   22.172
   5811.   21.086
   5861.   22.913
   5911.   22.256
33
    1.0130     1.110     1.032     0.618     0.608     0.579     0.531     0.579
     0.772     0.801     0.695     0.724     0.995     0.850     0.840     0.898
     0.926     0.936     0.907     0.974     0.950     0.965     0.985     0.936
    1.0150     1.225     1.370     1.390     1.400     1.450     2.030     2.030
    2.0300
    203.25    203.25     203.8     203.8     203.8     203.8     203.8     203.9
    203.9     203.90     203.9     203.9     203.9     203.9     204.0     204.1
    204.1     204.10     204.1     204.2     204.2     204.2     204.2     204.2
    204.2     201.90     202.1     202.2     202.3     202.4     202.4     202.4
    202.5
    5565.      5567.     5579.     5592.     5590.     5600.     5604.     5606.
    5609.      5616.    5618.      5621.     5624.     5626.     5631.     5644.
    5646.      5652.     5655.     5660.     5664.     5668.     5674.     5677.
    5682.      5734.     5784.     5792.     5834.     5866.     5867.     5883.
    5884.
 9
.000000001      1.00      0.75       0.5      .250     0.125    .06250 0.0000001
.000000001
     510.0     460.0     430.0     405.0     350.0     300.0      270.0     190.
     110.0
    5541.0     5545.     5546.     5549.     5554.     5558.     5562.     5578.
     5611.
 REPRESSURIZATION FOR S-IVB    OCT 16,1968
P$CASE                 PU      =     19.6     ,TU      =     75.     ,XML     =  17800.
  ,PSATL   =   19.6  $
0START PROBLEM WITH REPRESSURIZATION ONLY FOR FIRST 19 SEC.
P$PHASE                                   CONQLG =  1.0    ,    TIME     =  5541.0
            ,DTTOL   = 10.0
  ,EPSR    =  .00001,EPSA    =     .001    ,IFLOW  =  5        ,MDOTL   =     0.0
        ,    EPSP   = .0001
        , TIMEF=5565.      ,  DTIME= 2.0    ,FQLIQ=1.0
  ,NEXT    =  4      ,G      =     0.00059,CONSAT =  1.0       ,KBURP   =  1
  ,CONBRP =  0.0    ,CONQBO =     0.0     ,KRECIR =   0        ,CONFAC  =     1.0

1CONTINUE REPRESSURIZATION  AND START RECIRCULATION
P$PHASE                                                         TIME     =  5565.0
  ,TIMEF   =5611.0
  ,NEXT    =  4      ,G      =      .00052     ,KRECIR =  1    ,KBURP   =  1
1STOP REPRESSURIZATION  AND CONTINUE RECIRCULATION
P$PHASE                                                         TIME     =  5611.0
  ,NEXT    =  5      ,G      =      .00040      ,TIMEF   =5884.0,KBURP   =  0
     ,NEXT = 3
```

```
                      S-IV B TANK PRESSURE SIMULATION

 REPRESSURIZATION FOR S-IVB    OCT 16,1968

PSCASE              PU       =    19.6    ,TU      =    75.     ,XML     =  17800.
 ,PSATL   =  19.6  $

START PROBLEM WITH REPRESSURIZATION ONLY FOR FIRST 19 SEC.
PSPHASE                              CONQLG =  1.0     ,   TIME     =   5541.0
             ,DTTOL   = 10.0
 ,EPSR    =  .00001,EPSA    =    .001   ,IFLOW  =  5        ,MDOTL   =      0.0
        ,    EPSP  = .0001
        , TIMEF=5565.     ,  DTIME= 2.0   ,FQLIQ=1.0
 ,NEXT    =  4      ,G       =    0.00059,CONSAT =  1.0      ,KBURP   =  1
 ,CONBRP  =  0.0    ,CONQBO  =     0.0   ,KRECIR =   0       ,CONFAC  =      1.0
                                                              $


 1/0/0  TIME      PRESSURE     TEMP-ULL      SAT-TEMP     Q-LIQUID       Q-ULL     L/L STATION      ULL-VOL     P-HE BTL     MDOT-EVAP
 5541.00000       19.60000     75.00000      38.28936     12.32190      5.14810     251.57501    6294.96360     0.00000      0.00000
                  PRESS-VAP    PRESS-HE      U-VAP        MDOTC         MDOTE2       MDOTE3       Q-REC-LIQ
                  19.60000     0.00000      108.70668      0.00000      0.00000      0.00000      0.00000

  ULL-ENERGY      MASS-FUEL     MASS-HE      MASS-LIQ     TEMP-LIQ    MASS-SPRAY    HE IN BTL     TEMP-HE      TEMP-BTL    MASS VENTED
 34246.56557     315.03643     0.00000   17800.00000    38.28936      0.00000      0.00000      0.00000      0.00000      0.00000
     4.70090       0.00000      .00000      -0.00000      .00031      0.00000      0.00000      0.00000      0.00000      0.00000

WALL TEMPS =      0.000000     0.000000      0.000000


 2/4/1  TIME      PRESSURE     TEMP-ULL      SAT-TEMP     Q-LIQUID       Q-ULL     L/L STATION      ULL-VOL     P-HE BTL     MDOT-EVAP
 5545.00000       20.29443     77.32419      38.50124     13.05051      5.33365     251.57340    6294.91497     0.00000      0.00000
                  PRESS-VAP    PRESS-HE      U-VAP        MDOTC         MDOTE2       MDOTE3       Q-REC-LIQ
                  20.22852      .06590      112.15164      0.00000      0.00000      0.00000      0.00000

  ULL-ENERGY      MASS-FUEL     MASS-HE      MASS-LIQ     TEMP-LIQ    MASS-SPRAY    HE IN BTL     TEMP-HE      TEMP-BTL    MASS VENTED
 35447.84068     315.03643     2.00000   17800.00000    38.29064      0.00000      0.00000      0.00000      0.00000      0.00000
   575.25504       0.00000     1.00000      -0.00000      .00033      0.00000      0.00000      0.00000      0.00000      0.00000

WALL TEMPS =      0.000000     0.000000      0.000000


 2/3/1  TIME      PRESSURE     TEMP-ULL      SAT-TEMP     Q-LIQUID       Q-ULL     L/L STATION      ULL-VOL     P-HE BTL     MDOT-EVAP
 5546.00000       20.57904     78.26542      38.57394     13.23267      5.38003     251.57298    6294.90237     0.00000      0.00000
                  PRESS-VAP    PRESS-HE      U-VAP        MDOTC         MDOTE2       MDOTE3       Q-REC-LIQ
                  20.48315      .09589      113.53465      0.00000      0.00000      0.00000      0.00000

  ULL-ENERGY      MASS-FUEL     MASS-HE      MASS-LIQ     TEMP-LIQ    MASS-SPRAY    HE IN BTL     TEMP-HE      TEMP-BTL    MASS VENTED
 35936.31103     315.03643     2.87500   17800.00000    38.29098      0.00000      0.00000      0.00000      0.00000      0.00000
   404.78662       0.00000      .75000      -0.00000      .00034      0.00000      0.00000      0.00000      0.00000      0.00000

WALL TEMPS =      0.000000     0.000000      0.000000


 2/4/1  TIME      PRESSURE     TEMP-ULL      SAT-TEMP     Q-LIQUID       Q-ULL     L/L STATION      ULL-VOL     P-HE BTL     MDOT-EVAP
 5548.00000       20.98990     79.61296      38.67785     13.59699      5.47279     251.57212    6294.87661     0.00000      0.00000
                  PRESS-VAP    PRESS-HE      U-VAP        MDOTC         MDOTE2       MDOTE3       Q-REC-LIQ
                  20.84712      .14278      115.51872      0.00000      0.00000      0.00000      0.00000
```

```
 ULL-ENERGY    MASS-FUEL     MASS-HE     MASS-LIQ     TEMP-LIQ   MASS-SPRAY   HE IN BTL     TEMP-HE     TEMP-BTL   MASS VENTED
36643.88461    315.03643     4.20833  17800.00000     38.29166      0.00000     0.00000     0.00000      0.00000      0.00000
  303.93596      0.00000      .58333     -0.00000       .00034      0.00000     0.00000     0.00000      0.00000      0.00000

WALL TEMPS =    0.000000    0.000000     0.000000


 2/2/1  TIME    PRESSURE    TEMP-ULL     SAT-TEMP     Q-LIQUID      Q-ULL    L/L STATION    ULL-VOL     P-HE BTL    MDOT-EVAP
 5549.00000     21.15228    80.14169     38.71866     13.77915     5.51917   251.57169   6294.86347     0.00000      0.00000
                PRESS-VAP   PRESS-HE     U-VAP        MDOTC        MDOTE2     MDOTE3      Q-REC-LIQ
                20.99005      .16223    116.29844      0.00000     0.00000     0.00000     0.00000

 ULL-ENERGY    MASS-FUEL     MASS-HE     MASS-LIQ     TEMP-LIQ   MASS-SPRAY   HE IN BTL     TEMP-HE     TEMP-BTL   MASS VENTED
36923.75693    315.03643     4.75000  17800.00000     38.29200      0.00000     0.00000     0.00000      0.00000      0.00000
  256.09602      0.00000      .50000     -0.00000       .00035      0.00000     0.00000     0.00000      0.00000      0.00000

WALL TEMPS =    0.000000    0.000000     0.000000


 2/5/1  TIME    PRESSURE    TEMP-ULL     SAT-TEMP     Q-LIQUID      Q-ULL    L/L STATION    ULL-VOL     P-HE BTL    MDOT-EVAP
 5553.00000     21.60673    81.60450     38.83167     14.43014     5.70374   251.56989   6294.80920     0.00000      0.00000
                PRESS-VAP   PRESS-HE     U-VAP        MDOTC        MDOTE2     MDOTE3      Q-REC-LIQ
                21.38590      .22083    118.45908      0.00000     0.00000     0.00000     0.00000

 ULL-ENERGY    MASS-FUEL     MASS-HE     MASS-LIQ     TEMP-LIQ   MASS-SPRAY   HE IN BTL     TEMP-HE     TEMP-BTL   MASS VENTED
37707.56840    315.03643     6.35000  17800.00000     38.29344      0.00000     0.00000     0.00000      0.00000      0.00000
  139.44881      0.00000      .30000     -0.00000       .00037      0.00000     0.00000     0.00000      0.00000      0.00000

WALL TEMPS =    0.000000    0.000000     0.000000


 2/3/1  TIME    PRESSURE    TEMP-ULL     SAT-TEMP     Q-LIQUID      Q-ULL    L/L STATION    ULL-VOL     P-HE BTL    MDOT-EVAP
 5554.00000     21.68001    81.83730     38.84968     14.57348     5.74964   251.56943   6294.79528     0.00000      0.00000
                PRESS-VAP   PRESS-HE     U-VAP        MDOTC        MDOTE2     MDOTE3      Q-REC-LIQ
                21.44895      .23106    118.80339      0.00000     0.00000     0.00000     0.00000

 ULL-ENERGY    MASS-FUEL     MASS-HE     MASS-LIQ     TEMP-LIQ   MASS-SPRAY   HE IN BTL     TEMP-HE     TEMP-BTL   MASS VENTED
37834.02847    315.03643     6.62500  17800.00000     38.29380      0.00000     0.00000     0.00000      0.00000      0.00000
  113.69884      0.00000      .25000     -0.00000       .00037      0.00000     0.00000     0.00000      0.00000      0.00000

WALL TEMPS =    0.000000    0.000000     0.000000


 2/5/1  TIME    PRESSURE    TEMP-ULL     SAT-TEMP     Q-LIQUID      Q-ULL    L/L STATION    ULL-VOL     P-HE BTL    MDOT-EVAP
 5558.00000     21.86851    82.43066     38.89549     15.14683     5.93325   251.56754   6294.73823     0.00000      0.00000
                PRESS-VAP   PRESS-HE     U-VAP        MDOTC        MDOTE2     MDOTE3      Q-REC-LIQ
                21.60943      .25908    119.68156      0.00000     0.00000     0.00000     0.00000

 ULL-ENERGY    MASS-FUEL     MASS-HE     MASS-LIQ     TEMP-LIQ   MASS-SPRAY   HE IN BTL     TEMP-HE     TEMP-BTL   MASS VENTED
38160.00247    315.03643     7.37500  17800.00000     38.29531      0.00000     0.00000     0.00000      0.00000      0.00000
   51.87267      0.00000      .12500     -0.00000       .00038      0.00000     0.00000     0.00000      0.00000      0.00000

WALL TEMPS =    0.000000    0.000000     0.000000


 2/1/1  TIME    PRESSURE    TEMP-ULL     SAT-TEMP     Q-LIQUID      Q-ULL    L/L STATION    ULL-VOL     P-HE BTL    MDOT-EVAP
```

5562.00000	21.95822	82.70997	38.91708	15.57709	6.06947	251.56558	6294.67913	0.00000	0.00000
	PRESS-VAP	PRESS-HE	U-VAP	MDOTC	MDOTE2	MDOTE3	Q-REC-LIQ		
	21.68504	.27318	120.09521	0.00000	0.00000	0.00000	0.00000		
ULL-ENERGY	MASS-FUEL	MASS-HE	MASS-LIQ	TEMP-LIQ	MASS-SPRAY	HE IN BTL	TEMP-HE	TEMP-BTL	MASS VENTED
38315.11850	315.03643	7.75000	17800.00000	38.29687	0.00000	0.00000	0.00000	0.00000	0.00000
26.42924	0.00000	.06250	-0.00000	.00039	0.00000	0.00000	0.00000	0.00000	0.00000
WALL TEMPS =	0.000000	0.000000	0.000000						
2/2/1 TIME	PRESSURE	TEMP-ULL	SAT-TEMP	Q-LIQUID	Q-ULL	L/L STATION	ULL-VOL	P-HE BTL	MDOT-EVAP
5565.00000	21.99984	82.83974	38.92712	15.57779	6.06505	251.56410	6294.63432	0.00000	0.00000
	PRESS-VAP	PRESS-HE	U-VAP	MDOTC	MDOTE2	MDOTE3	Q-REC-LIQ		
	21.72023	.27961	120.28742	0.00000	0.00000	0.00000	0.00000		
ULL-ENERGY	MASS-FUEL	MASS-HE	MASS-LIQ	TEMP-LIQ	MASS-SPRAY	HE IN BTL	TEMP-HE	TEMP-BTL	MASS VENTED
38386.98524	315.03643	7.91992	17800.00000	38.29805	0.00000	0.00000	0.00000	0.00000	0.00000
21.55467	0.00000	.05078	-0.00000	.00039	0.00000	0.00000	0.00000	0.00000	0.00000
WALL TEMPS =	0.000000	0.000000	0.000000						

```
CONTINUE REPRESSURIZATION  AND START RECIRCULATION
P$PHASE                                                        TIME    =  5565.0
  ,TIMEF  =5611.0
  ,NEXT   =  4     ,G      =      .00052     ,KRECIR =  1     ,KBURP   =  1    $

 1/0/1  TIME      PRESSURE     TEMP-ULL     SAT-TEMP     Q-LIQUID       Q-ULL    L/L STATION     ULL-VOL    P-HE BTL    MDOT-EVAP
 5565.00000       21.99984     82.83974     38.92712     15.57779     6.06505    251.56410   6294.63432     0.00000      0.00000
                  PRESS-VAP    PRESS-HE     U-VAP        MDOTC        MDOTE2       MDOTE3      Q-REC-LIQ
                  21.72023       .27961     120.28743     0.00000     0.00000      0.00000    205.89225

  ULL-ENERGY      MASS-FUEL     MASS-HE     MASS-LIQ     TEMP-LIQ   MASS-SPRAY    HE IN BTL     TEMP-HE    TEMP-BTL   MASS VENTED
 38386.98524      315.03643     7.91992  17800.00000     38.29805     0.00000      0.00000     0.00000     0.00000      0.00000
    21.57229        0.00000      .05078     -0.00000       .00542     0.00000      0.00000     0.00000     0.00000      0.00000

WALL TEMPS =      0.000000     0.000000     0.000000

 2/1/5  TIME      PRESSURE     TEMP-ULL     SAT-TEMP     Q-LIQUID       Q-ULL    L/L STATION     ULL-VOL    P-HE BTL    MDOT-EVAP
 5569.00000       22.04566     82.97475     38.93839     15.58133     6.05655    251.53493   6293.75355     0.00000      0.00000
                  PRESS-VAP    PRESS-HE     U-VAP        MDOTC        MDOTE2       MDOTE3      Q-REC-LIQ
                  21.75968       .28618     120.48705     0.00000     0.00000      0.00000    223.06581

  ULL-ENERGY      MASS-FUEL     MASS-HE     MASS-LIQ     TEMP-LIQ   MASS-SPRAY    HE IN BTL     TEMP-HE    TEMP-BTL   MASS VENTED
 38461.36951      315.03643     8.09180  17800.00000     38.32131     0.00000      0.00000     0.00000     0.00000      0.00000
    15.74908        0.00000      .03516     -0.00000       .00584     0.00000      0.00000     0.00000     0.00000      0.00000

WALL TEMPS =      0.000000     0.000000     0.000000

 2/2/1  TIME      PRESSURE     TEMP-ULL     SAT-TEMP     Q-LIQUID       Q-ULL    L/L STATION     ULL-VOL    P-HE BTL    MDOT-EVAP
 5577.00000       22.10218     83.13848     38.95270     15.92907     6.12501    251.47752   6292.02001     0.00000      0.00000
                  PRESS-VAP    PRESS-HE     U-VAP        MDOTC        MDOTE2       MDOTE3      Q-REC-LIQ
                  21.80982       .29236     120.72884     0.00000     0.00000      0.00000    212.87521

  ULL-ENERGY      MASS-FUEL     MASS-HE     MASS-LIQ     TEMP-LIQ   MASS-SPRAY    HE IN BTL     TEMP-HE    TEMP-BTL   MASS VENTED
 38548.28135      315.03643     8.24805  17800.00000     38.36708     0.00000      0.00000     0.00000     0.00000      0.00000
     6.51488        0.00000      .00391     -0.00000       .00560     0.00000      0.00000     0.00000     0.00000      0.00000

WALL TEMPS =      0.000000     0.000000     0.000000

 1/2/3  TIME      PRESSURE     TEMP-ULL     SAT-TEMP     Q-LIQUID       Q-ULL    L/L STATION     ULL-VOL    P-HE BTL    MDOT-EVAP
 5581.00000       22.11848     83.18708     38.95727     16.15972     6.17348    251.44993   6291.18677     0.00000      0.00000
                  PRESS-VAP    PRESS-HE     U-VAP        MDOTC        MDOTE2       MDOTE3      Q-REC-LIQ
                  21.82581       .29267     120.80048     0.00000     0.00000      0.00000    197.34111

  ULL-ENERGY      MASS-FUEL     MASS-HE     MASS-LIQ     TEMP-LIQ   MASS-SPRAY    HE IN BTL     TEMP-HE    TEMP-BTL   MASS VENTED
 38571.28776      315.03643     8.25065  17800.00000     38.38909     0.00000      0.00000     0.00000     0.00000      0.00000
     5.61805        0.00000      .00000     -0.00000       .00523     0.00000      0.00000     0.00000     0.00000      0.00000

WALL TEMPS =      0.000000     0.000000     0.000000

 2/3/5  TIME      PRESSURE     TEMP-ULL     SAT-TEMP     Q-LIQUID       Q-ULL    L/L STATION     ULL-VOL    P-HE BTL    MDOT-EVAP
 5597.00000       22.18002     83.37944     38.97461     16.77140     6.27138    251.36506   6288.62405     0.00000      0.00000
                  PRESS-VAP    PRESS-HE     U-VAP        MDOTC        MDOTE2       MDOTE3      Q-REC-LIQ
```

```
                21.88656        .29346    121.08440     0.00000     0.00000     0.00000   119.77326

  ULL-ENERGY   MASS-FUEL       MASS-HE     MASS-LIQ    TEMP-LIQ  MASS-SPRAY   HE IN BTL     TEMP-HE    TEMP-BTL  MASS VENTED
 38661.96242   315.03643       8.25065  17800.00000    38.45427     0.00000     0.00000     0.00000     0.00000     0.00000
     5.71293     0.00000        .00000     -0.00000      .00335     0.00000     0.00000     0.00000     0.00000     0.00000

 WALL TEMPS =   0.000000      0.000000     0.000000


 2/2/5  TIME    PRESSURE      TEMP-ULL     SAT-TEMP    Q-LIQUID       Q-ULL  L/L STATION     ULL-VOL    P-HE BTL   MDOT-EVAP
 5611.00000     22.23367      83.54982     38.98973    17.18836     6.32134   251.29871  6286.62045     0.00000     0.00000
                PRESS-VAP     PRESS-HE     U-VAP       MDUTC        MDOTE2      MDOTE3     Q-REC-LIQ
                21.93952        .29416    121.33610     0.00000     0.00000     0.00000   159.10026
  ULL-ENERGY   MASS-FUEL       MASS-HE     MASS-LIQ    TEMP-LIQ  MASS-SPRAY   HE IN BTL     TEMP-HE    TEMP-BTL  MASS VENTED
 38742.32948   315.03643       8.25065  17800.00000    38.50084     0.00000     0.00000     0.00000     0.00000     0.00000
     5.76022     0.00000        .00000     -0.00000      .00432     0.00000     0.00000     0.00000     0.00000     0.00000

 WALL TEMPS =   0.000000      0.000000     0.000000
```

```
STOP REPRESSURIZATION  AND CONTINUE RECIRCULATION
PSPHASE                                                    TIME    =  5611.0
 ,NEXT   =  5    ,G     =    .00040     ,TIMEF  =5884.0,KBURP   =  0
   ,NEXT = 3
                                                   $

 1/0/5  TIME     PRESSURE     TEMP-ULL     SAT-TEMP     Q-LIQUID      Q-ULL     L/L STATION    ULL-VOL      P-HE BTL    MDOT-EVAP
 5611.00000      22.23368     83.54989     38.98973     17.18836     6.32134     251.29871   6286.62045    0.00000     0.00000
                 PRESS-VAP    PRESS-HE     U-VAP        MDOTC        MDOTE2       MDOTE3       Q-REC-LIQ
                 21.93952      .29416     121.33620     0.00000      0.00000      0.00000     159.10026

 ULL-ENERGY      MASS-FUEL     MASS-HE     MASS-LIQ     TEMP-LIQ    MASS-SPRAY   HE IN BTL    TEMP-HE      TEMP-BTL    MASS VENTED
 38742.32948     315.03643     8.25065   17800.00000    38.50084     0.00000      0.00000      0.00000      0.00000     0.00000
     5.79583       0.00000      .00000     -0.00000      .00432      0.00000      0.00000      0.00000      0.00000     0.00000

 WALL TEMPS =     0.000000    0.000000     0.000000


 2/2/5  TIME     PRESSURE     TEMP-ULL     SAT-TEMP     Q-LIQUID      Q-ULL     L/L STATION    ULL-VOL      P-HE BTL    MDOT-EVAP
 5619.00000      22.26583     83.64833     38.99879     17.40337     6.32527     251.24954   6285.13585    0.00000     0.00000
                 PRESS-VAP    PRESS-HE     U-VAP        MDOTC        MDOTE2       MDOTE3       Q-REC-LIQ
                 21.97126      .29457     121.48149     0.00000      0.00000      0.00000     143.68153

 ULL-ENERGY      MASS-FUEL     MASS-HE     MASS-LIQ     TEMP-LIQ    MASS-SPRAY   HE IN BTL    TEMP-HE      TEMP-BTL    MASS VENTED
 38788.70589     315.03643     8.25065   17800.00000    38.53535     0.00000      0.00000      0.00000      0.00000     0.00000
     5.79832       0.00000      .00000     -0.00000      .00395      0.00000      0.00000      0.00000      0.00000     0.00000

 WALL TEMPS =     0.000000    0.000000     0.000000


 2/1/5  TIME     PRESSURE     TEMP-ULL     SAT-TEMP     Q-LIQUID      Q-ULL     L/L STATION    ULL-VOL      P-HE BTL    MDOT-EVAP
 5627.00000      22.29853     83.74688     39.00801     17.61903     6.32856     251.19560   6283.50687    0.00000     0.00000
                 PRESS-VAP    PRESS-HE     U-VAP        MDOTC        MDOTE2       MDOTE3       Q-REC-LIQ
                 22.00353      .29500     121.62691     0.00000      0.00000      0.00000     172.92416

 ULL-ENERGY      MASS-FUEL     MASS-HE     MASS-LIQ     TEMP-LIQ    MASS-SPRAY   HE IN BTL    TEMP-HE      TEMP-BTL    MASS VENTED
 38835.10046     315.03643     8.25065   17800.00000    38.57322     0.00000      0.00000      0.00000      0.00000     0.00000
     5.80015       0.00000      .00000     -0.00000      .00467      0.00000      0.00000      0.00000      0.00000     0.00000

 WALL TEMPS =     0.000000    0.000000     0.000000


 2/1/5  TIME     PRESSURE     TEMP-ULL     SAT-TEMP     Q-LIQUID      Q-ULL     L/L STATION    ULL-VOL      P-HE BTL    MDOT-EVAP
 5635.00000      22.33114     83.84531     39.01720     17.83472     6.33181     251.14257   6281.90557    0.00000     0.00000
                 PRESS-VAP    PRESS-HE     U-VAP        MDOTC        MDOTE2       MDOTE3       Q-REC-LIQ
                 22.03572      .29542     121.77218     0.00000      0.00000      0.00000     175.02701

 ULL-ENERGY      MASS-FUEL     MASS-HE     MASS-LIQ     TEMP-LIQ    MASS-SPRAY   HE IN BTL    TEMP-HE      TEMP-BTL    MASS VENTED
 38881.50899     315.03643     8.25065   17800.00000    38.61044     0.00000      0.00000      0.00000      0.00000     0.00000
     5.80195       0.00000      .00000     -0.00000      .00472      0.00000      0.00000      0.00000      0.00000     0.00000

 WALL TEMPS =     0.000000    0.000000     0.000000


 2/3/5  TIME     PRESSURE     TEMP-ULL     SAT-TEMP     Q-LIQUID      Q-ULL     L/L STATION    ULL-VOL      P-HE BTL    MDOT-EVAP
 5667.00000      22.46391     84.23961     39.05461     18.69321     6.34860     250.91115   6274.91771    0.00000     0.00000
```

```
                PRESS-VAP    PRESS-HE     U-VAP        MDOTC       MDOTE2       MDOTE3       Q-REC-LIQ
                22.16677     .29714       122.35406    0.00000     0.00000      0.00000      196.28725
ULL-ENERGY      MASS-FUEL    MASS-HE      MASS-LIQ     TEMP-LIQ    MASS-SPRAY   HE IN BTL    TEMP-HE      TEMP-BTL     MASS VENTED
39067.28165     315.03643    8.25065      17800.00000  38.77288    0.00000      0.00000      0.00000      0.00000      0.00000
5.81289         0.00000      .00000       -0.00000     .00526      0.00000      0.00000      0.00000      0.00000      0.00000
WALL TEMPS =    0.000000     0.000000     0.000000

2/2/5  TIME     PRESSURE     TEMP-ULL     SAT-TEMP     Q-LIQUID    Q-ULL        L/L STATION  ULL-VOL      P-HE BTL     MDOT-EVAP
5683.00000      22.53123     84.43733     39.07358     19.10697    6.37138      250.78939    6271.24090   0.00000      0.00000
                PRESS-VAP    PRESS-HE     U-VAP        MDOTC       MDOTE2       MDOTE3       Q-REC-LIQ
                22.23322     .29801       122.64593    0.00000     0.00000      0.00000      208.04258
ULL-ENERGY      MASS-FUEL    MASS-HE      MASS-LIQ     TEMP-LIQ    MASS-SPRAY   HE IN BTL    TEMP-HE      TEMP-BTL     MASS VENTED
39160.44810     315.03643    8.25065      17800.00000  38.85835    0.00000      0.00000      0.00000      0.00000      0.00000
5.83270         0.00000      .00000       -0.00000     .00556      0.00000      0.00000      0.00000      0.00000      0.00000
WALL TEMPS =    0.000000     0.000000     0.000000

2/2/1  TIME     PRESSURE     TEMP-ULL     SAT-TEMP     Q-LIQUID    Q-ULL        L/L STATION  ULL-VOL      P-HE BTL     MDOT-EVAP
5715.00000      22.66923     84.83457     39.11247     19.91851    6.40071      250.52156    6263.15360   0.00000      0.00000
                PRESS-VAP    PRESS-HE     U-VAP        MDOTC       MDOTE2       MDOTE3       Q-REC-LIQ
                22.36943     .29980       123.23225    0.00000     0.00000      0.00000      232.80055
ULL-ENERGY      MASS-FUEL    MASS-HE      MASS-LIQ     TEMP-LIQ    MASS-SPRAY   HE IN BTL    TEMP-HE      TEMP-BTL     MASS VENTED
39347.60708     315.03643    8.25065      17800.00000  39.04634    0.00000      0.00000      0.00000      0.00000      0.00000
5.85608         0.00000      .00000       -0.00000     .00619      0.00000      0.00000      0.00000      0.00000      0.00000
WALL TEMPS =    0.000000     0.000000     0.000000

2/3/1  TIME     PRESSURE     TEMP-ULL     SAT-TEMP     Q-LIQUID    Q-ULL        L/L STATION  ULL-VOL      P-HE BTL     MDOT-EVAP
5723.00000      22.70426     84.93387     39.12235     20.08602    6.38704      250.45018    6260.99809   0.00000      0.00000
                PRESS-VAP    PRESS-HE     U-VAP        MDOTC       MDOTE2       MDOTE3       Q-REC-LIQ
                22.40401     .30025       123.37882    0.00000     0.00000      0.00000      238.93288
ULL-ENERGY      MASS-FUEL    MASS-HE      MASS-LIQ     TEMP-LIQ    MASS-SPRAY   HE IN BTL    TEMP-HE      TEMP-BTL     MASS VENTED
39394.39508     315.03643    8.25065      17800.00000  39.09645    0.00000      0.00000      0.00000      0.00000      0.00000
5.84089         0.00000      .00000       -0.00000     .00634      0.00000      0.00000      0.00000      0.00000      0.00000
WALL TEMPS =    0.000000     0.000000     0.000000

1/2/1  TIME     PRESSURE     TEMP-ULL     SAT-TEMP     Q-LIQUID    Q-ULL        L/L STATION  ULL-VOL      P-HE BTL     MDOT-EVAP
5727.00000      22.72184     84.98342     39.12730     20.16991    6.38007      250.41383    6259.90049   0.00000      0.00000
                PRESS-VAP    PRESS-HE     U-VAP        MDOTC       MDOTE2       MDOTE3       Q-REC-LIQ
                22.42136     .30048       123.45196    0.00000     0.00000      0.00000      241.99047
ULL-ENERGY      MASS-FUEL    MASS-HE      MASS-LIQ     TEMP-LIQ    MASS-SPRAY   HE IN BTL    TEMP-HE      TEMP-BTL     MASS VENTED
39417.74322     315.03643    8.25065      17800.00000  39.12196    0.00000      0.00000      0.00000      0.00000      0.00000
5.83317         0.00000      .00000       -0.00000     .00642      0.00000      0.00000      0.00000      0.00000      0.00000
WALL TEMPS =    0.000000     0.000000     0.000000
```

1/3/1 TIME	PRESSURE	TEMP-ULL	SAT-TEMP	Q-LIQUID	Q-ULL	L/L STATION	ULL-VOL	P-HE BTL	MDOT-EVAP
5728.00000	22.72623	84.99579	39.12854	20.19090	6.37831	250.40468	6259.62403	0.00000	0.00000
	PRESS-VAP	PRESS-HE	U-VAP	MDOTC	MDOTE2	MDOTE3	Q-REC-LIQ		
	22.42569	.30054	123.47022	0.00000	0.00000	0.00000	242.75397		
ULL-ENERGY	MASS-FUEL	MASS-HE	MASS-LIQ	TEMP-LIQ	MASS-SPRAY	HE IN BTL	TEMP-HE	TEMP-BTL	MASS VENTED
39423.57542	315.03643	8.25065	17800.00000	39.12839	0.00000	0.00000	0.00000	0.00000	0.00000
5.83122	0.00000	.00000	-0.00000	.00644	0.00000	0.00000	0.00000	0.00000	0.00000
WALL TEMPS =	0.000000	0.000000	0.000000						

1/1/2 TIME	PRESSURE	TEMP-ULL	SAT-TEMP	Q-LIQUID	Q-ULL	L/L STATION	ULL-VOL	P-HE BTL	MDOT-EVAP
5729.00000	22.73291	85.00460	39.13043	20.21181	6.37663	250.39617	6259.36719	0.00000	.09114
	PRESS-VAP	PRESS-HE	U-VAP	MDOTC	MDOTE2	MDOTE3	Q-REC-LIQ		
	22.43233	.30058	123.48274	0.00000	0.00000	0.00000	243.51712		
ULL-ENERGY	MASS-FUEL	MASS-HE	MASS-LIQ	TEMP-LIQ	MASS-SPRAY	HE IN BTL	TEMP-HE	TEMP-BTL	MASS VENTED
39433.43961	315.08400	8.25065	17799.95243	39.13461	0.00000	0.00000	0.00000	0.00000	0.00000
13.55834	.09114	.00000	-.09114	.00604	0.00000	0.00000	0.00000	0.00000	0.00000
WALL TEMPS =	0.000000	0.000000	0.000000						

1/1/2 TIME	PRESSURE	TEMP-ULL	SAT-TEMP	Q-LIQUID	Q-ULL	L/L STATION	ULL-VOL	P-HE BTL	MDOT-EVAP
5730.00000	22.74330	85.00752	39.13339	20.23258	6.37509	250.38874	6259.14289	0.00000	.15497
	PRESS-VAP	PRESS-HE	U-VAP	MDOTC	MDOTE2	MDOTE3	Q-REC-LIQ		
	22.44269	.30060	123.48580	0.00000	0.00000	0.00000	240.27991		
ULL-ENERGY	MASS-FUEL	MASS-HE	MASS-LIQ	TEMP-LIQ	MASS-SPRAY	HE IN BTL	TEMP-HE	TEMP-BTL	MASS VENTED
39449.88824	315.20922	8.25065	17799.82721	39.14050	0.00000	0.00000	0.00000	0.00000	0.00000
18.97137	.15497	.00000	-.15497	.00576	0.00000	0.00000	0.00000	0.00000	0.00000
WALL TEMPS =	0.000000	0.000000	0.000000						

1/2/2 TIME	PRESSURE	TEMP-ULL	SAT-TEMP	Q-LIQUID	Q-ULL	L/L STATION	ULL-VOL	P-HE BTL	MDOT-EVAP
5732.00000	22.77083	85.00274	39.14125	20.27390	6.37223	250.37582	6258.75257	0.00000	.22745
	PRESS-VAP	PRESS-HE	U-VAP	MDOTC	MDOTE2	MDOTE3	Q-REC-LIQ		
	22.47023	.30060	123.47482	0.00000	0.00000	0.00000	245.80442		
ULL-ENERGY	MASS-FUEL	MASS-HE	MASS-LIQ	TEMP-LIQ	MASS-SPRAY	HE IN BTL	TEMP-HE	TEMP-BTL	MASS VENTED
39494.77680	315.60105	8.25065	17799.43538	39.15169	0.00000	0.00000	0.00000	0.00000	0.00000
25.12016	.22745	.00000	-.22745	.00547	0.00000	0.00000	0.00000	0.00000	0.00000
WALL TEMPS =	0.000000	0.000000	0.000000						

2/1/2 TIME	PRESSURE	TEMP-ULL	SAT-TEMP	Q-LIQUID	Q-ULL	L/L STATION	ULL-VOL	P-HE BTL	MDOT-EVAP
5734.00000	22.80322	84.99038	39.15050	20.31506	6.36953	250.36422	6258.40241	0.00000	.26118
	PRESS-VAP	PRESS-HE	U-VAP	MDOTC	MDOTE2	MDOTE3	Q-REC-LIQ		
	22.50264	.30058	123.45166	0.00000	0.00000	0.00000	247.32750		
ULL-ENERGY	MASS-FUEL	MASS-HE	MASS-LIQ	TEMP-LIQ	MASS-SPRAY	HE IN BTL	TEMP-HE	TEMP-BTL	MASS VENTED
39548.24401	316.09398	8.25065	17798.94245	39.16249	0.00000	0.00000	0.00000	0.00000	0.00000
27.98339	.26118	.00000	-.26118	.00535	0.00000	0.00000	0.00000	0.00000	0.00000
WALL TEMPS =	0.000000	0.000000	0.000000						

APPENDIX B

LIQLEV PROGRAM

This program predicts the increase in liquid level in a tank during a depressurization phase by accounting for bubble growth and transient in the boundary layer. This analytical model is described in Section 4.3 of the report along with parametric data developed with the program. A description of the input is given here along with definition of input and output variables. A program listing in this appendix includes a sample set of input cards for one of the identifiable parametric cases. The output from this data is also presented.

INPUT INSTRUCTIONS

1. TITLE CARD (FORMAT 10A8)

2. CONSTANTS (FORMAT 8E10.4)

   CARD 1

   DELTA = Time step, sec

   DTANK = Tank diameter, ft

   HTZERØ = Liquid height initial, ft, assume cyl. tank

   VØLT = Tank volume total, cu ft

   XMLZRØ = Liquid mass, lb

   PINIT = Pressure initial, psia

   PFINAL = Pressure final after vent down, psia

   TINIT = Temperature bulk liquid, °R

   CARD 2

   THETIN = Problem time initial, sec

   GGØ = Gravity level, g's

3. CONSTANTS (FORMAT 8I10)

   MLTP = Multiple run flag; 0, case; 1, case follows

   NVMD = Number of time-vent rate entries, max. 20

   NEPS = Number of time-area ratio entries, max. 20

   NLATTM = Number of time-lateral spacing distances, max. 20

   NVERTM = Number of time-vertical spacing distances, max. 20

4. VENTING TABLE (FORMAT 8E10.4)

   TVMDØT = Problem time, sec

   XVMDØT = Vent rate, lbm/sec

5. INTERFACIAL AREA RATIO TABLE (FORMAT 8E10.4)

   TEPS = Problem time, sec

   XEPS = Ratio of bubble area to interfacial area plus bubble area

   Program will compute from wall area if NEPS = 0

6. LATERAL BUBBLE SPACING TABLE (FORMAT 8E10.4)

TSPAL = Problem time, sec

XSPACL = Bubble spacing factor, bubble diameters

7. VERTICAL BUBBLE SPACING TABLE (FORMAT 8E10.4)

TSPAV = Problem time, sec

XSPACV = Bubble spacing factor, bubble diameters

OUTPUT VARIABLES

THETA1 = Initial problem time, sec

XMVAP1 = Initial ullage vapor mass, lb

THETA2 = Problem time at each print out, sec

P2 = Tank pressure, psia

T2 = Liquid temperature, psia

XML2 = Liquid mass, lb

XMVAP2 = Ullage vapor balance mass, lb

H2 = Liquid height, ft

DHDT = Rate of change of H2, ft/sec

DELH = Change in H2 per time step, ft

HRATIØ = Fractional increase in liquid level above initial height, nd

DPDTHA = Pressure decay rate, psi/sec

DELP = Pressure change per time step, psi

EPS = Interfacial area ratio for boiling mass distribution, nd

BETA = Fraction of evaporated mass remaining in boundary layer, nd

VBL2 = Boundary layer vapor volume, cu ft

DELBLZ = Vapor boundary layer thickness at interface

AK3 = Free constant characterizing boundary layer thickness, $ft^{-1/2}$

VMDØT = Vent rate, lbm/sec

AK1 = Boundary layer constant, $ft^{1/2}$-sec^{-1}

AK2 = Thermal property constant, sec^{-1}

AK2/AK1 = Initial approximation for AK3, $ft^{-1/2}$

XMVBL2	=	Vapor mass in boundary layer, lb
XMDTBL	=	Mass leaving boundary layer at interface per time step, lb
XMVAP3	=	Ullage mass from volume calculation, lb
NCONV	=	Convergence iterations on boundary layer volume, nd

APPENDIX B

PROGRAM LISTING FOR LIQLEV

```
RUN(S)
LGO.
R
      PROGRAM LIQLEV(INPUT,OUTPUT)
      DIMENSION TVMDOT(20),XVMDOT(20),TEPS(20),XEPS(20),TSPAL(20),
     1          XSPACL(20),TSPAV (20),           XSPACV(20) ,TITLE(10),
     2          XFVBL(80),XSVFVB(80),XAK3(80),XSAVAK(80),XVBL2(80)    ,
     3  XAK4(80)
   50 READ 60,TITLE
      PRINT 60, TITLE
   60 FORMAT (1H1,10A8)
      READ 100, DELTA,DTANK,HTZERO,VOLT,XMLZRO,
     1          PINIT,PFINAL,TINIT,THETIN,GGO
  100 FORMAT(8E10.4)
      READ 200,MLTP, NVMD,NEPS,NLATTM,NVERTM
  200 FORMAT(8I10)
      READ 100, (TVMDOT(J),XVMDOT(J), J=1,NVMD)
      READ 100, (TEPS(J),XEPS(J), J= 1,NEPS)
      READ 100, (TSPAL(J),XSPACL(J), J=1,NLATTM)
      READ 100, (TSPAV(J),XSPACV(J), J=1,NVERTM)
      PRINT 300, DELTA,DTANK,HTZERO,VOLT,XMLZRO,
     1          PINIT,PFINAL,TINIT,THETIN,GGO
  300 FORMAT (* DELTA = *F10.2* DTANK = *F10.4* HTZERO = *F10.4* VOLT =*
     1F10.2*  XMLZRO = *F10.2/* PINIT = *F10.3*PFIN3L = *F10.3         *
     2TINIT = *F10.2*THETIN = *F10.2* GGO = *F10.5)
      PRINT 400, NVMD,NEPS,NLATTM,NVERTM
  400 FORMAT(*0NVMD =*I5*  NEPS =*I5*  NLATTM =*I5*  NVERTM = *I5)
      PRINT 500, (TVMDOT(J),XVMDOT(J), J=1,NVMD)
  500 FORMAT(1H0,10X,* TVMDOT*6X,* VMDOT*/(8X,F10.2,4X,F10.2)/)
      PRINT 600, (TEPS(J),XEPS(J), J=1,NEPS)
  600 FORMAT(1H0,10X *  TEPS *6X * XEPS */ (8X,F10.2,4X,F10.4)/)
      PRINT 700, (TSPAL(J), XSPACL(J), J= 1,NLATTM)
  700 FORMAT(1H0,10X * TSPAL *6X *XSPACL*/ (8X,F10.2,4X,F10.2)/)
      PRINT 800, (TSPAV(J), XSPACV(J), J= 1,NVERTM)
  800 FORMAT(1H0,10X,* TSPAV *6X *XSPACV*/ (8X,F10.2,4X,F10.2)/)
      PERIM = 3.1416 * DTANK
      AC = .7854*DTANK*DTANK
      NPRINT = 0
      DHOT = 0.0
      VBL1 = 0 .
      NCONV = 0
      P1 = PINIT
      T1 = TINIT
      H1 = HTZERO
      THETA1 = THETIN
      XML1 = XMLZRO
      ZHT1= HTZERO
      GO TO 1100
 1000 P1 = P2
      T1 = T2
      H1 = H2
      THETA1 = THETA2
      XML1   = XML2
      XMVAP1 = XMVAP2
```

```
      VBL1 = VBL2
      ZHT1 = ZHT2
      HLDAK3 = AK3
      NCONV = 0
 1100 RHOL =1.709E-01+7.454E-01*T1-4.421E-02*T1*T1+1.248E-03*(T1**3)
     1-1.738E-05*(T1**4)+9.424E-08*(T1**5)
      RHOV=-2.511E-01+4.294E-02*T1-2.860E-03*T1*T1+9.159E-05*(T1**3)
     1-1.422E-06*(T1**4)+1.001E-08*(T1**5)
      CS=0.078*(T1-34.)+2.12
      HFG=-2.0*(T1-34.)+194.5
 1200 DPDTS=2.49-.22*T1+.00407*T1*T1+.0000522*(T1**3)
      VOLLIQ = XML1/RHOL + VBL1
      VOLGAS = VOLT-VOLLIQ
      XMVAP3 = VOLGAS * RHOV
      IF (NPRINT)1220,1220,1230
 1220 XMVAP1 = XMVAP3
      PRINT 1225 , THETA1 , XMVAP1
 1225 FORMAT(/*THETA1 =*F8.2*XMVAP1 =*F8.2/)
      NPRINT = 1
 1230 DTDPS = 1.0/ DPDTS
      THETA2 = THETA1 + DELTA
      THETAV = 0.5*(THETA1 +THETA2)
      VMDOT = SLI(THETAV,NVMD,TVMDOT,XVMDOT)
 1300 DPDTHA = -VMDOT/(XML1*CS*DTDPS/HFG +XMVAP1*(1./P1-DTDPS/T1))
      DELP  = DPDTHA * DELTA
      P2 = P1 + DELP
      T2 = T1 + DTDPS* DELP
 1400 DELME = XML1*CS*(T2-T1)/HFG
      XML2 = XML1 + DELME
 1500 DELMV = VMDOT* DELTA
      IF(NEPS) 1600,1600,1700
 1600 AW = PERIM * H1
      EPS= AW/(AW+AC)
      GO TO 1800
 1700 EPS = SLI(THETAV,NEPS,TEPS,XEPS)
 1800 DELMEW = EPS * DELME
      SPACV = SLI(THETAV,NVERTM,TSPAV,XSPACV)
      SPACL = SLI(THETAV,NLATTM,TSPAL,XSPACL)
      AK1 =1.089*(10.80  *(1.+SPACL)*(1.+SPACV)*GGO*(RHOL-RHOV)/RHOL)**
     10.5
      AK2 = -EPS*CS*RHOL*DTDPS*DPDTHA/RHOV/HFG
      AK3 = AK2/AK1
C     ESTIMATE NEW ZHT
 1890 ZHT2 = ZHT1+ DHDT*DELTA
 1900 IF (AK3) 1905,1910,1910
 1905 AK3 = HLDAK3
 1910 DELBLZ = (0.375*DTANK*AK3*ZHT2)**.66667
      NN=-1
 1980 N = 0
      NN= NN - 1
 2000 SUM = 0.0
      DO 2100 L = 1,10
      XL=L
 2100 SUM = SUM + 4.**(L-1)*(DELBLZ**(XL+.5))/(DTANK**L)/(2.**XL+1.)
```

```
      FDELT = 8.0 * SUM/AK3 - ZHT2
      N = N + 1
      IF (N-20) 2200,2300,2300
2200  IF (ABS(FDELT) -.00001*ZHT2) 2400,2400,2250
2250  SUMM = 0.0
      DO 2270 K =1,10
      XK = K
2270  SUMM = SUMM + 4.**(K-1)*(DELBLZ**(XK-.5))/(DTANK**K)
      FPDELT = 4.0* SUMM/AK3
      DELBLZ = DELBLZ - FDELT/FPDELT
      GO TO 2000
2300  PRINT 2310 , DELBLZ, FDELT
2310  FORMAT(* ERROR MSG NON-CONVERGENCE DELBLZ =*F10.5* FDELT =*F10.5)
2400  DHDT = ((VBL2-VBL1) + (XML2-XML1)/RHOL)/AC/DELTA
      ZHT2 = ZHT1 + DHDT *DELTA
      IF (NN) 1980,1980,2500
2500  SUM=0.0
      DO 2600  L= 1,10
      XL=L
2600  SUM = SUM + (2.*XL+1.) * DELBLZ **(XL+1.5)/(XL +1.5)/ DTANK**(L-1)
      VBL2= SUM *3.1416/AK3
      AK2RK1 = AK2/AK1
      FVBL = VBL2-AK2*XML1*DELTA/RHOL + 2.1*AK1*DTANK*(DELBLZ**1.5)*
     1 DELTA - VBL1
2602  IF(NCONV-1 ) 2605,2609,2640
2605  NCONV = 1
      SAVAK3 = AK3
      SVFVBL = FVBL
2608  IF (FVBL) 2620,2690,2610
2609  IF (FVBL) 2640,2690,2610
2610  AK3 = 0.1*AK3
      GO TO 1890
2620  AK3 = 2.0*AK3
      NCONV = 0
      GO TO 1890
2640  IF(NCONV - 1) 2660, 2660,2645
2645  IF (FVBL) 2660,2690,2650
2650  SAVAK3 = AK3
      SVFVBL = FVBL
      AK3 = AK4
      FVBL = FVBL4
      GO TO 2670
2660  AK4 = AK3
      FVBL4 = FVBL
2670  IF (ABS(FVBL)-.001 *VBL2)2690,2690,2672
2672  AK3 = AK3-FVBL*(AK3-SAVAK3)/(FVBL-SVFVBL)
      AK3 = 0.5*(AK3 + SAVAK3)
2679  NCONV = NCONV + 1
      J = NCONV
      XFVBL(J) = FVBL4
      XSVFVB(J) = SVFVBL
      XAK4(J) = AK4
      XSAVAK(J) = SAVAK3
      XAK3(J) = AK3
```

```
      XVBL2(J) = VBL2
      IF (NCONV - 80) 1890,2680,2680
 2680 PRINT 2685,(XFVBL(J),XSVFVB(J),XAK4(J),XSAVAK(J),XAK3(J),XVBL2(J)
     1  , J=1,80)
 2685 FORMAT(*ERROR MSG NON-CONV FVBL = */(6F16.8))
      GO TO 3000
 2690 DHDT = ((VBL2-VBL1) +(XML2-XML1)/RHOL)/AC/DELTA
      ZHT2 = ZHT1 + DHDT *DELTA
      H2 = ZHT2
      DELH = H2 -H1
      HRATIO =(H2-HTZERO)/HTZERO
      BETA = VBL2* RHOV/ XMLZRO/(1.-EXP(-CS*(TINIT-T2)/HFG))
      XMVBL2 = VBL2 * RHOV
      XMDTBL = 2.1* AK1* DTANK*(DELBLZ**1.5) *DELTA*RHOV
      XMVAP2 = XMVAP1-(1.-EPS)*DELME-DELMV-XMDTBL
      VOLLIQ = XML2/RHOL + VBL2
      VOLGAS = VOLT-VOLLIQ
      XMVAP3 = VOLGAS * RHOV
 2700 PRINT 2800, THETA2,P2,T2,XML2,XMVAP2,H2,DHDT,DELH,HRATIO,DPDTHA,
     1              DELP,EPS,BETA,VBL2,DELBLZ,AK3,VMDOT,AK1,AK2,AK2RK1,
     2 XMVBL2, XMDTBL, XMVAP3, NCONV
 2800 FORMAT (/* THETA2 = *F8.2* P2      = *F8.3* T2      = *F8.3* XML2
     1= *F8.1* XMVAP2 = *F8.2* H 2     = *F8.4/* DHDT   = *F8.4* DELH   =
     2 *F8.4* HRATIO = *F8.4* DPDTHA = *F8.3* DELP   = *F8.3* EPS    = *
     3F8.4/* BETA   = *F8.4* VBL2   = *F8.2* DELBLZ = *F8.3* AK3    = *
     4F8.5* VMDOT  = *F8.3* AK1    = *F8.4/* AK2    = *F8.4* AK2/AK1 =*
     5 F8.5* XMVBL2 = *F8.3* XMDTBL = *F8.3* XMVAP3 = *F8.3* NCONV  = *
     6 I8/)
 2900 IF (P2-PFINAL) 3000,3000,1000
 3000 IF(MLTP) 4000,4000,50
 4000 STOP
      END
      FUNCTION SLI(ARG,NX,X,Y)
      DIMENSION X(100),Y(100)
      XA=ARG
      I=I-1
      N3=IABS(NX)
    5 IF(XA-X(1))170,20,10
   10 IF(I-1)20,20,40
   20 I=2
   40 IF(I-N3)80,60,60
   60 I=MAX0(2,N3/2)
   80 N2=I
      IF(X(I))100,100,90
   90 IF(X(I)-XA)140,250,100
  100 DO 120 I=2,N2
      IF(X(I)-XA)120,250,260
  120 CONTINUE
  140 DO 160 I=N2,N3
      IF(X(I)-XA)160,250,260
  160 CONTINUE
  170 IF(NX)180,180,200
  180 IF(XA-X(N3))230,240,240
  200 PRINT  210,  XA,(X(J),J=1,N3)
```

```
  210 FORMAT(15H1THE ARGUMENT (1PE14.7,46H ) WAS NOT IN THE RANGE OF THESLI00250
     1 FOLLOWING TABLE//(1P10E12.5))
      STOP
  230 I=1
      GO TO 250
  240 I=N3
  250 SLI=Y(I)
      RETURN
  260 SLI=Y(I-1)+(XA-X(I-1))*(Y(I)-Y(I-1))/(X(I)-X(I-1))
      RETURN
      END
R00
 TITLE   LIQUID LEVEL RISE  EPS FROM EVOLVE  MVDOT = 3.3
     10.0        21.667     14.416 10392.     16300.       19.5        13.8        38.3
      0.0        .00031
         1            2          11            2           2
      0.0          3.30     1000.        3.30
    0.0          0.0       20.          .0513   40.          .178      60.         .280
   80.           .362     100.          .422   120.          .470     140.         .520
  160.           .560     180.          .60    1000.          .60
      0.0          1.0     1000.         1.0
      0.0          1.0     1000.         1.0
>
```

```
TITLE   LIQUID LEVEL RISE  EPS FROM EVOLVE  MV-DT = 3.3
DELTA =      10.00 DTANK =    21.6670 HTZERO =    14.4160 VOLT =  10392.00  XMLZRO =   16300.00
PINIT =     19.500PFIN3L =     13.800 TINIT =     38.20THETIN =        0.00 BGO =     .00031

NVMD =    2  NEPS =    11  NLATTM =    2  NVERTV =     2

         TVMDOT       VMDOT
           0.00        3.30
        1000.00        3.30

           TEPS        XEPS
           0.00      0.0000
          20.00       .0513
          40.00       .1780
          60.00       .2800
          80.00       .3620
         100.00       .4220
         120.00       .4700
         140.00       .5200
         160.00       .5600
         180.00       .6000
        1000.00       .6000

          TSPAL      XSPACL
           0.00        1.00
        1000.00        1.00

          TSPAV      XSPACV

           0.00        1.00
        1000.00        1.00

THETA1 =    0.00XMVAP1 =  724.74

THETA2 =     10.00 P2      =    19.181 T2      =    38.192 VML2    =   16276.8 XMVAP2 =   714.62 H 2    =   14.4089
DHDT   =    -.0007 DELH    =    -.0071 HRATIO  =    -.0005 DPDTHA  =     -.032 DELP   =    -.319 EPS    =     .0128
BETA   =     .0127 VBL2    =      2.7- DELBLZ  =      .006 AK3     =    .00000 VMDOT  =    3.300 AK1    =     .1244
AK2    =     .0001 AK2/AK1 =    .00059 XMVBL2  =      .294 XMDTBL  =      .003 XMVAP3 =  725.031 NCONV  =        70

THETA2 =     20.00 P2      =    18.863 T2      =    38.084 VML2    =   16253.6 XMVAP2 =   703.94 H 2    =   14.4164
DHDT   =     .0008 DELH    =     .0075 HRATIO  =     .0000 DPDTHA  =     -.032 DELP   =    -.318 EPS    =     .0385
BETA   =     .0251 VBL2    =     10.79 DELBLZ  =      .024 AK3     =    .00003 VMDOT  =    3.300 AK1    =     .1245
AK2    =     .0002 AK2/AK1 =    .00179 XMVBL2  =     1.159 XMDTBL  =      .023 XMVAP3 =  714.424 NCONV  =        58

THETA2 =     30.00 P2      =    18.547 T2      =    37.975 VML2    =   16230.4 XMVAP2 =   692.32 H 2    =   14.4488
DHDT   =     .0032 DELH    =     .0325 HRATIO  =     .0023 DPDTHA  =     -.032 DELP   =    -.316 EPS    =     .0830
BETA   =     .0429 VBL2    =     28.08 DELBLZ  =      .064 AK3     =    .00014 VMDOT  =    3.300 AK1    =     .1245
AK2    =     .0005 AK2/AK1 =    .00392 XMVBL2  =     2.971 XMDTBL  =      .096 XMVAP3 =  702.886 NCONV  =        63

THETA2 =     40.00 P2      =    18.232 T2      =    37.865 VML2    =   16207.2 XMVAP2 =   679.45 H 2    =   14.5156
DHDT   =     .0067 DELH    =     .0668 HRATIO  =     .0069 DPDTHA  =     -.031 DELP   =    -.315 EPS    =     .1463
BETA   =     .0656 VBL2    =     58.02 DELBLZ  =      .131 AK3     =    .00041 VMDOT  =    3.300 AK1    =     .1245
AK2    =     .0009 AK2/AK1 =    .00705 XMVBL2  =     6.047 XMDTBL  =      .281 XMVAP3 =  690.099 NCONV  =        63
```

```
THETA2 =    50.00 P2      =   17.918 T2      =   37.754 XML2    =  16183.9 XMVAP2 =   665.62 H 2    =  14.6103
DHDT   =    .0095 DELH    =    .0947 HRATIO  =    .0135 DPDTHA  =    -.031 DELP   =    -.314 EPS    =    .2035
BETA   =    .0877 VBL2    =    98.28 DELBLZ  =     .222 AK3     =   .00091 VMDOT  =    3.300 AK1    =    .1245
AK2    =    .0012 AK2/AK1 =   .01000 XMVBL2  =   10.086 XMDTBL  =     .610 XMVAP3 =  676.360 NCONV  =       63

THETA2 =    60.00 P2      =   17.606 T2      =   37.642 XML2    =  16160.5 XMVAP2 =   651.12 H 2    =  14.7262
DHDT   =    .0116 DELH    =    .1150 HRATIO  =    .0215 DPDTHA  =    -.031 DELP   =    -.313 EPS    =    .2545
BETA   =    .1073 VBL2    =   146.34 DELBLZ  =     .331 AK3     =   .00165 VMDOT  =    3.300 AK1    =    .1246
AK2    =    .0016 AK2/AK1 =   .01277 XMVBL2  =   14.787 XMDTBL  =    1.089 XMVAP3 =  661.964 NCONV  =       16

THETA2 =    70.00 P2      =   17.294 T2      =   37.529 XML2    =  16137.1 XMVAP2 =   636.22 H 2    =  14.8571
DHDT   =    .0131 DELH    =    .1309 HRATIO  =    .0306 DPDTHA  =    -.031 DELP   =    -.312 EPS    =    .3005
BETA   =    .1239 VBL2    =   199.96 DELBLZ  =     .451 AK3     =   .00264 VMDOT  =    3.300 AK1    =    .1246
AK2    =    .0019 AK2/AK1 =   .01540 XMVBL2  =   19.888 XMDTBL  =    1.707 XMVAP3 =  647.170 NCONV  =       14

THETA2 =    80.00 P2      =   16.983 T2      =   37.415 XML2    =  16113.6 XMVAP2 =   621.14 H 2    =  14.9973
DHDT   =    .0140 DELH    =    .1402 HRATIO  =    .0403 DPDTHA  =    -.031 DELP   =    -.311 EPS    =    .3415
BETA   =    .1373 VBL2    =   257.01 DELBLZ  =     .579 AK3     =   .00386 VMDOT  =    3.300 AK1    =    .1246
AK2    =    .0022 AK2/AK1 =   .01788 XMVBL2  =   25.157 XMDTBL  =    2.443 XMVAP3 =  632.208 NCONV  =       17

THETA2 =    90.00 P2      =   16.674 T2      =   37.300 XML2    =  16090.0 XMVAP2 =   606.10 H 2    =  15.1413
DHDT   =    .0144 DELH    =    .1440 HRATIO  =    .0503 DPDTHA  =    -.031 DELP   =    -.310 EPS    =    .3770
BETA   =    .1475 VBL2    =   315.47 DELBLZ  =     .709 AK3     =   .00527 VMDOT  =    3.300 AK1    =    .1246
AK2    =    .0025 AK2/AK1 =   .02017 XMVBL2  =   30.382 XMDTBL  =    3.261 XMVAP3 =  617.287 NCONV  =       24

THETA2 =   100.00 P2      =   16.365 T2      =   37.184 XML2    =  16066.3 XMVAP2 =   591.26 H 2    =  15.2843
DHDT   =    .0143 DELH    =    .1430 HRATIO  =    .0602 DPDTHA  =    -.031 DELP   =    -.309 EPS    =    .4070
BETA   =    .1548 VBL2    =   373.59 DELBLZ  =     .839 AK3     =   .00681 VMDOT  =    3.300 AK1    =    .1247
AK2    =    .0028 AK2/AK1 =   .02227 XMVBL2  =   35.392 XMDTBL  =    4.127 XMVAP3 =  602.578 NCONV  =       18

THETA2 =   110.00 P2      =   16.057 T2      =   37.067 XML2    =  16042.6 XMVAP2 =   576.71 H 2    =  15.4238
DHDT   =    .0139 DELH    =    .1395 HRATIO  =    .0699 DPDTHA  =    -.031 DELP   =    -.308 EPS    =    .4340
BETA   =    .1597 VBL2    =   430.42 DELBLZ  =     .965 AK3     =   .00847 VMDOT  =    3.300 AK1    =    .1247
AK2    =    .0030 AK2/AK1 =   .02428 XMVBL2  =   40.100 XMDTBL  =    5.013 XMVAP3 =  588.166 NCONV  =       18

THETA2 =   120.00 P2      =   15.751 T2      =   36.948 XML2    =  16018.8 XMVAP2 =   562.52 H 2    =  15.5577
DHDT   =    .0134 DELH    =    .1340 HRATIO  =    .0792 DPDTHA  =    -.031 DELP   =    -.307 EPS    =    .4580
BETA   =    .1624 VBL2    =   485.22 DELBLZ  =    1.087 AK3     =   .01019 VMDOT  =    3.300 AK1    =    .1247
AK2    =    .0033 AK2/AK1 =   .02622 XMVBL2  =   44.447 XMDTBL  =    5.894 XMVAP3 =  574.114 NCONV  =       18

THETA2 =   130.00 P2      =   15.445 T2      =   36.828 XML2    =  15994.8 XMVAP2 =   548.66 H 2    =  15.6867
DHDT   =    .0129 DELH    =    .1291 HRATIO  =    .0881 DPDTHA  =    -.031 DELP   =    -.306 EPS    =    .4825
BETA   =    .1636 VBL2    =   538.22 DELBLZ  =    1.206 AK3     =   .01197 VMDOT  =    3.300 AK1    =    .1247
AK2    =    .0035 AK2/AK1 =   .02826 XMVBL2  =   48.462 XMDTBL  =    6.765 XMVAP3 =  560.392 NCONV  =       18
```

```
THETA2 =   140.00 P2      =   15.141 T2      =   36.707 XML2    =  15970.9 XMVAP2 =   535.10 H 2    =  15.8115
DHDT   =    .0125 DELH    =    .1248 HRATIO  =    .0968 DPDTHA  =    -.030 DELP   =    -.304 EPS    =    .5075
BETA   =    .1637 VBL2    =   589.66 DELBLZ  =    1.321 AK3     =   .01381 VMDOT  =    3.300 AK1    =    .1248
AK2    =    .0036 AK2/AK1 =   .03042 XMVBL2  =   52.176 XMDTBL  =    7.623 XMVAP3 =  546.972 NCONV  =       20

THETA2 =   150.00 P2      =   10.837 T2      =   36.585 XML2    =  15946.8 XMVAP2 =   521.87 H 2    =  15.9309
DHDT   =    .0119 DELH    =    .1194 HRATIO  =    .1251 DPDTHA  =    -.030 DELP   =    -.303 EPS    =    .5300
BETA   =    .1629 VBL2    =   639.15 DELBLZ  =    1.432 AK3     =   .01569 VMDOT  =    3.300 AK1    =    .1248
AK2    =    .0041 AK2/AK1 =   .03251 XMVBL2  =   55.563 XMDTBL  =    8.454 XMVAP3 =  533.882 NCONV  =       24

THETA2 =   160.00 P2      =   14.536 T2      =   36.461 XML2    =  15922.6 XMVAP2 =   508.98 H 2    =  16.0442
DHDT   =    .0113 DELH    =    .1133 HRATIO  =    .1129 DPDTHA  =    -.030 DELP   =    -.302 EPS    =    .5500
BETA   =    .1613 VBL2    =   686.37 DELBLZ  =    1.538 AK3     =   .01758 VMDOT  =    3.300 AK1    =    .1248
AK2    =    .0043 AK2/AK1 =   .03454 XMVBL2  =   58.606 XMDTBL  =    9.247 XMVAP3 =  521.140 NCONV  =       16

THETA2 =   170.00 P2      =   14.235 T2      =   36.337 XML2    =  15898.4 XMVAP2 =   496.39 H 2    =  16.1523
DHDT   =    .0108 DELH    =    .1081 HRATIO  =    .1204 DPDTHA  =    -.030 DELP   =    -.301 EPS    =    .5700
BETA   =    .1591 VBL2    =   731.70 DELBLZ  =    1.640 AK3     =   .01950 VMDOT  =    3.300 AK1    =    .1248
AK2    =    .0046 AK2/AK1 =   .03666 XMVBL2  =   61.347 XMDTBL  =   10.004 XMVAP3 =  508.704 NCONV  =       16

THETA2 =   180.00 P2      =   13.936 T2      =   36.211 XML2    =  15874.1 XMVAP2 =   484.08 H 2    =  16.2561
DHDT   =    .0104 DELH    =    .1038 HRATIO  =    .1276 DPDTHA  =    -.030 DELP   =    -.299 EPS    =    .5900
BETA   =    .1565 VBL2    =   775.47 DELBLZ  =    1.740 AK3     =   .02144 VMDOT  =    3.300 AK1    =    .1248
AK2    =    .0049 AK2/AK1 =   .03886 XMVBL2  =   63.824 XMDTBL  =   10.729 XMVAP3 =  496.540 NCONV  =       16

THETA2 =   190.00 P2      =   13.638 T2      =   36.083 XML2    =  15849.8 XMVAP2 =   472.20 H 2    =  16.3501
DHDT   =    .0094 DELH    =    .0940 HRATIO  =    .1342 DPDTHA  =    -.030 DELP   =    -.298 EPS    =    .6000
BETA   =    .1532 VBL2    =   815.61 DELBLZ  =    1.832 AK3     =   .02331 VMDOT  =    3.300 AK1    =    .1249
AK2    =    .0051 AK2/AK1 =   .04049 XMVBL2  =   65.879 XMDTBL  =   11.375 XMVAP3 =  484.808 NCONV  =       14
```

APPENDIX C

EVOLVE PROGRAM

This program predicts the bubble dynamics of a bubble population up to 1000 bubbles in a liquid in a specified gravity-temperature environment. The analytical model and an application to the S-IVB vehicle were presented in Section 4.4. In this appendix, the input is described, variables are defined, and a listing of the program is given. The program listing is followed by a typical set of data input cards. These cards describe a model experiment in the earth's gravity field where point heaters generate bubbles at eight locations on a heater plate using Freon 11 liquid. The first eight pages of output up to time 3.01 seconds show the type of data generated; these include time histories of bubble location and velocity in three dimensions and the bubble radius as well as overall tank conditions.

INPUT DESCRIPTION

CARD TYPE	FORMAT	CARD TYPE REPETITION	ITEM LIST
1	(20I4)	1	NPRØP,NPTIM,NRZ,NTL,NTLR,NTLZ,NRFT,NSITE,NB,IPRINTU,ISLIP,IRESTRT,IWAKE
2	(8E10.0)	(I=1,NPRØP)	PPZ(I), TPZ(I), SPZ(I), VPZ(I), RPLZ(I), UPLZ(I), RPGZ(I), UPGZ(I)
3	(7E10.0)	(I=1,NPTIM)	TIMPRØP(I), PTIM(I), QLTIM(I), WMLØTIM(I), SANTIM(I), GANTIM(I), GRATIM(I)
4	(8E10.0)	1	(TRFTIM(I), I=1,NRFT)
5[1] 5[2]	(8E10.0)	(I=1,NSITE)	XSITE(1,I), XSITE(2,I), XSITE(3,I) (RBSITX(I,J), FREQX(I,J), J=1,NRFT)
6	(6E13.6)	1	(TSITE(I), I=1,NSITE)
7	(8E10.0)	1	(TLTIME(I), I=1,NTL)
8	(8E10.0)	1	(RZTL(I), I=1,NTLR)
9	(8E10.0)	1	(ZZTL(I), I=1,NTLZ)
10[1] ↓ 10[NTLZ]	(8E10.0)	(I=1,NTL)	(TLTIMX(K,1,I), K=1,NTLR) ↓ (TLTIMX(K,NTLZ,I), K=1,NTLR)
11	(8E10.0)	1	(RADTX(I), ZRADT(I), I=1,NRZ)
12	(8E10.0)	1	(TIMPRNT(I), I=1,IPRINTU)
13	(8E10.0)	1	REYN12, REYN23, ACØF(1), EXPN(1), ACØF(2), EXPN(2), ACØF(3), EXPN(3)
14	(8E10.0)	1	DML1, TSUPRL, RBMIN, DTIMEX, TIME, HG, TIMEND, TBULKL
15	(8E10.0)	1	PARIMP, PIMPS, ZSURF, CWAKX, ARBDEN, DEGFAC, SCRAD
16	(6E13.6)	(I=1,NB)	- CARD TYPE 16 ONLY REQUIRED FOR NB > 0 - XB(1,I) XB(2,I), XB(3,I), RB(I)

The convention of the above Input Description is summarized:

List A, B, C, ... → A, B, C, ...

List (A(J), J=1,N) → A(1), A(2), A(3), ..., A(N)

which may require additional punch cards under a particular card type to complete N elements.

The bra [and ket] is a subtype card, e.g., 5[1], 5[2], 10[1] ... 10[NTLZ], which follow consecutively:

$$I = 1 \left\{ \begin{array}{l} 5[1] \\ 5[2] \end{array} \right.$$

$$I = 2 \left\{ \begin{array}{l} 5[1] \\ 5[2] \end{array} \right.$$

$$\vdots$$

$$I = \mathrm{NSITE} \left\{ \begin{array}{l} 5[1] \\ 5[2] \end{array} \right.$$

or

$$I = 1 \left\{ \begin{array}{l} 10[1] \\ \vdots \\ 10[\mathrm{NTLZ}] \end{array} \right.$$

$$I = 2 \left\{ \begin{array}{l} 10[1] \\ \vdots \\ 10[\mathrm{NTLZ}] \end{array} \right.$$

$$\vdots$$

$$I = \mathrm{NTL} \left\{ \begin{array}{l} 10[1] \\ \vdots \\ 10[\mathrm{NTLZ}] \end{array} \right.$$

Symbolically, this system is represented by nested loops:

- Loop over card type number

  (Third Operation)

  - Loop over bra-ket number

    (Second Operation)

    - Loop over list index

      (First Operation)

VARIABLE DEFINITION

NPRØP	number of entries in the fluid property table (≤ 30)
NPTIM	number of entries in the time versus system parameter table (≤ 30)
NRZ	number of entries in the axial height versus container radius table ($\equiv 2$)
NTL	number of time entries in the liquid temperature matrix (≤ 15)
NTLR	number of radial entries in the liquid temperature matrix (≤ 15)
NTLZ	number of axial height entries in the liquid temperature matrix (≤ 15)
NRFT	number of time entries in the time versus bubble site radius and frequency table (≤ 10)
NSITE	number of nucleation sites in the container (≤ 100)
NB	initial number of bubbles present (≤ 1000)
IPRINTU	number of printout times requested (≤ 1000)
ISLIP	0 for no-slip condition at container wall 1 for slip condition
IRESTRT	0 for no restart capability 1 for restart capability (generates card types 6 and 16)
IWAKE	0 no wake interactions 1 wake interactions
PPZ(I)	i^{th} saturation pressure (PSIA) entry in the fluid property table (must be monotonic)
TPZ(I)	i^{th} saturation temperature (^{o}R) entry corresponding to PPZ(I)
SPZ(I)	i^{th} liquid surface tension (LBF/FT) entry corresponding to TPZ(I)
VPZ(I)	i^{th} liquid viscosity (LBM/FT-SEC) entry corresponding to TPZ(I)
RPLZ(I)	i^{th} liquid density (LBM/FT^3) entry corresponding to TPZ(I)
UPLZ(I)	i^{th} liquid specific internal energy (BTU/LBM) corresponding to TPZ(I)

RPGZ(I)	i^{th} gas saturated density (LBM/FT^3) corresponding to TPZ(I)
UPGZ(I)	i^{th} gas specific internal energy (BTU/LBM) corresponding to TPZ(I)
TIMPRØP(I)	i^{th} time in the time (SEC) dependent parameter table
PTIM(I)	i^{th} container pressure (PSIA) corresponding to time TIMPRØP(I)
QLTIM(I)	i^{th} liquid heat rate per unit liquid height (BTU/SEC FT) corresponding to time TIMPRØP(I)
WMLØTIM(I)	i^{th} liquid outflow (+) (inflow (-)) (LBM/SEC) corresponding to time TIMPRØP(I)
SANTIM(I)	i^{th} surface angle (radians), clockwise (+) about x-axis relative to y-axis (plane of surface always parallel to x-axis), corresponding to time TIMPRØP(I)
GANTIM(I)	i^{th} gravity (or inertial field) angle (radians), clockwise (+) about x-axis relative to z-axis (gravity vector always contained in y-z plane), corresponding to time TIMPRØP(I)
GRATIM(I)	i^{th} gravity magnitude (earth's gravity ≡ 1) corresponding to time TIMPRØP(I)
TRFTIM(I)	i^{th} time (SEC) in the time dependent bubble site radius and frequency table
XSITE(1,I)	i^{th} site x-coordinate (FT)
XSITE(2,I)	i^{th} site y-coordinate (FT)
XSITE(3,I)	i^{th} site z-coordinate (FT)
RBSITX(I,J)	i^{th} site bubble radius (FT) corresponding to time TRFTIM(J)
FREQX(I,J)	i^{th} site bubble production frequency (SEC^{-1}) corresponding to time TRFTIM(J)
TSITE(I)	i^{th} site time of last bubble produced (used in restart, for initial problem set to zero); if restart option is chosen, these values are punched out in the proper format for use.
TLTIME(I)	i^{th} time (SEC) in the time dependent normalized liquid temperature matrix
RZTL(I)	i^{th} radial coordinate (FT), distance from z-axis, in the normalized liquid temperature matrix

ZZTL(I)	i^{th} axial z-coordinate (FT) in the normalized liquid temperature matrix
TLTIMX(K,J,I)	normalized liquid temperature at k^{th} radial coordinate, j^{th} axial coordinate, and i^{th} time corresponding to (RZTL(K), ZZTL(J), TLTIME(I)). This input is multiplied by the bulk liquid temperature calculated from the liquid energy equation to obtain the local temperature of the liquid.
RADTX(I)	i^{th} container radius (FT)
ZRADT(I)	i^{th} container axial height (FT) in the height versus radius table
TIMPRNT(I)	i^{th} printout time (SEC) desired
REYN 12	Reynolds number transition between regions I and II of bubble dynamics (normally ~ 80)
REYN 23	Reynolds number transition between regions II and III (normally ~ 5000)
ACØF(1)	constant coefficient in region I (normally ~ 24)
EXPN(1)	exponent coefficient in region I (normally ~-1.0)
ACØF(2)	constant coefficient in region II (normally ~ 1.975)
EXPN (2)	exponent coefficient in region II (normally ~ 0.5)
ACØF(3)	constant coefficient in region III (normally ~ 2.5)
EXPN(3)	exponent coefficient in region III (normally ~ 0.)
DML1	initial liquid mass (LBM)
TSUPRL	maximum superheat of liquid (^{o}R), difference between saturation temperature and maximum liquid temperature (+)
RBMIN	minimum bubble radius (FT) permitted, below this value the bubble is assumed to collapse, must be greater than zero
DTIMEX	time increment (SEC)
TIME	initial time (SEC)
HG	bubble heat convection coefficient (BTU/SEC FT^2)
TIMEND	problem stop time (SEC)
TBULKL	initial liquid temperature (^{o}R)
PARIMP	impact parameter (FT), the distance at which two bubbles coalesce (normally zero)
PIMPS	surface impact parameter (FT), the distance at which a bubble coalesces with surface

ZSURF	initial surface height (FT) estimate
CWAKX	wake parameter (normally zero, which stimulates program to use built in coefficient ~ 0.288)
ARBDEN	arbitrary weighting factor, which proportions the partitioning of vapor produced between the liquid-ullage interface and the total area of bubbles in the liquid medium (normally one)
DEGFAC	degeneracy factor, which accommodates consideration of a representative sector of the container (care must be taken that the bubble cross sections do not grow larger than the sector); this parameter reduces the program run time for problems which have geometric similitude and is equal to the number of sectors in the total cross section, (normally one).
SCRAD	pore radius (FT) of the container wall used to calculate the escape of bubbles from the container (normally zero)
XB(1,I)	i^{th} bubble x-coordinate (FT) of center of mass for bubbles initially present or for restart (punched out in proper format)
XB(2,I)	i^{th} bubble y-coordinate (FT)
XB(3,I)	i^{th} bubble z-coordinate (FT)
RB(I)	i^{th} bubble mass radius (FT)

PROGRAM LISTING FOR EVOLVE

```
REQUEST(EVOLVE,HI,R,ID=10188)
RUN(S,,,,,,,,1)
REWIND(LGO)
COPYBF(LGO,EVOLVE)
SET(0)
EVOLVE(LC,50000)
UNLOAD(EVOLVE)
EXIT.
UNLOAD(EVOLVE)
R
      PROGRAM EVOLVE(INPUT,OUTPUT,TAPE5=INPUT,TAPE6=OUTPUT,PUNCH)
      COMMON/PROPRT/PPZ(30),TPZ(30),SPZ(30),VPZ(30),RPLZ(30),UPLZ(30),
     X              RPGZ(30),UPGZ(30)
      COMMON/DYNAM/TIMPROP(30),PTIM(30),QLTIM(30),WMLOTIM(30),SANTIM(30)
     X           ,GANTIM(30),GRATIM(30)
      COMMON/TLIQX/TLTIMX(15,15,15),TLTIME(15),RZTL(15),ZZTL(15)
      COMMON/SITEX/RBSITX(100,10),FREQX(100,10),XSITE(3,100),TSITE(100),
     X             TRFTIM(10)
      COMMON/TANKX/RADTX(10),ZRADTX(10)
      COMMON/BUBBLE/WAKV(3,1000),VB(3,1000),XB(3,1000),RB(1000),
     X              RBA(1000),IB(1000),DMBGF(1000),DMB(1000),CDRAG(1000)
      COMMON/CONVERG/DBUBCO,DLIQCO,DLEVCO,DCONCO,DENRCO,DFORCO
      COMMON/SURFAS/ZSURF,SURFAN,ISLIP
      COMMON/LICUID/WMLO,DML1,DMLBF,TSUPRL,QL,REYN12,REYN23,ACOF(3),
     X         EXPN(3),TBULKL
      COMMON/GASPRO/HG,RBMIN,NB
      COMMON/GNRL/DTIME,DTIMEX,TIMEND,TIMPRNT(1000),IPRINTL,IPRINTU,
     X           NTAPE,IRESTRT,TIME,PIMPS,PARIMP
      COMMON/VOID/VOFRAC,DMBTOT
      COMMON/INTEGR/NTL,NTLR,NTLZ,NRFT,NSITE,NRZ,NPTIM,NPROP,IWAKE
      COMMON/ADCONST/CWAKE,BWAKE,SCRAD,ARBDEN,DEGFAC,ICRD(3)
      NTAPE=6
      CWAKE=0.288
      CALL MXCP(ICRD(1))
      KCPE=ICRD(1)*200B+22B
      ICRD(2)=MIORF(KCPE)
      N=25
      L=12
      ICRD(2)=LBYT(N,L,ICRD(2))*8
      CALL INITIAL
      CALL GOD
      IF(IRESTRT)1,1,2
    2 CALL RESTART
    1 CONTINUE
      END
      SUBROUTINE INITIAL
      COMMON/PROPRT/PPZ(30),TPZ(30),SPZ(30),VPZ(30),RPLZ(30),UPLZ(30),
     X              RPGZ(30),UPGZ(30)
      COMMON/DYNAM/TIMPROP(30),PTIM(30),QLTIM(30),WMLOTIM(30),SANTIM(30)
     X           ,GANTIM(30),GRATIM(30)
      COMMON/TLIQX/TLTIMX(15,15,15),TLTIME(15),RZTL(15),ZZTL(15)
      COMMON/SITEX/RBSITX(100,10),FREQX(100,10),XSITE(3,100),TSITE(100),
     X             TRFTIM(10)
      COMMON/TANKX/RADTX(10),ZRADTX(10)
```

```
      COMMON/BUBBLE/WAKV(3,1000),VB(3,1000),XB(3,1000),RB(1000),
     X                 RBA(1000),IB(1000),DMBGF(1000),DMB(1000),CDRAG(1000)
      COMMON/CONVERG/DBUBCO,DLIQCO,DLEVCO,DCONCO,DENRCO,DFORCO
      COMMON/SURFAS/ZSURF,SURFAN,ISLIP
      COMMON/LICUID/WMLO,DML1,DMLBF,TSUPRL,QL,REYN12,REYN23,ACOF(3),
     X          EXPN(3),TBULKL
      COMMON/GASPRO/HG,RBMIN,NB
      COMMON/GNRL/DTIME,DTIMEX,TIMEND,TIMPRNT(1000),IPRINTL,IPRINTU,
     X              NTAPE,IRESTRT,TIME,PIMPS,PARIMP
      COMMON/VOID/VOFRAC,DMBTOT
      COMMON/INTEGR/NTL,NTLR,NTLZ,NRFT,NSITE,NRZ,NPTIM,NPROP,IWAKE
      COMMON/ADCONST/CWAKE,BWAKE,SCRAD,ARBDEN,DEGFAC,ICRD(3)
      ITAPE=5
      WRITE(NTAPE,100)
  100 FORMAT(1H1,49X,19H INITIAL CONDITIONS///)
      READ(ITAPE,101)NPROP,NPTIM,NRZ,NTL,NTLR,NTLZ,NRFT    ,NSITE,NB,
     X                 IPRINTU,ISLIP,IRESTRT,IWAKE
  101 FORMAT(20I4)
      DO 20 I=1,NSITE
   20 TSITE(I)=0.
      TIME=0.
      READ(ITAPE,102)(PPZ(I),TPZ(I),SPZ(I),VPZ(I),RPLZ(I),UPLZ(I),
     X                 RPGZ(I),UPGZ(I),I=1,NPROP)
  102 FORMAT(8E10.0)
      WRITE(NTAPE,103)
  103 FORMAT(117H    PRESSURE       TEMPERATURE     SURF TENSION     VISCOSI
     XTY      LIQ DENSITY     LIQ ENERGY       GAS DENSITY      GAS ENERGY//)
      WRITE(NTAPE,104)(PPZ(I),TPZ(I),SPZ(I),VPZ(I),RPLZ(I),UPLZ(I),
     X                   RPGZ(I),UPGZ(I),I=1,NPROP)
  104 FORMAT(8(2X,E13.6))
      READ(ITAPE,105)(TIMPROP(I),PTIM(I),QLTIM(I),WMLOTIM(I),SANTIM(I),
     X                 GANTIM(I),GRATIM(I),I=1,NPTIM)
  105 FORMAT(7E10.0)
      WRITE(NTAPE,106)
  106 FORMAT(///,102H      TIME             PRESSURE         LIQ HEATING    LIQ
     XFLOW RATE      SURF ANGLE       GRAV ANGLE        GRAVITY//)
      WRITE(NTAPE,107)(TIMPROP(I),PTIM(I),QLTIM(I),WMLOTIM(I),SANTIM(I),
     X                 GANTIM(I),GRATIM(I),I=1,NPTIM)
  107 FORMAT(7(2X,E13.6))
      READ(ITAPE,102)(TRFTIM(I),I=1,NRFT)
      DO 1 N=1,NSITE
      READ(ITAPE,102) XSITE(1,N),XSITE(2,N),XSITE(3,N)
    1 READ(ITAPE,102)(RBSITX(N,I),FREQX(N,I),I=1,NRFT)
      READ(ITAPE,120)(TSITE(I),I=1,NSITE)
      DO 2 N=1,NSITE
      WRITE(NTAPE,110)N,XSITE(1,N),XSITE(2,N),XSITE(3,N),TSITE(N)
  108 FORMAT(///,42H      TIME          SITE RADIUS      SITE FREQ//)
  110 FORMAT(///,13H SITE NUMBER I4,5X,7H XSITE=E13.6,5X,7H YSITE=E13.6,
     X        5X,7H ZSITE=E13.6,5X,14H INITIAL TIME=E13.6)
      WRITE(NTAPE,108)
      DO 2 I=1,NRFT
    2 WRITE(NTAPE,111)TRFTIM(I),RBSITX(N,I),FREQX(N,I)
  111 FORMAT(3(2X,E13.6))
      READ(ITAPE,102)(TLTIME(I),I=1,NTL)
```

```
      READ(ITAPE,102)(RZTL(I),I=1,NTLR)
      READ(ITAPE,102)(ZZTL(I),I=1,NTLZ)
      DO 3 I=1,NTL
      DO 3 J=1,NTLZ
    3 READ(ITAPE,102)(TLTIMX(K,J,I),K=1,NTLR)
      DO 4 I=1,NTL
      WRITE(NTAPE,112)TLTIME(I)
  112 FORMAT(///,11H      TIME=E13.6//)
      WRITE(NTAPE,113)
  113 FORMAT(46H    RADIUS       AXIAL HEIGHT   NORM TEMPERATURE//)
      DO 4 J=1,NTLZ
      DO 4 K=1,NTLR
    4 WRITE(NTAPE,114)RZTL(K),ZZTL(J),TLTIMX(K,J,I)
  114 FORMAT(4(2X,E13.6))
      READ(ITAPE,102)(RADTX(I),ZRADTX(I),I=1,NRZ)
      READ(ITAPE,102)(TIMPRNT(I),I=1,IPRINTU)
      WRITE(NTAPE,115)
  115 FORMAT(///,29H  TANK RADIUS    AXIAL HEIGHT//)
      DO 5 I=1,NRZ
    5 WRITE(NTAPE,114)RADTX(I),ZRADTX(I)
      READ(ITAPE,102)REYN12,REYN23,ACOF(1),EXPN(1),ACOF(2),EXPN(2),
     X               ACOF(3),EXPN(3)
      WRITE(NTAPE,118)
  118 FORMAT(///,117H REYNOLDS 1-2   REYNOLDS 2-3        ACOEF 1      EXPO
     XNENT 1       ACOEF 2       EXPONENT 2        ACOEF 3       EXPONENT 3
     X//)
      WRITE(NTAPE,104)REYN12,REYN23,ACOF(1),EXPN(1),ACOF(2),EXPN(2),
     X                ACOF(3),EXPN(3)
      READ(ITAPE,102)DML1,TSUPRL,RBMIN,DTIMEX,TIME,HG,TIMEND,TBULKL
      WRITE(NTAPE,116)
  116 FORMAT(///,120H  LIQUID MASS    LIQ SUPRHEAT   MIN RADIUS       TIM
     XE STEP       TIME ZERO    BUBBLE CONV H       TIMEND         LIQUID T
     XEMP//)
      WRITE(NTAPE,104)DML1,TSUPRL,RBMIN,DTIMEX,TIME,HG,TIMEND,TBULKL
      READ(ITAPE,102)PARIMP,PIMPS,ZSURF,CWAKX,ARBDEN,DEGFAC,SCRAD
      IF(CWAKX-0.001)500,500,501
  501 CWAKE=CWAKX
  500 CONTINUE
      BWAKE=1.222*CWAKE**(-.267)
      CWAKE=0.202*CWAKE**(-.8)
      WRITE(NTAPE,119)
  119 FORMAT(///,118H BUB IMP PARAM  SURF IMP PARAM   ZSURF ZERO         C
     XWAKE           BWAKE      BOILING PARAM  SPATIAL DEGEN  SCREEN RADIU
     XS//)
      WRITE(NTAPE,104)PARIMP,PIMPS,ZSURF,CWAKE,BWAKE,ARBDEN,DEGFAC,SCRAD
      IF(NB)6,6,7
    7 DO 21 I=1,NB
   21 READ(ITAPE,120)XB(1,I),XB(2,I),XB(3,I),RB(I)
  120 FORMAT(6E13.6)
      DO 8 I=1,NB
    8 RBA(I)=RB(I)
      WRITE(NTAPE,117)
  117 FORMAT(///,56H     XB(1)            XB(2)            XB(3)            RA
     XDIUS//)
```

```
      DO 9 I=1,NB
    9 WRITE(NTAPE,114)XB(1,I),XB(2,I),XB(3,I),RB(I)
    6 CONTINUE
      RETURN
      END
      SUBROUTINE GOD
      COMMON/PROPRT/PPZ(30),TPZ(30),SPZ(30),VPZ(30),RPLZ(30),UPLZ(30),
     X             RPGZ(30),UPGZ(30)
      COMMON/DYNAM/TIMPROP(30),PTIM(30),QLTIM(30),WMLOTIM(30),SANTIM(30)
     X            ,GANTIM(30),GRATIM(30)
      COMMON/TLIQX/TLTIMX(15,15,15),TLTIME(15),RZTL(15),ZZTL(15)
      COMMON/SITEX/RBSITX(100,10),FREQX(100,10),XSITE(3,100),TSITE(100),
     X             TRFTIM(10)
      COMMON/TANKX/RADTX(10),ZRADTX(10)
      COMMON/BUBBLE/WAKV(3,1000),VB(3,1000),XB(3,1000),RB(1000),
     X             RBA(1000),IB(1000),DMBGF(1000),DMB(1000),CDRAG(1000)
      COMMON/CONVERG/DBUBCO,DLIQCO,DLEVCO,DCONCO,DENRCO,DFORCO
      COMMON/SURFAS/ZSURF,SURFAN,ISLIP
      COMMON/LICUID/WMLO,DML1,DMLBF,TSUPRL,QL,REYN12,REYN23,ACOF(3),
     X         EXPN(3),TBULKL
      COMMON/GASPRO/HG,RBMIN,NB
      COMMON/GNRL/DTIME,DTIMEX,TIMEND,TIMPRNT(1000),IPRINTL,IPRINTU,
     X            NTAPE,IRESTRT,TIME,PIMPS,PARIMP
      COMMON/VOID/VOFRAC,DMBTOT
      COMMON/INTEGR/NTL,NTLR,NTLZ,NRFT,NSITE,NRZ,NPTIM,NPROP,IWAKE
      COMMON/ADCONST/CWAKE,BWAKE,SCRAD,ARBDEN,DEGFAC,ICRD(3)
      IPRINTL=1
      CALL FANTASY(0)
    9 IF(TIME-TIMEND)1,2,2
    2 CALL FANTASY(2)
      RETURN
    1 SURFAN=LEVANG(TIME)
      CALL BIRTH
      CALL LIQLEV(0.)
      CALL LIQENRG(TIME,DTIME,WMLO,QL)
    3 CALL LIQUID
      IF(NB)5,5,6
    6 CALL BUBKIN
    5 CALL LIQLEV(DTIME)
      ZSURFT=ZSURF
      IF(NB)7,7,8
    8 CALL LOVE
      CALL LIQLEV(DTIME)
      IF(ZSURF-ZSURFT+RBMIN)81,7,7
   81 ZSURFT=ZSURF
      GO TO 8
    7 TIME=TIME+DTIME
      KCP=ICRD(1)*200B+23B
      ICP=MIORF(KCP)
      N=13
      L=24
      ICP=LBYT(N,L,ICP)
      IF(ICP.GT.(ICRD(2)-4))GO TO 2
      IF(IPRINTL-IPRINTU)10,10,9
```

```
 10 IF(TIME-TIMPRNT(IPRINTL))9,11,11
 11 IPRINTL=IPRINTL+1
    IF(TIME-TIMPRNT(IPRINTL))12,11,11
 12 CALL FANTASY(1)
    GO TO 9
    END
    SUBROUTINE FANTASY(NOUT)
    COMMON/PROPRT/PPZ(30),TPZ(30),SPZ(30),VPZ(30),RPLZ(30),UPLZ(30),
   X              RPGZ(30),UPGZ(30)
    COMMON/DYNAM/TIMPROP(30),PTIM(30),QLTIM(30),WMLOTIM(30),SANTIM(30)
   X             ,GANTIM(30),GRATIM(30)
    COMMON/TLIQX/TLTIMX(15,15,15),TLTIME(15),RZTL(15),ZZTL(15)
    COMMON/SITEX/RBSITX(100,10),FREQX(100,10),XSITE(3,100),TSITE(100),
   X             TRFTIM(10)
    COMMON/TANKX/RADTX(10),ZRADTX(10)
    COMMON/BUBBLE/WAKV(3,1000),VB(3,1000),XB(3,1000),RB(1000),
   X              RBA(1000),IB(1000),DMBGF(1000),DMB(1000),CDRAG(1000)
    COMMON/CONVERG/DBUBCO,DLIQCO,DLEVCO,DCONCO,DENRCO,DFORCO
    COMMON/SURFAS/ZSURF,SURFAN,ISLIP
    COMMON/LICUID/WMLO,DML1,DMLBF,TSUPRL,QL,REYN12,REYN23,ACOF(3),
   X         EXPN(3),TBULKL
    COMMON/GASPRO/HG,RBMIN,NB
    COMMON/GNRL/DTIME,DTIMEX,TIMEND,TIMPRNT(1000),IPRINTL,IPRINTU,
   X            NTAPE,IRESTRT,TIME,PIMPS,PARIMP
    COMMON/VOID/VOFRAC,DMBTOT
    COMMON/INTEGR/NTL,NTLR,NTLZ,NRFT,NSITE,NRZ,NPTIM,NPROP,IWAKE
    COMMON/ADCONST/CWAKE,BWAKE,SCRAD,ARBDEN,DEGFAC,ICRD(3)
    IF(NOUT-1)1,2,3
  1 WRITE(NTAPE,100)
100 FORMAT(1H1,///24X, 71H PROGRAM EVOLVE*** THE TEMPORAL AND SPATIAL
   XHISTORY OF A BUBBLE SOCIETY///)
    RETURN
  2 WRITE(NTAPE,101)
101 FORMAT(///,117H     TIME           PRESSURE       LIQUID MASS    LEVE
   XL ANGLE    LEVEL HEIGHT  VOID FRACTION    VOID MASS       GRAV ANGLE
   X  /)
    P=PZ(TIME)
    SURFIN=SURFAN*57.2958
    GRA=57.2958*GRANGL(TIME)
    WRITE(NTAPE,102)TIME,P,DML1,SURFIN,ZSURF,VOFRAC,DMBTOT,GRA
102 FORMAT(8(2X,E13.6))
    IF(NB)4,4,5
  5 WRITE(NTAPE,103)
103 FORMAT(///,119H     XB(1)           XB(2)            XB(3)            V
   XB(1)           VB(2)            VB(3)        MASS RADIUS   ACTUAL RADI
   XUS/)
    DO 6 I=1,NB
  6 WRITE(NTAPE,102)XB(1,I),XB(2,I),XB(3,I),VB(1,I),VB(2,I),VB(3,I),
   X                  RBA(I),RB(I)
  4 CONTINUE
    WRITE(NTAPE,104)
104 FORMAT( /,119H *************************************************
   X**********************************************************************
   X*///)
```

```
      RETURN
    3 WRITE(NTAPE,105)
  105 FORMAT(///,45X,27H THIS IS THE FINAL PRINTOUT//)
      GO TO 2
      END
      SUBROUTINE BIRTH
      COMMON/PROPRT/PPZ(30),TPZ(30),SPZ(30),VPZ(30),RPLZ(30),UPLZ(30),
     X                RPGZ(30),UPGZ(30)
      COMMON/DYNAM/TIMPROP(30),PTIM(30),QLTIM(30),WMLOTIM(30),SANTIM(30)
     X              ,GANTIM(30),GRATIM(30)
      COMMON/TLIQX/TLTIMX(15,15,15),TLTIME(15),RZTL(15),ZZTL(15)
      COMMON/SITEX/RBSITX(100,10),FREQX(100,10),XSITE(3,100),TSITE(100),
     X               TRFTIM(10)
      COMMON/TANKX/RADTX(10),ZRADTX(10)
      COMMON/BUBBLE/WAKV(3,1000),VB(3,1000),XB(3,1000),RB(1000),
     X                RBA(1000),IB(1000),DMBGF(1000),DMB(1000),CDRAG(1000)
      COMMON/CONVERG/DBUBCO,DLIQCO,DLEVCO,DCONCO,DENRCO,DFORCO
      COMMON/SURFAS/ZSURF,SURFAN,ISLIP
      COMMON/LICUID/WMLO,DML1,DMLBF,TSUPRL,QL,REYN12,REYN23,ACOF(3),
     X          EXPN(3),TBULKL
      COMMON/GASPRO/HG,RBMIN,NB
      COMMON/GNRL/DTIME,DTIMEX,TIMEND,TIMPRNT(1000),IPRINTL,IPRINTU,
     X             NTAPE,IRESTRT,TIME,PIMPS,PARIMP
      COMMON/VOID/VOFRAC,DMBTOT
      COMMON/INTEGR/NTL,NTLR,NTLZ,NRFT,NSITE,NRZ,NPTIM,NPROP,IWAKE
      COMMON/ADCONST/CWAKE,BWAKE,SCRAD,ARBDEN,DEGFAC,ICRD(3)
      DMLBF=0.
      NBMAX=1000
      NBN=0
      DT=DTIMEX
      IFIRST=0
   10 DO 1 I=1,NSITE
      TST=TSITE(I)
      FREQ=FREQZT(I,TST,TIME)
      XSURR=XSITE(2,I)*TAN(SURFAN)+ZSURF
      IF(XSURR-XSITE(3,I))19,19,18
   19 TSITE(I)=TIME
      GO TO 1
   18 IF(FREQ)1,1,2
    2 IF((TIME-TST)*FREQ-0.999999)3,4,4
    4 NBN=NBN+1
      IF(NB+NBN-NBMAX)14,14,15
   15 NBN=NBN-1
      WRITE(NTAPE,100)
  100 FORMAT(55H BUBBLE NUMBER LIMIT EXCEEDED,LAST ONE DROPPED,CONTINUE)
      GO TO 1
   14 XB(1,NB+NBN)=XSITE(1,I)
      XB(2,NB+NBN)=XSITE(2,I)
      XB(3,NB+NBN)=XSITE(3,I)
      RBA(NB+NBN)=RBSITZ(I,TIME)
      RB(NB+NBN)=RBSITZ(I,TIME)
      TSITE(I)=TIME
      GO TO 1
    3 IF((TIME-DT-TST)*FREQ-1.)1,5,5
```

```
 5 IF(IFIRST)6,6,7
 6 DT=1./FREQ+(TST-TIME)
   GO TO 1
 7 NBN=NBN+1
   IF(NB+NBN-NBMAX)16,16,17
17 NBN=NBN-1
   WRITE(NTAPE,100)
   GO TO 1
16 XB(1,NB+NBN)=XSITE(1,I)
   XB(2,NB+NBN)=XSITE(2,I)
   XB(3,NB+NBN)=XSITE(3,I)
   TSITE(I)=TIME+DT
   RBA(NB+NBN)=RBSITZ(I,TIME)
   RB(NB+NBN)=RBA(NB+NBN)
 1 CONTINUE
   IF(IFIRST)8,8,9
 8 IFIRST=1
   GO TO 10
 9 NB=NB+NBN
   DTIME=DT
   IF(NBN)11,11,12
12 NB1=NB-NBN+1
   DO 13 I=NB1,NB
   TL=TZ(XB(1,I),XB(2,I),XB(3,I),TIME)
   P=PZ(TIME)+2.*SIGZ(TL)/(144.*RBA(I))
   RHOG=RHGZ(P)
13 DMLBF=DMLBF+3.1416*4.*RHOG*RBA(I)**3/3.
11 RETURN
   END
   SUBROUTINE LIQENRG(TIM,DT,WMLO,QL)
   COMMON/PROPRT/PPZ(30),TPZ(30),SPZ(30),VPZ(30),RPLZ(30),UPLZ(30),
  X              RPGZ(30),UPGZ(30)
   COMMON/DYNAM/TIMPROP(30),PTIM(30),QLTIM(30),WMLOTIM(30),SANTIM(30)
  X             ,GANTIM(30),GRATIM(30)
   COMMON/TLIQX/TLTIMX(15,15,15),TLTIME(15),RZTL(15),ZZTL(15)
   COMMON/SITEX/RBSITX(100,10),FREQX(100,10),XSITE(3,100),TSITE(100),
  X              TRFTIM(10)
   COMMON/TANKX/RADTX(10),ZRADTX(10)
   COMMON/BUBBLE/WAKV(3,1000),VB(3,1000),XB(3,1000),RB(1000),
  X              RBA(1000),IB(1000),DMBGF(1000),DMB(1000),CDRAG(1000)
   COMMON/CONVERG/DBUBCO,DLIQCO,DLEVCO,DCONCO,DENRCO,DFORCO
   COMMON/SURFAS/ZSURF,SURFAN,ISLIP
   COMMON/LICUID/WMLO,DML1,DMLBF,TSUPRL,QL,REYN12,REYN23,ACOF(3),
  X          EXPN(3),TBULKL
   COMMON/GASPRO/HG,RBMIN,NB
   COMMON/GNRL/DTIME,DTIMEX,TIMEND,TIMPRNT(1000),IPRINTL,IPRINTU,
  X            NTAPE,IRESTRT,TIME,PIMPS,PARIMP
   COMMON/VOID/VOFRAC,DMBTOT
   COMMON/INTEGR/NTL,NTLR,NTLZ,NRFT,NSITE,NRZ,NPTIM,NPROP,IWAKE
   COMMON/ADCONST/CWAKE,BWAKE,SCRAD,ARBDEN,DEGFAC,ICRD(3)
   T1=TIM
   T2=TIM+DT
   CALL TABL(T1,WM1,TIMPROP(1),WMLOTIM(1),1,1,1,NPTIM,IFB)
   CALL TABL(T2,WM2,TIMPROP(1),WMLOTIM(1),1,1,1,NPTIM,IFB)
```

```
      CALL TABL(T1,QL1,TIMPROP(1),QLTIM(1),1,1,1,NPTIM,IFB)
      CALL TABL(T2,QL2,TIMPROP(1),QLTIM(1),1,1,1,NPTIM,IFB)
      QL=(QL1+QL2)*ZSURF/2.
      WMLO=(WM1+WM2)/2.
      RETURN
      END
      SUBROUTINE LIQUID
      COMMON/PROPRT/PPZ(30),TPZ(30),SPZ(30),VPZ(30),RPLZ(30),UPLZ(30),
     X              RPGZ(30),UPGZ(30)
      COMMON/DYNAM/TIMPROP(30),PTIM(30),QLTIM(30),WMLOTIM(30),SANTIM(30)
     X             ,GANTIM(30),GRATIM(30)
      COMMON/TLIQX/TLTIMX(15,15,15),TLTIME(15),RZTL(15),ZZTL(15)
      COMMON/SITEX/RBSITX(100,10),FREQX(100,10),XSITE(3,100),TSITE(100),
     X             TRFTIM(10)
      COMMON/TANKX/RADTX(10),ZRADTX(10)
      COMMON/BUBBLE/WAKV(3,1000),VB(3,1000),XB(3,1000),RB(1000),
     X              RBA(1000),IB(1000),DMBGF(1000),DMB(1000),CDRAG(1000)
      COMMON/CONVERG/DBUBCO,DLIQCO,DLEVCO,DCONCO,DENRCO,DFORCO
      COMMON/SURFAS/ZSURF,SURFAN,ISLIP
      COMMON/LICUID/WMLO,DML1,DMLBF,TSUPRL,QL,REYN12,REYN23,ACOF(3),
     X         EXPN(3),TBULKL
      COMMON/GASPRO/HG,RBMIN,NB
      COMMON/GNRL/DTIME,DTIMEX,TIMEND,TIMPRNT(1000),IPRINTL,IPRINTU,
     X            NTAPE,IRESTRT,TIME,PIMPS,PARIMP
      COMMON/VOID/VOFRAC,DMBTOT
      COMMON/INTEGR/NTL,NTLR,NTLZ,NRFT,NSITE,NRZ,NPTIM,NPROP,IWAKE
      COMMON/ADCONST/CWAKE,BWAKE,SCRAD,ARBDEN,DEGFAC,ICRD(3)
      DCON=1.
      P1=PZ(TIME)
      P2=PZ(TIME+DTIME)
      TSATL1=TSZT(P1)+TSUPRL
      TSATL2=TSZT(P2)+TSUPRL
      TB2=TBULKL
      UL1=ULSZ(TBULKL)
      ULS1=ULSZ(TSATL1)
      ULS2=ULSZ(TSATL2)
      PV1=P1/RHZL(TBULK)*0.1851
      HGST1=UGSZ(P1)+P1/RHGZ(P1)*0.1851
      DML1=DML1-DMLBF*DEGFAC
      IF(DML1)61,62,62
   62 IF(TBULK-TSATL1)63,64,64
   64 ISAT=1
      TBULK=TSATL1
      GO TO 65
   63 ISAT=0
   65 IF(P2-P1)66,66,67
   67 ISAT=0
   66 IT=0
      ITMAX=50
      ASSIGN 7 TO IS1
      ASSIGN 8 TO IS2
      TMLO=0.
      P11=P1
      DTLO=DTIME
```

```
      DTLIT=0.
      TFRAC=1.
      PIT=P2
      DMLIT=DML1
      DTGIT=DTIME
      DMFG=0.
      TLIT=TSATL2
      IF(ISAT)2,2,1
    2 DTLIT=DTIME
      DTLIT=DTLO
      PIT=P1+((P2-P1)/DTIME)*DTLIT
      TLIT=TSZT(PIT)
      RHOLIT=RHZL(TLIT)
      ULIT=ULSZ(TLIT)
   11 DMLIT=DML1-WMLO*DTLIT
      DQL=QL*DTLIT
      QTEST=(DMLIT*ULIT-DML1*UL1+((UL1+ULIT+0.1851*(PV1+PIT/RHOLIT))
     X      /2.)*(DML1-DMLIT))-DQL
      TMLO=DML1-DMLIT
      IF(ABS(QTEST)-0.001*DCON*DML1)5,5,6
    6 IF(QTEST)200,5,201
  200 GO TO IS1,(7,9,19,21)
  201 GO TO IS2,(8,9,10,21,22)
    7 ISAT=1
      ASSIGN 9 TO IS1
      ASSIGN 10 TO IS2
      QTFIX=DML1*(ULIT-UL1)
      DTFIX=0.
      QTSAVE=QTEST
      DTSAVE=DTLIT
    9 IT=IT+1
      DTLIT=(QTEST*DTFIX-QTFIX*DTLIT)/(QTEST-QTFIX)
      PIT=P1+((P2-P1)/DTIME)*DTLIT
      TLIT=TSZT(PIT)
      RHOLIT=RHZL(TLIT)
      ULIT=ULSZ(TLIT)
      IF(IT-ITMAX)11,11,12
   10 QTFIX=QTSAVE
      DTFIX=DTSAVE
      ASSIGN 7 TO IS1
      ASSIGN 9 TO IS2
      GO TO 9
   12 CONTINUE
    5 IF(DTLO-DTLIT)13,13,14
   13 IF(DTLO-DTIME)61,15,15
   15 DML1=DMLIT
      TBULKL=TLIT
      GO TO 17
    8 QTFIX=QTEST
      TLFIX=TLIT
      ASSIGN 19 TO IS1
      ASSIGN 8 TO IS2
      TLIT=TLIT-(TSATL2-TBULKL)-0.5
   18 IT=IT+1
```

```
      ULIT=ULSZ(TLIT)
      RHOLIT=RHZL(TLIT)
      IF(IT-ITMAX)11,11,12
   19 QTSAVE=QTEST
      TLSAVE=TLIT
      ASSIGN 21 TO IS1
      ASSIGN 22 TO IS2
   21 TLIT=(QTEST*TLFIX-QTFIX*TLIT)/(QTEST-QTFIX)
      GO TO 18
   22 QTFIX=QTSAVE
      TLFIX=TLSAVE
      ASSIGN 21 TO IS2
      GO TO 21
   14 UL1=ULIT
      PV1=PIT/RHOLIT*0.1851
      DTGIT=DTGIT-DTLIT
      TLIT=TSATL2
      P11=PIT
      PIT=P2
      IT=0
    1 HGIT=UGSZ(PIT)+PIT/RHGZ(PIT)*0.1851
      ULIT=ULSZ(TSATL2)
      RHOLIT=RHZL(TSATL2)
      HLA=(UL1+ULIT+0.1851*(PV1+PIT/RHOLIT))/2.
      HFGA=(HGST1+HGIT)/2.-HLA
      DMLG=WMLO*DTGIT
      DQL=QL*DTGIT
      DML2=(DQL+DMLIT*(UL1-HFGA)-DMLG*(HLA-HFGA))/(ULIT-HFGA)
      IF(DML2)61,61,23
   61 WRITE(NTAPE,100)
  100 FORMAT(1H1,///,51H PROBLEM IS TERMINATED,ALL LIQUID HAS BEEN CONSU
     XMED)
      CALL EXIT
   23 DMFG=DMLIT-DML2-TMLO-DMLG
      TBULKL=TSATL2
      DML1=DML2
   17 CONTINUE
      IF(NB)24,24,25
   25 TOTSURB=0.
      DXB=XRADT(ZSURF)-XRADT(0.)
      DYB=ZSURF
      SURFA=ABS(SURFAN)
      THETB=ATAN(DXB/DYB)
      ACO=SIN(1.5707963-THETB)/SIN(1.5707963+THETB-SURFA)
      BCO=SIN(1.5707963+THETB)/SIN(1.5707963-THETB-SURFA)
      RMAJR=XRADT(ZSURF)*(ACO+BCO)/2.
      DR=RMAJR-ACO*XRADT(ZSURF)
      ZUPR=ZSURF+DR*SIN(SURFA)
      RUPR=XRADT(ZUPR)
      DXB=DR*COS(SURFA)
      ANGLE=ACOS(DXB/RUPR)
      RMINR=RUPR*SIN(ANGLE)
      ARLU=3.1416*RMINR*RMAJR
      DO 26 I=1,NB
```

```
      IF(IB(I))27,27,28
   27 DMB(I)=4.*3.1416*RB(I)**2
      TOTSURB=TOTSURB+DMB(I)
      GO TO 26
   28 DXB=XRADT(XB(2,I)+RB(I))-XRADT(XB(2,I))
      DYB=RB(I)
      THETB=ATAN(DXB/DYB)
      DXB=XRADT(XB(2,I))
      ALPHA=ASIN(DXB/RB(I))
      THET1=ALPHA+THETB
      THET2=ALPHA-THETB
      DMB(I)=6.2832*RB(I)**2*(2.-COS(THET1)-COS(THET2))
      TOTSURB=TOTSURB+DMB(I)
   26 CONTINUE
      DMBDA=DMFG/(ARBDEN*DEGFAC*TOTSURB+ARLU)
      DO 29 I=1,NB
      DMBGF(I)=0.
   29 DMB(I)=DMB(I)*DMBDA*ARBDEN
   24 RETURN
      END
      SUBROUTINE LOVE
      COMMON/PROPRT/PPZ(30),TPZ(30),SPZ(30),VPZ(30),RPLZ(30),UPLZ(30),
     X              RPGZ(30),UPGZ(30)
      COMMON/DYNAM/TIMPROP(30),PTIM(30),QLTIM(30),WMLOTIM(30),SANTIM(30)
     X          ,GANTIM(30),GRATIM(30)
      COMMON/TLIQX/TLTIMX(15,15,15),TLTIME(15),RZTL(15),ZZTL(15)
      COMMON/SITEX/RBSITX(100,10),FREQX(100,10),XSITE(3,100),TSITE(100),
     X             TRFTIM(10)
      COMMON/TANKX/RADTX(10),ZRADTX(10)
      COMMON/BUBBLE/WAKV(3,1000),VB(3,1000),XB(3,1000),RB(1000),
     X              RBA(1000),IB(1000),DMBGF(1000),DMB(1000),CDRAG(1000)
      COMMON/CONVERG/DBUBCO,DLIQCO,DLEVCO,DCONCO,DENRCO,DFORCO
      COMMON/SURFAS/ZSURF,SURFAN,ISLIP
      COMMON/LICUID/WMLO,DML1,DMLBF,TSUPRL,QL,REYN12,REYN23,ACOF(3),
     X        EXPN(3),TBULKL
      COMMON/GASPRO/HG,RBMIN,NB
      COMMON/GNRL/DTIME,DTIMEX,TIMEND,TIMPRNT(1000),IPRINTL,IPRINTU,
     X            NTAPE,IRESTRT,TIME,PIMPS,PARIMP
      COMMON/VOID/VOFRAC,DMBTOT
      COMMON/INTEGR/NTL,NTLR,NTLZ,NRFT,NSITE,NRZ,NPTIM,NPROP,IWAKE
      COMMON/ADCONST/CWAKE,BWAKE,SCRAD,ARBDEN,DEGFAC,ICRD(3)
      DIMENSION INEW(1000),IGL(1000),JGL(1000)
      IFIRST=-1
   25 IFIRST=IFIRST+1
      ICOLSP=0
      DO 5 I=1,NB
    5 INEW(I)=0
      IGLOM=0
      DO 1 I=1,NB
      IF(RB(I)-RBMIN)6,6,7
    6 RB(I)=0.
      RBA(I)=0.
      ICOLSP=ICOLSP+1
      GO TO 1
```

```
 7 I1=I 1
   IF(I1-NB)4,4,1
 4 DO 41 J=I1,NB
   XIJ=XB(1,I)-XB(1,J)
   YIJ=XB(2,I)-XB(2,J)
   ZIJ=XB(3,I)-XB(3,J)
   RIJ=SQRT(XIJ*XIJ+YIJ*YIJ+ZIJ*ZIJ)
   DR=RIJ-(RB(I)+RB(J)+PARIMP)
   IF(DR)2,2,41
 2 IGLOM=IGLOM+1
   IGL(IGLOM)=I
   JGL(IGLOM)=J
41 CONTINUE
 1 CONTINUE
   IF(IGLOM)24,24,26
26 P=PZ(TIME)
   DO 3 IG=1,IGLOM
   II=IGL(IG)
   JJ=JGL(IG)
   IF(INEW(II))8,8,9
 8 IJ=II
   GO TO 10
 9 IJ=INEW(II)
10 XBI1=XB(1,IJ)
   XBI2=XB(2,IJ)
   XBI3=XB(3,IJ)
   XBJ1=XB(1,JJ)
   XBJ2=XB(2,JJ)
   XBJ3=XB(3,JJ)
   TLI=TZ(XBI1,XBI2,XBI3,TIME)
   TLJ=TZ(XBJ1,XBJ2,XBJ3,TIME)
   IF(RB(IJ))3,3,11
11 IF(RB(JJ))3,3,12
12 PI=P 2.*SIGZ(TLI)/(144.*RBA(IJ))
   PJ=P 2.*SIGZ(TLJ)/(144.*RBA(JJ))
   INEW(JJ)=IJ
   DMI=4.*3.1416*RHGZ(PI)*RBA(IJ)**3/3.
   DMJ=4.*3.1416*RHGZ(PJ)*RBA(JJ)**3/3.
   RB(JJ)=0.
   RBA(JJ)=0.
   TMIJ=DMI+DMJ
   XBAV1=XBI1+DMJ*(XBJ1-XBI1)/TMIJ
   XBAV2=XBI2+DMJ*(XBJ2-XBI2)/TMIJ
   XBAV3=XBI3+DMJ*(XBJ3-XBI3)/TMIJ
   TLAV=TZ(XBAV1,XBAV2,TIME)
   XB(1,IJ)=XBAV1
   XB(2,IJ)=XBAV2
   XB(3,IJ)=XBAV3
   IT=0
   RHGAV=AMIN1(RHGZ(PI),RHGZ(PJ))
13 RBAV=(3.*TMIJ/(4.*3.1416*RHGAV))**0.3333
   IT=IT+1
   PBAV=P+2.*SIGZ(TLAV)/(144.*RBAV)
   RHGAV=RHGZ(PBAV)
```

```
      IF(IT-3)13,14,14
   14 RBA(IJ)=RBAV
      IF(IB(IJ)+IB(JJ))3,3,141
  141 CALL CONFIGR(XB(1,IJ),XB(2,IJ),XB(3,IJ),XB(1,IJ),XB(2,IJ),XB(3,IJ)
     X        ,RB(IJ),IB(IJ),0,RBA(IJ))
    3 CONTINUE
      GO TO 27
   24 IF(IFIRST)23,28,23
   28 IFIRST=-1
   27 DO 15 I=1,NB
      XSURR=XB(2,I)*TAN(SURFAN)+ZSURF
      DXS=(XSURR-XB(3,I))*COS(SURFAN)
      IF(DXS-RB(I)-PIMPS)16,16,15
   16 IGLOM=IGLOM+1
      RB(I)=0.
   15 CONTINUE
      ICHANG=IGLOM+ICOLSP
      NB1=NB-1
      ICHA=0
      DO 17 I=1,NB
   20 IF(RB(I))18,18,17
   18 DO 19 J=I,NB1
      XB(1,J)=XB(1,J+1)
      XB(2,J)=XB(2,J+1)
      XB(3,J)=XB(3,J+1)
      RB(J)=RB(J+1)
      RBA(J)=RBA(J+1)
   19 IB(J)=IB(J+1)
      ICHA=ICHA+1
      IF(ICHA-ICHANG)20,21,21
   17 CONTINUE
   21 NB=NB-ICHANG
      IF(NB)23,23,221
  221 DO 22 I=1,NB
   22 CALL CONFIGR(XB(1,I),XB(2,I),XB(3,I),XB(1,I),XB(2,I),XB(3,I),
     X          RB(I),IB(I),0,RBA(I))
      IF(IFIRST)23,25,25
   23 RETURN
      END
      SUBROUTINE BUBKIN
      COMMON/PROPRT/PPZ(30),TPZ(30),SPZ(30),VPZ(30),RPLZ(30),UPLZ(30),
     X               RPGZ(30),UPGZ(30)
      COMMON/DYNAM/TIMPROP(30),PTIM(30),QLTIM(30),WMLOTIM(30),SANTIM(30)
     X             ,GANTIM(30),GRATIM(30)
      COMMON/TLIQX/TLTIMX(15,15,15),TLTIME(15),RZTL(15),ZZTL(15)
      COMMON/SITEX/RBSITX(100,10),FREQX(100,10),XSITE(3,100),TSITE(100),
     X              TRFTIM(10)
      COMMON/TANKX/RADTX(10),ZRADTX(10)
      COMMON/BUBBLE/WAKV(3,1000),VB(3,1000),XB(3,1000),RB(1000),
     X               RBA(1000),IB(1000),DMBGF(1000),DMB(1000),CDRAG(1000)
      COMMON/CONVERG/DBUBCO,DLIQCO,DLEVCO,DCONCO,DENRCO,DFORCO
      COMMON/SURFAS/ZSURF,SURFAN,ISLIP
      COMMON/LICUID/WMLO,DML1,DMLBF,TSUPRL,QL,REYN12,REYN23,ACOF(3),
     X          EXPN(3),TBULKL
```

```
      COMMON/GASPRO/HG,RBMIN,NB
      COMMON/GNRL/DTIME,DTIMEX,TIMEND,TIMPRNT(1000),IPRINTL,IPRINTU,
     X              NTAPE,IRESTRT,TIME,PIMPS,PARIMP
      COMMON/VOID/VOFRAC,DMBTOT
      COMMON/INTEGR/NTL,NTLR,NTLZ,NRFT,NSITE,NRZ,NPTIM,NPROP,IWAKE
      COMMON/ADCONST/CWAKE,BWAKE,SCRAD,ARBDEN,DEGFAC,ICRD(3)
      DIMENSION REGCO(1000)
      DCON=1.0
      DO 82 I=1,NB
      SUM=0.
      REGCO(I)=1.0
      TANKR=XRADT(XB(3,I))
      TANKA=3.1416*TANKR*TANKR
      ZUPR=XB(3,I)+RB(I)
      ZLWR=XB(3,I)-RB(I)
      DO 83 J=1,NB
      ZJ=XB(3,J)
      ZJU=JZ+RB(J)
      ZJL=ZJ-RB(J)
      IF(ZLWR-ZJ)84,85,86
   85 SUM=SUM+3.1416*RB(J)*RB(J)
      GO TO 83
   84 IF(ZUPR-ZJ)87,85,85
   87 IF(ZUPR-ZJL)83,83,88
   88 RINT=SQRT(RB(J)*RB(J)-(ZJ-ZUPR)*(ZJ-ZUPR))
      SUM=SUM+3.1416*RINT*RINT
      GO TO 83
   86 IF(ZLWR-ZJU)89,83,83
   89 RINT=SQRT(RB(J)*RB(J)-(ZLWR-ZJ)*(ZLWR-ZJ))
      SUM=SUM+3.1416*RINT*RINT
   83 CONTINUE
      REGCT=1.-SUM*DEGFAC/TANKA
   82 REGCO(I)=AMAX1(0.,REGCT)
   30 DO 1 I=1,NB
      CALL FORCES(XB(1,I),XB(2,I),XB(3,I),RB(I),RBA(I),IB(I),FMAG,THETA,
     X      PHI,TIME)
      CALL SPEED(XB(1,I),XB(2,I),XB(3,I),RB(I),RBA(I),FMAG,VMAG,IB(I),
     X     TIME,CDRAG(I))
      VMAG=VMAG*REGCO(I)
      VB(1,I)=VMAG*SIN(THETA)*COS(PHI)
      VB(3,I)=VMAG*COS(THETA)
    1 VB(2,I)=VMAG*SIN(THETA)*SIN(PHI)
      DO 32 I=1,NB
      WAKV(1,I)=0.
      WAKV(3,I)=0.
   32 WAKV(2,I)=0.
      CALL WAKES
      RHOL=RHZL(TBULKL)
      DO 31 I=1,NB
      RT=XRADT(XB(3,I))
   31 WAKV(3,I)=-WMLO/(RHOL*3.1416*RT*RT)+WAKV(3,I)
      ITMAX=50
      DO 2 I=1,NB
      P2=PZ(TIME+DTIME)
```

```
      P1=PZ(TIME)
      IOBS=IB(I)
      DO 3 J=1,3
      IT=0
      ASSIGN 17 TO IS2
      ASSIGN 18 TO IS3
      GO TO (4,5,51),J
    4 VBAV1=VB(1,I)
      VBAV2=0.
      VBAV3=0.
      GO TO 6
    5 VBAV2=VB(2,I)
      GO TO 6
   51 VBAV3=VB(3,I)
    6 XB1T=(WAKV(1,I)+VBAV1)*DTIME+XB(1,I)
      XB2T=(WAKV(2,I)+VBAV2)*DTIME+XB(2,I)
      XB3T=(WAKV(3,I)+VBAV3)*DTIME+XB(3,I)
   19 CALL ENERGY(XB(1,I),XB(2,I),XB(3,I),XB1T,XB2T,XB3T,RBA(I),DMB(I),
     X  DTIME,RBA2,P1, P2,TIME,DMBGF(I))
      IF(IOBS-1)191,192,192
  192 CALL CONFIGR(XB1T,XB2T,XB3T,XB1T,XB2T,XB3T,RB2,IOBS,0,RBA2)
      GO TO 193
  191 RB2=RBA2
  193 CALL FORCES(XB1T,XB2T,XB3T,RB2,RBA2,IOBS,FMAG,THETA,PHI,TIME+
     X       DTIME)
      CALL SPEED(XB1T,XB2T,XB3T,RB2,RBA2,FMAG,VMAG,TIME+DTIME,DUM)
      VMAG=VMAG*REGCO(I)
      GO TO (7,8,81),J
    7 VBAV1=(VMAG*SIN(THETA)*COS(PHI)+VB(1,I))/2.
      GO TO 9
    8 VBAV2=(VMAG*SIN(THETA)*SIN(PHI)+VB(2,I))/2.
      GO TO 9
   81 VBAV3=(VMAG*COS(THETA)+VB(3,I))/2.
    9 XB12=(WAKV(1,I)+VBAV1)*DTIME+XB(1,I)
      XB22=(WAKV(2,I)+VBAV2)*DTIME+XB(2,I)
      XB32=(WAKV(3,I)+VBAV3)*DTIME+XB(3,I)
      DXB1=XB1T-XB12
      DXB2=XB2T-XB22
      DXB3=XB3T-XB32
      GO TO (10,11,111),J
   10 DXB=DXB1
      XBT=XB1T
      GO TO 12
   11 DXB=DXB2
      XBT=XB2T
      GO TO 12
  111 DXB=DXB3
      XBT=XB3T
   12 IF(ABS(DXB)-0.001*DCON*(VMAG+0.001)*DTIME)3,3,14
   14 IF(DXB)15,3,16
   15 GO TO IS2,(17,23,27,28)
   16 GO TO IS3,(18,23,26,29)
   17 ASSIGN 23 TO IS2
      ASSIGN 26 TO IS3
```

```
      DFIX=DXB
      XFIX=XBT
      XB1T=XB12
      XB2T=XB22
      XB3T=XB32
      GO TO 19
   18 ASSIGN 27 TO IS2
      ASSIGN 23 TO IS3
      DFIX=DXB
      XFIX=XBT
      XB1T=XB12
      XB2T=XB22
      XB3T=XB32
      GO TO 19
   23 IT=IT+1
      XBT=(DXB*XFIX-DFIX*XBT)/(DXB-DFIX)
      GO TO (20,21,211),J
   20 XB1T=XBT
      GO TO 22
   21 XB2T=XBT
      GO TO 22
  211 XB3T=XBT
   22 IF(IT-ITMAX)19,19,3
   26 DSAVE=DXB
      XSAVE=XBT
      ASSIGN 23 TO IS3
      ASSIGN 28 TO IS2
      GO TO 23
   27 DSAVE=DXB
      XSAVE=XBT
      ASSIGN 23 TO IS2
      ASSIGN 29 TO IS3
      GO TO 23
   28 DFIX=DSAVE
      XFIX=XSAVE
      ASSIGN 23 TO IS2
      ASSIGN 26 TO IS3
      GO TO 23
   29 DFIX=DSAVE
      XFIX=XSAVE
      ASSIGN 27 TO IS2
      ASSIGN 23 TO IS3
      GO TO 23
    3 CONTINUE
      CALL CONFIGR(XB(1,I),XB(2,I),XB(3,I),XB1T,XB2T,XB3T,RB2,IOBS,1,
     X          RBA2)
      IB(I)=IOBS
      RB(I)=RB2
      RBA(I)=RBA2
      XB(1,I)=XB1T
      XB(2,I)=XB2T
      XB(3,I)=XB3T
      VB(1,I)=VBAV1+WAKV(1,I)
      VB(2,I)=VBAV2+WAKV(2,I)
```

```
      VB(3,I)=VBAV3*WAKV(3,I)
      CALL WALL(XB1T,XB2T,XB3T,RB2,VB(1,I),VB(2,I),VB(3,I),VC1,VC2,VC3,
     X   ISLIP)
      VB(1,I)=VB(1,I)+VC1
      VB(2,I)=VB(2,I)+VC2
      VB(3,I)=VB(3,I)+VC3
    2 CONTINUE
      RETURN
      END
      SUBROUTINE WAKES
      COMMON/PROPRT/PPZ(30),TPZ(30),SPZ(30),VPZ(30),RPLZ(30),UPLZ(30),
     X               RPGZ(30),UPGZ(30)
      COMMON/DYNAM/TIMPROP(30),PTIM(30),QLTIM(30),WMLOTIM(30),SANTIM(30)
     X            ,GANTIM(30),GRATIM(30)
      COMMON/TLIQX/TLTIMX(15,15,15),TLTIME(15),RZTL(15),ZZTL(15)
      COMMON/SITEX/RBSITX(100,10),FREQX(100,10),XSITE(3,100),TSITE(100),
     X             TRFTIM(10)
      COMMON/TANKX/RADTX(10),ZRADTX(10)
      COMMON/BUBBLE/WAKV(3,1000),VB(3,1000),XB(3,1000),RB(1000),
     X               RBA(1000),IB(1000),DMBGF(1000),DMB(1000),CDRAG(1000)
      COMMON/CONVERG/DBUBCO,DLIQCO,DLEVCO,DCONCO,DENRCO,DFORCO
      COMMON/SURFAS/ZSURF,SURFAN,ISLIP
      COMMON/LICUID/WMLO,DML1,DMLBF,TSUPRL,QL,REYN12,REYN23,ACOF(3),
     X         EXPN(3),TBULKL
      COMMON/GASPRO/HG,RBMIN,NB
      COMMON/GNRL/DTIME,DTIMEX,TIMEND,TIMPRNT(1000),IPRINTL,IPRINTU,
     X            NTAPE,IRESTRT,TIME,PIMPS,PARIMP
      COMMON/VOID/VOFRAC,DMBTOT
      COMMON/INTEGR/NTL,NTLR,NTLZ,NRFT,NSITE,NRZ,NPTIM,NPROP,IWAKE
      COMMON/ADCONST/CWAKE,BWAKE,SCRAD,ARBDEN,DEGFAC,ICRD(3)
      YWAKE=CWAKE*BWAKE/3.
      IF(IWAKE)8,8,9
    9 DO 6 I=1,NB
      DO 7 J=1,NB
      CALL WALL(XB(1,I),XB(2,I),XB(3,I),RB(I),VB(1,I),VB(2,I),VB(3,I),
     X         VCOR1,VCOR2,VCOR3,ISLIP)
      AIJ=0.
      VY1=0.
      VY2=0.
      VY3=0.
      RI=RB(I)
      RJ=RB(J)
      XI1=XB(1,I)
      XI2=XB(2,I)
      XI3=XB(3,I)
      XJ1=XB(1,J)
      XJ2=XB(2,J)
      XJ3=XB(3,J)
      RJI1=XI1-XJ1
      RJI2=XI2-XJ2
      RJI3=XI3-XJ3
      RMAG=SQRT(RJI1*RJI1+RJI2*RJI2+RJI3*RJI3)
      V1=VB(1,I)+VCOR1
      V2=VB(2,I)+VCOR2
```

```
      V3=VB(3,I)+VCOR3
      VMAG=SQRT(V1*V1+V2*V2+V3*V3)
      RV=RMAG*VMAG
      IF(RV)1,1,3
    1 WAKV(1,J)=WAKV(1,J)+AIJ*V1+VY1
      WAKV(2,J)=WAKV(2,J)+AIJ*V2+VY2
      WAKV(3,J)=WAKV(3,J)+AIJ*V3+VY3
      GO TO 2
    3 COSA=(RJI1*V1+RJI2*V2+RJI3*V3)/(RV)
      IF(COSA)1,1,4
    4 XR=RMAG*COSA
      COSA=AMIN1(COSA,1.)
      IF(XR-RI)1,5,5
    5 ALPHA=ACOS(COSA)
      YR=RMAG*SIN(ALPHA)
      YR=ABS(YR)
      B=BWAKE*(CDRAG(I)*3.1416*RI*RI*XR)**0.333333
      AIJ=CWAKE*(CDRAG(I)*3.1416*RI*RI/(XR*XR))**0.333333
      AIJ=AMIN1(AIJ,1.0)
      YIJ=YWAKE*(AIJ/CWAKE)**2.
      AIJ=AIJ*AVWAK(RJ,YR,B,1)
      YIJ=YIJ*AVWAK(RJ,YR,B,2)
      VY1=YIJ*VMAG*(RJI1-V1*XR/VMAG)/RMAG
      VY2=YIJ*VMAG*(RJI2-V2*XR/VMAG)/RMAG
      VY3=YIJ*VMAG*(RJI3-V3*XR/VMAG)/RMAG
      GO TO 1
    2 CONTINUE
    7 CONTINUE
    6 CONTINUE
    8 RETURN
      END
      FUNCTION AVWAK(R,Y,B,IC)
      A(X1,X2)=X1-0.8*X1*X2**1.5+0.25*X1*X2**3
      D(X3,X4)=0.5*X3*X4-0.571*X3*X4**2.5+0.2*X3*X4**4.
      IF(B-(Y+R))1,1,2
    1 YU=B
      GO TO 3
    2 YU=Y R
      YL=Y-R
    3 IF(B-(Y-R))4,4,5
    4 AVWAK=0.
      GO TO 6
    5 IF(B (Y-R))7,7,8
    7 YL=-B
      GO TO 9
    8 YL=Y-R
    9 RATU=ABS(YU/B)
      RATL=ABS(YL/B)
      IF(IC-1)12,12,11
   11 AVWAK=D(YU,RATU)-D(YL,RATL)
      GO TO 13
   12 AVWAK=A(YU,RATU)-A(YL,RATL)
   13 IF(R)4,4,10
   10 AVWAK=AVWAK/(2.*R)
```

```
  6 RETURN
    END
    SUBROUTINE WALL(X1,X2,X3,R,V1,V2,V3,VC1,VC2,VC3,IS)
    VC1=0.
    VC2=0.
    VC3=0.
    D=1.00001*R
    IF(R)1,1,2
  2 DXB=XRADT(X3+R)-XRADT(X3)
    THETB=ATAN(DXB/R)
    PHI=ATIN(X2,X1)
    XR=SQRT(X1*X1+X2*X2+X3*X3)
    THETA=ACOS(X3/XR)
    IF(X3-R)3,3,4
  3 IF(V3)31,1,1
 31 VC1=0.
    VC2=0.
    VC3=-V3
    GO TO 5
  1 VC1=0.
    VC2=0.
    VC3=0.
    GO TO 5
  4 IF(XRADT(X3)-D/COS(THETB))10,6,6
  6 DXB=(XRADT(X3)-XR*SIN(THETA))*COS(THETB)
    IF(DXB-D)7,7,1
  7 IF(IS)8,8,9
  8 VC1=-V1
    VC2=-V2
    VC3=-V3
    GO TO 5
  9 DN1=COS(PHI)*COS(THETB)
    DN2=SIN(PHI)*COS(THETB)
    DN3=-SIN(THETB)
    VDOTN=-(V1*DN1+V2*DN2+V3*DN3)
    VC1=VDOTN*DN1
    VC2=VDOTN*DN2
    VC3=VDOTN*DN3
    GO TO 5
 10 VC1=-V1
    VC2=-V2
    VC3=0.
  5 CONTINUE
    RETURN
    END
    SUBROUTINE FORCES(X1,X2,X3,R,RA,IOBS,FMAG,THETA,PHI,TIM)
    COMMON/PROPRT/PPZ(30),TPZ(30),SPZ(30),VPZ(30),RPLZ(30),UPLZ(30),
   X              RPGZ(30),UPGZ(30)
    COMMON/DYNAM/TIMPROP(30),PTIM(30),QLTIM(30),WMLOTIM(30),SANTIM(30)
   X             ,GANTIM(30),GRATIM(30)
    COMMON/TLIQX/TLTIMX(15,15,15),TLTIME(15),RZTL(15),ZZTL(15)
    COMMON/SITEX/RBSITX(100,10),FREQX(100,10),XSITE(3,100),TSITE(100),
   X             TRFTIM(10)
    COMMON/TANKX/RADTX(10),ZRADTX(10)
```

```
      COMMON/BUBBLE/WAKV(3,1000),VB(3,1000),XB(3,1000),RB(1000),
     X                RBA(1000),IB(1000),DMBGF(1000),DMB(1000),CDRAG(1000)
      COMMON/CONVERG/DBUBCO,DLIQCO,DLEVCO,DCONCO,DENRCO,DFORCO
      COMMON/SURFAS/ZSURF,SURFAN,ISLIP
      COMMON/LICUID/WMLO,DML1,DMLBF,TSUPRL,QL,REYN12,REYN23,ACOF(3),
     X          EXPN(3),TBULKL
      COMMON/GASPRO/HG,RBMIN,NB
      COMMON/GNRL/DTIME,DTIMEX,TIMEND,TIMPRNT(1000),IPRINTL,IPRINTU,
     X              NTAPE,IRESTRT,TIME,PIMPS,PARIMP
      COMMON/VOID/VOFRAC,DMBTOT
      COMMON/INTEGR/NTL,NTLR,NTLZ,NRFT,NSITE,NRZ,NPTIM,NPROP,IWAKE
      COMMON/ADCONST/CWAKE,BWAKE,SCRAD,ARBDEN,DEGFAC,ICRD(3)
      IF(RA)3,3,4
    3 FMAG=0.
      THETA=0.
      PHI=0.
      RETURN
    4 IF(IOBS)1,1,2
    1 G=GRAVITY(TIM)
      XU=X1+RA
      XL=X1-RA
      YU=X2+RA
      YL=X2-RA
      ZU=X3+RA
      ZL=X3-RA
      GRADTX=(TZ(XU,X2,X3,TIM)-TZ(XL,X2,X3,TIM))/(XU-XL)
      GRADTY=(TZ(X1,YU,X3,TIM)-TZ(X1,YL,X3,TIM))/(YU-YL)
      GRADTZ=(TZ(X1,X2,ZU,TIM)-TZ(X1,X2,ZL,TIM))/(ZU-ZL)
      ANGLE=GRANGL(TIM)
      P=PZ(TIM)
      TL=TZ(X1,X2,X3,TIM)
      PTOT=P+2.*SIGZ(TL)/(144.*RA)
      DELRO=RHZL(TL)-RHGZ(PTOT)
      SIGPRM=(SIGZ(TL+1.)-SIGZ(TL-1.))/2.
      FBOY=4.*3.1416*32.17*G*DELRO*RA**3/3.
      FST=-8.*3.1416*SIGPRM*RA*RA*32.17
      FX1=FST*GRADTX
      FX2=FST*GRADTY-FBOY*SIN(ANGLE)
      FX3=FST*GRADTZ+FBOY*COS(ANGLE)
      GO TO 5
    2 GO TO 3
    5 FMAG=SQRT(FX1*FX1+FX2*FX2+FX3*FX3)
      THETA=ACIS(FX3,FMAG)
      PHI=ATIN(FX2,FX1)
      RETURN
      END
      FUNCTION ACIS(X,R)
      IF(R)1,2,3
    2 ACIS=0.
      RETURN
    1 X1=-X
      R1=-R
      GO TO 4
    3 X1=X
```

```
      R1=R
    4 IF(X1)5,6,6
    5 THETA=ACOS(X1/R1)
      ACIS=3.1415927-THETA
      RETURN
    6 ACIS=ACOS(X1/R1)
      RETURN
      END
      FUNCTION ATIN(Y,X)
      IF(X)1,2,3
    2 IF(Y)4,5,6
    4 ATIN=4.712389
      RETURN
    5 ATIN=0.
      RETURN
    6 ATIN=1.5707963
      RETURN
    3 IF(Y)7,8,8
    7 THETA=ATAN(Y/X)
      ATIN=6.2831853+THETA
      RETURN
    8 ATIN=ATAN(Y/X)
      RETURN
    1 ATIN=3.1415927+ATAN(Y/X)
      RETURN
      END
      SUBROUTINE SPEED(X,Y,Z,RBUB,RBUBA,FMAG,VMAG,IOBS,TIM,CDR)
      COMMON/PROPRT/PPZ(30),TPZ(30),SPZ(30),VPZ(30),RPLZ(30),UPLZ(30),
     X              RPGZ(30),UPGZ(30)
      COMMON/DYNAM/TIMPROP(30),PTIM(30),QLTIM(30),WMLOTIM(30),SANTIM(30)
     X             ,GANTIM(30),GRATIM(30)
      COMMON/TLIQX/TLTIMX(15,15,15),TLTIME(15),RZTL(15),ZZTL(15)
      COMMON/SITEX/RBSITX(100,10),FREQX(100,10),XSITE(3,100),TSITE(100),
     X             TRFTIM(10)
      COMMON/TANKX/RADTX(10),ZRADTX(10)
      COMMON/BUBBLE/WAKV(3,1000),VB(3,1000),XB(3,1000),RB(1000),
     X              RBA(1000),IB(1000),DMBGF(1000),DMB(1000),CDRAG(1000)
      COMMON/CONVERG/DBUBCO,DLIQCO,DLEVCO,DCONCO,DENRCO,DFORCO
      COMMON/SURFAS/ZSURF,SURFAN,ISLIP
      COMMON/LICUID/WMLO,DML1,DMLBF,TSUPRL,QL,REYN12,REYN23,ACOF(3),
     X         EXPN(3),TBULKL
      COMMON/GASPRO/HG,RBMIN,NB
      COMMON/GNRL/DTIME,DTIMEX,TIMEND,TIMPRNT(1000),IPRINTL,IPRINTU,
     X           NTAPE,IRESTRT,TIME,PIMPS,PARIMP
      COMMON/VOID/VOFRAC,DMBTOT
      COMMON/INTEGR/NTL,NTLR,NTLZ,NRFT,NSITE,NRZ,NPTIM,NPROP,IWAKE
      COMMON/ADCONST/CWAKE,BWAKE,SCRAD,ARBDEN,DEGFAC,ICRD(3)
      CDR=1.0
      IF(FMAG)1,1,2
    1 VMAG=0
      RETURN
    2 TL=TZ(X,Y,Z,TIM)
      RHL=RHZL(TL)
      SIGL=SIGZ(TL)*32.17
```

```
      DMUL=VISCZ(TL)
      PI=3.1415927
      RE1=2.*RBUBA*RHL*((DMUL/(2.*RBUBA*RHL))**EXPN(1)*(2.*FMAG/
     X                 (ACOF(1)*PI*RHL*RBUBA*RBUBA)))**(1./(2.*EXPN(1)))
     X                 /DMUL
      RE2=2.*RBUBA*RHL*((DMUL/(2.*RBUBA*RHL))**EXPN(2)*(2.*FMAG/
     X                 (ACOF(2)*PI*RHL*RBUBA*RBUBA)))**(1./(2.*EXPN(2)))
     X                 /DMUL
      IF(RE1-REYN12)3,3,4
    3 VMAG=RE1*DMUL/(2.*RBUBA*RHL)
      GO TO 7
    4 DNETVOS=3.*FMAG/(PI*RBUBA*SIGL)
      DCDR=ACOF(3)*(1.-EXP(-EXPN(3)*DNETVOS))-ACOF(2)*RE2**EXPN(2)
      IF(DCDR)5,5,6
    5 VMAG=RE2*DMUL/(2.*RBUBA*RHL)
      GO TO 7
    6 CDR=ACOF(3)*(1.-EXP(-EXPN(3)*DNETVOS))
      VMAG=(8.*FMAG*RHL/(PI*CDR))**0.5/(2.*RBUBA*RHL)
      RETURN
    7 CDR=2.*FMAG/(PI*RHL*RBUBA*RBUBA*VMAG*VMAG)
      RETURN
      END
      SUBROUTINE ENERGY(X11,X12,X13,X21,X22,X23,R1,DMG,DT,R2,P1,P2,TIME,
     X       DMGAP)
      COMMON/PROPRT/PPZ(30),TPZ(30),SPZ(30),VPZ(30),RPLZ(30),UPLZ(30),
     X               RPGZ(30),UPGZ(30)
      COMMON/DYNAM/TIMPROP(30),PTIM(30),QLTIM(30),WMLOTIM(30),SANTIM(30)
     X             ,GANTIM(30),GRATIM(30)
      COMMON/TLIQX/TLTIMX(15,15,15),TLTIME(15),RZTL(15),ZZTL(15)
      COMMON/SITEX/RBSITX(100,10),FREQX(100,10),XSITE(3,100),TSITE(100),
     X              TRFTIM(10)
      COMMON/TANKX/RADTX(10),ZRADTX(10)
      COMMON/BUBBLE/WAKV(3,1000),VB(3,1000),XB(3,1000),RB(1000),
     X               RBA(1000),IB(1000),DMBGF(1000),DMB(1000),CDRAG(1000)
      COMMON/CONVERG/DBUBCO,DLIQCO,DLEVCO,DCONCO,DENRCO,DFORCO
      COMMON/SURFAS/ZSURF,SURFAN,ISLIP
      COMMON/LICUID/WMLO,DML1,DMLBF,TSUPRL,QL,REYN12,REYN23,ACOF(3),
     X         EXPN(3),TBULKL
      COMMON/GASPRO/HG,RBMIN,NB
      COMMON/GNRL/DTIME,DTIMEX,TIMEND,TIMPRNT(1000),IPRINTL,IPRINTU,
     X            NTAPE,IRESTRT,TIME,PIMPS,PARIMP
      COMMON/VOID/VOFRAC,DMBTOT
      COMMON/INTEGR/NTL,NTLR,NTLZ,NRFT,NSITE,NRZ,NPTIM,NPROP,IWAKE
      COMMON/ADCONST/CWAKE,BWAKE,SCRAD,ARBDEN,DEGFAC,ICRD(3)
      ECON=1.
      IT=0
      DMGAP=0.
      TL1=TZ(X11,X12,X13,TIME)
      ITMAX=50
      TL2=TZ(X21,X22,X23,TIME+DT)
      PG1=P1+2.*SIGZ(TL1)/(144.*R1)
      RHG1=RHGZ(PG1)
      UG1=UGSZ(PG1)
      TS1=TSZT(P1)
```

```
      TG1=TSZT(PG1)
      TS2=TSZT(P2)
      UL1=ULSZ(TL1)
      UL2=ULSZ(TL2)
      HG1=UG1+PG1/RHG1*0.1851
      HL1=UL1+P1/RHZL(TL1)*0.1851
      HL2=UL2+P2/RHZL(TL2)*0.1851
      HGFA=(HL1+HL2)/2.
      R2=R1
      IF(DMG)5,6,6
    5 CDMG=1.
      GO TO 7
    6 CDMG=0.
    7 DM1=4.*3.1416*RHG1*R1**3/3.
      ASSIGN 15 TO IS2
      ASSIGN 16 TO IS3
    1 IF(R2)32,32,33
   32 RI=-R2
      SIGN=-1.
      PG2=P2+2.*SIGZ(TL2)/(144.*RBMIN)
      GO TO 34
   33 RI=R2
      SIGN=1.
      PG2=P2+2.*SIGZ(TL2)/(144.*R2)
   34 TG2=TSZT(PG2)
      DQ=6.2832*HG*(R1*R1*(TS1-TL1)+R2*R2*(TS2-TL2)*SIGN)*DT
      RHG2=RHGZ(PG2)
      UG2=UGSZ(PG2)
      HG2=UG2+PG2/RHG2*0.1851
      RHGI=SIGN*RHG2
      HFGA=(HG1+HG2)/2.
      HGFX=HFGA-HGFA
      DMQGF=DQ/HGFX
      DM2=4.*3.1416*RHGI*RI**3/3.
      PVW=DM1*PG1*0.1851/RHG1-DM2*PG2*0.1851/RHG2
      IF(DMQGF)2,3,3
    2 CQ=0.
      GO TO 4
    3 CQ=1.
    4 DMGAP=4.*3.1416*(RHG1*R1**3-RHGI*RI**3)/3.+DMG-DMQGF
      IF(DMGAP)8,9,9
    8 CP=0.
      GO TO 10
    9 CP=1.
   10 DENERG=4.*3.1416*(RHGI*UG2*RI**3-RHG1*UG1*R1**3)/3.+DMGAP*((1.-CP)
     X        *HFGA+CP*HGFX)+DMQGF*((1.-CQ)*HFGA+CQ*HGFX)-DMG*((1.-CDMG)*
     X        HFGA+CDMG*HGFX)-PVW
      IF(ABS(DENERG)-ECON*0.001*DM1*UG1)12,12,11
   11 IF(DENERG)13,12,14
   13 GO TO IS2,(15,23,27,28)
   14 GO TO IS3,(16,23,26,29)
   15 R2=(3.*(DM1+DMG)/(4.*3.1416*RHG1))**0.3333
      ASSIGN 23 TO IS2
      ASSIGN 26 TO IS3
```

```
      DFIX=DENERG
      RFIX=R1
      GO TO 17
   16 R2=(3.*(DM1+DMG)/(4.*3.1416*RHG1))**0.3333
      ASSIGN 27 TO IS2
      ASSIGN 23 TO IS3
      DFIX=DENERG
      RFIX=R1
   17 IF(ABS((R1-R2)/R1)-0.0001)18,1,1
   18 R2=R1*1.05
      GO TO 1
   23 IT=IT+1
      R2=(DENERG*RFIX-DFIX*R2)/(DENERG-DFIX)
      IF(IT-ITMAX)1,1,12
   26 DSAVE=DENERG
      RSAVE=R2
      ASSIGN 23 TO IS3
      ASSIGN 28 TO IS2
      GO TO 23
   27 DSAVE=DENERG
      RSAVE=R2
      ASSIGN 23 TO IS2
      ASSIGN 29 TO IS3
      GO TO 23
   28 DFIX=DSAVE
      RFIX=RSAVE
      ASSIGN 23 TO IS2
      ASSIGN 26 TO IS3
      GO TO 23
   29 DFIX=DSAVE
      RFIX=RSAVE
      ASSIGN 27 TO IS2
      ASSIGN 23 TO IS3
      GO TO 23
   12 IF(R2-RBMIN)30,31,31
   30 R2=RBMIN
   31 RETURN
      END
      SUBROUTINE CONFIGR(X11,X12,X13,X21,X22,X23,R2,IOBS,IREDC,R1)
      COMMON/PROPRT/PPZ(30),TPZ(30),SPZ(30),VPZ(30),RPLZ(30),UPLZ(30),
     X              RPGZ(30),UPGZ(30)
      COMMON/DYNAM/TIMPROP(30),PTIM(30),QLTIM(30),WMLOTIM(30),SANTIM(30)
     X            ,GANTIM(30),GRATIM(30)
      COMMON/TLIQX/TLTIMX(15,15,15),TLTIME(15),RZTL(15),ZZTL(15)
      COMMON/SITEX/RBSITX(100,10),FREQX(100,10),XSITE(3,100),TSITE(100),
     X             TRFTIM(10)
      COMMON/TANKX/RADTX(10),ZRADTX(10)
      COMMON/BUBBLE/WAKV(3,1000),VB(3,1000),XB(3,1000),RB(1000),
     X              RBA(1000),IB(1000),DMBGF(1000),DMB(1000),CDRAG(1000)
      COMMON/CONVERG/DBUBCO,DLIQCO,DLEVCO,DCONCO,DENRCO,DFORCO
      COMMON/SURFAS/ZSURF,SURFAN,ISLIP
      COMMON/LICUID/WMLO,DML1,DMLBF,TSUPRL,QL,REYN12,REYN23,ACOF(3),
     X         EXPN(3),TBULKL
      COMMON/GASPRO/HG,RBMIN,NB
```

```
      COMMON/GNRL/DTIME,DTIMEX,TIMEND,TIMPRNT(1000),IPRINTL,IPRINTU,
     X             NTAPE,IRESTRT,TIME,PIMPS,PARIMP
      COMMON/VOID/VOFRAC,DMBTOT
      COMMON/INTEGR/NTL,NTLR,NTLZ,NRFT,NSITE,NRZ,NPTIM,NPROP,IWAKE
      COMMON/ADCONST/CWAKE,BWAKE,SCRAD,ARBDEN,DEGFAC,ICRD(3)
      DCON=1.
      IF(XRADT(X13)-R1)501,501,502
  501 IF(ISLIP)503,503,502
  503 XZ2=X13
      GO TO 50
  502 XZ2=X23
   50 IF(XZ2-R1)1,2,2
    1 XZ2=R1
      IBOT=1
      GO TO 3
    2 IBOT=0
    3 XZ1=AMAX1(X13,R1)
      XR1=SQRT(X11*X11+X12*X12+XZ1*XZ1)
      XR2=SQRT(X21*X21+X22*X22+XZ2*XZ2)
      IOBS=0.
      TH1=ACOS(XZ1/XR1)
      TH2=ACOS(XZ2/XR2)
      DXB=XRADT(XZ2+R1)-XRADT(XZ2)
      THETB=ATAN(DXB/R1)
      IREDC1=IREDC
      PHI1=ATIN(X12,X11)
      PHI2=ATIN(X22,X21)
      RT=R1/COS(THETB)
   19 DXB=(XRADT(XZ2)-XR2*SIN(TH2))*COS(THETB)
      IF(DXB-R1)5,5,4
    4 X23=XZ2
      R2=R1
      RETURN
    5 IF(XRADT(XZ2)-RT)9,51,51
    9 X21=0.
      X22=0.
      IOBS=1
      RI=R1
      ITMAX=25
      VOLB=4.*3.1416*RI**3/3.
      IT=0
      ASSIGN 37 TO IS2
      ASSIGN 38 TO IS3
      X23=XZ2
   36 XZ2=AMAX1(X23,RI)
      DXB=XRADT(XZ2)*COS(THETB)
      ALPHA=ASIN(DXB/RI)
      THET1=ALPHA+ABS(THETB)
      THET2=ALPHA-ABS(THETB)
      VOLC1=3.1416*RI**3*(2.+COS(THET1))*(1.-COS(THET1))**2/3.
      VOLC2=3.1416*RI**3*(2.+COS(THET2))*(1.-COS(THET2))**2/3.
      VOCON=3.1416*RI**3*(COS(THET1)+COS(THET2))*(SIN(THET1)**2+
     X                   SIN(THET1)*SIN(THET2)+SIN(THET2)**2)/3.
      VTOT=VOCON+VOLC1+VOLC2
```

```
      DV=VOLB-VTOT
      IF(ABS(DV)-0.001*DCON*VOLB)39,39,40
   40 IF(DV)41,39,42
   41 GO TO IS2,(37,43,47,48)
   42 GO TO IS3,(38,43,46,49)
   37 ASSIGN 43 TO IS2
      ASSIGN 46 TO IS3
      DVFIX=DV
      RFIX=R1
      GO TO 44
   38 ASSIGN 47 TO IS2
      ASSIGN 43 TO IS3
      DVFIX=DV
      RFIX=R1
   44 RI=R1*1.1
      GO TO 36
   43 IT=IT+1
      RI=(DV*RFIX-DVFIX*RI)/(DV-DVFIX)
      IF(IT-ITMAX)36,36,39
   46 ASSIGN 43 TO IS3
      ASSIGN 48 TO IS2
      DVSAVE=DV
      RSAVE=RI
      GO TO 43
   47 ASSIGN 43 TO IS2
      ASSIGN 49 TO IS3
      DVSAVE=DV
      RSAVE=RI
      GO TO 43
   48 RFIX=RSAVE
      DVFIX=DVSAVE
      ASSIGN 43 TO IS2
      ASSIGN 46 TO IS3
      GO TO 43
   49 RFIX=RSAVE
      DVFIX=DVSAVE
      ASSIGN 47 TO IS2
      ASSIGN 43 TO IS3
      GO TO 43
   39 R2=RI
      X23=XZ2
      CALL SCREEN(X21,X22,R1,RN,3,IREDC1)
      IF(R1-RN)45,451,45
  451 RETURN
   45 IREDC1=0
      R1=RN
      GO TO 50
   51 IF(ISLIP)6,6,7
    7 DX=R1-DXB
      XZ2=XZ2+DX*SIN(THETB)
      X21=X21-DX*COS(THETB)*COS(PHI2)
      X22=X22-DX*COS(THETB)*SIN(PHI2)
      IF(XRADT(XZ2)-RT)9,10,10
   10 CALL SCREEN(X21,X22,X23,R1,RN,1,IREDC1)
```

```
      IF(R1-RN)11,12,11
 12   R2=R1
      RETURN
 11   DR=R1-RN
      R1=RN
      RT=R1/COS(THETB)
      IREDC1=0
      IF(XRADT(XZ2)-RT)9,13,13
 13   X21=X21+(DR)*COS(THETB)*COS(PHI2)
      X22=X22+(DR)*COS(THETB)*SIN(PHI2)
      X23=X23-(DR)*SIN(THETB)
      R2=R1
      RETURN
  6   DX1=(XRADT(XZ1)-XR1*SIN(TH1))*COS(THETB)
      IF(DX1-R1)52,52,53
 52   IF(XRADT(XZ1)-RT)54,55,55
 54   XZ2=XZ1
      GO TO 9
 55   X23=XZ1+(R1-DX1)*SIN(THETB)
      X21=X11-(R1-DX1)*COS(THETB)*COS(PHI1)
      X22=X12-(R1-DX1)*COS(THETB)*SIN(PHI1)
      IF(XRADT(X23)-RT)56,57,57
 56   XZ2=X23
      GO TO 9
 57   CALL SCREEN(X21,X22,X23,R1,RN,1,IREDC1)
      IREDC1=0
      DR=R1-RN
      R1=RN
      RT=R1/COS(THETB)
      IF(XRADT(X23)-RT)56,58,58
 58   X21=X21+DR*COS(THETB)*COS(PHI1)
      X22=X22+DR*COS(THETB)*SIN(PHI1)
      X23=X23-DR*SIN(THETB)
      R2=R1
      RETURN
 53   DTHETA=ABS(TH1-TH2)
      DR=SQRT(XR1*XR1*SIN(DTHETA)**2+(XR2-XR1*COS(DTHETA))**2)
      DX1=(XRADT(XZ1)-XR1*SIN(TH1))*COS(THETB)
      DX2=(XRADT(XZ2)-XR2*SIN(TH2))*COS(THETB)
      DDR=DR*(R1-DX2)/(DX1-DX2)
      ANGLE=ACOS((DX1-DX2)/DR)
      IF(TH1-TH2)59,60,60
 59   ANG=1.5707963-ANGLE-THETB
      SIG=1.
      GO TO 61
 60   ANG=1.5707963-THETB+ANGLE
      SIG=-1.
 61   DRHO=SIG*DR*COS(ANG)
      DZ=DR*SIG*SIN(ANG)
      X23=XZ1+DZ
      RPRO=XR2*COS(PHI2-PHI1)
      DR=RPRO-XR1
      XSIDE=XR2*SIN(PHI2-PHI1)*DRHO/DR
      RHB=XRADT(X23)-R1
```

```
      DPHI=ASIN(XSIDE/RHB)
      PHI=PHI1+DPHI
      X21=RHB*COS(PHI)
      X22=RHB*SIN(PHI)
      CALL SCREEN(X21,X22,X23,R1,RN,1,IREDC1)
      IREDC1=0
      DR=R1-RN
      R1=RN
      RT=R1/COS(THETB)
      IF(XRADT(X23)-RT)56,62,62
   62 X21=X21+DR*COS(THETB)*COS(PHI)
      X22=X22+DR*COS(THETB)*SIN(PHI)
      X23=X23-DR*SIN(THETB)
      R2=R1
      RETURN
      END
      SUBROUTINE LIQLEV(DT)
      COMMON/PROPRT/PPZ(30),TPZ(30),SPZ(30),VPZ(30),RPLZ(30),UPLZ(30),
     X              RPGZ(30),UPGZ(30)
      COMMON/DYNAM/TIMPROP(30),PTIM(30),QLTIM(30),WMLOTIM(30),SANTIM(30)
     X            ,GANTIM(30),GRATIM(30)
      COMMON/TLIQX/TLTIMX(15,15,15),TLTIME(15),RZTL(15),ZZTL(15)
      COMMON/SITEX/RBSITX(100,10),FREQX(100,10),XSITE(3,100),TSITE(100),
     X             TRFTIM(10)
      COMMON/TANKX/RADTX(10),ZRADTX(10)
      COMMON/BUBBLE/WAKV(3,1000),VB(3,1000),XB(3,1000),RB(1000),
     X              RBA(1000),IB(1000),DMBGF(1000),DMB(1000),CDRAG(1000)
      COMMON/CONVERG/DBUBCO,DLIQCO,DLEVCO,DCONCO,DENRCO,DFORCO
      COMMON/SURFAS/ZSURF,SURFAN,ISLIP
      COMMON/LIQUID/WMLO,DML1,DMLBF,TSUPRL,QL,REYN12,REYN23,ACOF(3),
     X         EXPN(3),TBULKL
      COMMON/GASPRO/HG,RBMIN,NB
      COMMON/GNRL/DTIME,DTIMEX,TIMEND,TIMPRNT(1000),IPRINTL,IPRINTU,
     X            NTAPE,IRESTRT,TIME,PIMPS,PARIMP
      COMMON/VOID/VOFRAC,DMBTOT
      COMMON/INTEGR/NTL,NTLR,NTLZ,NRFT,NSITE,NRZ,NPTIM,NPROP,IWAKE
      COMMON/ADCONST/CWAKE,BWAKE,SCRAD,ARBDEN,DEGFAC,ICRD(3)
      DCON=1.
      P=PZ(TIME+DT)
      TMLDB=0.
      DMBTOT=0.
      IF(NB)83,83,84
   84 DO 80 I=1,NB
   80 TMLDB=TMLDB+DMBGF(I)*DEGFAC
   83 TOTML=DML1+TMLDB
      IF(TMLDB)81,81,82
   82 TBULKL=(DML1*TBULKL+TSZT(P)*TMLDB)/TOTML
   81 DML1=TOTML
      RHOL=RHZL(TBULKL)
      TOTVOLL=DML1/RHOL
      TSAT=TSZT(P)
      TOTVOLB=0.
      RHOLS=RHZL(TSAT)
      IF(NB)85,85,86
```

```
86 DO 1 I=1,NB
   TL=TZ(XB(1,I),XB(2,I),XB(3,I),TIME+DT)
   PT=P+2.*SIGZ(TL)/(144.*RBA(I))
   RHOG=RHGZ(PT)
   DMBTOT=DMBTOT+4.*3.1416*RHOG*RBA(I)**3/3.
 1 TOTVOLB=TOTVOLB+4.*3.1416*RBA(I)**3/3.
   TOTVOLB=TOTVOLB*DEGFAC
   DMBTOT=DMBTOT*DEGFAC
85 ASSIGN 27 TO IS2
   ASSIGN 23 TO IS3
   TOTVOL=TOTVOLL+TOTVOLB
   VOFRAC=TOTVOLB/TOTVOL
   IT=0
   ZFIX=0.
   ITMAX=50
   VFIX=TOTVOL
 2 SURFIN=SURFAN
   VTEST=TOTVOL-VOLFZT(ZSURF,SURFIN)
   IF(ABS(VTEST)-0.001*DCON*TOTVOL)21,21,3
 3 IF(VTEST)4,21,5
 4 GO TO IS2,(23,27,28)
 5 GO TO IS3,(23,26,29)
23 IT=IT+1
   ZSURF=(VTEST*ZFIX-VFIX*ZSURF)/(VTEST-VFIX)
   IF(IT-ITMAX)2,2,6
 6 GO TO 21
26 VSAVE=VTEST
   ZSAVE=ZSURF
   ASSIGN 23 TO IS3
   ASSIGN 28 TO IS2
   GO TO 23
27 VSAVE=VTEST
   ZSAVE=ZSURF
   ASSIGN 23 TO IS2
   ASSIGN 29 TO IS3
   GO TO 23
28 VFIX=VSAVE
   ZFIX=ZSAVE
   ASSIGN 23 TO IS2
   ASSIGN 26 TO IS3
   GO TO 23
29 VFIX=VSAVE
   ZFIX=ZSAVE
   ASSIGN 27 TO IS2
   ASSIGN 23 TO IS3
   GO TO 23
21 SURFAN=SURFIN
   DO 7 I=1,NB
 7 DMBGF(I)=0.
   RETURN
   END
   FUNCTION VOLFZT(ZSURF,SURFIN)
   COMMON/PROPRT/PPZ(30),TPZ(30),SPZ(30),VPZ(30),RPLZ(30),UPLZ(30),
  X                RPGZ(30),UPGZ(30)
```

```
      COMMON/DYNAM/TIMPROP(30),PTIM(30),QLTIM(30),WMLOTIM(30),SANTIM(30)
     X              ,GANTIM(30),GRATIM(30)
      COMMON/TLIQX/TLTIMX(15,15,15),TLTIME(15),RZTL(15),ZZTL(15)
      COMMON/SITEX/RBSITX(100,10),FREQX(100,10),XSITE(3,100),TSITE(100),
     X               TRFTIM(10)
      COMMON/TANKX/RADTX(10),ZRADTX(10)
      COMMON/BUBBLE/WAKV(3,1000),VB(3,1000),XB(3,1000),RB(1000),
     X                RBA(1000),IB(1000),DMBGF(1000),DMB(1000),CDRAG(1000)
      COMMON/CONVERG/DBUBCO,DLIQCO,DLEVCO,DCONCO,DENRCO,DFORCO
      COMMON/SURFAS/ZSURF,SURFAN,ISLIP
      COMMON/LICUID/WMLO,DML1,DMLBF,TSUPRL,QL,REYN12,REYN23,ACOF(3),
     X          EXPN(3),TBULKL
      COMMON/GASPRO/HG,RBMIN,NB
      COMMON/GNRL/DTIME,DTIMEX,TIMEND,TIMPRNT(1000),IPRINTL,IPRINTU,
     X              NTAPE,IRESTRT,TIME,PIMPS,PARIMP
      COMMON/VOID/VOFRAC,DMBTOT
      COMMON/INTEGR/NTL,NTLR,NTLZ,NRFT,NSITE,NRZ,NPTIM,NPROP,IWAKE
      COMMON/ADCONST/CWAKE,BWAKE,SCRAD,ARBDEN,DEGFAC,ICRD(3)
      DXB=XRADT(ZSURF)-XRADT(0.)
    2 THETB=ATAN(DXB/ZSURF)
      THETAB=ABS(THETB)
      SURFA=ABS(SURFIN)
      DSID=XRADT(ZSURF)*SIN(SURFA)*COS(THETB)/SIN(1.5707693-SURFA-THETB)
      IF(DSID-ZSURF)7,7,6
    6 SURFIN=ATAN(ZSURF/XRADT(0.))*SIGN(1.,SURFIN)
      SURFA=ABS(SURFIN)
    7 IF(THETAB-0.001)4,4,71
   71 IF(THETB)3,4,5
    4 VOLFZT=3.1416*XRADT(ZSURF)**2*ZSURF
      RETURN
    3 ACO=SIN(1.5707963-THETB)/SIN(1.5707963*THETB-SURFA)
      BCO=SIN(1.5707963+THETB)/SIN(1.5707963-THETB-SURFA)
      RMAJR=XRADT(ZSURF)*(ACO+BCO)/2.
      DR=RMAJR-ACO*XRADT(ZSURF)
      ZUPR=ZSURF+DR*SIN(SURFA)
      RUPR=XRADT(ZUPR)
      DXB=DR*COS(SURFA)
      ANGLE=ACOS(DXB/RUPR)
      RMINR=RUPR*SIN(ANGLE)
      ARLU=3.1416*RMINR*RMAJR
      ZLWR=ZSURF-(RMAJR-ABS(DR))*SIN(SURFA)
      VOLFZT=3.1416*ZLWR*(XRADT(0.)**2+XRADT(0.)*XRADT(ZLWR)*XRADT(ZLWR)
     X        **2)/3.
      RLWR=XRADT(ZLWR)
      VOLFZT=VOLFZT+RLWR*(3.1416*RLWR**2*SIN(1.5707963-THETAB)-ARLU*
     X        SIN(1.5707963-THETAB-SURFA))/SIN(THETAB)
      RETURN
    5 ACO=SIN(1.5707963-THETB)/SIN(1.5707963+THETB-SURFA)
      BCO=SIN(1.5707963+THETB)/SIN(1.5707963-THETB-SURFA)
      RMAJR=XRADT(ZSURF)*(ACO+BCO)/2.
      ZUPR=ZSURF+(RMAJR-ACO*XRADT(ZSURF))*SIN(SURFA)
      RUPR=XRADT(ZUPR)
      DXB=(RMAJR-ACO*XRADT(ZSURF))*COS(SURFA)
      ANGLE=ACOS(DXB/RUPR)
```

```
      RMINR=RUPR*SIN(ANGLE)
      ARLU=3.1416*RMINR*RMAJR
      ZLWR=ZSURF-(RMAJR-ABS(RMAJR-ACO*XRADT(ZSURF)))*SIN(SURFA)
      RLWR=XRADT(ZLWR)
      RZERO=XRADT(0.)
      VOLFXT=3.1416*ZLWR*(RZERO**2+RZERO*RLWR+RLWR**2)/3.
      VOLFZT=VOLFXT+RLWR*(ARLU*SIN(1.5707963-THETAB-SURFA)*(1.+2.*TAN(
     X     THETAB)*TAN(SURFA))-3.1416*RLWR**2*SIN(1.5707963-THETAB))/
     X   SIN(THETAB)
      RETURN
      END
      FUNCTION UGSZ(P)
      COMMON/PROPRT/PPZ(30),TPZ(30),SPZ(30),VPZ(30),RPLZ(30),UPLZ(30),
     X             RPGZ(30),UPGZ(30)
      COMMON/DYNAM/TIMPROP(30),PTIM(30),QLTIM(30),WMLOTIM(30),SANTIM(30)
     X            ,GANTIM(30),GRATIM(30)
      COMMON/TLIQX/TLTIMX(15,15,15),TLTIME(15),RZTL(15),ZZTL(15)
      COMMON/SITEX/RBSITX(100,10),FREQX(100,10),XSITE(3,100),TSITE(100),
     X             TRFTIM(10)
      COMMON/TANKX/RADTX(10),ZRADTX(10)
      COMMON/BUBBLE/WAKV(3,1000),VB(3,1000),XB(3,1000),RB(1000),
     X              RBA(1000),IB(1000),DMBGF(1000),DMB(1000),CDRAG(1000)
      COMMON/CONVERG/DBUBCO,DLIQCO,DLEVCO,DCONCO,DENRCO,DFORCO
      COMMON/SURFAS/ZSURF,SURFAN,ISLIP
      COMMON/LICUID/WMLO,DML1,DMLBF,TSUPRL,QL,REYN12,REYN23,ACOF(3),
     X        EXPN(3),TBULKL
      COMMON/GASPRO/HG,RBMIN,NB
      COMMON/GNRL/DTIME,DTIMEX,TIMEND,TIMPRNT(1000),IPRINTL,IPRINTU,
     X            NTAPE,IRESTRT,TIME,PIMPS,PARIMP
      COMMON/VOID/VOFRAC,DMBTOT
      COMMON/INTEGR/NTL,NTLR,NTLZ,NRFT,NSITE,NRZ,NPTIM,NPROP,IWAKE
      COMMON/ADCONST/CWAKE,BWAKE,SCRAD,ARBDEN,DEGFAC,ICRD(3)
      CALL TABL(P,UGSZ,PPZ(1),UPGZ(1),1,1,1,NPROP,IFB)
      RETURN
      END
      FUNCTION ULSZ(T)
      COMMON/PROPRT/PPZ(30),TPZ(30),SPZ(30),VPZ(30),RPLZ(30),UPLZ(30),
     X             RPGZ(30),UPGZ(30)
      COMMON/DYNAM/TIMPROP(30),PTIM(30),QLTIM(30),WMLOTIM(30),SANTIM(30)
     X            ,GANTIM(30),GRATIM(30)
      COMMON/TLIQX/TLTIMX(15,15,15),TLTIME(15),RZTL(15),ZZTL(15)
      COMMON/SITEX/RBSITX(100,10),FREQX(100,10),XSITE(3,100),TSITE(100),
     X             TRFTIM(10)
      COMMON/TANKX/RADTX(10),ZRADTX(10)
      COMMON/BUBBLE/WAKV(3,1000),VB(3,1000),XB(3,1000),RB(1000),
     X              RBA(1000),IB(1000),DMBGF(1000),DMB(1000),CDRAG(1000)
      COMMON/CONVERG/DBUBCO,DLIQCO,DLEVCO,DCONCO,DENRCO,DFORCO
      COMMON/SURFAS/ZSURF,SURFAN,ISLIP
      COMMON/LICUID/WMLO,DML1,DMLBF,TSUPRL,QL,REYN12,REYN23,ACOF(3),
     X        EXPN(3),TBULKL
      COMMON/GASPRO/HG,RBMIN,NB
      COMMON/GNRL/DTIME,DTIMEX,TIMEND,TIMPRNT(1000),IPRINTL,IPRINTU,
     X            NTAPE,IRESTRT,TIME,PIMPS,PARIMP
      COMMON/VOID/VOFRAC,DMBTOT
```

```
      COMMON/INTEGR/NTL,NTLR,NTLZ,NRFT,NSITE,NRZ,NPTIM,NPROP,IWAKE
      COMMON/ADCONST/CWAKE,BWAKE,SCRAD,ARBDEN,DEGFAC,ICRD(3)
      CALL TABL(T,ULSZ,TPZ(1),UPLZ(1),1,1,1,NPROP,IFB)
      RETURN
      END
      FUNCTION SIGZ(T)
      COMMON/PROPRT/PPZ(30),TPZ(30),SPZ(30),VPZ(30),RPLZ(30),UPLZ(30),
     X             RPGZ(30),UPGZ(30)
      COMMON/DYNAM/TIMPROP(30),PTIM(30),QLTIM(30),WMLOTIM(30),SANTIM(30)
     X          ,GANTIM(30),GRATIM(30)
      COMMON/TLIQX/TLTIMX(15,15,15),TLTIME(15),RZTL(15),ZZTL(15)
      COMMON/SITEX/RBSITX(100,10),FREQX(100,10),XSITE(3,100),TSITE(100),
     X            TRFTIM(10)
      COMMON/TANKX/RADTX(10),ZRADTX(10)
      COMMON/BUBBLE/WAKV(3,1000),VB(3,1000),XB(3,1000),RB(1000),
     X             RBA(1000),IB(1000),DMBGF(1000),DMB(1000),CDRAG(1000)
      COMMON/CONVERG/DBUBCO,DLIQCO,DLEVCO,DCONCO,DENRCO,DFORCO
      COMMON/SURFAS/ZSURF,SURFAN,ISLIP
      COMMON/LICUID/WMLO,DML1,DMLBF,TSUPRL,QL,REYN12,REYN23,ACOF(3),
     X        EXPN(3),TBULKL
      COMMON/GASPRO/HG,RBMIN,NB
      COMMON/GNRL/DTIME,DTIMEX,TIMEND,TIMPRNT(1000),IPRINTL,IPRINTU,
     X           NTAPE,IRESTRT,TIME,PIMPS,PARIMP
      COMMON/VOID/VOFRAC,DMBTOT
      COMMON/INTEGR/NTL,NTLR,NTLZ,NRFT,NSITE,NRZ,NPTIM,NPROP,IWAKE
      COMMON/ADCONST/CWAKE,BWAKE,SCRAD,ARBDEN,DEGFAC,ICRD(3)
      CALL TABL(T,SIGZ,TPZ(1),SPZ(1),1,1,1,NPROP,IFB)
      RETURN
      END
      FUNCTION RHZL(T)
      COMMON/PROPRT/PPZ(30),TPZ(30),SPZ(30),VPZ(30),RPLZ(30),UPLZ(30),
     X             RPGZ(30),UPGZ(30)
      COMMON/DYNAM/TIMPROP(30),PTIM(30),QLTIM(30),WMLOTIM(30),SANTIM(30)
     X          ,GANTIM(30),GRATIM(30)
      COMMON/TLIQX/TLTIMX(15,15,15),TLTIME(15),RZTL(15),ZZTL(15)
      COMMON/SITEX/RBSITX(100,10),FREQX(100,10),XSITE(3,100),TSITE(100),
     X            TRFTIM(10)
      COMMON/TANKX/RADTX(10),ZRADTX(10)
      COMMON/BUBBLE/WAKV(3,1000),VB(3,1000),XB(3,1000),RB(1000),
     X             RBA(1000),IB(1000),DMBGF(1000),DMB(1000),CDRAG(1000)
      COMMON/CONVERG/DBUBCO,DLIQCO,DLEVCO,DCONCO,DENRCO,DFORCO
      COMMON/SURFAS/ZSURF,SURFAN,ISLIP
      COMMON/LICUID/WMLO,DML1,DMLBF,TSUPRL,QL,REYN12,REYN23,ACOF(3),
     X        EXPN(3),TBULKL
      COMMON/GASPRO/HG,RBMIN,NB
      COMMON/GNRL/DTIME,DTIMEX,TIMEND,TIMPRNT(1000),IPRINTL,IPRINTU,
     X           NTAPE,IRESTRT,TIME,PIMPS,PARIMP
      COMMON/VOID/VOFRAC,DMBTOT
      COMMON/INTEGR/NTL,NTLR,NTLZ,NRFT,NSITE,NRZ,NPTIM,NPROP,IWAKE
      COMMON/ADCONST/CWAKE,BWAKE,SCRAD,ARBDEN,DEGFAC,ICRD(3)
      CALL TABL(T,RHZL,TPZ(1),RPLZ(1),1,1,1,NPROP,IFB)
      RETURN
      END
      FUNCTION RHGZ(P)
```

```
      COMMON/PROPRT/PPZ(30),TPZ(30),SPZ(30),VPZ(30),RPLZ(30),UPLZ(30),
     X              RPGZ(30),UPGZ(30)
      COMMON/DYNAM/TIMPROP(30),PTIM(30),QLTIM(30),WMLOTIM(30),SANTIM(30)
     X          ,GANTIM(30),GRATIM(30)
      COMMON/TLIQX/TLTIMX(15,15,15),TLTIME(15),RZTL(15),ZZTL(15)
      COMMON/SITEX/RBSITX(100,10),FREQX(100,10),XSITE(3,100),TSITE(100),
     X             TRFTIM(10)
      COMMON/TANKX/RADTX(10),ZRADTX(10)
      COMMON/BUBBLE/WAKV(3,1000),VB(3,1000),XB(3,1000),RB(1000),
     X              RBA(1000),IB(1000),DMBGF(1000),DMB(1000),CDRAG(1000)
      COMMON/CONVERG/DBUBCO,DLIQCO,DLEVCO,DCONCO,DENRCO,DFORCO
      COMMON/SURFAS/ZSURF,SURFAN,ISLIP
      COMMON/LICUID/WMLO,DML1,DMLBF,TSUPRL,QL,REYN12,REYN23,ACOF(3),
     X       EXPN(3),TBULKL
      COMMON/GASPRO/HG,RBMIN,NB
      COMMON/GNRL/DTIME,DTIMEX,TIMEND,TIMPRNT(1000),IPRINTL,IPRINTU,
     X           NTAPE,IRESTRT,TIME,PIMPS,PARIMP
      COMMON/VOID/VOFRAC,DMBTOT
      COMMON/INTEGR/NTL,NTLR,NTLZ,NRFT,NSITE,NRZ,NPTIM,NPROP,IWAKE
      COMMON/ADCONST/CWAKE,BWAKE,SCRAD,ARBDEN,DEGFAC,ICRD(3)
      CALL TABL(P,RHGZ,PPZ(1),RPGZ(1),1,1,1,NPROP,IFB)
      RETURN
      END
      FUNCTION PZ(TIM)
      COMMON/PROPRT/PPZ(30),TPZ(30),SPZ(30),VPZ(30),RPLZ(30),UPLZ(30),
     X              RPGZ(30),UPGZ(30)
      COMMON/DYNAM/TIMPROP(30),PTIM(30),QLTIM(30),WMLOTIM(30),SANTIM(30)
     X          ,GANTIM(30),GRATIM(30)
      COMMON/TLIQX/TLTIMX(15,15,15),TLTIME(15),RZTL(15),ZZTL(15)
      COMMON/SITEX/RBSITX(100,10),FREQX(100,10),XSITE(3,100),TSITE(100),
     X             TRFTIM(10)
      COMMON/TANKX/RADTX(10),ZRADTX(10)
      COMMON/BUBBLE/WAKV(3,1000),VB(3,1000),XB(3,1000),RB(1000),
     X              RBA(1000),IB(1000),DMBGF(1000),DMB(1000),CDRAG(1000)
      COMMON/CONVERG/DBUBCO,DLIQCO,DLEVCO,DCONCO,DENRCO,DFORCO
      COMMON/SURFAS/ZSURF,SURFAN,ISLIP
      COMMON/LICUID/WMLO,DML1,DMLBF,TSUPRL,QL,REYN12,REYN23,ACOF(3),
     X       EXPN(3),TBULKL
      COMMON/GASPRO/HG,RBMIN,NB
      COMMON/GNRL/DTIME,DTIMEX,TIMEND,TIMPRNT(1000),IPRINTL,IPRINTU,
     X           NTAPE,IRESTRT,TIME,PIMPS,PARIMP
      COMMON/VOID/VOFRAC,DMBTOT
      COMMON/INTEGR/NTL,NTLR,NTLZ,NRFT,NSITE,NRZ,NPTIM,NPROP,IWAKE
      COMMON/ADCONST/CWAKE,BWAKE,SCRAD,ARBDEN,DEGFAC,ICRD(3)
      CALL TABL(TIM,PZ,TIMPROP(1),PTIM(1),1,1,1,NPTIM,IFB)
      RETURN
      END
      FUNCTION TSZT(P)
      COMMON/PROPRT/PPZ(30),TPZ(30),SPZ(30),VPZ(30),RPLZ(30),UPLZ(30),
     X              RPGZ(30),UPGZ(30)
      COMMON/DYNAM/TIMPROP(30),PTIM(30),QLTIM(30),WMLOTIM(30),SANTIM(30)
     X          ,GANTIM(30),GRATIM(30)
      COMMON/TLIQX/TLTIMX(15,15,15),TLTIME(15),RZTL(15),ZZTL(15)
      COMMON/SITEX/RBSITX(100,10),FREQX(100,10),XSITE(3,100),TSITE(100),
```

```
X              TRFTIM(10)
      COMMON/TANKX/RADTX(10),ZRADTX(10)
      COMMON/BUBBLE/WAKV(3,1000),VB(3,1000),XB(3,1000),RB(1000),
X               RBA(1000),IB(1000),DMBGF(1000),DMB(1000),CDRAG(1000)
      COMMON/CONVERG/DBUBCO,DLIQCO,DLEVCO,DCONCO,DENRCO,DFORCO
      COMMON/SURFAS/ZSURF,SURFAN,ISLIP
      COMMON/LICUID/WMLO,DML1,DMLBF,TSUPRL,QL,REYN12,REYN23,ACOF(3),
X          EXPN(3),TBULKL
      COMMON/GASPRO/HG,RBMIN,NB
      COMMON/GNRL/DTIME,DTIMEX,TIMEND,TIMPRNT(1000),IPRINTL,IPRINTU,
X             NTAPE,IRESTRT,TIME,PIMPS,PARIMP
      COMMON/VOID/VOFRAC,DMBTOT
      COMMON/INTEGR/NTL,NTLR,NTLZ,NRFT,NSITE,NRZ,NPTIM,NPROP,IWAKE
      COMMON/ADCONST/CWAKE,BWAKE,SCRAD,ARBDEN,DEGFAC,ICRD(3)
      CALL TABL(P,TSZT,PPZ(1),TPZ(1),1,1,1,NPROP,IFB)
      RETURN
      END
      FUNCTION XRADT(Z)
      COMMON/PROPRT/PPZ(30),TPZ(30),SPZ(30),VPZ(30),RPLZ(30),UPLZ(30),
X               RPGZ(30),UPGZ(30)
      COMMON/DYNAM/TIMPROP(30),PTIM(30),QLTIM(30),WMLOTIM(30),SANTIM(30)
X             ,GANTIM(30),GRATIM(30)
      COMMON/TLIQX/TLTIMX(15,15,15),TLTIME(15),RZTL(15),ZZTL(15)
      COMMON/SITEX/RBSITX(100,10),FREQX(100,10),XSITE(3,100),TSITE(100),
X              TRFTIM(10)
      COMMON/TANKX/RADTX(10),ZRADTX(10)
      COMMON/BUBBLE/WAKV(3,1000),VB(3,1000),XB(3,1000),RB(1000),
X               RBA(1000),IB(1000),DMBGF(1000),DMB(1000),CDRAG(1000)
      COMMON/CONVERG/DBUBCO,DLIQCO,DLEVCO,DCONCO,DENRCO,DFORCO
      COMMON/SURFAS/ZSURF,SURFAN,ISLIP
      COMMON/LICUID/WMLO,DML1,DMLBF,TSUPRL,QL,REYN12,REYN23,ACOF(3),
X          EXPN(3),TBULKL
      COMMON/GASPRO/HG,RBMIN,NB
      COMMON/GNRL/DTIME,DTIMEX,TIMEND,TIMPRNT(1000),IPRINTL,IPRINTU,
X             NTAPE,IRESTRT,TIME,PIMPS,PARIMP
      COMMON/VOID/VOFRAC,DMBTOT
      COMMON/INTEGR/NTL,NTLR,NTLZ,NRFT,NSITE,NRZ,NPTIM,NPROP,IWAKE
      COMMON/ADCONST/CWAKE,BWAKE,SCRAD,ARBDEN,DEGFAC,ICRD(3)
      CALL TABL(Z,XRADT,ZRADTX(1),RADTX(1),1,1,1,NRZ,IFB)
      RETURN
      END
      FUNCTION VISCZ(T)
      COMMON/PROPRT/PPZ(30),TPZ(30),SPZ(30),VPZ(30),RPLZ(30),UPLZ(30),
X               RPGZ(30),UPGZ(30)
      COMMON/DYNAM/TIMPROP(30),PTIM(30),QLTIM(30),WMLOTIM(30),SANTIM(30)
X             ,GANTIM(30),GRATIM(30)
      COMMON/TLIQX/TLTIMX(15,15,15),TLTIME(15),RZTL(15),ZZTL(15)
      COMMON/SITEX/RBSITX(100,10),FREQX(100,10),XSITE(3,100),TSITE(100),
X              TRFTIM(10)
      COMMON/TANKX/RADTX(10),ZRADTX(10)
      COMMON/BUBBLE/WAKV(3,1000),VB(3,1000),XB(3,1000),RB(1000),
X               RBA(1000),IB(1000),DMBGF(1000),DMB(1000),CDRAG(1000)
      COMMON/CONVERG/DBUBCO,DLIQCO,DLEVCO,DCONCO,DENRCO,DFORCO
      COMMON/SURFAS/ZSURF,SURFAN,ISLIP
```

```
      COMMON/LICUID/WMLO,DML1,DMLBF,TSUPRL,QL,REYN12,REYN23,ACOF(3),
     X          EXPN(3),TBULKL
      COMMON/GASPRO/HG,RBMIN,NB
      COMMON/GNRL/DTIME,DTIMEX,TIMEND,TIMPRNT(1000),IPRINTL,IPRINTU,
     X          NTAPE,IRESTRT,TIME,PIMPS,PARIMP
      COMMON/VOID/VOFRAC,DMBTOT
      COMMON/INTEGR/NTL,NTLR,NTLZ,NRFT,NSITE,NRZ,NPTIM,NPROP,IWAKE
      COMMON/ADCONST/CWAKE,BWAKE,SCRAD,ARBDEN,DEGFAC,ICRD(3)
      CALL TABL(T,VISCZ,TPZ(1),VPZ(1),1,1,1,NPROP,IFB)
      RETURN
      END
      FUNCTION LEVANG(TIM)
      COMMON/PROPRT/PPZ(30),TPZ(30),SPZ(30),VPZ(30),RPLZ(30),UPLZ(30),
     X              RPGZ(30),UPGZ(30)
      COMMON/DYNAM/TIMPROP(30),PTIM(30),QLTIM(30),WMLOTIM(30),SANTIM(30)
     X          ,GANTIM(30),GRATIM(30)
      COMMON/TLIQX/TLTIMX(15,15,15),TLTIME(15),RZTL(15),ZZTL(15)
      COMMON/SITEX/RBSITX(100,10),FREQX(100,10),XSITE(3,100),TSITE(100),
     X             TRFTIM(10)
      COMMON/TANKX/RADTX(10),ZRADTX(10)
      COMMON/BUBBLE/WAKV(3,1000),VB(3,1000),XB(3,1000),RB(1000),
     X              RBA(1000),IB(1000),DMBGF(1000),DMB(1000),CDRAG(1000)
      COMMON/CONVERG/DBUBCO,DLIQCO,DLEVCO,DCONCO,DENRCO,DFORCO
      COMMON/SURFAS/ZSURF,SURFAN,ISLIP
      COMMON/LICUID/WMLO,DML1,DMLBF,TSUPRL,QL,REYN12,REYN23,ACOF(3),
     X          EXPN(3),TBULKL
      COMMON/GASPRO/HG,RBMIN,NB
      COMMON/GNRL/DTIME,DTIMEX,TIMEND,TIMPRNT(1000),IPRINTL,IPRINTU,
     X          NTAPE,IRESTRT,TIME,PIMPS,PARIMP
      COMMON/VOID/VOFRAC,DMBTOT
      COMMON/INTEGR/NTL,NTLR,NTLZ,NRFT,NSITE,NRZ,NPTIM,NPROP,IWAKE
      COMMON/ADCONST/CWAKE,BWAKE,SCRAD,ARBDEN,DEGFAC,ICRD(3)
      CALL TABL(TIM,LEVANG,TIMPROP(1),SANTIM(1),1,1,1,NPTIM,IFB)
      RETURN
      END
      FUNCTION GRAVITY(TIM)
      COMMON/PROPRT/PPZ(30),TPZ(30),SPZ(30),VPZ(30),RPLZ(30),UPLZ(30),
     X              RPGZ(30),UPGZ(30)
      COMMON/DYNAM/TIMPROP(30),PTIM(30),QLTIM(30),WMLOTIM(30),SANTIM(30)
     X          ,GANTIM(30),GRATIM(30)
      COMMON/TLIQX/TLTIMX(15,15,15),TLTIME(15),RZTL(15),ZZTL(15)
      COMMON/SITEX/RBSITX(100,10),FREQX(100,10),XSITE(3,100),TSITE(100),
     X             TRFTIM(10)
      COMMON/TANKX/RADTX(10),ZRADTX(10)
      COMMON/BUBBLE/WAKV(3,1000),VB(3,1000),XB(3,1000),RB(1000),
     X              RBA(1000),IB(1000),DMBGF(1000),DMB(1000),CDRAG(1000)
      COMMON/CONVERG/DBUBCO,DLIQCO,DLEVCO,DCONCO,DENRCO,DFORCO
      COMMON/SURFAS/ZSURF,SURFAN,ISLIP
      COMMON/LICUID/WMLO,DML1,DMLBF,TSUPRL,QL,REYN12,REYN23,ACOF(3),
     X          EXPN(3),TBULKL
      COMMON/GASPRO/HG,RBMIN,NB
      COMMON/GNRL/DTIME,DTIMEX,TIMEND,TIMPRNT(1000),IPRINTL,IPRINTU,
     X          NTAPE,IRESTRT,TIME,PIMPS,PARIMP
      COMMON/VOID/VOFRAC,DMBTOT
```

```
      COMMON/INTEGR/NTL,NTLR,NTLZ,NRFT,NSITE,NRZ,NPTIM,NPROP,IWAKE
      COMMON/ADCONST/CWAKE,BWAKE,SCRAD,ARBDEN,DEGFAC,ICRD(3)
      CALL TABL(TIM,GRAVITY,TIMPROP(1),GRATIM(1),1,1,1,NPTIM,IFB)
      RETURN
      END
      FUNCTION GRANGL(TIM)
      COMMON/PROPRT/PPZ(30),TPZ(30),SPZ(30),VPZ(30),RPLZ(30),UPLZ(30),
     X              RPGZ(30),UPGZ(30)
      COMMON/DYNAM/TIMPROP(30),PTIM(30),QLTIM(30),WMLOTIM(30),SANTIM(30)
     X             ,GANTIM(30),GRATIM(30)
      COMMON/TLIQX/TLTIMX(15,15,15),TLTIME(15),RZTL(15),ZZTL(15)
      COMMON/SITEX/RBSITX(100,10),FREQX(100,10),XSITE(3,100),TSITE(100),
     X             TRFTIM(10)
      COMMON/TANKX/RADTX(10),ZRADTX(10)
      COMMON/BUBBLE/WAKV(3,1000),VB(3,1000),XB(3,1000),RB(1000),
     X              RBA(1000),IB(1000),DMBGF(1000),DMB(1000),CDRAG(1000)
      COMMON/CONVERG/DBUBCO,DLIQCO,DLEVCO,DCONCO,DENRCO,DFORCO
      COMMON/SURFAS/ZSURF,SURFAN,ISLIP
      COMMON/LICUID/WMLO,DML1,DMLBF,TSUPRL,QL,REYN12,REYN23,ACOF(3),
     X         EXPN(3),TBULKL
      COMMON/GASPRO/HG,RBMIN,NB
      COMMON/GNRL/DTIME,DTIMEX,TIMEND,TIMPRNT(1000),IPRINTL,IPRINTU,
     X            NTAPE,IRESTRT,TIME,PIMPS,PARIMP
      COMMON/VOID/VOFRAC,DMBTOT
      COMMON/INTEGR/NTL,NTLR,NTLZ,NRFT,NSITE,NRZ,NPTIM,NPROP,IWAKE
      COMMON/ADCONST/CWAKE,BWAKE,SCRAD,ARBDEN,DEGFAC,ICRD(3)
      CALL TABL(TIM,GRANGL,TIMPROP(1),GANTIM(1),1,1,1,NPTIM,IFB)
      RETURN
      END
      FUNCTION RBSITZ(N,TIM)
      COMMON/PROPRT/PPZ(30),TPZ(30),SPZ(30),VPZ(30),RPLZ(30),UPLZ(30),
     X              RPGZ(30),UPGZ(30)
      COMMON/DYNAM/TIMPROP(30),PTIM(30),QLTIM(30),WMLOTIM(30),SANTIM(30)
     X             ,GANTIM(30),GRATIM(30)
      COMMON/TLIQX/TLTIMX(15,15,15),TLTIME(15),RZTL(15),ZZTL(15)
      COMMON/SITEX/RBSITX(100,10),FREQX(100,10),XSITE(3,100),TSITE(100),
     X             TRFTIM(10)
      COMMON/TANKX/RADTX(10),ZRADTX(10)
      COMMON/BUBBLE/WAKV(3,1000),VB(3,1000),XB(3,1000),RB(1000),
     X              RBA(1000),IB(1000),DMBGF(1000),DMB(1000),CDRAG(1000)
      COMMON/CONVERG/DBUBCO,DLIQCO,DLEVCO,DCONCO,DENRCO,DFORCO
      COMMON/SURFAS/ZSURF,SURFAN,ISLIP
      COMMON/LICUID/WMLO,DML1,DMLBF,TSUPRL,QL,REYN12,REYN23,ACOF(3),
     X         EXPN(3),TBULKL
      COMMON/GASPRO/HG,RBMIN,NB
      COMMON/GNRL/DTIME,DTIMEX,TIMEND,TIMPRNT(1000),IPRINTL,IPRINTU,
     X            NTAPE,IRESTRT,TIME,PIMPS,PARIMP
      COMMON/VOID/VOFRAC,DMBTOT
      COMMON/INTEGR/NTL,NTLP,NTLZ,NRFT,NSITE,NRZ,NPTIM,NPROP,IWAKE
      COMMON/ADCONST/CWAKE,BWAKE,SCRAD,ARBDEN,DEGFAC,ICRD(3)
      DIMENSION DUMMY(10)
      DO 2 I=1,NRFT
    2 DUMMY(I)=RBSITX(N,I)
      CALL TABL(TIM,RBSITZ,TRFTIM(1),DUMMY(1),1,1,1,NRFT,IFB)
```

```
      RETURN
      END
      FUNCTION FREQZT(N,TIM1,TIM2)
      COMMON/PROPRT/PPZ(30),TPZ(30),SPZ(30),VPZ(30),RPLZ(30),UPLZ(30),
     X                RPGZ(30),UPGZ(30)
      COMMON/DYNAM/TIMPROP(30),PTIM(30),QLTIM(30),WMLOTIM(30),SANTIM(30)
     X            ,GANTIM(30),GRATIM(30)
      COMMON/TLIQX/TLTIMX(15,15,15),TLTIME(15),RZTL(15),ZZTL(15)
      COMMON/SITEX/RBSITX(100,10),FREQX(100,10),XSITE(3,100),TSITE(100),
     X                TRFTIM(10)
      COMMON/TANKX/RADTX(10),ZRADTX(10)
      COMMON/BUBBLE/WAKV(3,1000),VB(3,1000),XB(3,1000),RB(1000),
     X                RBA(1000),IB(1000),DMBGF(1000),DMB(1000),CDRAG(1000)
      COMMON/CONVERG/DBUBCO,DLIQCO,DLEVCO,DCONCO,DENRCO,DFORCO
      COMMON/SURFAS/ZSURF,SURFAN,ISLIP
      COMMON/LICUID/WMLO,DML1,DMLBF,TSUPRL,QL,REYN12,REYN23,ACOF(3),
     X          EXPN(3),TBULKL
      COMMON/GASPRO/HG,RBMIN,NB
      COMMON/GNRL/DTIME,DTIMEX,TIMEND,TIMPRNT(1000),IPRINTL,IPRINTU,
     X              NTAPE,IRESTRT,TIME,PIMPS,PARIMP
      COMMON/VOID/VOFRAC,DMBTOT
      COMMON/INTEGR/NTL,NTLR,NTLZ,NRFT,NSITE,NRZ,NPTIM,NPROP,IWAKE
      COMMON/ADCONST/CWAKE,BWAKE,SCRAD,ARBDEN,DEGFAC,ICRD(3)
      DIMENSION DUMMY(10)
      DO 2 I=1,NRFT
    2 DUMMY(I)=FREQX(N,I)
      CALL TABL(TIM1,FR1,TRFTIM(1),DUMMY(1),1,1,1,NRFT,IFB)
      CALL TABL(TIM2,FR2,TRFTIM(1),DUMMY(1),1,1,1,NRFT,IFB)
      FREQZT=(FR1+FR2)/2.
      RETURN
      END
      FUNCTION TZ(X,Y,Z,TIM)
      COMMON/PROPRT/PPZ(30),TPZ(30),SPZ(30),VPZ(30),RPLZ(30),UPLZ(30),
     X                RPGZ(30),UPGZ(30)
      COMMON/DYNAM/TIMPROP(30),PTIM(30),QLTIM(30),WMLOTIM(30),SANTIM(30)
     X            ,GANTIM(30),GRATIM(30)
      COMMON/TLIQX/TLTIMX(15,15,15),TLTIME(15),RZTL(15),ZZTL(15)
      COMMON/SITEX/RBSITX(100,10),FREQX(100,10),XSITE(3,100),TSITE(100),
     X                TRFTIM(10)
      COMMON/TANKX/RADTX(10),ZRADTX(10)
      COMMON/BUBBLE/WAKV(3,1000),VB(3,1000),XB(3,1000),RB(1000),
     X                RBA(1000),IB(1000),DMBGF(1000),DMB(1000),CDRAG(1000)
      COMMON/CONVERG/DBUBCO,DLIQCO,DLEVCO,DCONCO,DENRCO,DFORCO
      COMMON/SURFAS/ZSURF,SURFAN,ISLIP
      COMMON/LICUID/WMLO,DML1,DMLBF,TSUPRL,QL,REYN12,REYN23,ACOF(3),
     X          EXPN(3),TBULKL
      COMMON/GASPRO/HG,RBMIN,NB
      COMMON/GNRL/DTIME,DTIMEX,TIMEND,TIMPRNT(1000),IPRINTL,IPRINTU,
     X              NTAPE,IRESTRT,TIME,PIMPS,PARIMP
      COMMON/VOID/VOFRAC,DMBTOT
      COMMON/INTEGR/NTL,NTLR,NTLZ,NRFT,NSITE,NRZ,NPTIM,NPROP,IWAKE
      COMMON/ADCONST/CWAKE,BWAKE,SCRAD,ARBDEN,DEGFAC,ICRD(3)
      DIMENSION DUM1(15,15),DUM2(15,15)
      R=SQRT(X*X+Y*Y)
```

```
      I=1
    4 IF(TIM-TLTIME(I))1,2,3
    3 I=I+1
      IF(I-NTL)4,4,5
    5 IU=NTL
      IL=NTL-1
      GO TO 6
    1 IU=I
      IL=I-1
      IF(I-1)7,7,6
    7 IU=2
      IL=1
    6 DO 8 I=1,NTLR
      DO 8 J=1,NTLZ
    8 DUM1(J,I)=TLTIMX(I,J,IL)
      DO 9 I=1,NTLR
      DO 9 J=1,NTLZ
    9 DUM2(J,I)=TLTIMX(I,J,IU)
      CALL DTABL2(R,Z,TN1,ZZTL(1),1,NTLZ,1,1,IFB,RZTL(1),DUM1(1,1),1,
     X          15,NTLR)
      CALL DTABL2(R,Z,TN2,ZZTL(1),1,NTLZ,1,1,IFB,RZTL(1),DUM2(1,1),1,
     X          15,NTLR)
      TN=TN1+(TN2-TN1)*(TIM-TLTIME(IL))/(TLTIME(IU)-TLTIME(IL))
      GO TO 10
    2 IL=I
      DO 11 I=1,NTLR
      DO 11 J=1,NTLZ
   11 DUM1(J,I)=TLTIMX(I,J,IL)
      CALL DTABL2(R,Z,TN,ZZTL(1),1,NTLZ,1,1,IFB,RZTL(1),DUM1(1,1),1,
     X              15,NTLR)
   10 TZ=TN*TBULKL
      RETURN
      END
      SUBROUTINE SCREEN(X,Y,Z,RI,RO,ISOBS,IREDUC)
      COMMON/PROPRT/PPZ(30),TPZ(30),SPZ(30),VPZ(30),RPLZ(30),UPLZ(30),
     X                RPGZ(30),UPGZ(30)
      COMMON/DYNAM/TIMPROP(30),PTIM(30),QLTIM(30),WMLOTIM(30),SANTIM(30)
     X              ,GANTIM(30),GRATIM(30)
      COMMON/TLIQX/TLTIMX(15,15,15),TLTIME(15),RZTL(15),ZZTL(15)
      COMMON/SITEX/RBSITX(100,10),FREQX(100,10),XSITE(3,100),TSITE(100),
     X               TRFTIM(10)
      COMMON/TANKX/RADTX(10),ZRADTX(10)
      COMMON/BUBBLE/WAKV(3,1000),VB(3,1000),XP(3,1000),RB(1000),
     X                RBA(1000),IB(1000),DMBGF(1000),DMB(1000),CDRAG(1000)
      COMMON/CONVERG/DBUBCO,DLIQCO,DLEVCO,DCONCO,DENRCO,DFORCO
      COMMON/SURFAS/ZSURF,SURFAN,ISLIP
      COMMON/LICUID/WMLO,DML1,DMLBF,TSUPRL,QL,REYN12,REYN23,ACOF(3),
     X          EXPN(3),TBULKL
      COMMON/GASPRO/HG,RBMIN,NB
      COMMON/GNRL/DTIME,DTIMEX,TIMEND,TIMPRNT(1000),IPRINTL,IPRINTU,
     X              NTAPE,IRESTRT,TIME,PIMPS,PARIMP
      COMMON/VOID/VOFRAC,DMBTOT
      COMMON/INTEGR/NTL,NTLR,NTLZ,NRFT,NSITE,NRZ,NPTIM,NPROP,IWAKE
      COMMON/ADCONST/CWAKE,BWAKE,SCRAD,ARBDEN,DEGFAC,ICRD(3)
```

```
      IF(RI*SCRAD)1,1,3
    3 IF(IREDUC)1,1,2
    2 CALL FORCES(X,Y,Z,RI,RI,ISOBS,FMAG,THETA,PHI,TIME)
      TL=TZ(X,Y,Z,TIME)
      FSCRAD=2.*3.1416*SCRAD*SIGZ(TL)
      DR=XRADT(Z+RI)-XRADT(Z)
      DM=SQRT(DR*DR+RI*RI)
      THETN=ACIS(DR,DM)
      PHN=ATIN(Y,X)
      FNO=FMAG*(SIN(THETA)*COS(PHI)*COS(THETN)*COS(PHN)+SIN(THETA)*
     X          SIN(PHI)*COS(THETN)*SIN(PHN)-COS(THETA)*SIN(THETN))
      FNO=FNO/32.17
      IF(FNO)1,1,4
    4 P=PZ(TIME)+2.*SIGZ(TL)/(144.*RI)
      ANO=FNO/(144.*P)
      DNO=ANO/(3.1416*SCRAD*SCRAD)
      FSCRAD=FSCRAD*DNO
      IF(FSCRAD-FNO)5,5,1
    1 RO=RI
      GO TO 6
    5 RO=0.
    6 RETURN
      END
      SUBROUTINE RESTART
      COMMON/PROPRT/PPZ(30),TPZ(30),SPZ(30),VPZ(30),RPLZ(30),UPLZ(30),
     X             RPGZ(30),UPGZ(30)
      COMMON/DYNAM/TIMPROP(30),PTIM(30),QLTIM(30),WMLOTIM(30),SANTIM(30)
     X            ,GANTIM(30),GRATIM(30)
      COMMON/TLIQX/TLTIMX(15,15,15),TLTIME(15),RZTL(15),ZZTL(15)
      COMMON/SITEX/RBSITX(100,10),FREQX(100,10),XSITE(3,100),TSITE(100),
     X             TRFTIM(10)
      COMMON/TANKX/RADTX(10),ZRADTX(10)
      COMMON/BUBBLE/WAKV(3,1000),VB(3,1000),XB(3,1000),RB(1000),
     X             RBA(1000),IB(1000),DMBGF(1000),DMB(1000),CDRAG(1000)
      COMMON/CONVERG/DBUBCO,DLIQCO,DLEVCO,DCONCO,DENRCO,DFORCO
      COMMON/SURFAS/ZSURF,SURFAN,ISLIP
      COMMON/LICUID/WMLO,DML1,DMLBF,TSUPRL,QL,REYN12,REYN23,ACOF(3),
     X          EXPN(3),TBULKL
      COMMON/GASPRO/HG,RBMIN,NB
      COMMON/GNRL/DTIME,DTIMEX,TIMEND,TIMPRNT(1000),IPRINTL,IPRINTU,
     X            NTAPE,IRESTRT,TIME,PIMPS,PARIMP
      COMMON/VOID/VOFRAC,DMBTOT
      COMMON/INTEGR/NTL,NTLR,NTLZ,NRFT,NSITE,NRZ,NPTIM,NPROP,IWAKE
      COMMON/ADCONST/CWAKE,BWAKE,SCRAD,ARBDEN,DEGFAC,ICRD(3)
      IF(NB)1,1,2
    2 PUNCH 100,(TSITE(I),I=1,NSITE)
      DO 21 I=1,NB
   21 PUNCH 100,XB(1,I),XB(2,I),XB(3,I),RBA(I)
  100 FORMAT(6E13.6)
    1 RETURN
      END
R
 11   2   2   2   2   3   4   8   0 149   1   1   1
  12.061     524.69  1.317E-3  3.087E-4    93.132      21.296  0.30456     60.195
```

12.562	526.69	1.307E-3	3.060E-4	92.968	21.705	0.31633	60.324
13.080	528.69	1.297E-3	3.033E-4	92.804	22.114	0.32846	60.452
13.614	530.69	1.287E-3	3.005E-4	92.640	22.522	0.34094	60.581
14.165	532.69	1.277E-3	2.978E-4	92.475	22.931	0.35378	60.712
14.733	534.69	1.267E-3	2.951E-4	92.310	23.341	0.36700	60.845
15.319	536.69	1.257E-3	2.924E-4	92.144	23.750	0.38059	60.975
15.924	538.69	1.247E-3	2.896E-4	91.978	24.160	0.39458	61.106
16.546	540.69	1.237E-3	2.869E-4	91.812	24.570	0.40895	61.241
17.188	542.69	1.227E-3	2.842E-4	91.645	24.979	0.42374	61.374
17.848	544.69	1.217E-3	2.815E-4	91.477	25.389	0.43893	61.512
0.	14.7	0.	0.	0.	0.	1.	
100.	14.7	0.	0.	0.	0.	1.	
0.0	0.125	0.126	100.0				
0.	0.	0.25					
0.008	1.35	0.008	1.35	0.008	1.35	0.008	1.35
0.	0.03100	0.25					
0.008	1.31	0.008	1.31	0.008	1.31	0.008	1.31
0.229	0.	0.25					
0.0	0.0	0.0	0.0	0.0	0.0		
0.1145	0.1985	0.25					
0.0	0.0	0.0	0.0	0.0	0.0		
-0.1145	0.1985	0.25					
0.0	0.0	0.0	0.0	0.0	0.0		
-0.229	0.	0.25					
0.0	0.0	0.0	0.0	0.0	0.0		
-0.1145	-0.1985	0.25					
0.0	0.0	0.0	0.0	0.0	0.0		
0.1145	-0.1985	0.25					
0.0	0.0	0.0	0.0	0.0	0.0		
0.350		0.0	0.0	0.0		0.0	0.0
0.0		0.0					
0.0	100.0						
0.0	0.349						
0.0	0.25	0.95					
1.0	1.0						
1.0	1.0						
1.0	1.0						
1.0	1.0						
1.0	1.0						
1.0	1.0						
0.349	0.0	0.349	1.0				
0.4	0.6	0.8	1.0	1.2	1.4	1.6	1.8
2.0	2.2	2.4	2.6	2.8	3.0	3.2	3.4
3.6	3.8	4.0	4.2	4.4	4.6	4.8	5.0
5.2	5.4	5.6	5.8	6.0	6.2	6.4	6.6
6.8	7.0	7.2	7.4	7.6	7.8	8.0	8.2
8.4	8.6	8.8	9.0	9.2	9.4	9.6	9.8
10.0	10.2	10.4	10.6	10.8	11.0	11.2	11.4
11.6	11.8	12.0	12.2	12.4	12.6	12.8	13.0
13.2	13.4	13.6	13.8	14.0	14.2	14.4	14.6
14.8	15.0	15.2	15.4	15.6	15.8	16.0	16.2
16.4	16.6	16.8	17.0	17.2	17.4	17.6	17.8
18.0	18.2	18.4	18.6	18.8	19.0	19.2	19.4
19.6	19.8	20.0	20.2	20.4	20.6	20.8	21.0

21.2	21.4	21.6	21.8	22.0	22.2	22.4	22.6
22.8	23.0	23.2	23.4	23.6	23.8	24.0	24.2
24.4	24.6	24.8	25.0	25.2	25.4	25.6	25.8
26.0	26.2	26.4	26.6	26.8	27.0	27.2	27.4
27.6	27.8	28.0	28.2	28.4	28.6	28.8	29.0
29.2	29.4	29.6	29.8	30.0			
2.0	2000.	24.	-1.	19.7	-.725	2.64	0.13
33.6	0.	0.0001	.02	0.	0.003	30.0	534.69
0.0	0.0	0.95	0.0	1.0	1.0	0.0	

INITIAL CONDITIONS

PRESSURE	TEMPERATURE	SURF TENSION	VISCOSITY	LIQ DENSITY	LIQ ENERGY	GAS DENSITY	GAS ENERGY
1.206100E+01	5.246900E+02	1.317000E-03	3.087000E-04	9.313200E+01	2.129600E+01	3.045600E-01	6.019500E+01
1.256200E+01	5.266900E+02	1.307000E-03	3.060000E-04	9.296800E+01	2.170500E+01	3.163300E-01	6.032400E+01
1.308000E+01	5.286900E+02	1.297000E-03	3.033000E-04	9.280400E+01	2.211400E+01	3.284600E-01	6.045200E+01
1.361400E+01	5.306900E+02	1.287000E-03	3.005000E-04	9.264000E+01	2.252200E+01	3.409400E-01	6.058100E+01
1.416500E+01	5.326900E+02	1.277000E-03	2.978000E-04	9.247500E+01	2.293100E+01	3.537800E-01	6.071200E+01
1.473300E+01	5.346900E+02	1.267000E-03	2.951000E-04	9.231000E+01	2.334100E+01	3.670000E-01	6.084500E+01
1.531900E+01	5.366900E+02	1.257000E-03	2.924000E-04	9.214400E+01	2.375000E+01	3.805900E-01	6.097500E+01
1.592400E+01	5.386900E+02	1.247000E-03	2.896000E-04	9.197800E+01	2.416000E+01	3.945800E-01	6.110600E+01
1.654600E+01	5.406900E+02	1.237000E-03	2.869000E-04	9.181200E+01	2.457000E+01	4.089500E-01	6.124100E+01
1.718800E+01	5.426900E+02	1.227000E-03	2.842000E-04	9.164500E+01	2.497900E+01	4.237400E-01	6.137400E+01
1.784800E+01	5.446900E+02	1.217000E-03	2.815000E-04	9.147700E+01	2.538900E+01	4.389300E-01	6.151200E+01

TIME	PRESSURE	LIQ HEATING	LIQ FLOW RATE	SURF ANGLE	GRAV ANGLE	GRAVITY
0.	1.470000E+01	0.	0.	0.	0.	1.000000E+00
1.000000E+02	1.470000E+01	0.	0.	0.	0.	1.000000E+00

SITE NUMBER 1 XSITE= 0. YSITE= 0. ZSITE= 2.500000E-01 INITIAL TIME= 3.500000E-01

TIME	SITE RADIUS	SITE FREQ
0.	8.000000E-03	1.350000E+00
1.250000E-01	8.000000E-03	1.350000E+00
1.260000E-01	8.000000E-03	1.350000E+00
1.000000E+02	8.000000E-03	1.350000E+00

SITE NUMBER 2 XSITE= 0. YSITE= 3.100000E-02 ZSITE= 2.500000E-01 INITIAL TIME= 0.

TIME	SITE RADIUS	SITE FREQ
0.	8.000000E-03	1.310000E+00
1.250000E-01	8.000000E-03	1.310000E+00
1.260000E-01	8.000000E-03	1.310000E+00
1.000000E+02	8.000000E-03	1.310000E+00

SITE NUMBER 3 XSITE= 2.290000E-01 YSITE= 0. ZSITE= 2.500000E-01 INITIAL TIME= 0.

TIME SITE RADIUS SITE FREQ

```
 0.               0.            0.
 1.250000E-01     0.            0.
 1.260000E-01     0.            0.
 1.000000E+02    -0.           -0.

SITE NUMBER    4      XSITE= 1.145000E-01      YSITE= 1.985000E-01      ZSITE= 2.500000E-01      INITIAL TIME= 0.

   TIME          SITE RADIUS     SITE FREQ

 0.               0.            0.
 1.250000E-01     0.            0.
 1.260000E-01     0.            0.
 1.000000E+02    -0.           -0.

SITE NUMBER    5      XSITE=-1.145000E-01      YSITE= 1.985000E-01      ZSITE= 2.500000E-01      INITIAL TIME= 0.

   TIME          SITE RADIUS     SITE FREQ

 0.               0.            0.
 1.250000E-01     0.            0.
 1.260000E-01     0.            0.
 1.000000E+02    -0.           -0.

SITE NUMBER    6      XSITE=-2.290000E-01      YSITE= 0.                ZSITE= 2.500000E-01      INITIAL TIME= 0.

   TIME          SITE RADIUS     SITE FREQ

 0.               0.            0.
 1.250000E-01     0.            0.
 1.260000E-01     0.            0.
 1.000000E+02    -0.           -0.

SITE NUMBER    7      XSITE=-1.145000E-01      YSITE=-1.985000E-01      ZSITE= 2.500000E-01      INITIAL TIME= 0.

   TIME          SITE RADIUS     SITE FREQ

 0.               0.            0.
 1.250000E-01     0.            0.
 1.260000E-01     0.            0.
 1.000000E+02    -0.           -0.
```

SITE NUMBER 8 XSITE= 1.145000E-01 YSITE=-1.985000E-01 ZSITE= 2.500000E-01 INITIAL TIME= 0.

TIME	SITE RADIUS	SITE FREQ
0.	0.	0.
1.250000E-01	0.	0.
1.260000E-01	0.	0.
1.000000E+02	-0.	-0.

TIME= 0.

RADIUS	AXIAL HEIGHT	NORM TEMPERATURE
0.	0.	1.000000E+00
3.490000E-01	0.	1.000000E+00
0.	2.500000E-01	1.000000E+00
3.490000E-01	2.500000E-01	1.000000E+00
0.	9.500000E-01	1.000000E+00
3.490000E-01	9.500000E-01	1.000000E+00

TIME= 1.000000E+02

RADIUS	AXIAL HEIGHT	NORM TEMPERATURE
0.	0.	1.000000E+00
3.490000E-01	0.	1.000000E+00
0.	2.500000E-01	1.000000E+00
3.490000E-01	2.500000E-01	1.000000E+00
0.	9.500000E-01	1.000000E+00
3.490000E-01	9.500000E-01	1.000000E+00

TANK RADIUS	AXIAL HEIGHT
3.490000E-01	0.
3.490000E-01	1.000000E+00

REYNOLDS 1-2	REYNOLDS 2-3	ACOEF 1	EXPONENT 1	ACOEF 2	EXPONENT 2	ACOEF 3	EXPONENT 3
2.000000E+00	2.000000E+03	2.400000E+01	-1.000000E+00	1.970000E+01	-7.250000E-01	2.640000E+00	1.300000E-01

LIQUID MASS	LIQ SUPRHEAT	MIN RADIUS	TIME STEP	TIME ZERO	BUBBLE CONV H	TIMEND	LIQUID TEMP
3.360000E+01	0.	1.000000E-04	2.000000E-02	0.	3.000000E-03	3.000000E+01	5.346900E+02

BUB IMP PARAM	SURF IMP PARAM	ZSURF ZERO	CWAKE	BWAKE	BOILING PARAM	SPATIAL DEGEN	SCREEN RADIUS
0.	0.	9.500000E-01	5.468112E-01	1.703780E+00	1.000000E+00	1.000000E+00	0.

PROGRAM EVOLVE*** THE TEMPORAL AND SPATIAL HISTORY OF A BUBBLE SOCIETY

TIME	PRESSURE	LIQUID MASS	LEVEL ANGLE	LEVEL HEIGHT	VOID FRACTION	VOID MASS	GRAV ANGLE
4.200000E-01	1.470000E+01	3.356239E+01	0.	9.500736E-01	0.	0.	0.

****

TIME	PRESSURE	LIQUID MASS	LEVEL ANGLE	LEVEL HEIGHT	VOID FRACTION	VOID MASS	GRAV ANGLE
6.200000E-01	1.470000E+01	3.356239E+01	0.	9.500736E-01	0.	0.	0.

****

TIME	PRESSURE	LIQUID MASS	LEVEL ANGLE	LEVEL HEIGHT	VOID FRACTION	VOID MASS	GRAV ANGLE
8.033588E-01	1.470000E+01	3.356239E+01	0.	9.500736E-01	5.899267E-06	7.855549E-07	0.

XB(1)	XB(2)	XB(3)	VB(1)	VB(2)	VB(3)	MASS RADIUS	ACTUAL RADIUS
0.	3.100000E-02	2.731092E-01	0.	0.	5.329752E-01	8.000000E-03	8.000000E-03

****

TIME	PRESSURE	LIQUID MASS	LEVEL ANGLE	LEVEL HEIGHT	VOID FRACTION	VOID MASS	GRAV ANGLE
1.003359E+00	1.470000E+01	3.356239E+01	0.	9.500736E-01	5.899267E-06	7.855549E-07	0.

XB(1)	XB(2)	XB(3)	VB(1)	VB(2)	VB(3)	MASS RADIUS	ACTUAL RADIUS
0.	3.100000E-02	3.797042E-01	0.	0.	5.329752E-01	8.000000E-03	8.000000E-03

****

TIME	PRESSURE	LIQUID MASS	LEVEL ANGLE	LEVEL HEIGHT	VOID FRACTION	VOID MASS	GRAV ANGLE
1.210741E+00	1.470000E+01	3.356238E+01	0.	9.500736E-01	1.179846E-05	1.571110E-06	0.

XB(1)	XB(2)	XB(3)	VB(1)	VB(2)	VB(3)	MASS RADIUS	ACTUAL RADIUS
0.	3.100000E-02	4.902337E-01	0.	0.	5.329752E-01	8.000000E-03	8.000000E-03
0.	5.361886E-05	3.229459E-01	0.	4.325822E-04	5.728357E-01	8.000000E-03	8.000000E-03

****

TIME	PRESSURE	LIQUID MASS	LEVEL ANGLE	LEVEL HEIGHT	VOID FRACTION	VOID MASS	GRAV ANGLE
1.410741E+00	1.470000E+01	3.356238E+01	0.	9.500736E-01	1.179806E-05	1.571110E-06	0.

XB(1)	XB(2)	XB(3)	VB(1)	VB(2)	VB(3)	MASS RADIUS	ACTUAL RADIUS
0.	3.100000E-02	5.968287E-01	0.	0.	5.329752E-01	8.000000E-03	8.000000E-03
0.	1.453936E-04	4.375905E-01	0.	4.816182E-04	5.735470E-01	8.000000E-03	8.000000E-03

****

TIME	PRESSURE	LIQUID MASS	LEVEL ANGLE	LEVEL HEIGHT	VOID FRACTION	VOID MASS	GRAV ANGLE
1.606718E+00	1.470000E+01	3.356238E+01	0.	9.500736E-01	1.769759E-05	2.356665E-06	0.

XB(1)	XB(2)	XB(3)	VB(1)	VB(2)	VB(3)	MASS RADIUS	ACTUAL RADIUS
0.	3.100000E-02	7.012795E-01	0.	0.	5.329752E-01	8.000000E-03	8.000000E-03
0.	2.457860E-04	5.500724E-01	0.	5.386402E-04	5.742954E-01	8.000000E-03	8.000000E-03
0.	3.098663E-02	2.986959E-01	0.	-1.685954E-04	6.089241E-01	8.000000E-03	8.000000E-03

****

TIME	PRESSURE	LIQUID MASS	LEVEL ANGLE	LEVEL HEIGHT	VOID FRACTION	VOID MASS	GRAV ANGLE
1.806718E+00	1.470000E+01	3.356238E+01	0.	9.500736E-01	1.769759E-05	2.356665E-06	0.

XB(1)	XB(2)	XB(3)	VB(1)	VB(2)	VB(3)	MASS RADIUS	ACTUAL RADIUS
0.	3.100000E-02	8.078745E-01	0.	0.	5.329752E-01	8.000000E-03	8.000000E-03
0.	3.609775E-04	6.650211E-01	0.	6.084825E-04	5.751195E-01	8.000000E-03	8.000000E-03
0.	3.095177E-02	4.206526E-01	0.	-1.791542E-04	6.105062E-01	8.000000E-03	8.000000E-03

****

TIME	PRESSURE	LIQUID MASS	LEVEL ANGLE	LEVEL HEIGHT	VOID FRACTION	VOID MASS	GRAV ANGLE
2.011481E+00	1.470000E+01	3.356238E+01	0.	9.500736E-01	2.359665E-05	3.142220E-06	0.

XB(1)	XB(2)	XB(3)	VB(1)	VB(2)	VB(3)	MASS RADIUS	ACTUAL RADIUS
0.	3.100000E-02	9.170087E-01	0.	0.	5.329752E-01	8.000000E-03	8.000000E-03
0.	4.950918E-04	7.828867E-01	0.	6.957997E-04	5.760366E-01	8.000000E-03	8.000000E-03
0.	3.091375E-02	5.458583E-01	0.	-1.911908E-04	6.122726E-01	8.000000E-03	8.000000E-03
0.	7.221207E-05	3.675696E-01	0.	4.006902E-04	6.370353E-01	8.000000E-03	8.000000E-03

****

TIME	PRESSURE	LIQUID MASS	LEVEL ANGLE	LEVEL HEIGHT	VOID FRACTION	VOID MASS	GRAV ANGLE
2.211481E+00	1.470000E+01	3.356238E+01	0.	9.500736E-01	1.769759E-05	2.356665E-06	0.

XB(1)	XB(2)	XB(3)	VB(1)	VB(2)	VB(3)	MASS RADIUS	ACTUAL RADIUS
0.	5.380042E-04	8.920768E-01	0.	0.	5.329752E-01	8.000000E-03	8.000000E-03
0.	3.087404E-02	6.623239E-01	0.	-2.049769E-04	5.694803E-01	8.000000E-03	8.000000E-03
0.	1.521906E-04	4.917112E-01	0.	4.109020E-04	6.141198E-01	8.000000E-03	8.000000E-03

****

TIME	PRESSURE	LIQUID MASS	LEVEL ANGLE	LEVEL HEIGHT	VOID FRACTION	VOID MASS	GRAV ANGLE
2.410076E+00	1.470000E+01	3.356238E+01	0.	9.500736E-01	1.769759E-05	2.356665E-06	0.

XB(1)	XB(2)	XB(3)	VB(1)	VB(2)	VB(3)	MASS RADIUS	ACTUAL RADIUS

0.	3.085339E-02	7.717834E-01	0.	0.	5.329752E-01	8.000000E-03	8.000000E-03
0.	2.391114E-04	6.096714E-01	0.	4.597032E-04	5.736903E-01	8.000000E-03	8.000000E-03
0.	3.098504E-02	3.229287E-01	0.	-1.235749E-04	6.043270E-01	8.000000E-03	8.000000E-03

****

TIME	PRESSURE	LIQUID MASS	LEVEL ANGLE	LEVEL HEIGHT	VOID FRACTION	VOID MASS	GRAV ANGLE
2.612222E+00	1.470000E+01	3.356238E+01	0.	9.500736E-01	2.359665E-05	3.142220E-06	0.

XB(1)	XB(2)	XB(3)	VB(1)	VB(2)	VB(3)	MASS RADIUS	ACTUAL RADIUS
0.	3.085339E-02	8.795222E-01	0.	0.	5.329752E-01	8.000000E-03	8.000000E-03
0.	3.380709E-04	7.257262E-01	0.	5.154600E-04	5.744695E-01	8.000000E-03	8.000000E-03
0.	3.095940E-02	4.452270E-01	0.	-1.295727E-04	6.055634E-01	8.000000E-03	8.000000E-03
0.	1.876980E-05	2.767385E-01	0.	4.471013E-04	6.345147E-01	8.000000E-03	8.000000E-03

****

TIME	PRESSURE	LIQUID MASS	LEVEL ANGLE	LEVEL HEIGHT	VOID FRACTION	VOID MASS	GRAV ANGLE
2.812222E+00	1.470000E+01	3.356238E+01	0.	9.500736E-01	1.769759E-05	2.356665E-06	0.

XB(1)	XB(2)	XB(3)	VB(1)	VB(2)	VB(3)	MASS RADIUS	ACTUAL RADIUS
0.	4.025633E-04	8.373347E-01	0.	0.	5.329752E-01	8.000000E-03	8.000000E-03
0.	3.093278E-02	5.632942E-01	0.	-1.363071E-04	5.668742E-01	8.000000E-03	8.000000E-03
0.	1.105110E-04	4.019258E-01	0.	4.666303E-04	6.124445E-01	8.000000E-03	8.000000E-03

****

TIME	PRESSURE	LIQUID MASS	LEVEL ANGLE	LEVEL HEIGHT	VOID FRACTION	VOID MASS	GRAV ANGLE
3.012222E+00	1.470000E+01	3.356238E+01	0.	9.500736E-01	1.179847E-05	1.571110E-06	0.

XB(1)	XB(2)	XB(3)	VB(1)	VB(2)	VB(3)	MASS RADIUS	ACTUAL RADIUS
0.	3.090462E-02	6.767095E-01	0.	0.	5.329752E-01	8.000000E-03	8.000000E-03
0.	2.105984E-04	5.246160E-01	0.	-1.445421E-04	5.672443E-01	8.000000E-03	8.000000E-03